STATE OF CALIFORNIA • DEPARTMENT OF TRANSPORTATION

# TECHNICAL REPORT DOCUMENTATION PAGE

TR0003 (REV 10/98)

**ADA Notice**

For individuals with sensory disabilities, this document is available in alternate formats. For information call (916) 654-6410 or TDD (916) 654-3880 or write Records and Forms Management, 1120 N Street, MS-89, Sacramento, CA 95814.

| 1. REPORT NUMBER | 2. GOVERNMENT ASSOCIATION NUMBER | 3. RECIPIENT'S CATALOG NUMBER |
|---|---|---|
| CA13-1233 | | |

**4. TITLE AND SUBTITLE**

Reusable Instrumented Test Pile for Improved Pile Design in Granular Soils

**5. REPORT DATE**

March 2013

**6. PERFORMING ORGANIZATION CODE**

N/A

**7. AUTHOR**

Jason DeJong (1), Aravinthan Thurairajah (2), Daniel Wilson (1), Mason Ghafghazi (1)

**8. PERFORMING ORGANIZATION REPORT NO.**

**9. PERFORMING ORGANIZATION NAME AND ADDRESS**

(1) Department of Civil & Environmental Engineering, University of California, One Shields Ave., Davis, CA 95616

(2) Golder Associates Ltd., 500-4260 Still Creek Drive, Burnaby, British Columbia, Canada V5C 6C6 (formerly doctoral student at UC Davis)

**10. WORK UNIT NUMBER**

Contract No. 65A0264

**11. CONTRACT OR GRANT NUMBER**

**12. SPONSORING AGENCY AND ADDRESS**

California Department of Transportation
Division of Research, Innovation, & System Information, MS-83
1227 O Street
Sacramento, CA 95814

**13. TYPE OF REPORT AND PERIOD COVERED**

Final Report

**14. SPONSORING AGENCY CODE**

913

**15. SUPPLEMENTARY NOTES**

This report presents the work of Aravinthan Thurairajah for his doctoral dissertation. The work was advised by Prof. Jason DeJong, and Dr. Wilson and Dr. Ghafghazi contributed to the mechanical design and/or the data analysis. The reusable test pile development is continuing.

**16. ABSTRACT**

Caltrans' investment in driven piling to support bridges and other structures has averaged about $25M/year over the last decade. The systems constructed have performed well, but conservatism exists due to uncertainties in soil properties, pile drivability, soil-pile interaction, and pile setup. A new method that could achieve modest saving of 5% in design could save in excess of $1M per annum. This thesis presents the development of a reusable instrumented test pile (RTP) as an in situ testing device for improved pile design in granular soils. The RTP system consists of short instrumented sections that provide measurements of axial load, radial stress, pore pressure, and acceleration, and are connected in series with standard Becker pipe sections. The RTP – Becker pipe string is driven using the standard Becker pile driving hammer, and the TRP system was designed to handle the high installation stresses in granular soils while retaining sufficient resolution in the instrumentation readings for subsequent analyses of shaft and tip resistances. RTP measurements obtained during driving provide detailed information regarding pile drivability, measurements during static tests capture load transfer along the pile, and measurements during pile setup capture capacity gain over time. The design, fabrication, calibration, proof testing, and full scale field deployment are presented herein.

| 17. KEY WORDS | 18. DISTRIBUTION STATEMENT | |
|---|---|---|
| Pile design, becker penetration test, foundation design, sand, gravel | No. restrictions. This document is available to the public through the National Technical Information Service, Springfield, VA 22161 | |
| **19. SECURITY CLASSIFICATION** *(of this report)* | **20. NUMBER OF PAGES** | **21. COST OF REPORT CHARGED** |
| Unclassified | 282 | |

**DISCLAIMER STATEMENT**

This document is disseminated in the interest of information exchange. The contents of this report reflect the views of the authors who are responsible for the facts and accuracy of the data presented herein. The contents do not necessarily reflect the official views or policies of the State of California or the Federal Highway Administration. This publication does not constitute a standard, specification or regulation. This report does not constitute an endorsement by the Department of any product described herein.

For individuals with sensory disabilities, this document is available in Braille, large print, audiocassette, or compact disk. To obtain a copy of this document in one of these alternate formats, please contact: the Division of Research and Innovation, MS-83, California Department of Transportation, P.O. Box 942873, Sacramento, CA 94273-0001.

Division of Research & Innovation

# Reusable Instrumented Test Pile for Improved Pile Design in Granular Soils

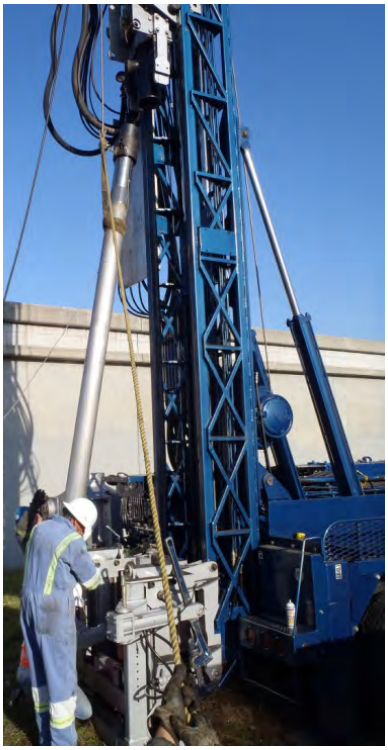

DRSI Research Task No. 1233,
DRSI Project No. P656,
Contract No. 65A0264

Reusable Instrumented Test Pile for Improved Pile Design in Granular Soils

By

ARAVINTHAN THURAIRAJAH
B.Sc. (University of Peradeniya, Sri Lanka) 2004
M.S. (University of Nevada, Reno) 2007

DISSERTATION

Submitted in partial satisfaction of the requirements for the degree of

DOCTOR OF PHILOSOPHY

in

Civil and Environmental Engineering

in the

OFFICE OF GRADUATE STUDIES

of the

UNIVERSITY OF CALIFORNIA

DAVIS

Approved:

_____
Jason T. DeJong, Chair

_____
Ross W. Boulanger

_____
Daniel W. Wilson

Committee in Charge

2013

Aravinthan Thurairajah
March 2013
Civil and Environmental Engineering

Reusable Instrumented Test Pile for Improved Pile Design in Granular Soils

# Abstract

Caltrans' investment in driven piling to support bridges and other structures has averaged about $25M/year over the last decade. The systems constructed have performed well, but conservatism exists due to uncertainties in soil properties, pile drivability, soil-pile interaction, and pile setup. A new method that could achieve modest saving of 5% in design could save in excess of $1M per annum. This thesis presents the development of a reusable instrumented test pile (RTP) as an in situ testing device for improved pile design in granular soils (coarser than No. 200 sieve). The RTP system consists of short instrumented sections that provide measurements of axial load, radial stress, pore pressure, and acceleration, and are connected in series with standard Becker pipe sections. The RTP – Becker pipe string is driven using the standard Becker pile driving hammer, and the TRP system was designed to handle the high installation stresses in granular soils while retaining sufficient resolution in the instrumentation readings for subsequent analyses of shaft and tip resistances. RTP measurements obtained during driving provide detailed information regarding pile drivability, measurements during static tests capture load transfer along the pile, and measurements

during pile setup capture capacity gain over time. The design, fabrication, calibration, proof testing, and full scale field deployment are presented herein.

# Dedication

To my parents and teachers

## Acknowledgements

I am grateful to all those who extended themselves in many ways for the completion of this dissertation work. This dissertation work would not have been possible without the help, support, and guidance of many people. I am indebted to all of them.

First and foremost I would like to express my deepest gratitude to my supervisor Professor Jason DeJong. He helped me immensely in many ways during my studies at UC Davis and especially in this dissertation work. He guided me in several aspects of development on my technical abilities as a graduate student researcher, not only by giving me the opportunity to work on this exciting research and guiding me throughout, but also teaching me how to present my work in precise and elegant manner. I also grateful for the numerous meetings I had with him during this period always made me motivated and made me work even harder. He also taught me to work effectively and handle things in professional way when needed. I am really glad and proud that I have had an opportunity to work closely with such a wonderful person.

I would like to acknowledge my dissertation committee members Professor Ross Boulanger and Dr. Dan Wilson for their valuable comments and suggestion in this dissertation work. Dr. Dan Wilson extended all his support in data processing for more than a year and also contributed in deciding instrumentation and data acquisition units.

My sincere thanks to Tom Shantz of Caltrans for funding this research project and his valuable timely input in the research work. Without this funding this research work could not

have been possible at all. Also, I would like to thanks Caltrans for providing us a well-documented test site for the field deployment.

My sincere thanks to Jim Benson of Great West Drilling, Inc. and their staff for their time, availability to our questions, multiple testing we performed during the development stages in their shop yard and at their project site, and two field testing programs at the Oakland, CA field site.

I would like to extend my thanks to John Lemke of Geodaq Inc. for developing the down hole data acquisition units feasible for this project and Dr. Mason Ghafghazi for his valuable time and help in data processing.

I like to acknowledge Dr. Robbie Jaeger, a good friend and colleague as graduate student at UC Davis, for his time and help in setting up the initial data acquisition unit and being available to any discussion even if it is outside the research work. I would like to thank Chris Krage, Clayton Proto, and Collin Anderson for their help during the field testing.

I would like to acknowledge the contribution of Bill Sluis and Daret Kehlet of department of civil engineering at UC Davis. From the beginning to the day of field testing, Bill and Daret brought all our ideas to feasible reality. I would also like to acknowledge the contribution on instrumentation and data acquisition by Ray Gerhard, Anatoliy Ganchenko, and Lars Pederson of the Center for Geotechnical Modeling at UC Davis.

I like to thank to all my friends for the positive encouragements they gave me. Also, I would like to thank all my wonderful teachers I had throughout my education that directly or

indirectly contributed towards my doctoral degree. I am grateful to all my teachers at Hartley college, Point Pedro, Sri Lanka, Royal college, Colombo, Sri Lanka, University of Peradeniya, Sri Lanka, University of Nevada, Reno and University of California, Davis. I am very grateful for Professor Raj Siddharthan of University of Nevada, Reno for being my well-wisher and guiding me through my carrier for a long time.

I wish to express my sincere gratitude to my mother Rajeswary Thurairajah for being strong and caring me over the years. Without her I will not be anywhere closer to the position I am in now, my sister Ahila and my brother in law Sivathasan and their wonderful family for the positive encouragement and the great support they provided, and my brother Alaheswaran Thurairajah, for being a great support to me during this time period. I would also like to extend my thanks to my other two sisters Cavitha and Punitha for their support.

Also I would like to thank my fiancé Mathura for her encouragements and patiently waiting for me to finish my dissertation.

# TABLE OF CONTENTS

# LIST OF TABLES

# LIST OF FIGURES

# Chapter 1: Introduction and Motivation

## 1.1 Motivation and Potential Benefit

A new in-situ system that provides measurements to assess pile drivability and performance on a site-specific project basis has the potential to improve the efficiency and reduce the cost of Caltrans deep foundation systems. Caltrans investment in driven piling to support bridges and other structures has averaged $25M/year to $30M/year over the last decade. The final constructed systems have performed well, with no significant failures. However, the design methods for these piling systems contain uncertainty and likely excessive conservatism. The uncertainty in design is due, in large part, to an inability to capture the full complexity of the soil deposit, soil properties, pile drivability, dynamic soil/pile interaction, and pile setup on a site-specific project basis. This conservatism can have significant cost implications. Even a modest saving of 5% in design efficiency will save in excess of $1,000,000 per annum. In addition to this, increased certainty of pile driving conditions expected during construction may reduce change orders to a great extent. The reusable test pile (RTP) presented herein is developed as a new in situ testing device to meet this need. The total project cost for RTP development has the potential to be recovered within the first few RTP deployments at Caltrans project sites.

## 1.2 Reusable Test Pile (RTP) Concept

The reusable test pile (RTP) is intended to operate as a mobile test pile that is deployed during the site investigation program at Caltrans project sites where a deep foundation system is required. Ideally the RTP could be installed, load tested, and removed within one to two days. Data collected would include information regarding pile drivability, driving dynamics, residual stresses, pile setup, and load distribution along the pile during tensile loading testing. The information collected would be summarized and useful during the project design and bidding processes.

Eventually it is hoped that a direct RTP-based pile design method for static capacity will be developed (which was beyond the scope of this project). In the interim the pile load test data collected may be used to assess the ability of a given design method to capture the site conditions (by comparing the measured RTP data with that estimated by a conventional design method). If agreement is good, then the designer would have increased confidence in using the respective method for design of the full scale foundation system, potentially with a reduced safety factor.

The RTP dynamic driving data in combination with the static pullout data would also provide detailed information along the entire pile length that could significantly improve calibration of a CAPWAP model. This would further improve estimates of static pile capacity as well as investigate and optimize the pile driving system.

The RTP data, both the basic driving record as well as a RTP data-calibrated CAPWAP analysis, would be useful for piling contractors during the project bidding to more accurately estimate anticipated driving conditions. This would result in mobilization of the most suitable equipment (e.g. rig type, hammer size) and an accurate estimate of the time and materials (e.g. fuel) required for installation of the full scale foundation system.

### 1.3 RTP Performance Requirements

The RTP was designed within a set of practical constraints to ensure adaptation to practice to the extent possible. These design constraints included:

- Mobility: The mobility of the RTP system must balance the issues of portability and pile size effects. The system must be sufficiently small such that instrumented sections can be transported and handled with relative ease. At the same time, the RTP diameter should be as large as possible in order to minimize pile diameter scaling effects.
- Commercial Integration: To the extent possible, the equipment required for installation and removal of the RTP system will be commercially available through a project service contract. This specification was desirable to manage overall project costs and to minimize the amount of equipment and/or vehicles that Caltrans must manage and own over the long term.
- Durability and Robustness: The RTP system must be capable of surviving of dynamic piling driving, extraction, and handling by field personnel. For context, the RTP may be

installed up to 60 m (200 feet) depths eventually, which could require up to 5,000 hammer blows for a single installation.

- Measurement Types: The measurements required for the initial RTP system include the following, in order of priority: (1) axial force at the tip and select locations along the RTP length, (2) pile head position, (3) axial acceleration at the tip and select locations along the RTP length, (4) pore pressure at select locations along the RTP length, and (5) radial stress at select locations along the RTP length.
- Measurement Capacity & Sensitivity: The sensors required for obtaining the above measurements must be capable of surviving extreme loads during pile driving and extraction while being able to resolve small changes between pile hammer blows and during pile setup.
- Measurement Frequency and Duration: The frequency and duration of sampling will vary depending on the mode of testing (i.e. pile driving, pile setup, static pile load test) and project conditions (i.e. driving resistance, soil type). The system must be sufficiently flexible to capture the dynamics during pile driving and long term pile setup.

## 1.4 RTP System Overview

The RTP system is a modular system that contains a series of instrumented pipe sections, equipped with sensors and a down-hole computer that are assembled at selected spacing in a Becker drill pipe string and installed by dynamic pile driving using the Becker drill rig. A schematic of the system configured for driving is presented in Figure 1.1. The central

component is the modular instrumented pipe sections, which are 61 cm (2 ft) long with an outer diameter of 168 mm (6.625 in). Each contains axial force, axial acceleration, pore pressure, and radial stress transducer. The modular sections are assembled in series with standard 152 cm (5 ft) and 305 cm (10 ft) long Becker drill pipes, enabling positioning of the instrumented sections in the drill string at target final elevations specified by project specific soil stratigraphy. Down-hole data acquisition computers in each RTP section record and process sensor data before transmitting it to the surface. A separate above ground data acquisition system measures vertical pile displacement and Becker hammer performance. The RTP system is installed with the Becker hammer system and the tensile load test is performed with the hydraulic lifting system. The modular nature of the RTP system and its integration with the Becker system enables testing to be completed (with a limited pile setup period) in one day.

## 1.5 Overview of Dissertation

This dissertation presents the design, fabrication, calibration, and verification of the newly developed RTP system. It includes laboratory and field scale work, which is presented as follows.

Chapter 2 contains a review of previous research performed in the area of instrumented model piles as well as details about the Becker drilling system and a review of driven pile setup behavior installed in the San Francisco bay mud deposit. Chapter 3 details the new RTP system

including its performance specifications, final design including sensor selections and system components (e.g. instrumented sections, vibration isolation system, data acquisition systems), intermediate testing required to finalized the design, and equipment and methods for RTP calibration. Chapter 4 presents the Oakland field test site where RTP deployment occurred, including its regional geology, engineering soil properties, and prior Caltrans load test results, as well as an overview of the RTP testing program performed. Chapter 5 analyzes RTP performance during driven installation, including driving rates and hammer performance as well as pile driving analysis of dynamic force and acceleration measurements obtained in the instrumented sections during driving. Chapter 6 examines the residual driving stresses within the RTP following driving, pile setup over a period of 3 hours, and RTP capacity from tensile (pullout) loading testing immediately after pile installation and following a period of setup. Chapter 7 presents conclusions and recommendations for future work based on the RTP performance.

**FIGURES**

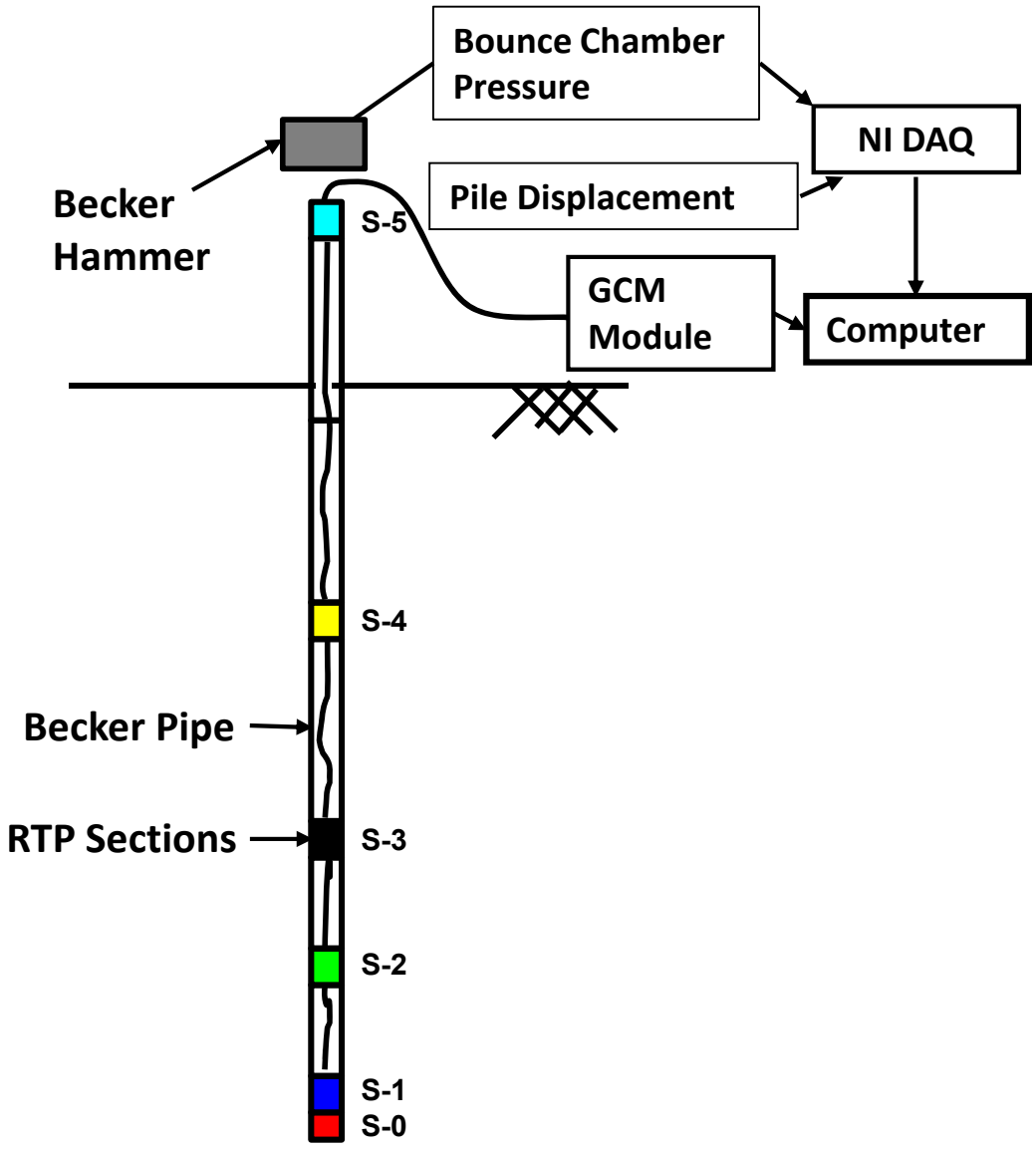


**Figure 1.1: Schematic diagram of RTP system with above ground measurements and Becker hammer (not to scale).**

# Chapter 2: Review of Previous Research

## 2.1 Introduction

The reusable test pile (RTP) was developed for use during a project's site investigation phase in order to obtain quantitative measurements of pile performance during installation, setup, and load testing. For ease of use, the RTP was designed to be directly compatible with the conventional Becker hammer drilling system. After development, the RTP was evaluated through a series of tests in Oakland, CA at a site comprised of a stratigraphy with the common units of surficial fill, young bay mud, and sand.

Given this scope of work (all discussed in more detail in subsequent chapters), literature from several topics is relevant. Herein the following topics are presented and reviewed: instrumented test piles, Becker drilling system, and pile load tests monitoring residual stresses and setup in young bay mud. In addition to brief descriptions of the different systems, focus is placed on aspects particularly relevant to the development, testing, and evaluation of the RTP system.

## 2.2 Instrumented Test Piles

All instrumented piles developed to date have varied accordingly to meet their specific project objective. Importantly, nearly all were installed by hydraulic jacking rather than driving, and many focused on characterization of pile performance in clay. As a result, few focused on the ability to predict driven pile capacity in granular soil. One primary reason for this is the challenges associated with this latter objective in instrumentation and data acquisition durability during the harsh installation process. A summary of all the different instrumented pile methods developed is summarized in Table 2.1. The primary object of this project is to develop an insitu testing device to capture the pile installation behavior in granular soils, though the device must also work well in clayey soils.

### 2.2.1 Cone Penetration Test (CPT) Probe

The cone penetrometer was originally developed for site investigation purposes to characterize soil properties, stratigraphy, and variability. It was not used for pile design until the 1930s (de Rutter 1982). The standard 10 and 15 $cm^2$ cones (ASTM D3441-05) provide measures of base (tip) resistance, pore pressure (often at the $u_2$ shoulder location), and shaft (friction sleeve) resistance immediately behind the tip (e.g. Lunne et al. 1997). Typical results from cone soundings and their interpretation for soil type identification and estimation of soil properties is reported by Lunne et al. (1997), Mayne (2007), Robertson (2009), and others. Variants on the conventional cone can also provide multiple pore pressure measurements and multiple sleeve

friction measurements (e.g. Lunne et al. 1997, DeJong and Frost 2002). The cone is installed by hydraulic jacking at a rate of 2 cm/s per 1 m stroke.

The advantage of the cone penetrometer is its nearly ubiquitous use around the world for site investigations. Therefore this information is often readily available for pile design. Shortcomings of the CPT include its inability to penetrate very dense sands and gravels, its jacking installation not mimicking dynamic driving installation, its small diameter (relative to typical pile diameters) introducing scaling effects that must be accounted for, and the lack of shaft resistance measurements along the cone rod string. Nonetheless, recent CPT-based design methods such as Fugro-05, ICP-05, NGI-05, and UWA-05 (Kolk et al. 2005, Fugro 2004, Jardine et al. 2005, Clausen et al. 2005, Lehane et al. 2005) perform well in predicting pile capacity in sands. Fewer cone-based methods exist for estimating the capacity of piles installed in clays since empirical methods based on the normalized undrained strength ratio perform well (e.g. Randolph 2003), with the Canadian Foundation Engineering Manual (Canadian Geotechnical Society 2006) method likely being the most widely adopted.

A study by Schneider (2007) explored the factors that influence the relationship between measured cone tip resistance and the shaft friction of displacement piles. The primary factors identified were:

- initial increase in radial stress due to displacement of soil during pile installation,
- level of soil displacement induced by type of driving shoe,
- reduction of radial stress as a function of distance behind the tip,
- friction fatigue behavior on radial stress reduction as pile advances further,

- changes of radial stress during loading,
- constant volume interface friction angle between soil and steel, and
- changes of these mechanisms with setup time.

Of all cone based pile design methods, the UWA-05 method (Lehane et al. 2005) captures the above factors in the most explicit, mechanics-based formulation. As described by Schneider (2007), this method was developed based on previous research on friction fatigue, pile setup, prior CPT based design methods, and regression analysis on a large pile load test data base.

The primary equation for the unit base pile resistance is:

$$q_{b0.1}/\overline{q_c} = 0.15 + 0.45A_{rb,eff} \quad (2.1)$$

where,

$q_{b0.1}$ = unit base resistance of pile

$\overline{q_c}$ = cone resistance averaged using Dutch method

$A_{rb,eff}$ = effective area ratio, = 1 – FFR × $\left(\frac{D_i}{D}\right)^2$ (2.2)

where,

$D_i$ = pile inner diameter

D = pile outer diameter for closed ended pile, and effective diameter ($D^* = D \times A_{rb,eff}^2$) for open ended piles

FFR = Final filling ratio measured at the end of driving, averaged over $3D_i$.

If FFR is not measured, it can be approximated as a function of $D_i$ in meters as:

$$\text{FFR} = min\left[1, \left({D_i\,(m)}/{1.5}\right)^{0.2}\right] \quad (2.3)$$

The associated equations for unit shaft friction are:

$$\tau_f = \sigma'_{rf} \times \tan\delta_{cv} = \frac{f}{f_c} \times (\sigma'_{rc} + \Delta\sigma'_{rd}) \tan\delta_{cv} \quad (2.4)$$

where,

$\tau_f$ = local shear stress at failure along the shaft of the pile

$\delta_{cv}$ = constant volume interface friction angle

$\sigma'_{rf}$ = radial effective stress at failure

$\sigma'_{rc}$ = radial effective stress after installation and equalization

$\Delta\sigma'_{rd}$ = increase in radial stress due to loading stress path (dilation)

$\frac{f}{f_c}$ = 1 for compression loading and 0.75 in tension

The radial effective stress after installations and equalization is given as:

$$\sigma'_{rc} = 0.03 \times q_c \times A_{r,eff}^{0.3} \times \left[max\left(\frac{h}{D}, 2\right)^{-0.5}\right] \quad (2.5)$$

where,

$q_c$ = local cone resistance

D = pile outer diameter

h = relative distance above the pile tip

$$h = pile\ length - depth \quad (2.6)$$

$A_{r,eff}$ = effective area ratio

$$A_{r,eff} = 1 - IFR\left(\frac{D_i}{D}\right)^2 \quad (2.7)$$

where,

$IFR$ = incremental filling ratio

$D_i$ = pile inner diameter

A simplified approximation for average incremental filling ratio can be given by:

$$IFR_{avg} = min\left[1, \left(\frac{D_i\,(m)}{1.5}\right)^{0.2}\right] \quad (2.8)$$

This design method is appealing from a fundamental perspective, but the effort to separate and explicitly consider different factors also results in a level of complexity that exceeds the other methods and that arguably exceeds the level of detail available in current measurements and databases. Subsequent implementation of UWA-05 at several sites has shown it to perform very well, in most cases exceeding the performance of more simplified methods (Lehane et. al. 2012). The UWA-05 approach and formulation is appealing for the RTP based pile design approach that is planned to be developed in the next phase of the project.

This is due to the manner in which individual parameters that influence pile design are utilized in calculations and that many of these parameters will be directly measured by RTP in the field.

### 2.2.2 Piezo Lateral Stress (PLS) Cell

The piezo lateral stress cell (PLS) pile was developed in 1978 to evaluate pile performance in clay (Morrison 1984). The PLS cell is 470 mm long and 384 mm outer diameteral cylinder. The PLS cell consisted of a pore pressure sensor, load cell, lateral stress cell and temperature sensor. A cylindrical lateral stress cell measures the horizontal stress acting on a discrete segment of the instrumented pile, and therefore measures the local lateral stress acting on the pile shaft. The PLS pile was installed by hydraulic jacking at the rate of 20 mm/s (Azzuz and Lutz 1986). The PLS pile was tested successfully in Empire, Louisiana at a site comprised of a thick deposit of plastic clay where previous full scale pile testing results were available (Azzuz and Lutz 1986) and also at three Boston blue clay sites (Baligh et al. 1985).

Results showed the PLS pile to be effective in measuring the unit skin friction of a long pile and to improve the prediction of skin friction for full-scale cylindrical driven piles in clay (Morrison 1984). The PLS pile had limitations in predicting driven pile capacity in granular soil. Namely, the thin outer cylinder (0.38 mm (0.015 in) thickness) of the lateral load cell would be easily damaged during penetration in granular material (sands, gravels). Further, for both clays and sands full-scale installation by driving was not performed.

Figure 2.1 presents representative results of the dissipation of excess pore pressure following PLS pile penetration in both dilative and contractive soil layers. Expectedly, the dissipation of excess pore pressure results in consolidation and an associated change in the horizontal stress. Results of this coupling are presented in Figure 2.2 where the effective radial stress increases and excess pore pressures decrease in contractive clays. The time duration over which pore pressure dissipation occurs is dependent on the vertical and horizontal coefficient of consolidation and directly indicates the pile setup time (due only to excess pore pressure dissipation and not to other thixotropic effects). As discussed by Fleming et al. (2009), this dissipation process can be analyzed in a dimensionless manner such that it can be upscaled to predict the excess pore pressure dissipation time expected for full scale piles.

### 2.2.3 Grosch & Reese (G&R) Model Pile

The Grosch & Reese (G&R) model pile was developed to study the effect of cyclic axial loading on the load transfer of piles in offshore structures (Grosch and Reese 1980). The model pile was fabricated from 6061 aluminum tubing with 25.4 mm (1 in) outer diameter and 0.71 mm (0.028 in) wall thickness. This closed end model pile was installed into the ground by a screw jack with a reversible variable speed motor. The screw jack applied cyclic loading similar to field conditions, albeit at a lower cyclic frequency. Two strain gaged load cells were positioned 254 mm (10 in) apart to determine the average shaft resistance between them. A pore pressure transducer was located at midpoint between these two axial load cells. The G&R model pile was tested at Sabine, Texas in the Sabine River (Grosch and Reese 1980).

The G&R model pile installation effectively demonstrated the pore pressure behavior and associated consolidation in soft normally consolidated clay due to pile insertion. The G&R pile was installed and tested in soft soils (e.g. clay and silt), but was not tested in sands. This is due to the thin aluminum wall being susceptible to damage during pile insertion. In addition, the jacking method did not replicate the driven pile installation process.

Example results from the G&R model pile installed in the field are presented in Figures 2.3 to 2.6. Figure 2.3 shows one of the initial displacement cyclic load tests performed at a field site. The degradation of load transfer with cycling is clearly evident. Figure 2.4 presents the reduction in load transfer and the associated pore pressure variation during cyclic loading for both the initial A-1 test with +/-1.44 mm (+/-0.055 in) displacement cycles as well as for the subsequent A-2 test with small cyclic displacements (+/-1.44 mm). During the initial A-1 test negative excess pore pressure developed in the soft clay. Subsequent cycling at a smaller displacement did not cause any further reduction in load transfer or excess pore pressure generation. The linkage between cyclic displacement amplitude and excess pore pressure generation is further examined in Figure 2.5, where excess pore pressure is not generated until the pile displacement reached 0.838 mm (0.033 in). Interestingly, the magnitude of excess pore pressure generated at the two higher levels of cyclic displacement was constant. The exact mechanism linking the generation of excess pore pressure with a minimum cyclic displacement, while experimentally observed, was not fully understood. However, a simplified model for capturing the reduction in unit shaft resistance with cyclic loading was developed, and is summarized in Figure 2.6.

### 2.2.4 Norwegian Geotechnical Institute (NGI) Model Pile

The Norwegian Geotechnical Institute (NGI) model pile was developed to study the performance of offshore piles subjected to both static and cyclic loading with particular focus on tension loading of pile anchors (Karlsrud and Haugen 1985). The NGI model pile was a 5 m long closed ended pipe pile with 153 mm outer diameter. The model pile was installed into the ground by jacking at a rate of 1.0 – 1.4 mm/s. The NGI model pile was instrumented with 6 levels of strain gages to measure axial loads in order to calculate average skin friction over discrete depth intervals. Four levels of pore and earth pressure gages were installed to measure pore and lateral earth pressures during driving and subsequent equilibration. The NGI model pile was tested successfully in over consolidated clay deposits at the Haga test site outside Oslo, Norway (Karlsrud and Haugen 1985).

The NGI model pile study effectively measured the skin friction of the clay due to pile installation and linked the measurements to laboratory results of remolded, reconsolidated clay. Similar to the other model piles, the NGI model pile has limitations that would prevent it from being used to predict driven pile capacity in granular soils. These include structural sections designed for application in clay, inadequate instrumentation to measure the tip resistance, and the pile installation method not representing the dynamic pile driving.

The total horizontal stress and excess pore pressure immediately after the NGI model pile installation and during pile setup is presented in Figure 2.7. As excess pore pressure dissipates, total horizontal stress reduces with time. However, the effective stress increases with dissipation of excess pore pressure. This in turn results in an increase in the pile shaft

capacity with time. The pore pressure dissipation record in combination with the pile dimensions can be used to estimate the pile shaft capacity after pore pressure equilibration and the time required for pore pressure dissipation for full-scale piles.

The shaft friction measured by the NGI pile during penetration was compared against the undrained strength measured by the vane shear test as well as calculated shaft friction values computed by the $\alpha$ and $\lambda$ methods (Karlsrud et al. 1985). Results are presented in Figure 2.8. As evident, the measured shaft friction did not agree with the shaft frictions obtained from other methods. As the model pile penetrates, the soil adjacent to the pile wall undergoes high strains and is fully remolded. Therefore, the shaft friction measured by the NGI pile relates more to the remolded undrained strength than the (reconsolidated) peak strength.

### 2.2.5 Three Inch Model Pile and X-Probe

The three inch (3-in) model pile was developed to study the soil parameters affecting long flexible piles in the offshore environment under static and cyclic loading conditions (Bogard and Matlock 1990b). The model pile was developed as a primary tool to investigate plugging and non-plugging pile conditions, and had a length of about 4.9 m (16 feet) and a diameter of 76.2 mm (3 in). The model pile was installed by jacking with a hydraulic ram. Instrumentation consisted of two load cells to estimate shaft friction, a total pressure cell located midway between the axial load cells to measure total lateral pressure, a pore pressure transducer also located midway between axial load cells to measure pore pressure, and a

displacement transducer to measure relative displacement between the pile and soil. The model pile was successfully tested at different soil conditions including soft clay, stiff clay and calcareous soils (Bogard and Matlock 1990a, 1990b, 1990c, Bogard et al. 1985).

The primary use of the X-probe, similar to the 3-in model pile and developed by the same researchers, was for routine site investigation at proposed sites for offshore oil and gas facilities (Bogard et al. 1985). The X-probe was 1.4 m (56.5 in) length and 43.7 mm (1.72 in) in diameter. The installation method was the same as for the 3–in model pile. The X-Probe was instrumented with a pore pressure transducer, a total lateral pressure transducer, a shear sensing element (a 200 $cm^2$ cylindrical sleeve supported by a load cell), and a displacement transducer.

The 3-in model pile and X-probe tests effectively captured the time rate strength gain and provided insights for development of soil resistance versus axial pile displacement curves for use in design. Similar to other model piles, the 3 inch model pile and X-probe had limitations that would prevent them from being used to predict driven pile capacity in granular soils. These limitations included structural sections designed for application in clay, inadequate instrumentation to measure the tip resistance, and the pile installation method not representing the large scale driven pile.

Example results from the 3-in model pile are presented in Figures 2.9 and 2.10. Figure 2.11 presents the gradual increase in effective lateral pressure measured adjacent to the 3-in model pile following driving. As evident, the pore pressure dissipation is characteristic of that in normally consolidated soils, which results in gradual consolidation and an increase in the

effective lateral stress. The resulting impact on tensile pile capacity is presented in Figure 2.12. Tension load tests were performed following different amounts of pore pressure dissipation (reconsolidation) following driving. The static pullout test performed after only 14 minutes of equilibration time resulted in a unit load transfer of about 24 kPa (0.5 ksf). However, after full dissipation, 69 hours later, the unit load transfer increased to about 65 kPa (1.35 ksf).

### 2.2.6 In Situ Model Pile (IMP)

The In Situ Model Pile (IMP) was developed to predict driven steel pipe pile behavior in clayey soils (Coop and Wroth 1989). The pile section was 1135 mm long and 80 mm diameter, and consisted of two concentric cylinders. The inner cylinder was rigidly connected to pile head and the outer brass cylinder consisted of interchangeable instrumented sections. Each instrumented section contained two pore pressure sensors, two total radial stress transducers, and an axial load cell. In addition to these instrumented sections, the tip was instrumented with a pore pressure transducer and an axial load cell. The IMP was hydraulically jacked into ground for installation and was successfully tested at heavily over consolidated and normally consolidated clay sites.

The IMP study further confirmed the formation of a residual shear surface adjacent to pile shaft during pile installation. Like in the other model piles, IMP also had its limitations that would prevent it from being used to predict driven pile capacity in granular soil. These included

the structural sections designed for application in clay, inadequate instrumentation to measure the tip resistance, and the pile installation method not representing the dynamic pile driving.

A summary of all pore pressure and total radial stress profiles measured by the IMP during five separate installations is presented in Figure 2.13. The predicted total radial stress and pore pressure using cavity expansion theory is also plotted. As evident, the measured total radial stress and pore pressure were lower in magnitude than that predicted from cavity expansion theory. Per Coop and Wroth (1989), this difference was due to stress relief immediately behind the pile tip as predicted by Levadoux and Baligh (1980) using their strain path method for cone penetrometers. In addition, experimental results indicated that the effective radial stress at the leading instrumented section was generally higher than that on the following instrumented sections. This was attributed to the soil continuing to degrade with additional pile penetration (Bond and Jardine 1991). Absolute and normalized shaft friction profiles (versus depth) are presented in Figure 2.12 to investigate this issue further. Firstly, it is clear that the absolute value of shaft friction was identical for both the lower and upper instrumented sections. However, when normalized by the effective radial stress it is clear that the normalized strength ratio has decreased as a function of distance behind the driving tip.

### 2.2.7 Imperial College Instrumented Pile (ICP)

The Imperial College Instrumented Pile (ICP) was developed with the objective to establish a theory to explain the behavior of displacement piles based on effective stresses

(Bond and Jardine 1991). The ICP pile was tested in a variety of soils from sensitive soft clays to medium dense sand. The ICP pile sections were 7 m long and 10.2 cm in diameter. The ICP was instrumented with three clusters of sensors spaced 1 m apart. Each instrumented section consisted of a high capacity axial load cell, surface stress transducer to measure radial and shear stress on pile wall, pore pressure transducer, and temperature sensor. The closed ended ICP model pile was jacked into ground to prevent damage to the sensors.

The ICP study effectively captured the influence of penetration rate on mobilized skin friction and the associated formation of shear surfaces, the zone of affected soil adjacent to a pile due to installation (Bond and Jardine 1991). It was also effective in providing quantitative data to support the concept of friction fatigue, where the shaft friction at a specific elevation degrades as the pile continues to advance past it. Like other model piles, the ICP also had limitations that would prevent it from being used to predict driven pile capacity in granular soil. These included structural sections designed primarily for application in clay and the pile installation method not mimicking dynamic pile driving.

Example results from ICP model tests obtained during installation at a sand site are presented in Figures 2.13 and 2.14. Measurement profiles obtained at three distances behind the pile tip are presented. The distance behind the pile tip was normalized by the pile radius. Figure 2.13 presents the radial effective stress during installation of ICP. As the pile advances, the radial effective stress of the soil acting on the pile at a specific elevation decreases with normalized penetration distance. In general, the radial effective stress decreases by between 25% and 50% between normalized h/D distances of 8 to 50. This reduction is due to the

gradual reworking and degradation of the soil adjacent to the pile, which results in contraction and relaxation of the radial stress. The associated effect of this relaxation on the unit shaft friction is clearly evident in Figure 2.14. In fact the magnitude of degradation is more severe. This is attributed to both the reduction in radial stress and a reduction in the coefficient of friction due to crushing of soil adjacent to the pile.

### 2.2.8 Multiple Deployment Model Pile (MDMP)

The main objective behind MDMP development was to simulate the installation and stress history that full scale piles experience during all three stages of its service life: installation, setup, and loading (Paikowsky and Hart 2000). The MDMP was a very similar design to the three inch model pile (Paikowsky and Hart 2000). The MDMP instrumentation included three load cells, three accelerometers, a displacement transducer, a pore pressure transducer, and a total pressure cell. A conventional standard penetration test (SPT) hammer was used to drive the MDMP, or a hydraulic system was used to jack the MDMP into the ground. When driving installation was used pile dynamic analyses could also be performed. A drill casing was advanced prior to MDMP deployment in order to prevent damage during penetration through crustal soil layers and to control the depth interval where the MDMP measured the soil response.

The MDMP study built on and confirmed results with prior model piles. Namely, it effectively captured capacity gain with time in clay soil and quantified soil-pile interface load

transfer (shaft friction). Similar to the other model piles, the MDMP was limited to installation in clay therefore preventing it from being used to predict driven pile capacity in granular soil.

Figure 2.15 presents the excess pore pressure dissipation following MDMP field installation at clayey site. The dissipation data was used to examine radial drainage conditions and pile setup periods. Figure 2.16 presents the associated change in the effective stress measurement during pore pressure dissipation (pile setup period) after installation. Again consistent with prior work, the effective radial stress increases as the excess pore pressure dissipates. Interestingly, the final effective radial stress is estimated to be about 300% larger than the initial horizontal effective stress. The ability to perform dynamic MDMP installation using the SPT hammer enabled pile driving analysis (PDA) on a model pile for the first time. These results were useful to begin assessing and comparing driving dynamics between a model pile and a full scale pile. Example results during the impact driving of MDMP are presented in Figure 2.17.

### 2.2.9 Summary of Instrumented Test Piles

In summary, the instrumented test piles and associated research programs to date have provided significant contributions towards the understanding of pile performance and design. Important outcomes specifically relevant to the RTP project presented herein include the importance of geometrical section survivability, instrumentation durability, effective positioning of sensors, adequate instrumentation, sensor selections and handling, pile diameter

scaling and the importance of pile installation method among others. The challenge of replicating pile driving dynamics during installation in sand of an instrumented model has not been accomplished successfully and was expected to be a major challenge in development of the RTP.

## 2.3 Becker System

The Becker hammer drill system (Figure 2.18) was selected as the pile driving installation system for the reusable instrumented test pile (RTP) as detailed further in Chapter 3. The Becker hammer drill system has the following advantages (Harder and Seed 1986, Harder 1988) over other existing field systems or alternate systems that could have been developed:

- The Becker drill system is a standardized commercially available system. As a result, Becker system services are available and competitively priced. Caltrans would not be required to develop, own, or maintain the installation system for the RTP.
- The Becker drill system is equipped with a standard ICE-180 impact pile driving hammer, which is a light, but standard pile driving hammer. As a result, the Becker drill system can install the RTP under realistic pile driving conditions.
- The Becker drill system is equipped with a 890 kN (200 kip) hydraulic jacking unit that is capable of performing tension pile load tests (Benson 2010).

- Becker pipe sections, with a diameter of 168 mm (6.625 in), are sufficiently large such that diameter scale effects are reduced, and yet sufficiently small that they can be safely handled and transported.

A brief review of the Becker drill system is provided here due to it being the selected platform for RTP installation and extraction.

### 2.3.1 Background

The Becker hammer drill system was developed in Alberta, Canada during late 1950s (Harder and Seed 1986). It was developed as a new method to rapidly penetrate and obtain disturbed samples of gravel and cobble deposits in western Canada. The system has seen widespread adoption and is now widely used in both Canada and the United States in geotechnical investigations for drilling, sampling and penetration testing in coarse grained granular soils.

### 2.3.2 Equipment

Becker testing is performed by driving the specially designed double wall cylinder (Becker) pipes into the ground using a double acting diesel pile driving hammer attached to Becker driving rig. Extraction of the pipe string is performed by a hydraulic jacking system.

Images of the equipment are presented in Figure 2.18 and a schematic presenting the primary components of the overall system is presented in Figure 2.19.

#### 2.3.2.1 Becker Pipe Sections

Becker pipe sections are available in standard dimensions of 3.048 m (10 feet) and 1.524 m (5 feet) long with outer diameters of 140 mm (5 1/2 inches), 168 mm (6 5/8 inches), and 229 mm (9 inches). Triple starting thread connections are fabricated from 4140 alloy steel and welded to a center pipe section of cold-rolled steel. For the 168 mm (6 5/8 in) diameter pipe, which is the most common in the western United States and that adopted for the RTP, the wall thickness is 20.64 mm (13/16 in). These heavy wall Becker pipe sections are robust for harsh driving conditions, and can even withstand penetration through boulders and into weak bedrock formations. The pipe string can be driven into ground as open or closed ended by unplugging or plugging the tip section as needed.

#### 2.3.2.2 Diesel Hammer

The International Construction Equipment (ICE) Model 180 double acting diesel hammer is the standard hammer for Becker drill rigs. Specifications of the hammer are summarized in Table 2.2. The maximum theoretical energy rating of the hammer is 10.85 kJ (8000 foot pounds) per blow. During field driving the hammer operates at about 30% efficiency as detailed by Sy (1993). Typically the hammer operates at a frequency 90-95 blows per minute.

The closed and sealed upper chamber of the hammer system stores part of the kinetic driving energy for next blow by the entrapped air compressing as piston goes up. A schematic diagram of a typical diesel hammer function is presented in Figure 2.20 (Note that is similar to, but not the exact ICE 180 hammer installed on the Becker rig used in this project). By measuring the pressure of the trapped air, commonly referred to as the bounce chamber pressure, an estimate of driving energy can be obtained for each blow (Harder and Seed 1986).

#### 2.3.2.3 Puller Assembly

After driving with the Becker is complete a hydraulic puller assembly is used to retract the Becker pipe string (i.e. pullout or tension load test). The Becker pipe string is gripped with tapered slips and raised by two 223 kN (50 ton) hydraulic grips (Benson 2010). Thus the puller assembly has total of 445 kN (100 ton) pullout capacity and can pull out with the maximum stroke length of 1.44 m (56.7 in).

### 2.3.3 Tests Performed Using Becker System

Generally, the Becker system is used for either obtaining soil samples while advancing the hole or for performing a "Becker penetration test". Soil sampling and characterization can be performed with an open ended driving shoe during installation while the Becker penetration test is performed with a closed ended driving shoe.

Soil sampling occurs by disturbed soil entering the inner pipe of the drill string through the cutting shoe. Compressed air is delivered to the bottom of the borehole through the annulus between the inner and outer pipe walls. The compressed air is then released and lifts the cut soil particles up through the inner casing to the ground surface. The transferred soil is collected in a cyclone as shown schematically in Figure 2.19. Soil sampling with the Becker system is typically performed at sites where other insitu penetration samplers such as the SPT are not feasible. Collected samples are heavily disturbed (with gravel and cobble particles often being fractured) but are still useful in identify the type of soil at specific depths and for developing a stratigraphic profile of the site.

The "Becker penetration test" (BPT), is performed with a closed ended tip section and the number of blows per foot of penetration is measured. Similar to the SPT N-value, the Becker penetration test provides an indication of soil resistance (i.e. density, stiffness) to penetration. Unlike the SPT, the BPT does not obtain a soil sample. Instead, the BPT can be performed continuously during pipe penetration in a manner similar to monitoring blows per foot during pile driving. The BPT number is typically converted to an equivalent standard penetration test (SPT) blow count as design charts based on BPT N numbers are not available. The equivalent SPT blow counts are often used in empirical correlations originally developed for sands.

The most common method for conversion of BPT N values to equivalent SPT N values is that developed by Harder (Harder 1988). Figure 2.21 shows the correction curves to correct the measured Becker blow counts and bounce chamber pressure to standardized BPT blow

counts. For example, two sets of measured average bounce chamber pressure and corresponding Becker blow count for 0.3 m (1 feet) penetration are marked in Figure 2.21 with open square and open circle. By following the blow count correction curves, standard BPT blow counts are obtained corresponding to closed square and closed circle. Corrected corresponding SPT blow counts are obtained with an empirical correlation between corrected BPT blow counts and standard SPT blow counts as presented in Figure 2.22.

## 2.4 Pile Setup in San Francisco Bay Mud

A study on the setup of driven piles in San Francisco bay mud by Hunt et al. (2000) and Pestana et al. (2002) are reviewed herein. This is relevant since deployment and evaluation of the reusable instrumented test pile (RTP) occurred in Oakland, CA, at a test site with a stratigraphy that included a young bay mud deposit about 4.75 m (15.5 ft) thick (details provided in Chapter 4). Results from this prior study, including pore pressure generation during pile driving, pore pressure dissipation after driving, and pile setup behavior are of particular interest.

A closed ended pipe pile 61 cm in diameter was driven 36 m, fully penetrating two bay mud layers. The pile installation occurred at a test site in San Francisco near Islais Creek which belongs to Department of Transportation, California (Caltrans). Prior to installation 10 pore pressure transducers were installed in 6 borehole locations at 8.5 m, 12.8 m, and 23.8 m depths and at radial distances ranging from 0.35 m to 4.7 m from the pile location. These pore

pressures were allowed to equilibrate to hydrostatic conditions prior to pile installation. Pore pressures were continuously monitored during pile installation and after, until all measurements returned to hydrostatic conditions. In addition to pore pressure monitoring, inclinometers were also installed to monitor the lateral deformation of the ground during pile installation and pile setup. Instrumentation monitoring occurred before pile installation, during pile installation, and during setup until full dissipation of excess pore pressure occurred.

### 2.4.1 Excess Pore Pressure Generation and Dissipation

Field measurements (Pestana et al., 2002) showed that excess pore pressure generation in San Francisco bay mud due to pile driving can significantly exceed the total over burden stress. Excess pore pressures generated were highest near the pile, as expected, but were also shown to be significant up to one pile diameter away from the pile wall. The gradual dissipation of excess pore pressure with time, from immediately after the installation of driven pile is shown in Figure 2.23. Behavior is consistent with that expected for normally consolidated clays (i.e. positive excess pore pressure gradually dissipating towards hydrostatic conditions), with a period of 2 years required for complete dissipation at the shallower depths. Figure 2.24 presents the normalized excess pore pressure (consolidation) versus time. At shallower and closer locations to the pile wall 75 days were required for 80% excess pore pressure dissipation.

### 2.4.2 Pile Setup

Field measurements of radial consolidation, monitored by vertical inclinometers installed at different distances from the pile, indicated soil movement towards the pile during pore pressure equilibration. Vertical inclinometers in the borehole casings, surrounding pile location, at different radial distances help to study soil deformation during pile driving and consolidation during pile setup period. A polar coordinate system capturing radial deflections towards or away from the pile and angular deflection around the pile was used to analyze soil movement (Pestana et al. 2002)

Lateral deformation results are summarized in Figure 2.25 as profiles of total and incremental radial displacement at different time periods following installation. Plots in the upper portion present the cumulative lateral soil movement due to consolidation after pile installation. Absolute measurements were taken on day 1, 47, and 678. The resulting absolute movement from day 1 to days 47 and 678 are presented in the lower figures. The negative values indicate soil movement towards to pile in time. As expected, the rate of deformation decreases in time with a majority of deformation occurring within the first 47 days after installation (Pestana, 2002).

As clearly evident, the rate of radial displacement decreases in time, which is consistent with the rate of pore pressure dissipation. The consolidation and radial displacement of soil towards the pile results in an increase in the radial stress acting on the pile wall.

## 2.5 Summary

This chapter has reviewed prior studies and developments regarding instrumented test piles, the Becker drilling system, and pile setup in clays. The designs, sensors, installation methods, and methods of interpretation in the development of prior instrumented piles informed design and equipment selections decisions presented in Chapter 3. The capabilities, practically, and demonstrated performance and durability of the Becker drilling system reviewed herein resulted in its selection as the installation system for the RTP. Further, the RTP's technical specifications of the system components, down to materials and threaded connections, were heavily influenced by the standardized Becker system design. Finally, the generation and subsequent equilibration of excess pore pressure around a pile installed in local soft clay (young bay mud) provide a reference for analyzing the performance of the RTP installed in the same regional soft clay deposit.

**REFERENCES**


ASTM D3441 - 05., (2005). "Standard test method for mechanical cone penetration tests of soil." *ASTM international*, 387-392.

Azzouz, A.S. and Lutz, D.G., (1986). "Shaft behavior of a model pile in plastic empire clays." *Journal of Geotechnical Engineering, ASCE,* 112(4): 389-406.

Baligh, M.M., Martin, , R.T., Azzouz, A.S., and Morrison, M.J., (1985). "The Piezo-Lateral Stress Cell." *Proceedings of the 11th International Conference on Soil Mechanics and Foundation Engineering,* San Francisco, CA, 841-844.

Benson, J., (2010). Personal communication, *Great West Drilling Inc*.

Bogard, J.D. and Matlock, H., (1990a). "Application of model pile tests to axial pile design." *Proceedings on 22nd Annual Offshore Technology Conference,* Houston, TX, 271-278.

Bogard, J.D. and Matlock, H., (1990b). "In situ pile segment model experiments at Empire, Louisiana." *Proceedings on 22nd Annual Offshore Technology Conference,* Houston, TX, 459-467.

Bogard, J.D. and Matlock, H., (1990c). "In situ pile segment model experiments at Harvey, Louisiana." *Proceedings on 22nd Annual Offshore Technology Conference,* Houston, TX, 469-477.

Bogard, J.D., Matlock, H., Audibert, J.M.E., and Bamford, S.R., (1985). "Three years' experience with model pile segment tool tests." *Proceedings on 17th Annual Offshore Technology Conference,* Houston, TX, 65-72.

Bond, A.J. and Jardine, R.J., (1991). "Effects of installing displacement piles in a high OCR clay." *Géotechnique*, 41(3): 341-363.

Canadian Geotechnical Society (2006) *Canadian Foundation Engineering Manual*, 4th Edition, 488 p.

Clausen, C.J.F., Aas, P.M., and Karlsrud, K., (2005). "Bearing capacity of driven piles in sand, the NGI approach." *Proceedings of the International Symposium on Frontiers Offshore Geomechanics*, ISFOG, Perth, 677-681.

Coop, M.R. and Wroth, C.P., (1989). "Field studies of an instrumented model pile in clay." *Géotechnique*, 39(4): 679-696.

DeJong, J.T. and Frost, J.D., (2002). "A multisleeve friction attachment for the cone penetrometer." *American Society of Testing and Material, Journal of Geotechnical Testing,* 25(2): 111-127.

de Ruiter, J., (1982). "The static cone penetration test, State-of-the-art report." *Proceedings of the Second European Symposium on Penetration Testing*, Amsterdam, 389-405.

Fleming, W.G.K., Weltman, A.J., Randolph, M.F., and Elson, W.K., (2009). "Piling engineering." *3rd edition, Taylor and Francis*, New York, 398p.

Fugro (2004). "Axial pile capacity design method for offshore driven piles in sand." *Report to API*, P-1003, Issue 3.

Grosch, J.J. and Reese, S.C., (1980). "Filed tests of small scale-pile segments in a soft clay deposit under repeated axial loading." *Proceedings on the 12th Annual Offshore Technology Conference,* Dallas, TX, 143-151.

Harder, Jr., L.F., (1988). "Use of penetration tests to determine the cyclic loading resistance of gravelly soils during earthquake shaking." *PhD thesis, University of California, Berkeley,* CA. 465p

Harder, Jr., L.F. and Seed, H.B., (1986). "Determination of penetration resistance for coarse-grained soils using the Becker hammer drill." Report UCB/EERC-86/06, Earthquake Engineering Research Center, University of California, Berkeley, CA. 144p

Hunt, C.E., Pestana, J.M., Bray, and Riemer, M.F., (2000). "Effect of pile installation on static and dynamic properties of soft clays." *Innovations and Applications in Geotechnical Site Characterization, GeoDenver 2000,* Denver, CO, 199-212.

ICE Inc., "Operating and service manual for ICE Model-180 diesel pile hammer." *International Construction Equipment. Inc.*, Matthews, NC. 80p.

Jardine, R.J., Chow, F.C., Overy, R.F., and Standing, J.R., (2005). "ICP design methods for driven piles in sands and clays." *Thomas Telfort*, London, 97p.

Karlsrud, K. and Haugen, T., (1985). "Axial static capacity of steel model piles in overconsolidated clay." *Proceedings on 11th International Conference on Soil Mechanics and Foundation Engineering,* San Francisco, CA, 1401-1406.

Kolk, H.J., Baaijens, A.E., and Senders, M., (2005). "Design criteria for pipe piles in silica sands." *Proceedings of the International Symposium on Frontiers Offshore Geomechanics*, ISFOG, Perth, 711-716.

Lehane, B.M., Jardine, R.J., Bond, A.J., Frank, R., (1993). "Mechanisms of shaft friction in sand from instrumented pile tests." *Journal of Geotechnical Engineering, ASCE*, 119(1): 19-35.

Lehane, B.M., Li, Y., Williams, R., (2012). "Shaft capacity of displacement piles in clay using the CPT." *Journal of Geotechnical and Geoenvironmental Engineering., ASCE. "In Press".*

Lehane, B.M., Schneider, J.A., and Xu, X., (2005a). "A review of design methods for offshore driven piles in Siliceous sand." *UWA Report, GEO 05358*, *University of Western Australia*, Australia.

Lehane, B.M., Schneider, J.A., and Xu, X., (2005b). "The UWA-05 method for prediction of axial capacity if driven piles in sand." *Proceedings of the International Symposium on Frontiers Offshore Geomechanics*, ISFOG, Perth, 683-689.

Levadoux, J.N. and Baligh, M.M., (1980). "Pore pressures during cone penetration in clays." *Report R80-15, Department of Civil Engineering, Massachusetts Institute of Technology,* Massachusetts.

Lunne, T., Robertson, P.K. and Powell, J.J.M., (1997). "Cone penetration testing in geotechnical practice." *Blackie Acadamic, EF Spon/Routledge Publishers*, New York.

Mayne, P.W., (2007). "NCHRP synthesis 368 in cone penetration test." *Transportation Research Board, National Academics Press,* Washington, D.C.

Morrison, M.J., (1984). "In situ measurement on a model pile in clay." *PhD thesis, Massachusetts Institute of Technology,* Massachusetts.

Paikowsky, S.G. and Hart, L.J., (2000). "Development and field testing of multiple deployment model pile." *FHWA-RD-99-194, Federal Highway Administration, US Department of Transportation,* McLean, VA., 236

Pestana, J.M., Hunt, C.E., and Bray, J.D., (2002). "Soil deformation and excess pore pressure field around a closed-ended pile." Journal of Geotechnical and Geoenvironmental Engineering, ASCE, 128(1): 1-12.

Randolph, M.F., (2003). "43rd Rankine Lecture: Science and empiricism in pile foundation design." *Géotechnique*, 53(10): 847-875.

Robertson, P.K., (2009). "Interpretation of cone penetration tests – a unified approach." *Canadian Geotechnical Journal*, 46: 1337-1355.

Schneider, J.A., (2007). "Analysis of piezocone data for displacement pile design." *PhD thesis*, University of Western Australia, Australia. 653p

Sy, A., (1993). "Energy measurements and correlations of the Standard penetration test (SPT) and the Becker penetration test (BPT)." Ph.D. thesis, Department of Civil Engineering, University of British Columbia, Vancouver, BC, Canada, 213p.

**Table 2.1: Summary of some instrumented test piles developed in the past (Paikiwsky. et. al.2000)**

| | Cone Penetrator | PLS | G&R Test Pile | NGI Test Pile | 3" Model Pile | X – Probe | IMP | Imperial College Pile | MDMP |
|---|---|---|---|---|---|---|---|---|---|
| **Diameter (mm)** | 35.7 | 38.4 | 25.4 | 153 | 76.2 | 43.7 | 80 | 102 | 76.2 |
| **Length (cm)** | Varies | 26.8 + Tip extension | 88.9 | 500.4 | 1850 | 143.5 | 113.5 | 700 | 287 |
| **Friction Sleeve ($cm^2$)** | 150 | Area of tip extension (about 2000) | 200 | NA | 1850 | 200 | Variable | Variable | 2000 between load cells |
| **Tip type** | $60^0$ Solid cone | $60^0$ Solid cone | Solid Aluminum plug | Closed ended | Open or closed ended | $60^0$ Solid cone | Open or closed ended | $60^0$ Solid cone | $60^0$ Solid cone or flat nose or open ended |

| | Cone Penetrator | PLS | G&R Test Pile | NGI Test Pile | 3" Model Pile | X – Probe | IMP | Imperial College Pile | MDMP |
|---|---|---|---|---|---|---|---|---|---|
| **Load cell locations (Type)** | One on tip, one on sleeve | One on top (Strain gauged load cell) | None | One on Top (Vibrating wire strain gauge | Two on sleeve | One on sleeve | Two on sleeve of leading cluster , one on sleeve of following cluster | Three behind tip on sleeve, each on a cluster 1m apart, one at top (High capacity axial load cells) | One behind tip and two on sleeve (Top & middle electric load cell; bottom strain gauge load cell) |
| **Pore pressure transducer location (Type)** | At tip, behind tip, above friction sleeve (Piezo cone). | In between PLS cell and tip extensio n | One at the middle of friction sleeve | Four along the sleeve | One in middle of sleeve (Kistler 4043A) | One on sleeve (Kistler 4043A) | Four on sleeve - Two on each cluster (Druck PDCR-81 | One behind tip on sleeve, two on a cluster 1m apart (Druck PDCR-81) | One in the middle of sleeve - Transducer housing (Kistler 4140A20) |
| **Lateral Pressure Transducer Location (Type)** | None | Top of tip extension (Piezo Lateral Stress cell) | None | Four along sleeve (Vibrating Wire) | One - Middle of sleeve (Sensotec Model 13) | One - on sleeve (Sensotec Model 14) | Four on sleeve - Two on each cluster | Three behind tip on sleeve, each a cluster 1m apart (Cambridge earth pressure cell) | One, middle of the sleeve - Transducer housing (Electric Strain Gauges) |

| | Cone Penetrator | PLS | G&R Test Pile | NGI Test Pile | 3" Model Pile | X – Probe | IMP | Imperial College Pile | MDMP |
|---|---|---|---|---|---|---|---|---|---|
| **Displacement Transducer** | None | None | None | One at Top | Slip Joint – DC LVDT between cutting shoe and instrumented portion, Cutting shoe act as anchor during loading | Slip Joint – DC LVDT between cutting shoe and instrumented portion, Cutting shoe act as anchor during loading | None | Three at top | One - behind tip |
| **Accelerometer** | None | None | None | None | Four (2 on each load cell) | None | None | None | Four, one at top of rod, one at each load cell |
| **Temperature Sensor** | Special cone | One in PLS cell | None | None | None | None | None | Three behind tip on sleeve, each on every surface stress transducer | None |

| | Cone Penetrator | PLS | G&R Test Pile | NGI Test Pile | 3" Model Pile | X – Probe | IMP | Imperial College Pile | MDMP |
|---|---|---|---|---|---|---|---|---|---|
| **Slop Sensor** | Omni-directional inclinometer – Special cone | None | None | None | None | None | None | None | None |
| **Driving Mechanism** | Jacking (20mm/s) | Jacking (20mm/s) | Reversible, variable speed screw jack | Jacking (4 - 15 cm/min) | Driving / Pushing | Pushing | Jacking | Jacking (fast 400-600 mm/min: slow 50-100 mm/min) | Driving with SPT hammer/ Pushing |
| **Pile Type** | Probe | Probe | 6061 Aluminum tube | Steel Pipe | Steel Pipe | Probe | Steel Pipe | Steel Pipe | Steel Pipe with 3/8" wall thickness |

**Table 2.2: Becker hammer (ICE – 180) specifications (ICE Inc.)**

| Description | Units |
|---|---|
| Total net operating weight | 20.25 kN (4550 lbs) |
| Ram net weight | 7.67 kN (1725 lbs) |
| Anvil net weight | 1.68 kN (377 lbs) |
| Hammer overall length | 3.43 m (135 in) |
| Rated ram stroke at sea level | 95.5 cm (37.6 in) |
| Maximum equivalent additional ram stroke from Bounce chamber at sea level | 45.92 cm (18.08 in) |
| Maximum equivalent ram stroke from free fall plus equivalent bounce chamber stroke at sea level | 144 cm (56.68 in) |
| Maximum equivalent energy rating | 10.85 kNm (8000 ft.lbs) |
| Blows per minute | 90 - 95 |

**FIGURES**

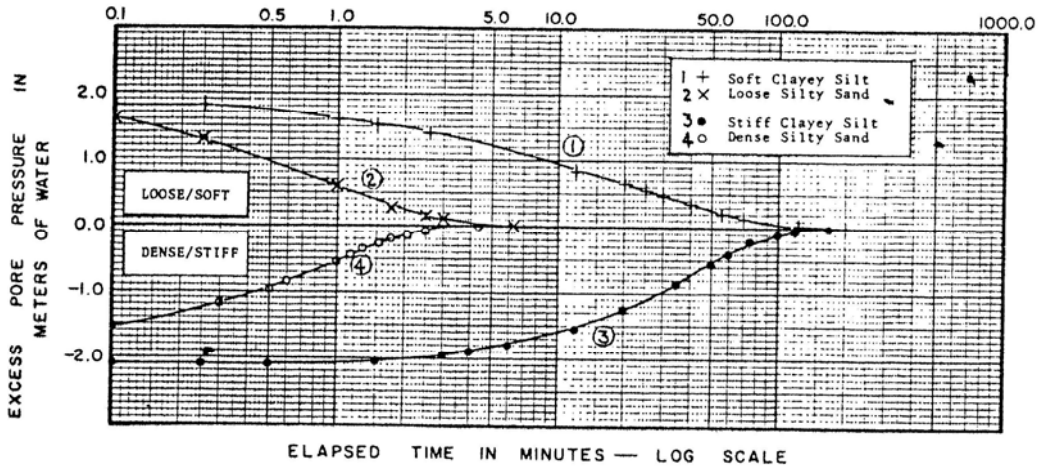


**Figure 2.1: Excess pore pressure dissipation following PLS cell probe penetration into dilative and contractive soil deposits (Wissa et al. 1975).**

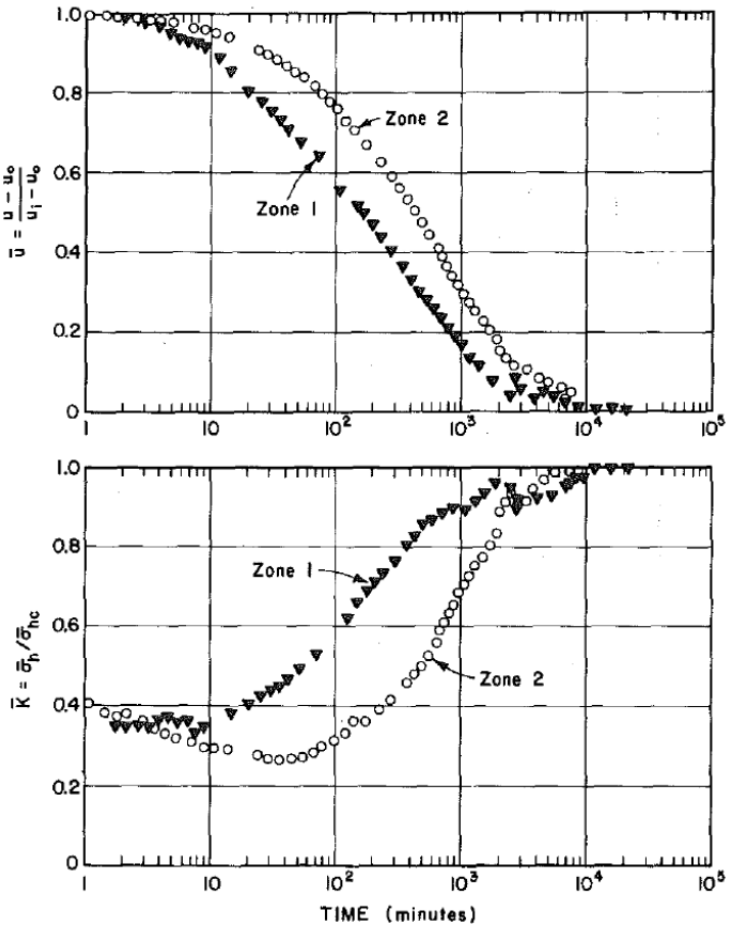


**Figure 2.2: Variation of normalized pore pressure and normalized effective stresses with setup period. Plots produced based on measurements using PLS cell. Zone 1 is (35-50 m) uniform firm gray clay and zone 2 (62-77m) very stiff gray clay (Azzouz et al. 1985).**

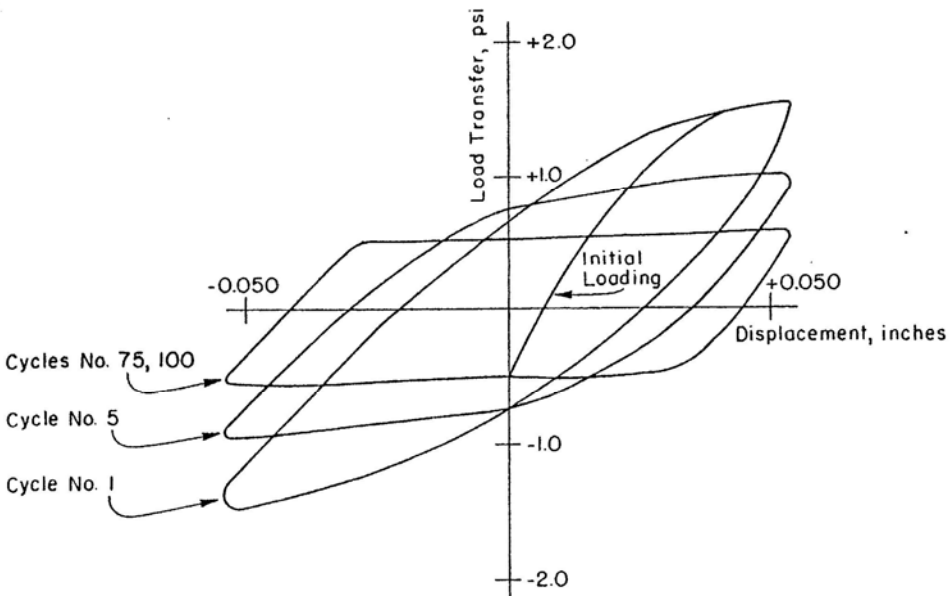


**Figure 2.3: Result of initial cyclic test, test A-1, with symmetric displacements of ±1.44 mm (±0.055 inches) measured with G & R instrumented test pile in clay layer (Grosch et al. 1980).**

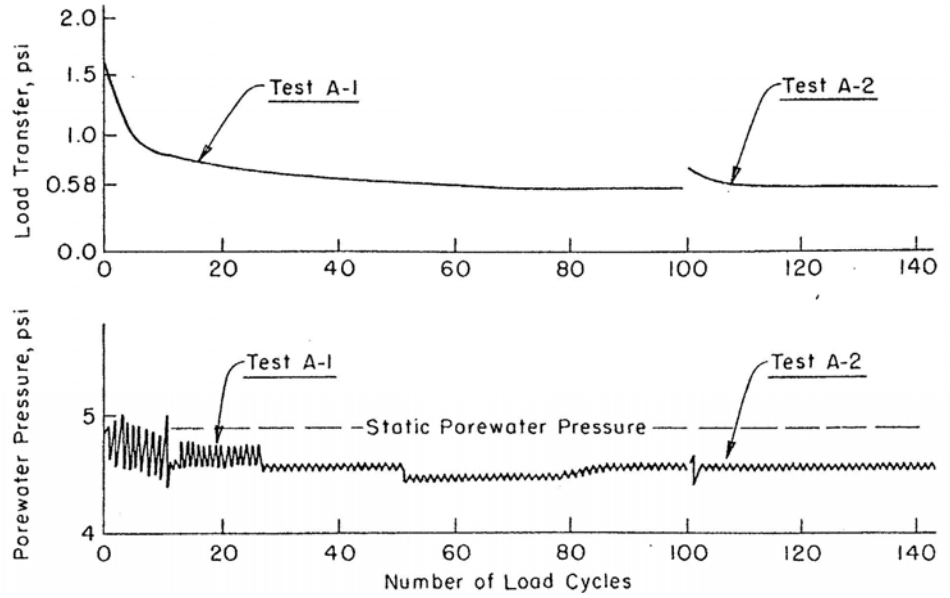


**Figure 2.4: Variation of load transfer and pore pressure with number of cycles measured with G & R instrumented test pile. Test A-1 is initial cyclic test, symmetric displacement of ±1.44 mm (±0.055 inches) in clay layer. Test A-2 is retesting with symmetric displacement of ±1.44 mm (±0.005 inches) in clay (Grosch et al. 1980).**

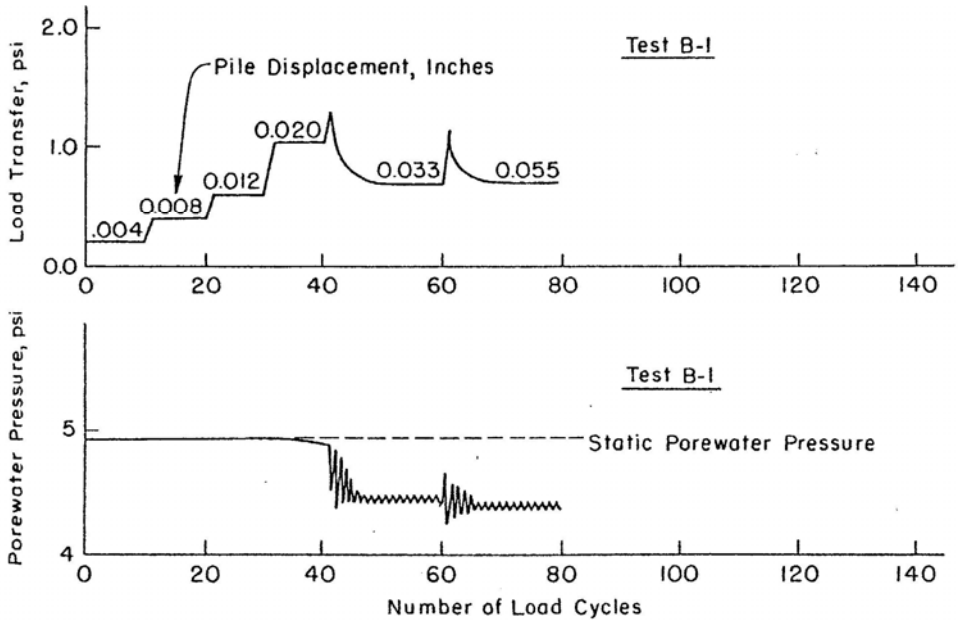


**Figure 2.5: Variation of load transfer and pore pressure with number of cycles measured with G & R instrumented test pile. Test B-1 is initial cyclic test starting from symmetric displacement of ±0.10 mm (±0.004 inches) to displacement of ±1.44 mm (±0.055 inches) in clay layer (Grosch et al. 1980).**

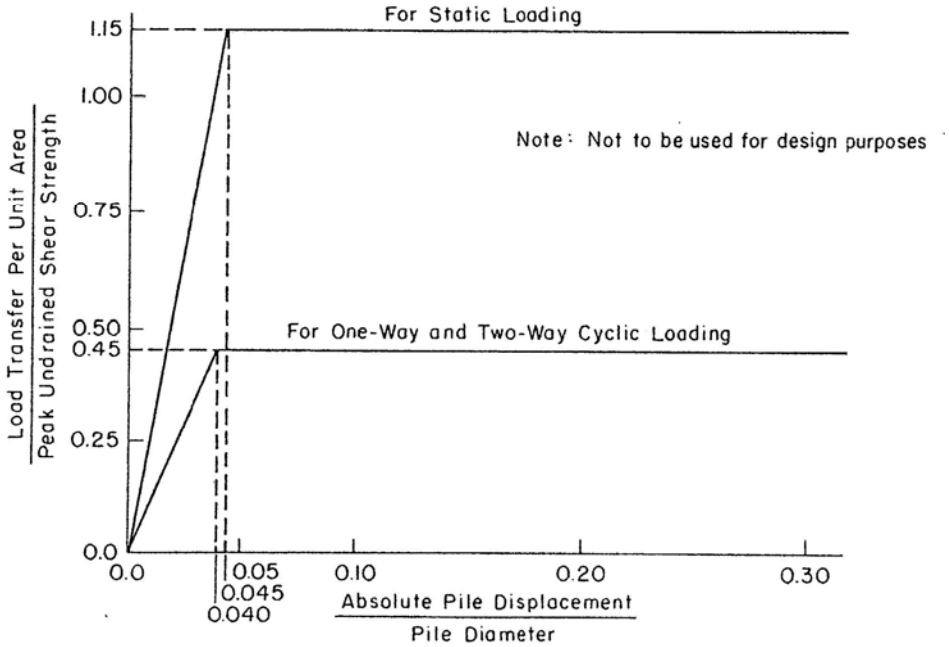


**Figure 2.6: Model of normalized load transfer with normalized pile displacement in clay (Grosch et al. 1980).**

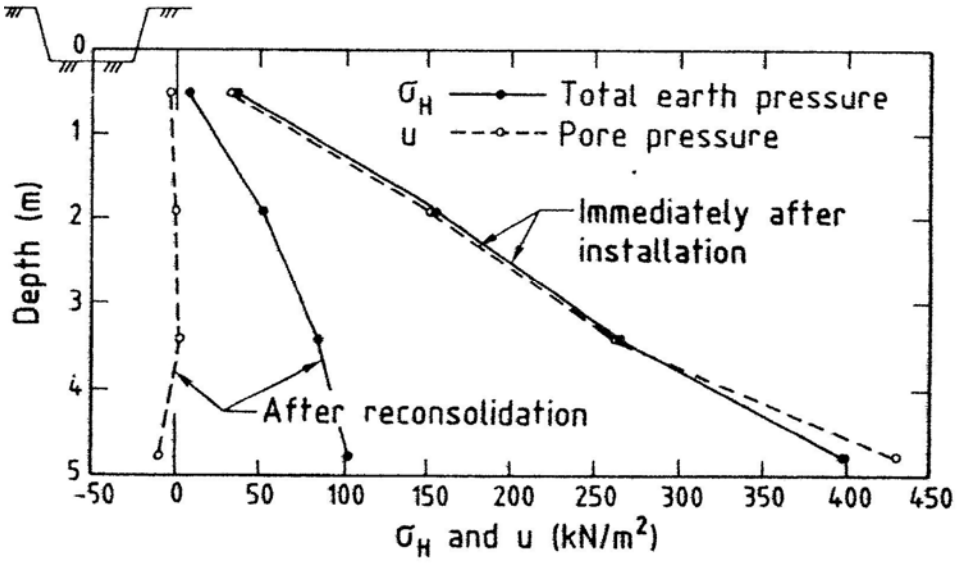


**Figure 2.7: Total horizontal stress and excess pore pressure measured with NGI model pile immediately after pile installation and after setup in overly consolidated clay (Karlsrud et al. 1985).**

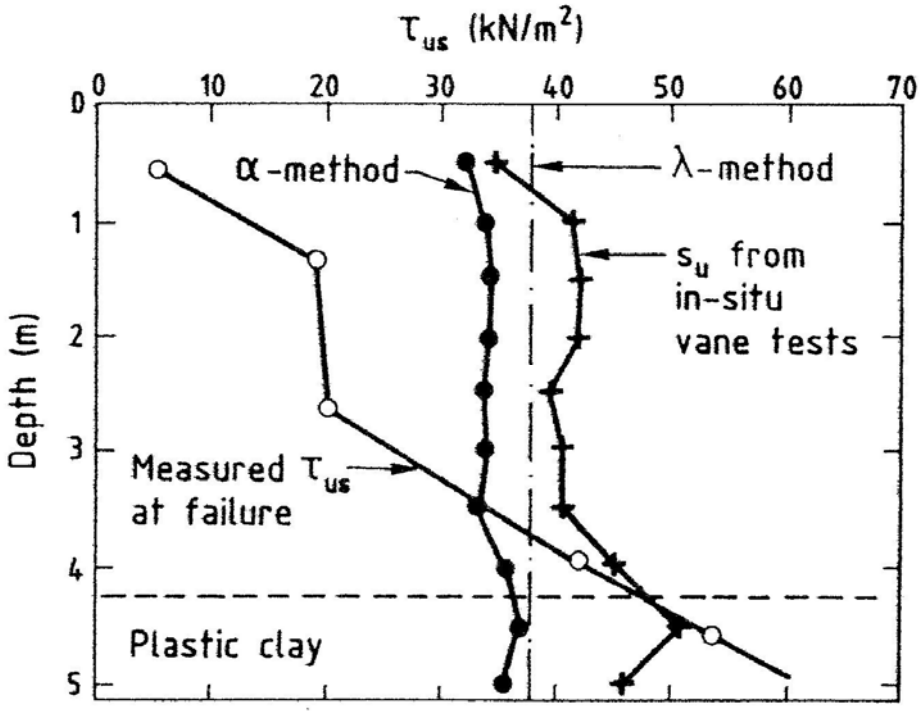


**Figure 2.8: Measured shaft friction with NGI model pile in overly consolidated clay layer compared to calculated shaft friction. Soil profile shown as homogeneous clay on top of plastic clay deposit (Karlsrud et al. 1985).**

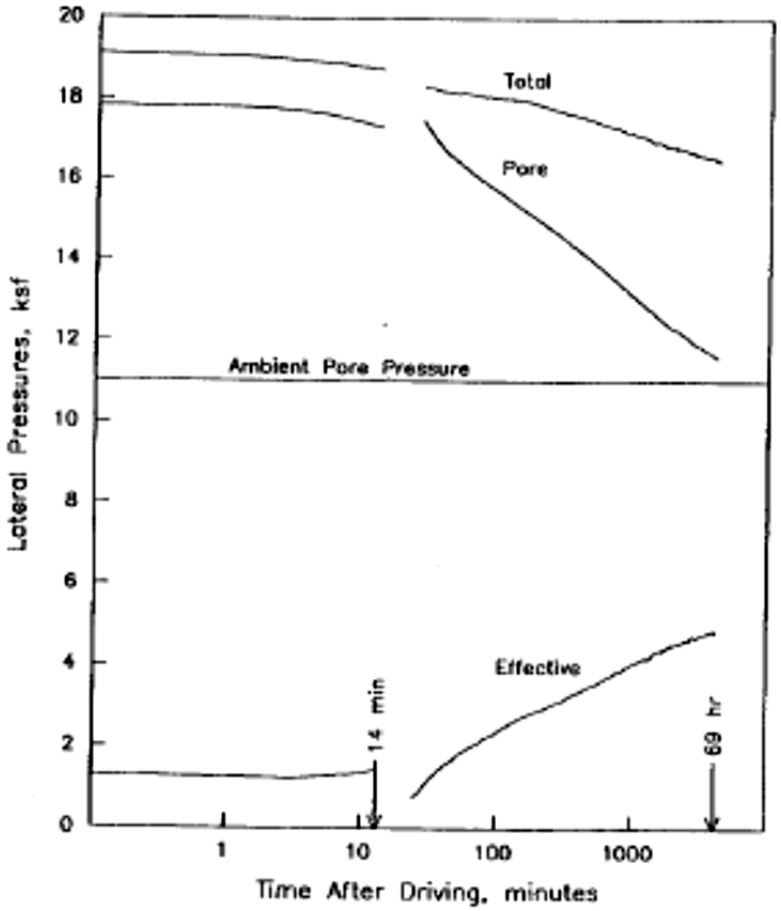


**Figure 2.9: Variation of lateral pressures with time after installation of 3 inch closed ended model pile in homogeneous normally consolidated clay (Bogard et al. 1990).**

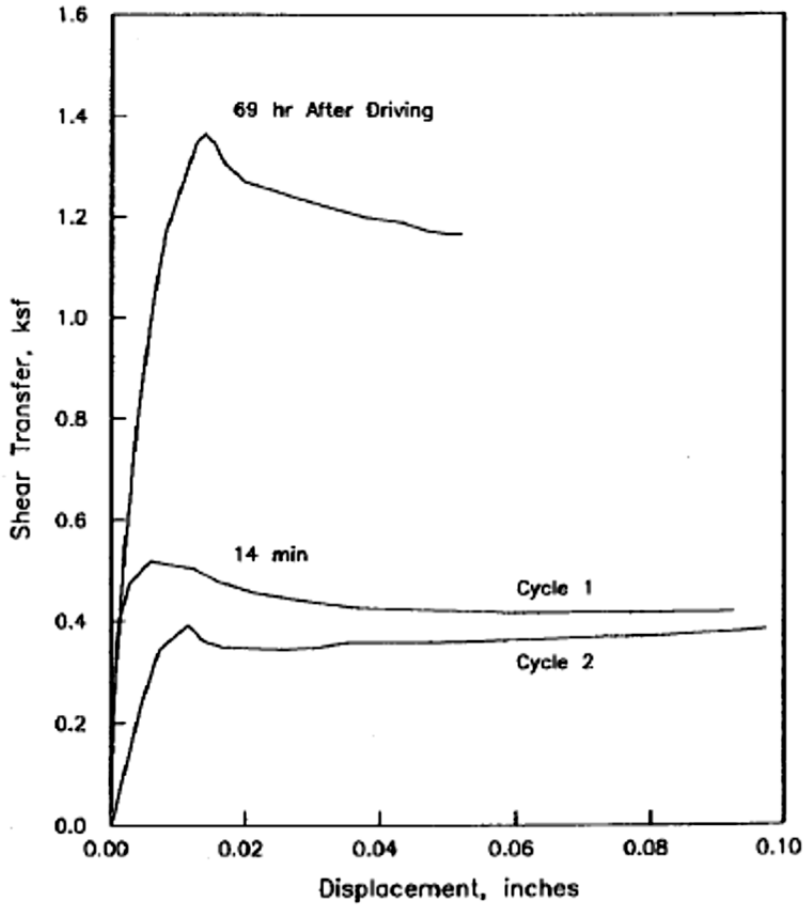


**Figure 2.10: Results of static tension load test after installation and setup of 3 inch model pile in homogeneous normally consolidated clay. Cycles 1 and 2 show the results from cyclic tension tests for first and second cycle. (Bogard et al. 1990).**

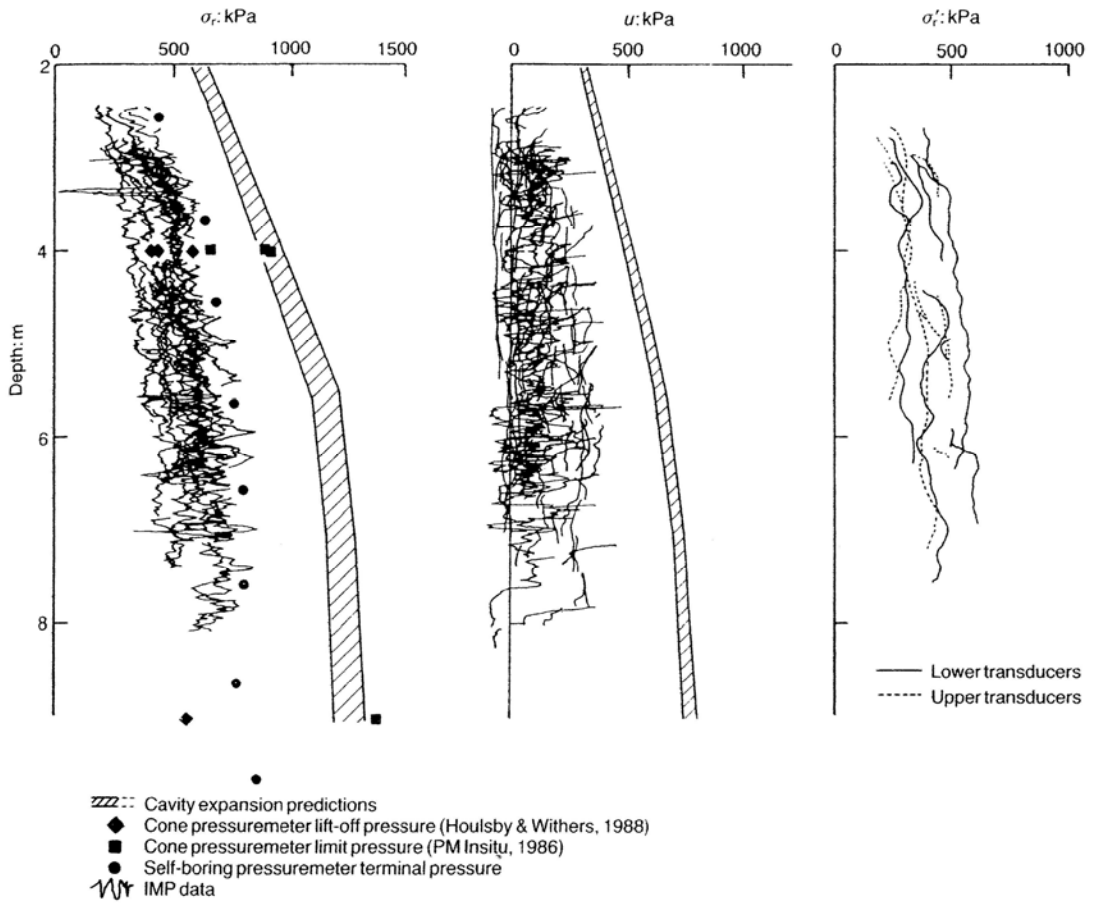


**Figure 2.11: Summary plot of pore pressure and total radial stress measurements obtained by each of the IMP transducers during continuous penetration of clay layer in five installations (Coop et al. 1989).**

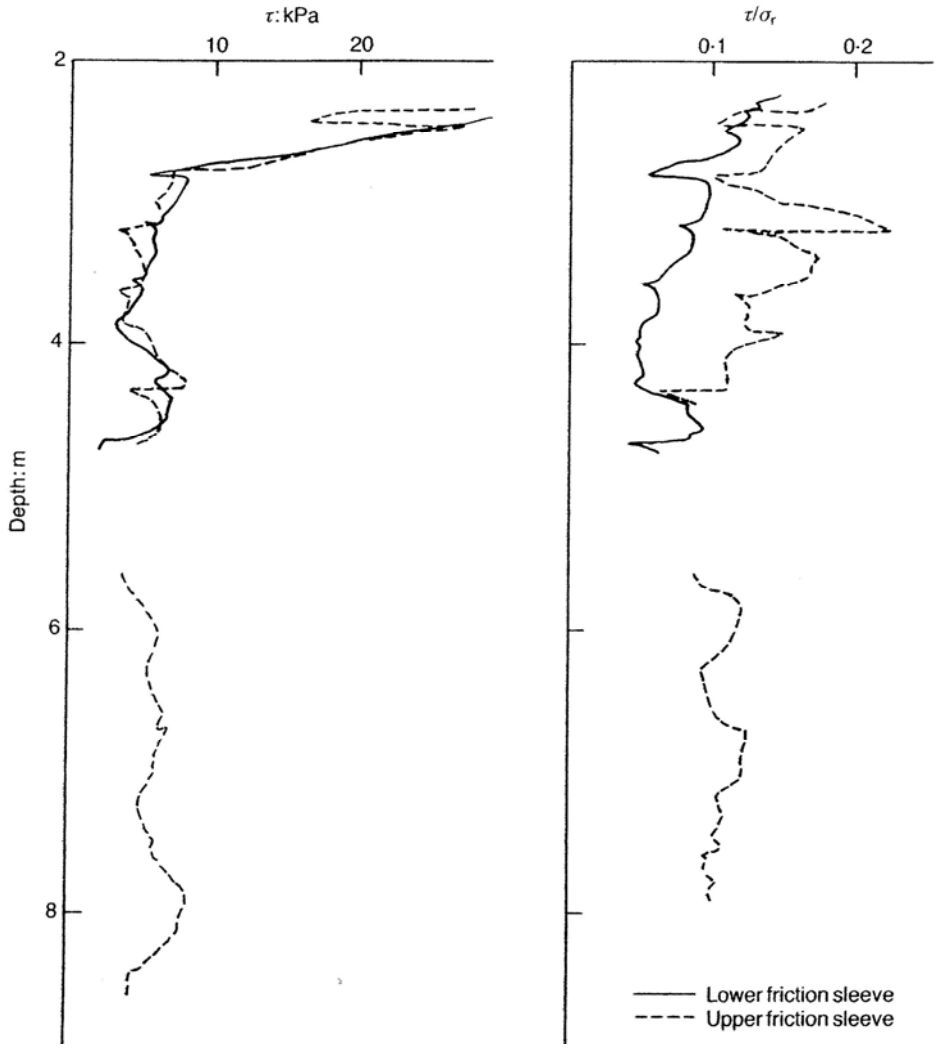


**Figure 2.12: Measurement from sleeve friction of leading and following instrumented sections of IMP in clay layer and normalized values of sleeve friction by effective radial stress (Coop et al. 1989).**

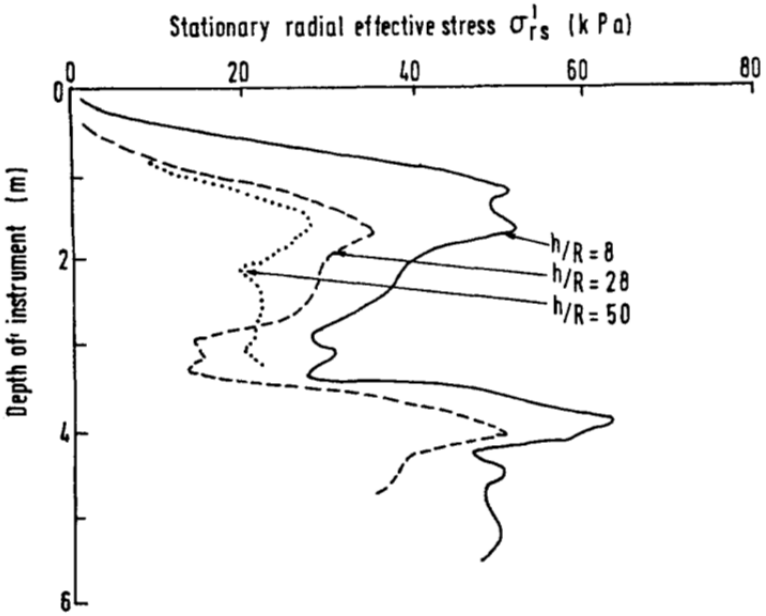


**Figure 2.13: Radial effective stress during installation of ICP measured in sand layer at three h/R ratios from the tip (Lehane et al. 1993).**

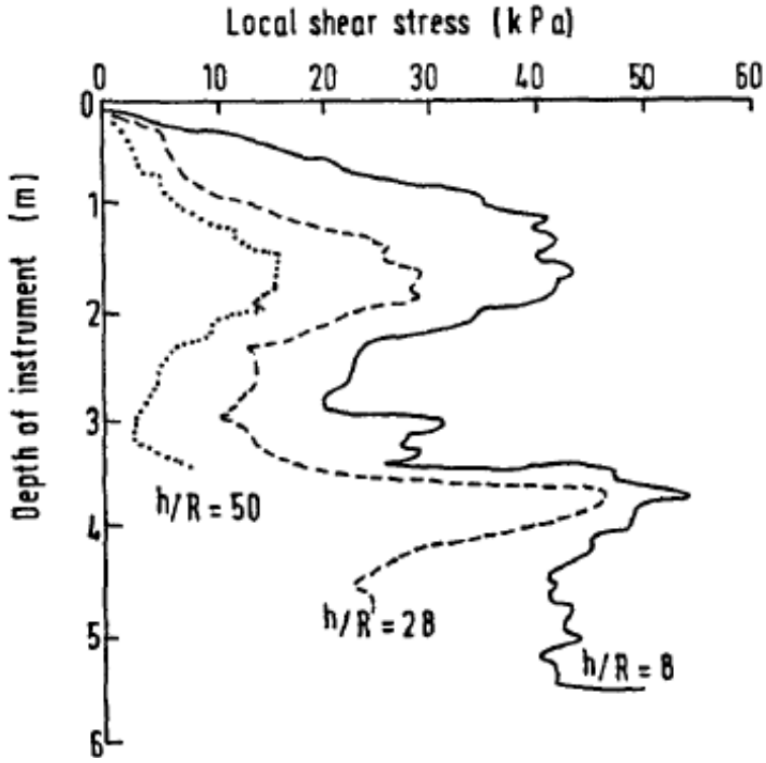


**Figure 2.14: Local shear stress during installation of ICP measured in sand layer at three h/R from the tip (Lehane et al. 1993).**

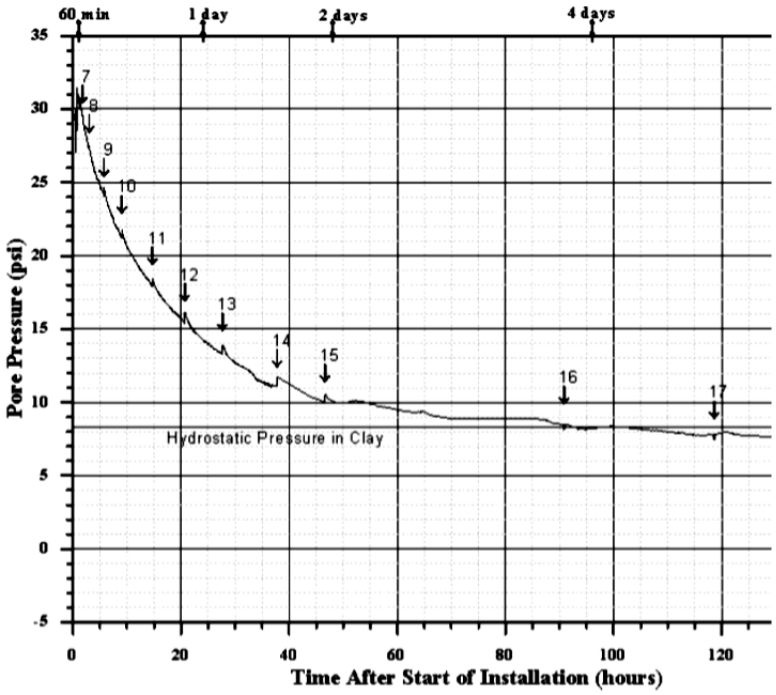


**Figure 2.15: Excess pore pressure generation due to installation and dissipation after the installation of MDMP in a clayey site. Static load testing carried out during pore pressure dissipation, test 7 to test 17, shows sudden increase in measurements (Paikowsky. et al. 2000).**

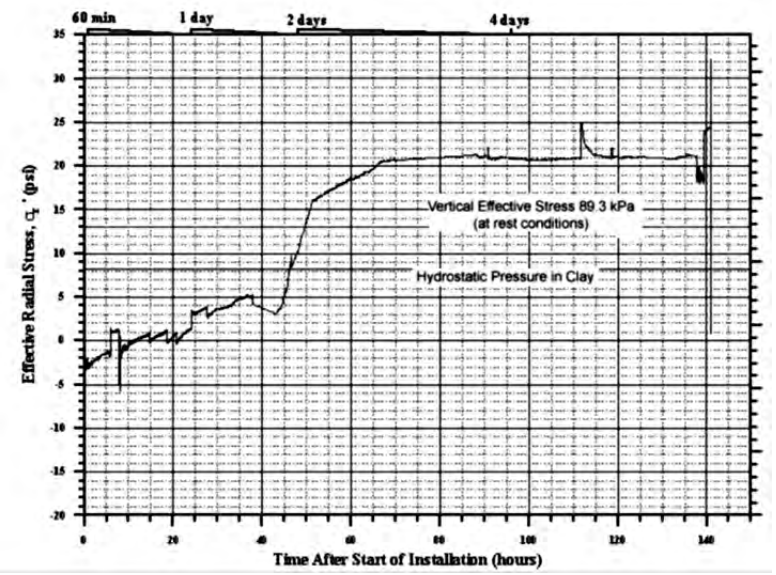


**Figure 2.16: Effective radial stress measurement during setup period following installation of MDMP in clayey soils (Paikowsky et al. 2000).**

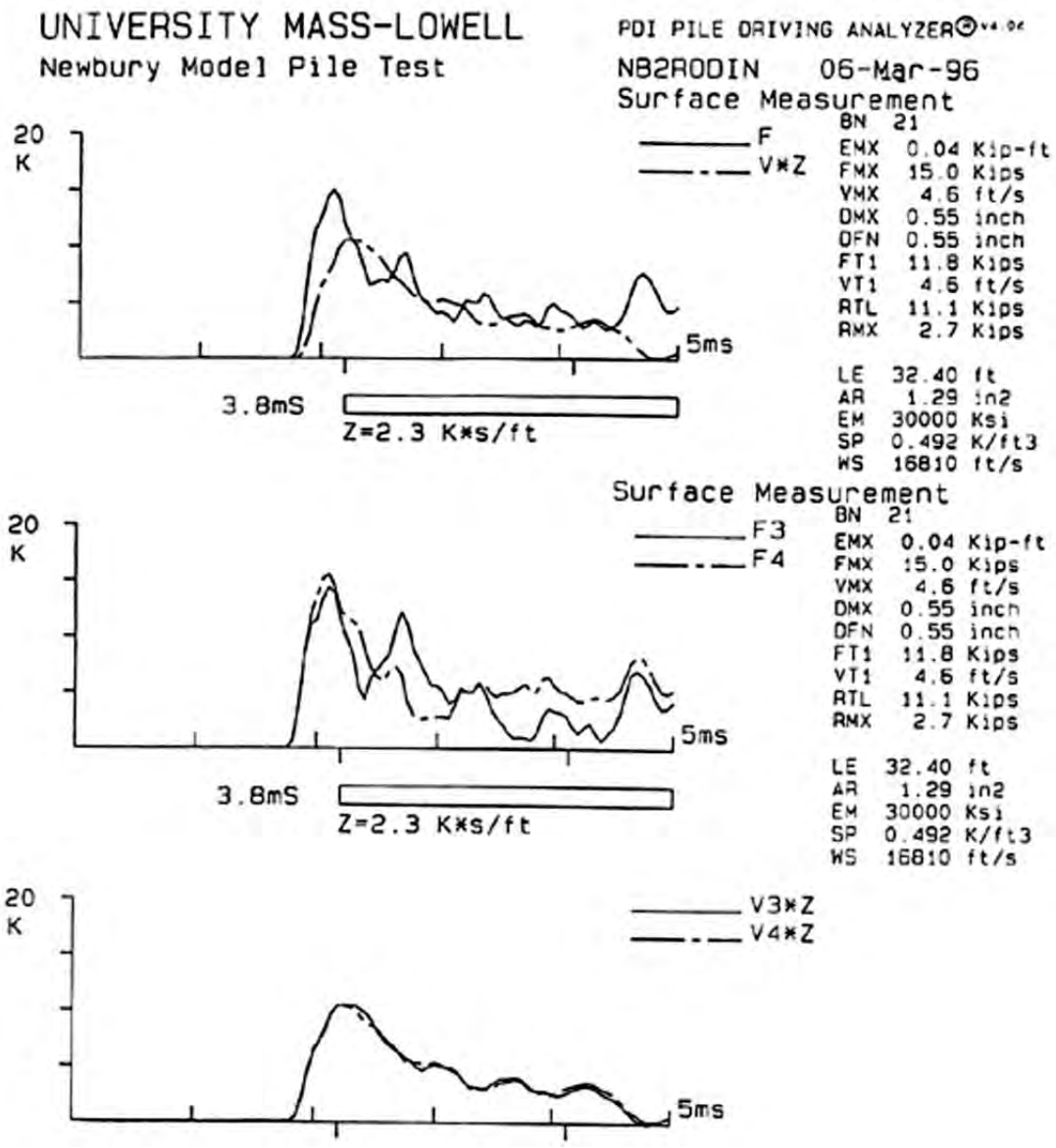


**Figure 2.17: PDA dynamic measurements during the installation of MDMP (Paikowsky et al. 2000).**

(a)

(b)

(c)

**Figure 2.18: Becker hammer drill system (a) moving Becker drill rig, (b) Drill ring with driving hammer in upward right position, and (c) Becker pipes being transported to field site.**

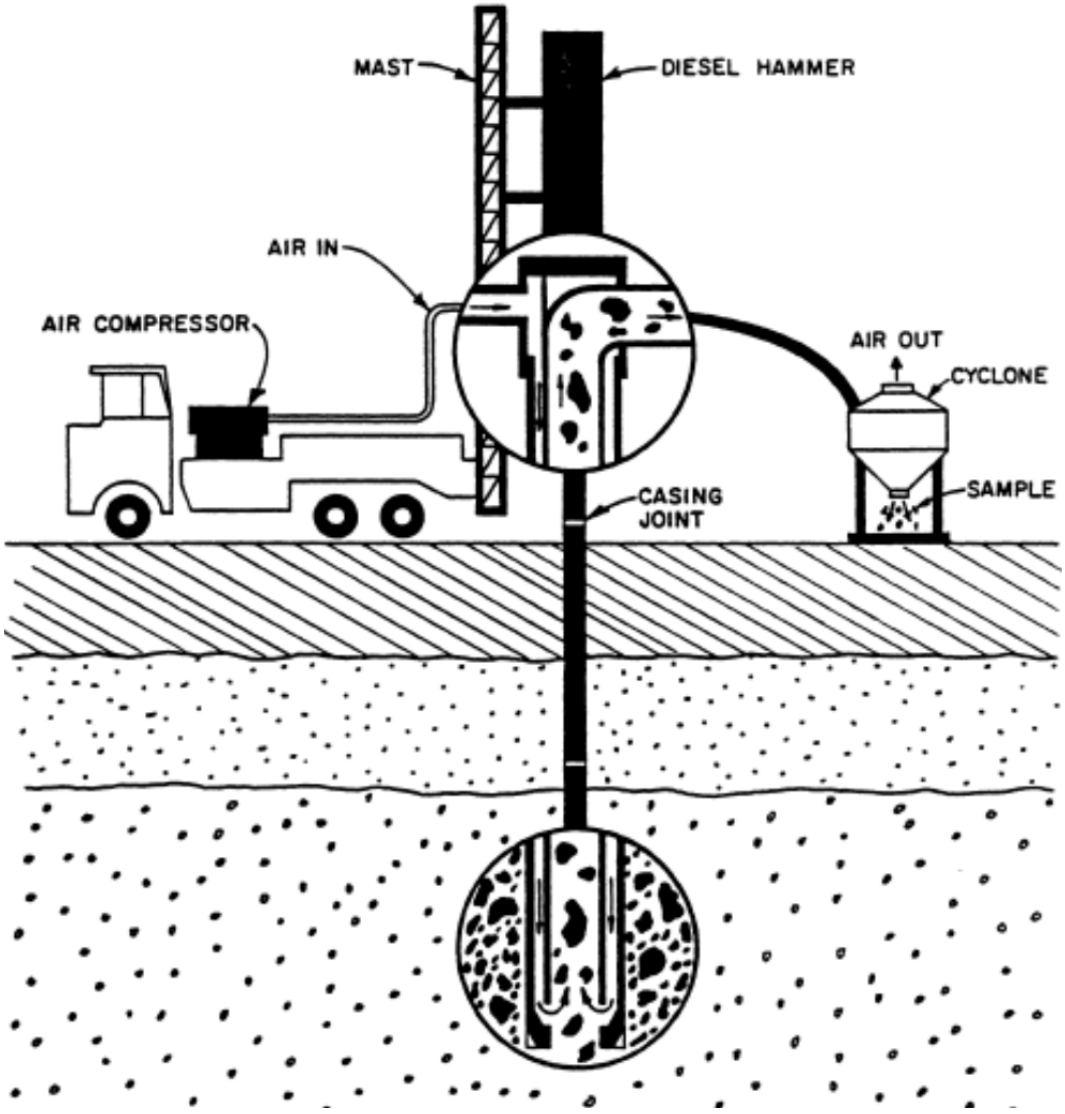


**Figure 2.19: Schematic diagram of Becker sampling operation (Harder and Seed 1986).**

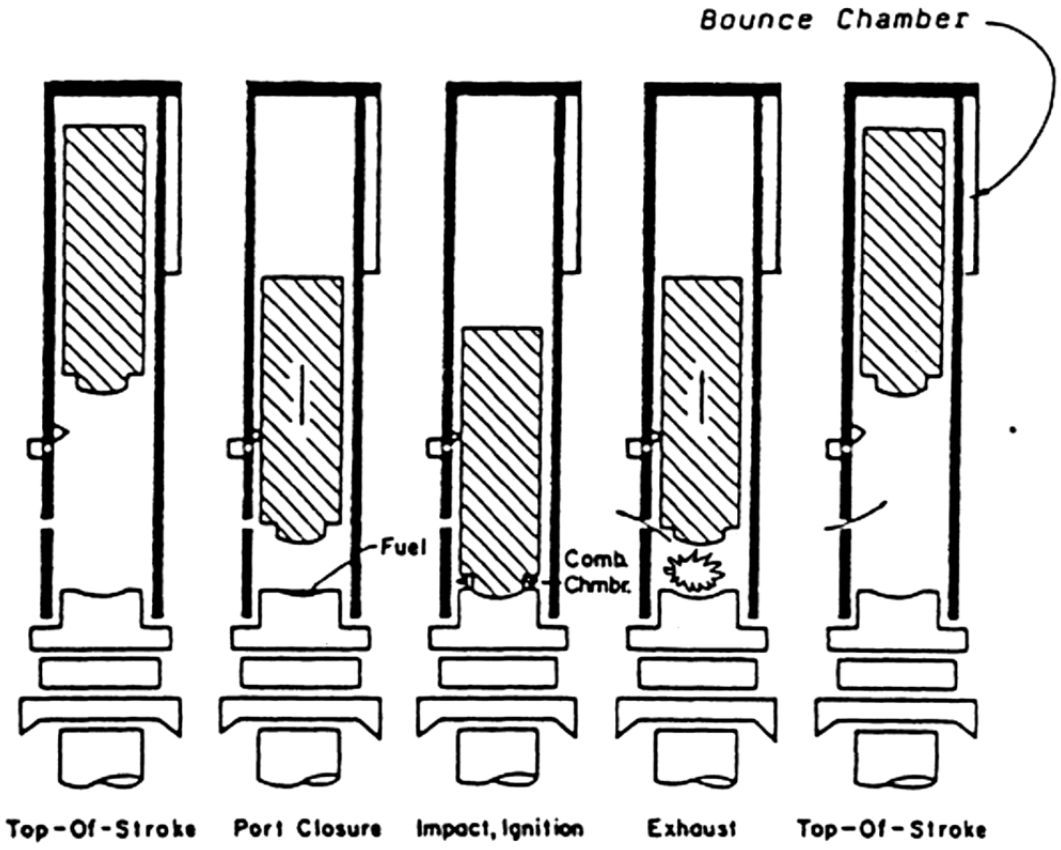


**Figure 2.20: Schematic diagram of diesel hammer operation and bounce chamber pressure (Harder and Seed 1986).**

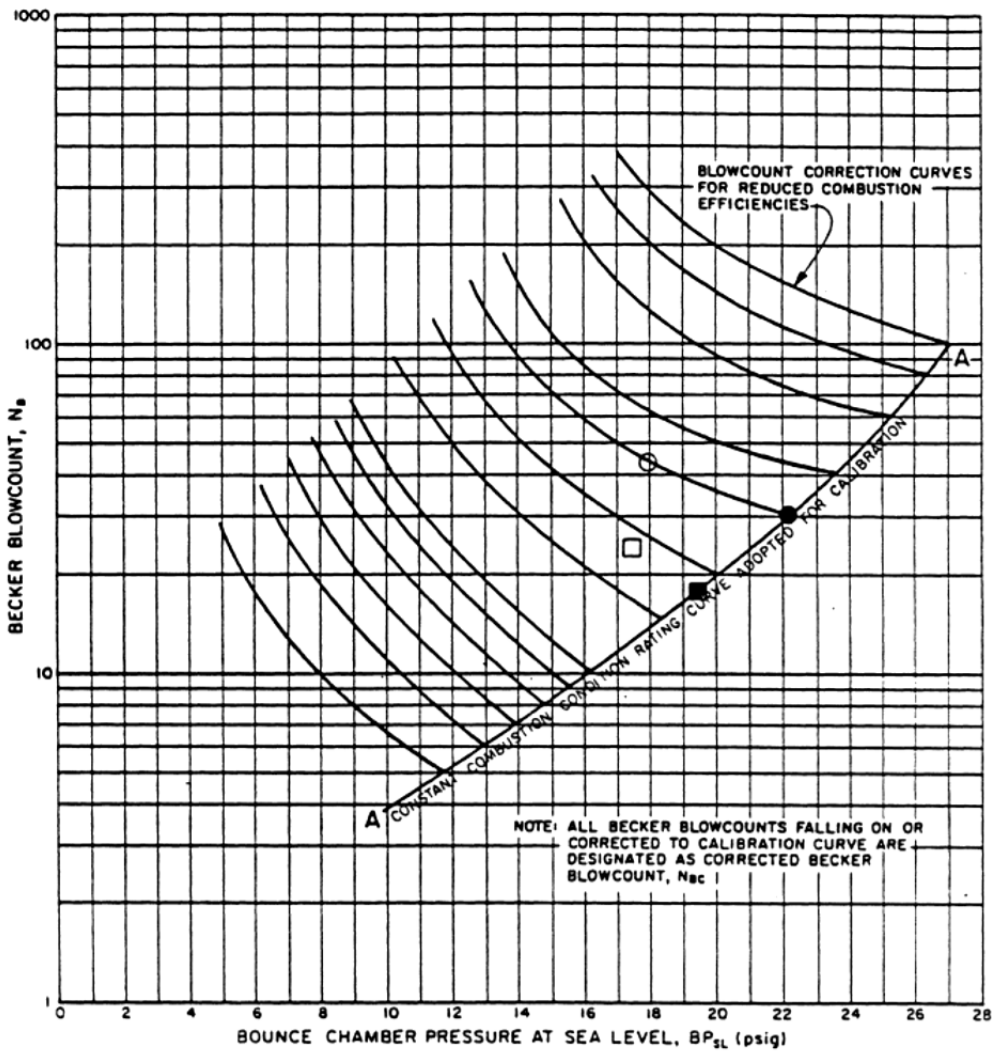


**Figure 2.21: Curves to correct the measured Becker blow counts and bounce chamber pressure to standard BPT blow count (Harder 1988).**

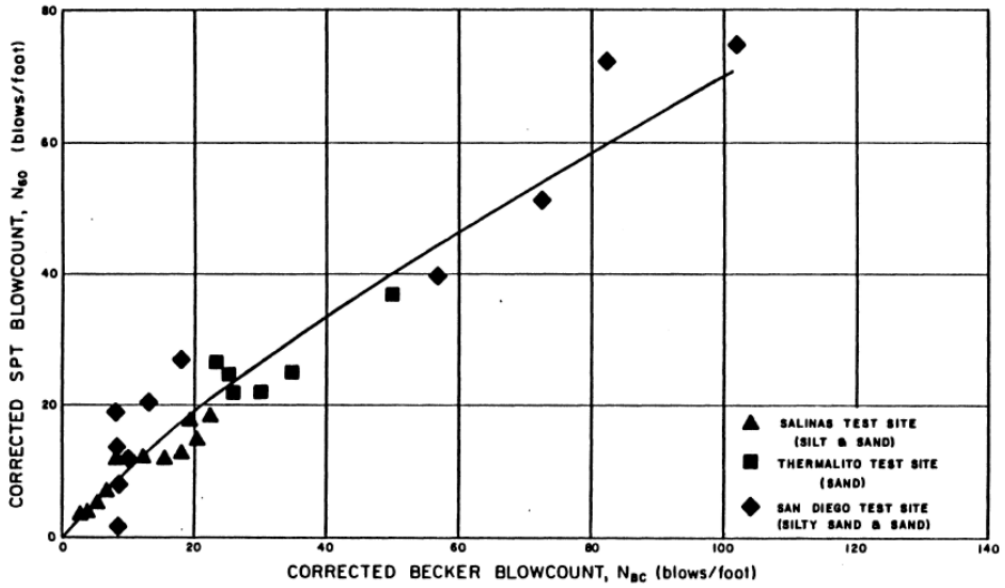


**Figure 2.22: Correlation between corrected Becker blow counts and standard SPT blow counts (Harder 1988).**

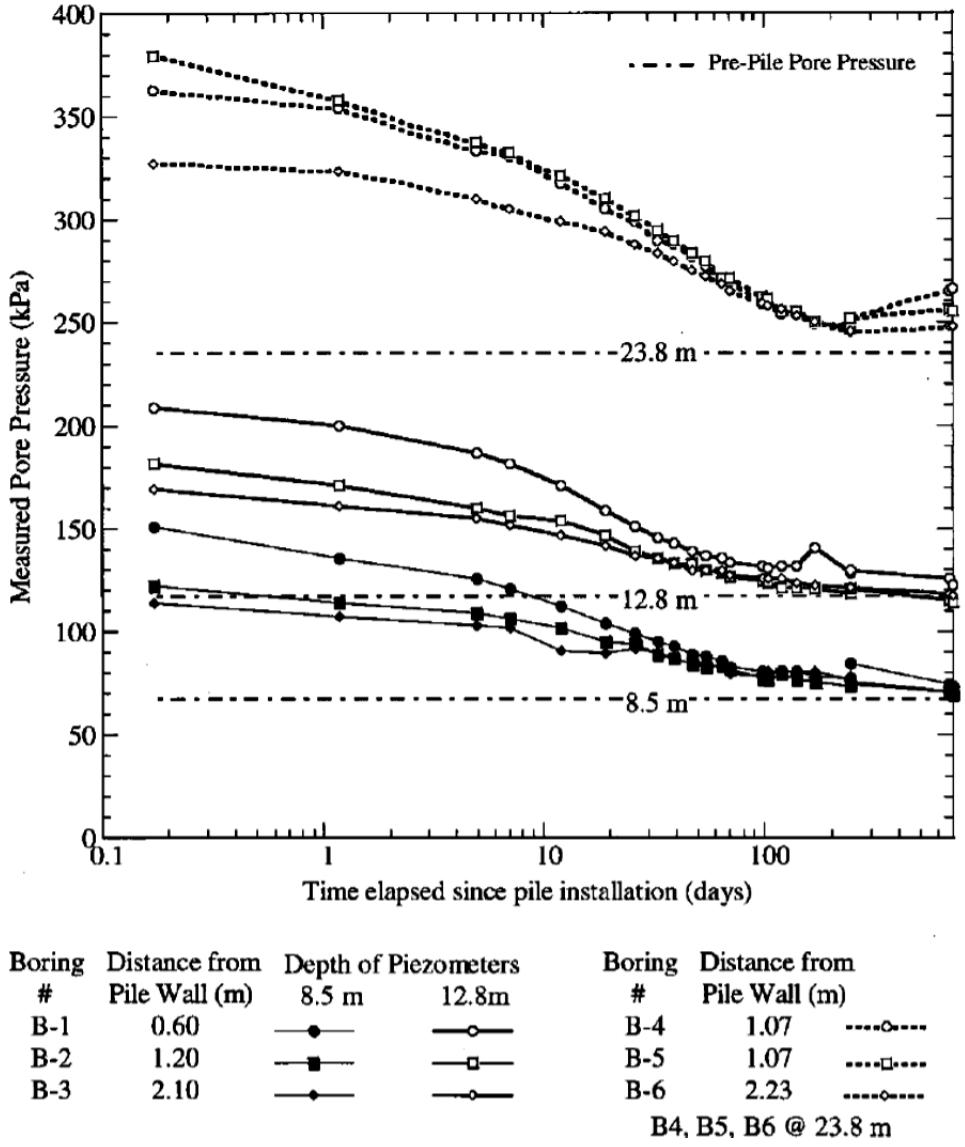


**Figure 2.23: Pore pressure monitoring after pile installation at San Francisco bay mud (Pestana et al. 2002).**

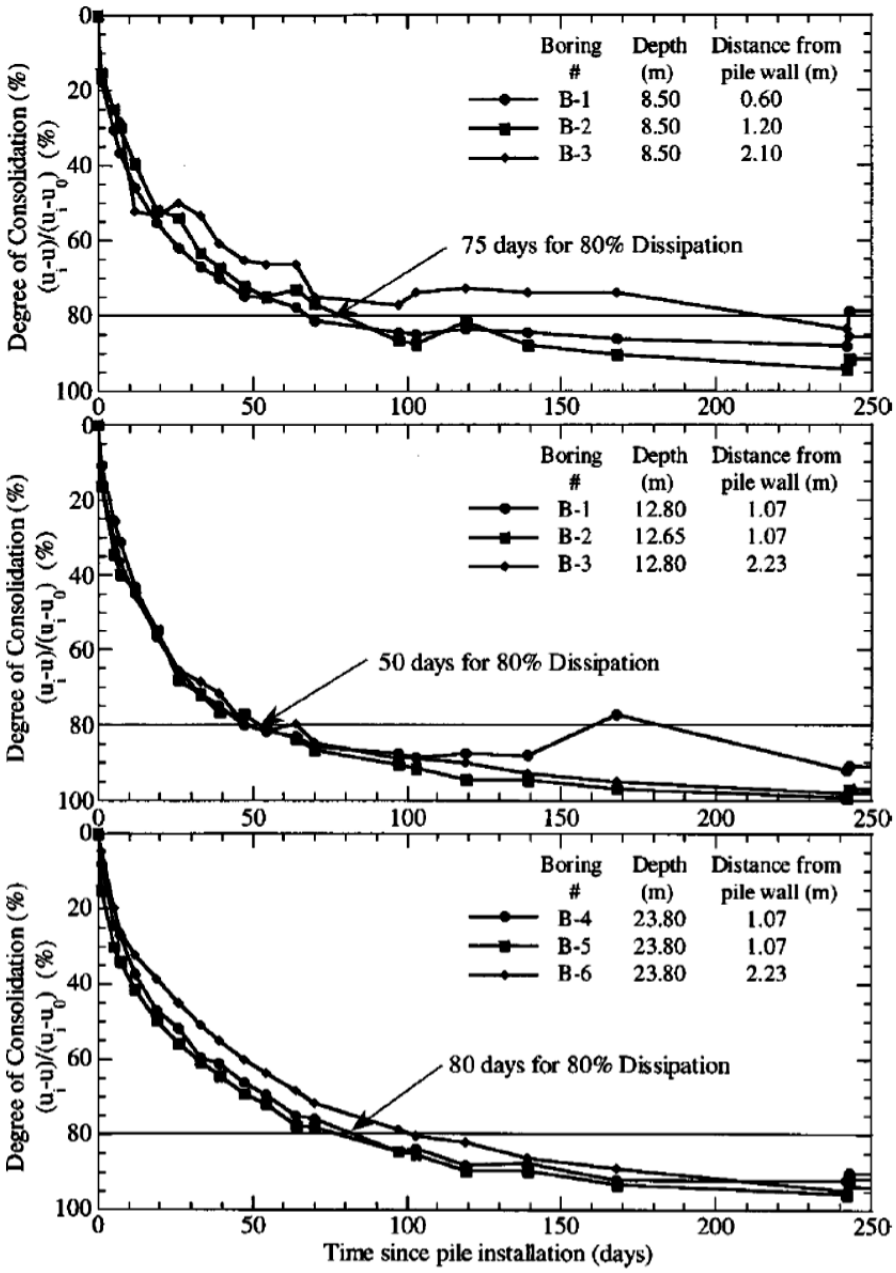


**Figure 2.24: Excess pore pressure dissipation at three depths (Pestana et al. 2002).**

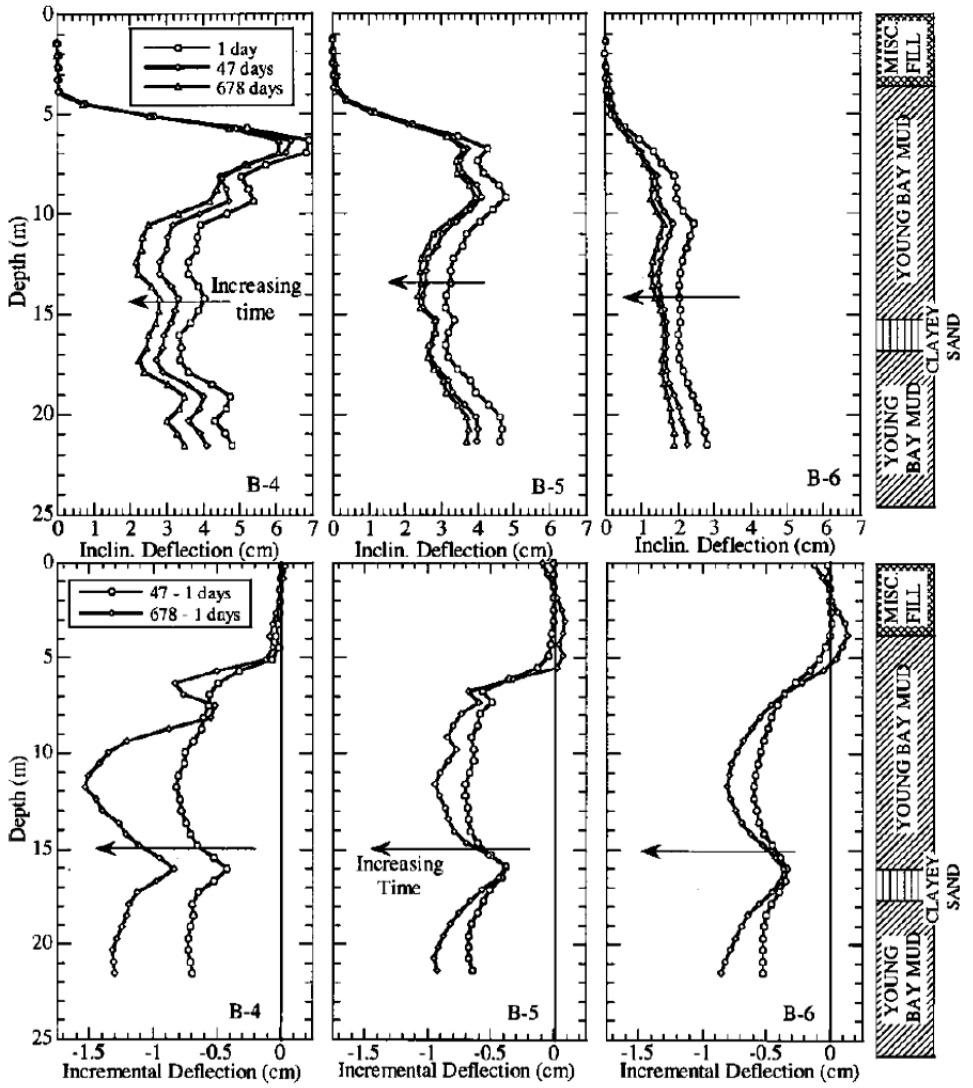


**Figure 2.25: Consolidation induced radial deformation at three borehole locations. Top row presents inclinometer location after pile installation and movement during consolidation and bottom row presents incremental displacement after initial displacement (Pestana et al. 2002).**

# Chapter 3: Reusable Test Pile (RTP) Design

## 3.1 Overview

The objective of the RTP system is to provide quantitative measurement responses of driving dynamics, setup, and load testing along the pile length. The RTP system is expected to serve as a mobile in-situ testing device that is installed by dynamic pile driving. As a result, the performance specifications were broad, covering a range of issues, and challenging, requiring equipment robustness and measurement sensitivity. The final RTP design, detailed herein, centers around 61 cm (24 in) long pipe sections instrumented for measurement of axial load, radial stress, acceleration, and pore pressure. Several additional components were designed to complete the system. Development of the RTP system required several intermediary field tests to proof equipment prototypes. Calibrations before and after field testing verified the robustness of the equipment, while identifying aspects of sensor design and data acquisition systems requiring improvement. These issues are discussed herein.

## 3.2 Performance Specification

The performance specification for the RTP system can generally be categorized into the following sections: mobility, commercial integration, durability and robustness, measurement types, measurement sensitivity and reliability, measurement frequency and duration. These criteria were specified as follows:

### 3.2.1 Mobility

The mobility of the RTP system was focused on balancing the issues of portability and pile size effects. The system must be sufficiently small such that instrumented sections can be transported and handled with relative ease. When on-site cable winches can be used to handle the instrumented sections during testing. However, in the laboratory during development, calibration, etc. and during transport the sections must be sufficiently small that two persons can handle the RTP sections safely. At the same time, the RTP diameter should be as large as possible in order to minimize pile diameter scaling effects. It is recognized that the scaling effects could not be eliminated, but an effort was made for the diameter to be larger than about 10 cm as soil arching around model piles at smaller diameters installed in coarse sands can affect behavior (e.g. Fivorante et al. 2002).

### 3.2.2 Commercial Integration

To the extent possible, the equipment required for installation and removal of the RTP system will be commercially available through a project service contract. The components of the RTP system that are unique to the system should be minimized in size and weight to the extent possible. This specification was desirable to manage overall project costs and to minimize the amount of equipment and/or vehicles that Caltrans must manage and own over the long term.

### 3.2.3 Durability and Robustness

The RTP system must survive dynamic piling driving, extraction, and handling by field personnel. The RTP may be installed up to 60 m (200 feet) depths eventually, which could require up to 10,000 hammer blows for a single installation. The RTP system will be clamped upon extraction, requiring sufficient surface area along the instrumented section capable of surviving high-pressure gripping forces. Handling of the RTP system will occur by contracting drillers; therefore rough handling and possible dropping of equipment should be expected.

### 3.2.4 Measurement Types

The measurements required for the initial RTP system include the following, in order of priority:

- Axial force at the tip and select locations along the RTP length
- Pile head position
- Axial acceleration at the tip and select locations along the RTP length
- Pore pressure at select locations along the RTP length
- Radial stress at select locations along the RTP length
- Temperature for data correction
- Inclination to verify RTP installation

### 3.2.5 Measurement Capacity & Sensitivity

The sensors required for obtaining the above measurements must be capable of surviving extreme loads during pile driving and extraction while being able to resolve small changes between pile hammer blows and during pile setup. The capacities required were not specifically known, but were estimated to be 1000 g for accelerations, 1000 kN (250 kips) for axial load, 700 kPa (100 psi) for pore pressure, and 700 kPa (100 psi) for radial stress. At the same time, sensitivity levels of 0.1 g, 1 N (0.25 kip), 7 kPa (1 psi), and 3.5 kPa (0.5 psi), respectively were desired based on how the data would be used in analysis (presented in later chapters). It was recognized that some of these specifications exceed the typical accuracy level of 0.1% common to most commercial sensors and therefore would be difficult to achieve.

### 3.2.6 Measurement Frequency and Duration

The frequency and duration of sampling will be varied depending on the mode of testing (i.e. pile driving, pile setup, static pile load test) and project conditions (i.e. driving resistance, soil type). The following general guidelines were specified:

- Fast sampling during pile driving at a frequency sufficient to clearly resolve dynamics forces and accelerations.

- Variable sampling frequency during pile setup to capture the faster initial changes in pore pressure immediately following driving and the more gradual changes over longer periods as the pore pressure equilibrates to the hydrostatic pressure.

Therefore it is preferable to have a system where the sampling frequency can be changed “on the fly”. The total measurement time may be up to several days (~100 hrs).

- Moderate sampling frequency, of about 10 Hz, during pile load testing would be sufficient as no high frequency content is expected. The total sampling time may be up to 12 hours.

Table 3.1 summarizes the measurements expected to be of priority during each operating modes.

### 3.3 RTP System Overview

The RTP system implemented within the above specifications was largely driven by the following critical decisions. First, it was decided that the RTP system would be compatible with the Becker drill system (described in Chapter 2). Specifically, the RTP system would be installed by the Becker pile-driving hammer and extracted by the spider hydraulic clamp system. This decision resulted in use of a commercially available system that is well established and does not require any ownership or maintenance by Caltrans. Second, the RTP system would be modular in design, with short instrumented sections being compatible with the industry standard Becker drill pipe size. This decision resulted in the RTP system components being easily handled and transported to site in a small truck or trailer, also resulting in significant overall cost reduction. Third, all sensor measurements would be recorded, processed, and digitized by downhole

computer systems and then digitally transmitted to the surface. Reduced length of cables keep the system practical and improves data quality by transmitting digital rather than analog signals over length. This decision required the development of a new downhole computer system and an associated vibration isolation system that would enable the computer to survive during dynamic pile driving. Fourth, the pile displacement during driving and pile load testing would be measured at the pile head above ground using a separate data acquisition system. An independent system for continuous pile head position measurement would enable automatic counting of pile blows per foot and reliable data during pile load testing.

The above decisions resulted in the RTP system assembly is shown schematically in Figure 3.1. The central component is the modular instrumented pipe sections, which are 61 cm (2 ft) long with an outer diameter of 168 mm (6.625 in). Each instrumented section contains axial force, axial acceleration, pore pressure, and radial stress measurements. In addition, an instrumented RTP tip section was developed that measures axial force and acceleration only to stay above ground. The modular sections are assembled in series with standard 152 cm (5 ft) and 305 cm (10 ft) long Becker pipes, enabling positioning of the instrumented sections in the drill string at target final elevations required by project-specific soil stratigraphy. Down-hole data acquisition units (GST module) in each RTP section provides signal conditioning (sensor excitation, gain, and filtering), digitizes and buffers the signals, and transmits the data serially (i.e. through additional GST modules in line) to the control unit (GCM) above ground. The digital transmission results in only a single 4-wire cable running along the RTP connecting all instrumented modules (GST modules) in a single line to the above ground computer (GCM module). The GCM provides control of which modules and sensors are connected and should

be recorded as well as control of sampling rate and the number of sample points (and therefore the total sampling time). A separate above ground data acquisition system (based on National Instruments (NI) hardware) collects data from displacement gages (string potentiometers) to measure vertical displacement of the pile and the bounce chamber pressure in the Becker hammer during driving. The NI system is also used to record pile displacement during field load testing. The modular nature of the RTP system and its integration with the Becker system enables testing to be completed in one day with limited time for pile setup.

## 3.4 RTP Detailed Design

This section describes the individual components of RTP system, including dimensional and part specifications as well as performance.

### 3.4.1 Instrumented Section Design

The modular RTP instrumented sections contain different components for either instrumentation or mounting of sensors, for recording of the sensors by the downhole computer, or for vibration isolation of the downhole computer (GST module). All of these components are housed within a 61 cm (2 ft.) long and 168 mm (6.625 in.) outer diameter (127 cm (5.0 in.) inner diameter) custom Becker pipe section. Each pipe section weighs about 35 kg (80 lbs). The sections were fabricated by Foremost Industries (Canada) out of 4140 alloy steel and machined with triple lead threads to be compatible with the standard Becker pipe. Figure

3.2 presents the geometry, instrumentation, downhole data acquisition unit, and the vibration isolation system of the RTP section in detail.

#### 3.4.1.1 Axial Force Measurement

Axial forces measurements were obtained using a full Wheatstone bridge mounted on a reduced wall thickness section of the 2 ft. pipe section. As detailed below in section 3.5.1, selection of the RTP wall thickness was investigated in the field to maximize resolution while still ensuring durability. After testing wall thicknesses ranging from 12.7 mm (0.5 in.) to 20.6 mm (0.8 in.), evaluating calibration factors changes pre- and post-testing, considering the minimum wall thickness present on standard Becker pipe, and considering design space constraints a final wall thickness of 12.7 mm (0.5 inches) was selected.

The length of the reduced wall thickness section was maximized to ensure strain uniformity throughout this section. Ideally the reduced thickness section would have no changes in cross-section geometry over a length between three to five times the pipe diameter (per communication with Vishay Precision Group). This was practically impossible given the overall pipe section length and space requirements for other components. In the end the length of the reduced cross section for axial strain measurement was 124 mm (4.875 inches).

The axial force Wheatstone bridge was installed on the outside of the reduced pipe section. Two CEA-06-250UT-10C strain gages (Table 3.2) manufactured by Vishay Micro Measurements comprised in each arm of the strain gage bridge to complete Poisson's bridge.

These Tee Rosettes strain gages were mounted in 4 locations at the same distance from the end longitudinally, but 90 degrees apart on the diameter. 34 gage wiring connected the strain gages and a 26 gage four conductor cable was used to relay the strain gage measurements through a hole in the pipe section wall to the downhole computer. Figure 3.3a presents a schematic of the system while Figure 3.3b presents a picture after gage installation. Gages were installed following methods specified by Vishay Micro Measurements with M-Bond 610 epoxy for gage mounting. The bridge was protected and waterproofed using the M-Coat F coating system by Vishay Micro Measurements. As evident in Figure 3.4, the strain gages were located in an annulus between the reduced pipe section and a thin cylinder used to measure radial stress (described in section 3.4.1.2). This annulus was sealed with O-rings for waterproofing.

#### 3.4.1.2 Radial Stress Measurement

Radial stress (i.e. lateral earth pressure) measurement is a long-standing challenge in geotechnical engineering. It is particularly challenging in this system due to the durability requirement (must survive during pile driving) and the expected low radial stress to be acting on the pile. The radial stress was measured using hoop strain measurements of a thin cylinder (2.54 mm (0.1 in.) thickness and 140 mm (5.5 in) in length) fabricated from 4140 alloy steel.

The thin walled cylinder was strain gaged to measure hoop strain and axial strain (to separate Poisson's effects on hoop strain measurements) in the section. The thin walled cylinder was isolated from the axial load transfer of the pile using a set of Delrin positioning

rings and waterproofing elastomer O-rings. As detailed in section 3.5.3 below, this design was complicated and required several iterations. Early versions using the Delrin material alone for positioning the cylinder resulted in the thin cylinder deforming (becoming egg-shaped), allowing soil into the annulus where the strain gages were positioned. The Delrin rings combined with O-rings in the direction of transferring axial load improved the positioning of the thin cylinder without transferring dynamic axial load from the hammer into the thin cylinder.

Half bridge circuits were used to measure the hoop strain and axial strain of the thin walled cylinder separately. CEA-06-250UT-10C strain gages manufactured by Vishay Micro Measurements (Table 3.2) were mounted on the inside of the thin cylinder using the same techniques described in the previous section. In active bridge completion resistors of 2000 Ohms were installed within the computer (GST) module to complete the Wheatstone bridge.

A diagram and picture of thin wall cylinder assembly in a RTP unit, including assembly of the Delrin ring, load isolation O-ring, and water sealing O-ring, is presented in Figure 3.4a and 3.4b.

#### 3.4.1.3 Pore Pressure & Acceleration Measurement

Pore pressure sensors and accelerometers were mounted on a custom bulkhead unit that mounted directly to the pipe wall from inside. The direct mounting was critical to ensure complete coupling of the accelerometer with the pipe section. It was also important to evaluate the potential of obtaining dynamic pore pressure measurements during driving.

The accelerometer selected was a model 1221L-1000 manufactured by Silicon Design for special order with 1000 g range (Table 3.2). The pore pressure transducer selected was a model ABH500PSC1B manufactured by Honeywell with a 500 psi range (Table 3.2).

The bulkhead module was comprised of two components and the pore pressure transducer was secured between them. The side facing the internal pipe wall was machined with same curvature as the wall to have a tight, waterproof seal. O-rings were used between the module and wall, and between the module and the pressure transducer, to ensure complete sealing of the module. In addition, a through hole and a recess for placement of a porous element were machined into the exterior pipe wall between four mounting bolts. The accelerometer was secured tightly to the top of the module using a bolt and epoxy. The module was located 111 mm (4.375 in) from the strain gages measuring axial resistance. Figure 3.5a shows the module assembly on RTP wall and Figure 3.5b shows a picture of the components.

In the field, porous stones were saturated in 1000 cSt viscous silicone oil under 100 kPa vacuum. Porous stones were submerged under vacuum until no air bubbles emerged from the silicone oil. Silicone oil was injected using a long needle to fill the cavity between the pore pressure sensing face and the outer pipe wall. Vacuum was then applied for 5 minutes to the hole with the outer surface of the RTP in an upright position. After the vacuum in the field, a saturated synthetic porous filter was placed in the hole and covered with a masking tape to prevent drainage during handling. Images from the saturation process in the field are shown in Figure 3.6.

#### 3.4.1.4 Vibration Isolation System for Downhole Data Acquisition Unit (GST Module)

The GST was selected to be used in field to acquire the desired data and at the same time, small enough to fit inside the pipe section. The customized downhole data acquisition unit (GST module described below in section 3.4.4.1) must be isolated from the 1000+g dynamic loading that the RTP pipe is subjected to during driving. To accomplish this, a custom enclosure for the GST module was developed and this enclosure was mounted within a spring-dashpot type damping system. The custom enclosure was fabricated from Delrin (selected due to its durability, machinability, and low unit weight) and contained stainless tube sections at each end of the Delrin box that sensor cable connectors passed through to connect with the internally mounted computer. Once installed, the enclosure was filled and sealed with epoxy to provide complete waterproofing.

The GST module enclosure was then mounted between two guide rails to prevent rotation. Damping material (i.e. springs, rubber, etc.) was installed around the stainless tube sections and cross-brackets secured the damping material in place. The vibration isolation system design was versatile as it allowed for evaluation of numerous different combinations of damping materials. Testing included laboratory drop hammer testing as well as a field trial. Details of this testing is provided in section 3.5.3.1. The end result of this testing sequence was selection of a helical compression spring and soft Sorbothane rubber (manufactured by Sorbothane, Inc., website: www.sorbothane.com) disk combination. Initial deformations were absorbed by the compression spring. After travel of 10.2 mm (0.4 in.) the 25.4 mm (1 in.) thick Sorbothane rubber disk began to compress. Deformations continued until the rubber absorbed

the energy and displacements reversed directions. Overall, the vibration isolation system was shown to reduce 1000 g accelerations on the pipe to less than 250 g accelerations on the GST module enclosure.

Figure 3.7 presents a schematic of the GST module and vibration isolation system assembled inside the RTP unit. Figure 3.8a shows a picture of GST modules curing in the lab after being filled with epoxy. Figure 3.8b shows a picture of an assembled GST module inside the pipe section.

### 3.4.2 Closed Ended Instrumented Driving Shoe

Recognizing that separation of base resistance from shaft resistance is critical for pile analysis and design, extra efforts were made in instrumenting the pile tip. A custom closed-ended tip section was developed for the RTP system.

The closed ended tip section was 41.9 cm (16.5 inches) long with a diameter equal to the pipe sections (16.8 cm (6.625 inches)), made of 4140 alloy steel, and having same threads to connect with regular Becker pipes. A schematic diagram of the instrumented driving shoe section is presented in Figures 3.9. Instrumentation included only axial strain and acceleration. The axial strain measurement was accomplished using the same sensors, wiring scheme, and waterproofing sealant system as that used for the other instrumented sections (described above in Section 3.4.1.1). The exception was that the strain gages were mounted on the inside of the pipe section directly where the wall thickness was 2.0 cm (0.8125 inches). The strain

gages were mounted at a distance of 21.6 cm (8.5 inches) behind the tip of the pile. The accelerometer sensor (the same used in the instrumented sections and described above in Section 3.4.1.3) was mounted directly on the back of the solid steel tip (see Figure 3.9), resulting in positioning at a distance of 12.7 cm (5 inches) from the tip face. Table 3.2 summarizes the specification of sensors mounted on driving shoe.

Due to the short length of the driving shoe there was insufficient space to install a data acquisition system (GST module). Instead, one instrumented section (S1) was equipped with an additional computer board such so that the driving tip sensors (acceleration, axial load) could be measured in addition to the standard sensors mounted in the instrumented pipe section above the shoe.

### 3.4.3 Above Ground Measurements

The instrumentation above ground, outside of the Becker pipe string, focused on measurement of the RTP displacement during dynamic driving and static load testing and on the bounce chamber pressure that develops within the Becker hammer during driving.

Displacement monitoring of the RTP during pile driving was accomplished using a long string potentiometer with a range of 6.35 m (250 inches). The instrument base was mounted on the base platform of the driving guide and the wire was extended and connected to a cap positioned between the top of the RTP and the hammer driving spout. The resolution of the string potentiometer was sufficient to detect displacements of about 1 mm. The long string

potentiometer used was manufactured by Celesco Transducer Products, Inc. and the sensor model number was PT5A-250-N34-UP-500-M6M.

Displacement monitoring during static RTP pull-out (tension) tests used the long string potentiometer described above as well as a second shorter range string potentiometer (range of 25.4 cm, 10 inches). The shorter instrument base was mounted on an isolated aluminum reference beam that was referenced to the ground surface a distance of about 3 m (9.8 ft) from the RTP installation location. This was important as nearby surface ground and/or Becker rig movements during the pile load tests affected the long string potentiometer measurement. The higher resolution short range string potentiometer referenced to stable ground provided a more accurate displacement measurement for the static RTP load tests. The short string potentiometer used was manufactured by Celesco Transducer Products, Inc. and was sensor model number PT1A-10-UP-500-MC4.

A pressure sensor was connected to the Becker hammer system to continuously measure the chamber pressure. The chamber pressure refers to the pressure that accumulates in the sealed chamber above the Becker impact mass when the impact mass rises following a hammer impact and the associated diesel combustion. The chamber pressure, typically referred to as the 'bounce pressure', provides an indication of the energy being applied by the Becker hammer (Harder and Seed 1986, Harder 1988). It is dependent on both the operation conditions of the hammer (which is operator controlled) and the driving conditions. Generally, higher bounce pressure reflects harder driving conditions. It is typical to record the maximum bounce pressure using an analog pressure gage for the Becker Penetration Test (Harder and

Seed 1986). In the RTP system the bounce pressure was measured continuously during RTP driving. The pressure transducer used was the same as that installed on the instrumented pipe sections to measure pore pressure in the ground, and was manufactured by Honeywell and was sensor model number ABH500PSC1B.

Figure 3.10 shows the pictures of above ground sensors in field application. Table 3.3 summarizes the specification details of sensors used above ground.

### 3.4.4 Data Acquisition System

Measurement of all of the above sensors, which totaled more than 30 when the RTP was fully assembled, was performed with two different data acquisition systems. All instrumentation within the RTP instrumented and tip sections were recorded with the Geodaq GST modules and a GCM control module. The displacement and pressure measurements obtained above ground were recorded with a LabVIEW based National Instruments data acquisition system. During RTP testing in the field, an operator coordinates and controls operation of each system. A schematic showing the overall wiring and layout of both data acquisition systems is presented in Figure 3.1.

#### 3.4.4.1 Geodaq data acquisition RTP Measurements

The down hole data acquisition system in the RTP was necessary to collect, filter, gain, and digitize data in close proximity to the sensors. After evaluation of numerous commercially available data acquisition systems it was determined that only the GST/GCM system by GeoDaq, Inc. could meet, with limited customization, the performance requirements outlined above in Section 3.2.

The Geodaq system consists of GST modules positioned within each instrumented section, a GCM controller located above ground, and a 12 V DC power supply. The GST modules are downhole signal conditioners and data acquisition computers potted in the custom Delrin housing (Section 3.4.1.4) and vibration isolated from the RTP pipe sections. Each sensor channel on the GST module was dedicated to a specific sensor and provides 5 Vdc excitation to the sensor, amplifies and filters the signal as required, and then digitizes the signal. The GST modules can digitize data at a varying sampling frequency from 200 Hz to 8333 Hz. The analog to digital conversion of each signal was performed at 16 bit resolution.

Digital communication and data transmission enables the use of a single cable that is daisy-chained between all instrumented sections. The single four wire cable provides power to all of the modules and facilities digital communication. The use of a single robust cable was critical for practical operation; separate four-wire cables for each sensor would be practically prohibitive when adding additional pipe sections during RTP installation.

Control of the data acquisition occurs through the GCM which is commanded by the computer software. Variables that can be controlled include the sampling frequency, number of sample points in a sampling event, delay period between sampling events, and specification of which GST modules (i.e. which sensors) are to be sampled. The control software is command line based.

Once a command is sent to the GCM, the GCM communicates the sampling protocol with all downhole GST modules. The GST modules then excite the sensors, filter and gain the analog signals, convert the signal to a digital form and buffer the data locally, and transmit the recorded digital signals up to the GCM. The GCM deciphers the digital transmissions from all GST modules and writes tab delimited data files to the computer. The transmission time of the signals from the GST modules to writing of the data file in the computer is dependent on the number of GST modules, number of channels on each GST modules being sampled, and number of samples in each event. Typically GST modules will complete transmission and will be ready for the next sampling event in about 20-60 seconds depending on number of GST modules sampled at maximum recorded points.

Operation of the Geodaq system was most intensive during driving installation of the RTP. Data was collected at the maximum sampling rate of 8333 Hz with a maximum of 20,000 data points recorded per channel. Following data recording for about 2.4 seconds a transmission time of about 50 seconds was required to transfer the data from all of the GST modules up to the GCM controller and to write a composite data file to the computer. During load testing, the number of sampling points was reduced to 1000 to reduce the sampling period

in order to have quicker data transfer to computer and more frequent data collection. During pile setup (over a period of 3+ hours), a different approach was used. Short sampling events at a high frequency were performed at specific time intervals. The average value during each sampling event was reported as the representative value. This mode of operation enabled the time delay between sampling events to be varied in time in a manner consistent with pore pressure dissipation trends (i.e. the required sampling frequency decreased as a function of the logarithmic trend). The sampling frequency and number of points sampled with the different operational conditions of the RTP during field testing is provided in Table 3.4.

#### 3.4.4.2 National Instruments DAQ for Above Ground Measurements

A National Instruments based data acquisition system (referred to as NI-DAQ herein) was developed for recording of the above ground displacement and pressure sensors. A separate data acquisition system was necessary as continuous recording of RTP displacement during driving was necessary as sampling requirement, digital communication, robustness and small size requirement for above ground unit is significantly different than the downhole system. The NI-DAQ system operated continuously during driving while the Geodaq system recorded intermittently during driving. Synchronization of the two systems was approximately coordinated based on the computer clocks.

The NI-DAQ system consisted of signal conditioner units powered with a 24Vdc power supply and National Instruments data acquisition board. The signal conditioner units used for

the string potentiometers were manufactured by Phoenix Contact and were model number Phoenix MCR Strain Gage (LN). The signal conditioner units used for the bounce chamber pressure were manufactured by Advantech and were model number ADAM 3016. For the string potentiometers, the conditioners only served as 10V excitation sources as the proportional voltage signal did not need to be conditioned before being connected to the data acquisition board. For the pore pressure transducer, an excitation voltage of 5V was supplied and filtering and gaining was applied to the received signal. A USB based data acquisition board model number NI-USB 6218 was used to sample the data. The components of the NI-DAQ are described in Table 3.5. Table 3.6 presents the signal conditioner models and gains used through the signal conditioner for data acquisition.

A custom NI LabVIEW software program developed at UC Davis was used to record during testing. During RTP dynamic driving and load testing all sensors were sampled continuously at a 200 Hz sampling frequency. The sampling frequency was dynamically (on-the-fly) reduced to 2 Hz during waiting periods such as when attaching an additional Becker pipe section. This reduction in sampling rate helped to avoid collection of unnecessary data to ease data management.

## 3.5 Field Testing Performed During RTP Equipment Development

Although much of the RTP design was accomplished by theoretical calculations and applying sufficient safety factors, it was essential to evaluate prototypes experimentally in either the laboratory or in the field prior to production of multiple units. The three primary prototype testing events are presented in this section. In chronological sequence, these testing events were used to (1) evaluate the optimum Becker wall thickness for measuring axial strain during driving, to obtain direct field measurements of the axial acceleration and forces that are generated during Becker hammer operation, and gain practical exposure to how the Becker system operates, (2) assess and verify the performance (durability, reliability, accuracy) of all sensors selected and their respective mounting systems under full scale operational conditions, and (3) optimize and finalize the design and configuration of the GST module vibration isolation system. The results of each of these evaluation programs are presented in the following sections.

### 3.5.1 Determination of Optimum Wall Thickness for Measurement of Axial Resistance and Performance of Becker Hammer System

Field testing experience with the Becker system was necessary to evaluate (1) performance of Becker hammer during dynamic driving, (2) to optimize the pipe wall thickness selected for axial strain measurements, and (3) to have practical hands-on understanding so that the RTP design would be compatible and relatively user friendly during operation. In

particular, representative axial acceleration and force time histories during nominally easy and hard driving conditions were necessary for design of the RTP system to progress. Second, theoretical calculations indicated that the wall thickness of the instrumented Becker system could be much thinner than that minimum thickness that existed in the commercially produced standard pipe section. Practical field testing was necessary to discern the appropriate balance between theory and practice. Third, the eventual success of the RTP system hinges largely on its practically. As such, it was important for the research team to have a basic understanding of how the Becker system operates and what considerations must be made in the RTP design process.

Field testing was performed with the Becker system in coordination with Great West Drilling Inc., the primary Becker testing company in the western United States. The testing program was relatively simple, and consisted of repeated dynamic loading with the Becker hammer onto a pipe section with sections of varying thicknesses. The instrumented pipe test section was prepared from a 45.7 cm (18 in.) long, 16.8 cm (6.625 in) outer diameter and 12.7 cm (5 in.) inner diameter (wall thickness of 2 cm) 4140 alloy steel pipe. The outer and inner diameters and the material of this section were identical to the conventional Becker pipe. The test section was machined in three sections with reduced outer diameters of 15.88 cm (corresponding wall thickness of 1.59 cm), 15.56 cm (1.43 cm wall thickness), and 15.24 cm (1.27 cm wall thickness) as shown in Figure 3.11a. These three sections and a full thickness section were instrumented to measure the axial strains (force) during hammer impacts. In each section a full Wheatstone bridge was installed using two tee rosette strain gages (Manufactured by Vishay Micro Measurements, model CEA-06-250UT-10C). In addition, two 500 g

accelerometers were attached to opposite sides of this test section to measure axial acceleration. A picture of the section attached with the strain gages is shown in Figure 3.11b.

The instrumented test section was positioned between the Becker hammer and a large I-beam that was lying on a gravel deposit. A schematic of the setup is shown in Figure 3.12. The steel I-beam had dimensions of 30.5 cm width by 30.5 cm tall by 152 cm long. The purpose of the I-beam was to prevent the test specimen from being driven into the soil during driving (since gaging and wiring was on the outside of the pipe section) while still allowing the underlying soil to provide representative damping. Testing was performed with two different Becker hammer impact energy levels. Qualitatively these are described as "low" and "high" energy levels. The "low" energy represents the minimum practical system performance that can be controlled by the operator while the "high" energy represents the maximum performance of the Becker system.

Results from field testing and subsequent recalibration of the system in the laboratory led to a conclusion that a wall thickness of 1.27 cm (0.5 in.) was appropriate for the final design. The following observations contributed to this decision. Thicker wall sections resulted in reduced resolution of the axial load. Thinner wall sections exhibited no differences in the calibration factors before and after testing, indicating no possibility of measurable permanent deformations during the test. On the other hand, the minimum wall thickness on commercially available Becker pipe sections that transfers axial load (shoulder at the end of pin threaded section) is 0.95 cm (0.375 in). The acceleration and force time histories also indicated that accelerations can reach high as 1000 g and axial forces can be high as 1000 kN (225 kips). These

values were confirmed with typical Becker hammer records measured by Pile Driving Inc. (PDI). Representative recorded accelerations, axial load measurements, and the micro-strain generated in the 1.27 cm (0.5 in.) thick section from low and higher energy impacts are presented in Figure 3.13.

### 3.5.2 Verification of Instrumentation Setup and Performance of Sensors during Field Driving Conditions

Verification of the final design for the RTP instrumentation design was necessary prior to production of multiple sections. This included evaluation of both the sensors themselves as well as the mounting systems that house the sensors on an instrumented section. In this testing all sensors were individually wired directly to up-hole signal conditioning modules, which were in turn connected to a National Instruments data acquisition unit that was controlled by custom LabVIEW software; as a result, no evaluations of the Geodaq system or the vibration isolation system were performed at this stage. Figure 3.14 presents a schematic of the tested design.

Field testing occurred at the Oakland, CA site described in Chapter 4 and utilized for the final testing program of the RTP described in detail in Chapters 5 and 6. In short, it is a site with several meters of fill underlain by young bay mud, which in turn is underlain by two dense sand layers with a softer clayey sand layer between them. Testing was performed by Great West Drilling, Inc., using their standard Becker penetration rig.

The fully instrumented 61 cm (2 ft) long RTP section, with an uninstrumented 42 cm (16.5 in.) tip section, was driven into the ground to a depth of 12.5 m (41 ft) in the multilayered soil profile, terminating in the lower dense sand layer. A second RTP section, instrumented to measure axial load only, was attached to the top of the Becker pipe string to measure the load being applied by the Becker hammer above ground. Pullout tensile load tests were also performed to evaluate the performance of the above ground linear potentiometers and to assess the ability of the Becker rig to perform slow pullout tests. Data was recorded from both instrumented sections during driving and pullout testing. Images during testing are shown in Figure 3.15.

Calibration of the sensors in the laboratory after testing (methods are described in Section 3.6) proved the reliability of instrumented section design and selection of sensors. Overall, both performed well in harsh driving environment. All sensors maintained linearity and exhibited no drift or shift in the calibration constants. The mounting systems for all sensors survived driving conditions. It was noticed that special attention must be paid to saturation of the pore pressure system; this process was improved, resulting in the method described above in Section 3.4.1.3. The primary concerning result was the significant amount (about 10 %) of axial load that was transferred to thin walled cylinder section designed to measure only the radial stress. This section was designed to be axial force isolated with the Delrin rings at the ends while underlying O-rings maintained the water seal. Figure 3.16 shows the arrangement of O-rings and Delrin rings as tested in the field. It was determined that the Delrin rings, which is a stiff plastic material and were machined to tight tolerances to avoid soil penetrating into

any gap between the thin walled sleeve and the ring, were loaded during elastic pile compression.

### 3.5.3 Development of GST Module Vibration Isolation System and Improvement to Load Transfer Mechanism on Section Measuring Radial Stress

The vibration isolation system developed to isolate the down hole GST modules from dynamic hammer loading and the modification of the Delrin ring design to prevent dynamic axial loads from affecting radial stress measurements were evaluated through a third field testing program. This testing program was performed in the UC Davis structural engineering laboratory and at Great West Drilling Inc.'s, headquarters at Fontana, CA. The field site consists of relatively thin layer of fill material below which a soft stone caliche formation exists.

#### 3.5.3.1 Development of Vibration Isolation System

As mentioned above, a relatively simple spring-dashpot type vibration isolation system was developed to protect the GST modules from the hard Becker driving conditions. The system, discussed previously in Section 3.4.1.4 above, basically consists of a Delrin protective housing for the GST module that translates vertically. Its vertical travel is limited rigidly by two aluminum cross-bars and Sorbothane damping material and it is prevented from rotating by side notches in the protective housing which guide movement along the side rails.

Optimization of this system was directly dependent on the configuration of materials/parts required to provide the damping. The device design allowed +/- 1.0 cm (+/- 0.4 in.) of vertical travel with compression of the spring and further travel with compression of damping material. Numerous different types of damping materials and springs with different thicknesses, stiffnesses, etc. were evaluated.

The vibration isolation system was first evaluated and optimized in the UC Davis structural engineering laboratory using a manual drop test system. The laboratory hammer system consisted of 227 kg (500 lb.) mass that could be dropped from a maximum height of 1.35 m (53 in). The potential energy that could be generated in the laboratory was about 25% of the nominal value for the Becker hammer system (Table 3.7). Since the Becker hammer itself typically operates at about 30% energy efficiency (Sy 1983) the laboratory system can be considered roughly comparable to field driving energy. The test operation was as follows. The tip section, with the instrumented section connected behind, was placed with the tip partially embedded into sand inside a large container. The dead weight was dropped, directly impacting the top of the instrumented section. Accelerations on the pipe wall and on the isolated GST module container were recorded and compared to evaluate the amount of damping provided for a given configuration.

After many laboratory trials, it was concluded that the combination of a 3.6 cm (1.4 in.) long compression spring with a spring constant of 2.45 N/mm (14 lbs/in) and a 2.5 cm (1 in.) thick disk (3.81 cm (1.5 in) outer diameter, 1.9 cm (0.75 in) inner diameter cylinder) of Sorbothane (www.sorbothane.com, durometer: 80, shore 00) elastic damping material was the

best combination. The spring and damper assembly in a RTP section is also shown in Figure 3.7. Figure 3.17 shows the acceleration comparison obtained from one of the laboratory drop tests performed with this configuration.

The instrumented section with the vibration isolation system was then tested in the field under very hard driving conditions. After penetration to ~2 m (6 ft) depth the blows per 0.3 m of penetration exceeded 150. The total depth of driving was 5 m (16 ft). The vibration isolation system as well as the GST module performed well throughout driving. Acceleration comparisons between the instrumented pipe section and the vibration isolated GST module are shown in Figure 3.18. The GST module itself performed throughout testing with no damage occurring.

#### 3.5.3.2 Modification to Reduce the Dynamic Axial Load Transfer into the Radial Stress Measurement Section

Modification of the system that positioned the thin walled cylinder designed to measure radial stress was required based on the field testing reported in Section 3.4.2. The problem was undesired partial transfer of the axial load to the thin walled cylinders through the Delrin positioning rings. To mitigate this problem, soft elastomer O-rings were introduced between the instrumented pipe and the Delrin rings (which were reduced in width). These O-rings provided additional cushion during dynamic loading. The modified section design is shown in Figure 3.19. The design modification was successful during both the laboratory and field tests

in nearly eliminating the amount of axial force in the pipe transferred to the thin walled cylinder (i.e. < 1% transferred). However, field testing in the soft stone deposit revealed that under very hard driving conditions the radial stress cell section is vulnerable to damage. Figure 3.20 shows the damaged section after extrusion from field testing. This is not surprising given the small thickness of the section and potential for it to deform radially. This indicated that the thin walled section likely would not perform well if driving conditions exceeded about 100 blows per foot.

Following the field testing results, the instrumented design was re-evaluated to determine if the radial stress measurement could be made more robust while maintaining sufficient measurement sensitivity. It was decided that minor modifications were not possible with the given geometric space constrains. Therefore, the system must be entirely re-designed to explore another system. In consultation with Caltrans it was decided that the current design be adopted for the RTP system with the understanding that the radial stress measurement system may fail under hard driving conditions.

## 3.6 Calibration Methods for the RTP

The RTP components were tested and calibrated before and after field testing. Calibrations were performed with field condition configurations; i.e. all communication cables, down hole GST modules, above ground computer control (GCM controller), and laptop were used to capture system effects. The entire system was calibrated for static loading in the

laboratory at the University of California, Davis. This section presents calibration of sections measuring axial load, radial stress, and pore pressure. Other sensors (accelerometer) were also tested in the laboratory for quality control.

### 3.6.1 Calibration of Axial Load Section

Six instrumented pipe sections as well as the instrumented tip section were calibrated in the laboratory. Sections were calibrated up to the maximum compressive design load of 1000 kN (225 kips) in load increments of 222 kN (50 kips) using the 1780 kN (400 kip) capacity Tinius Olson load frame. The sections and tip were always conditioned with at least 10 cycles of pre-loading before calibration. Calibration load cycles were performed in triplicate to ensure repeatability and to assess consistency of the calibration factor. The coefficient of determination ($R^2$ value) for the linear regression was used to assess the quality of the calibration. The statistical term $R^2$ value equal to 1.000 indicates a perfect correlation and lower values indicate a poorer fit. The calibration process is shown in Figure 3.21 and calibration results are presented in Table 3.8.

Calibration results before the field testing program described in Chapters 5 and 6 shows very high $R^2$ values. All sections met the desired performance level prior to field testing. Following the field testing recalibration of sections S2 and S5 exhibited similar performance. Recalibration of sections S0 (tip) and S1 ($1^{st}$ instrumented section) were not possible due to RTP section damage during the second day of testing (Installation 2). The wiring of axial gages was

ruined as soil entered through the failed radial stress section. The axial load measurement on section S4 began malfunctioning at the beginning of Installation 1 (day 1) and therefore this section was also not available for recalibration (It was later determined that the malfunction was due to a loose soldering connection). Section S3 exhibited a scattered response at lower loading and unloading conditions during recalibration. This behavior is reflected in its lower $R^2$ value. However the change in the overall calibration factor was less than 1.5% for this section. Section S5 (above ground) and section S2 did not show any sign of permanent deformation or damage to strain gauge wiring. The total changes in the calibration factor for these units were less than 1%.

### 3.6.2 Calibration of Radial Stress Section

Four instrumented sections (i.e. all sections except the tip (S0) and above ground section (S5)), contained radial stress measurements on the thin walled cylinder. The radial stress acting on the thin walled cylinder was recorded in terms of hoop strain using strain gages mounted to the inside of the cylinder. Technically, deformation of the thin walled cylinder is due to both radial compression inducing hoop strains as well as Poisson's effect hoop strain induced by axial strain. A method for calibration for both the radial and axial deformation of the thin walled section independently was developed and reported herein. The axial strain calibration was used to assess the amount of load transfer to the thin walled section through the Delrin rings described earlier. However, the axial strain measurement in the thin walled cylinder was not used in data reduction or reporting of radial stress values in later chapters due

to the damage incurred in the thin walled sections during testing and due to the small amount of load axial load transferred from the pipe section to the thin walled cylinder being much smaller than that due to the hoop strain.

A new system was developed for calibrating the strain gauged thin wall cylinder in the laboratory. A cylindrical calibration chamber (Figure 3.22) with a pressurized inner bladder was used. The inner bladder expanded between two solid walls and applied uniform radial pressure on the thin walled cylinder. Assembly of inner tube and pressure chamber is illustrated in Figure 3.23. An initial loading and unloading sequence was performed to ensure proper seating of the pressurized bladder. The pressure was varied from 0 to 550 kPa (0 - 80 psi) in increments of 138 kPa (20 psi). 550 kPa (80 psi) loading was the design value determined considering the maximum expected penetration depth of the RTP. An air pressure regulator with a pressure gage was used to control the applied pressure. Figure 3.24 shows the pressure regulator and pressure gage used in the calibration process.

The radial stress calibration results before and after the field testing is presented in Table 3.9. Calibrations show good correlations before the field testing. Due to hard driving conditions encountered at the end of Installation 2 most radial sections were physically damaged. Even not visually damaged sections sustained wiring/gaging damage, resulting in recalibration being impossible after field testing.

The four RTP sections (S1 to S4) containing the radial stress measurement arrangement were also calibrated for axial load. The ability to measure the axial load helped assess the axial load transferred to the thin walled cylinder during loading of the pipe. The thin wall cylinder

alone was axially loaded to a maximum load of 67 kN (15 kips) in load increments of 11 kN (2.5 kips). Multiple loading and unloading cycles were applied initially to ensure proper seating.

The calibration results of axial load measurement on the thin walled sections are presented in Table 3.10. Calibrations show good correlation before the field testing. As described above, damage during field testing resulted in recalibration after testing being impossible.

### 3.6.3 Calibration of Pore Pressure Transducer

Four instrumented sections (i.e. all sections except the tip (S0) and above ground section (S5)), were instrumented with pressure transducers. The bounce chamber pressure of the Becker hammer also measured with the same model pressure transducer. All the transducers were calibrated in the laboratory. Pressure sensors installed on the RTP sections (see Figure 3.5) were calibrated in their assembled condition to ensure complete sealing of the sensor within the mounting bracket and of the mounting bracket to the pipe wall. The transducer used for the measurement of bounce chamber pressure was calibrated with the fixture used to connect to the Becker hammer system in the field.

The sensors assembled in the RTP sections were calibrated with the field data acquisition in place; i.e. the sensor was connected to the GST module, which in turn was connected to the GCM controller. This approach captures any effects of the data acquisition

system on the calibration factor. Similarly, the pressure sensor used to measure bounce chamber pressure was calibrated with the NI-DAQ field system.

Calibration of the pore pressure sensor assembly in the RTP section consisted of the following steps. A mounting bracket that created a sealed connection with the outside of a pipe was installed and secured with vacuum grease and hose clamps. The fluid cavity in the pipe wall and bracket was filled with water and connected to a burette filled with water. Vacuum was applied to remove any air entrapped in the water and to ensure proper sealing of the bracket to the pipe wall. During calibration the water in the burette was pressurized with compressed air. The water level during calibration was monitored to ensure that no leakage occurred during pressurization. Figure 3.25 shows the calibration process of the pore pressure transducers.

The calibration results for the pore pressure transducers are presented in Table 3.11. The $R^2$ values show high correlation of calibration factors both before and after field testing. There is no significant change in the calibration factors either, with a maximum deviation of 0.7% before and after the field testing observed for the pore pressure sensor installed in section S2.

### 3.6.4 Calibration Factors for Accelerometers and String Potentiometers

Factory calibration factors for the accelerometers and string potentiometers were used. All were tested and verified in the laboratory against calibrated reference sensors.

## 3.7 Summary

This chapter has presented the design and specifications of the new RTP system, including details of mechanical components, sensor selection, configuration, mounting, and calibration, and data acquisition systems. A series of intermediate testing programs were required to test and evaluate prototype designs before the final RTP system was fabricated. Particular challenges in the design were the downhole computer isolation system, radial stress measurement system with the thin walled cylinders, and saturation of the pore pressure sensor. As detailed in the following chapters, the RTP system overall performed well in the first comprehensive RTP field testing program, providing valuable data and demonstrating feasibility while also revealing areas where the design should be further improved.

**REFERENCES**

Fioravante, V., (2002). "On the shaft friction modeling of non-displacement piles in sand." *Soils and Foundations,* 42(2): 23-33.

Harder, Jr., L.F., (1988). "Use of penetration tests to determine the cyclic loading resistance of gravelly soils during earthquake shaking." *PhD thesis, University of California, Berkeley,* CA. 465p

Harder, Jr., L.F. and Seed, H.B., (1986). "Determination of penetration resistance for coarse-grained soils using the Becker hammer drill." *Report UCB/EERC-86/06, Earthquake Engineering Research Center, University of California, Berkeley*, CA. 144p.

Sy, A., (1993). "Energy measurements and correlations of the Standard penetration test (SPT) and the Becker penetration test (BPT)." *Ph.D. thesis, Department of Civil Engineering, University of British Columbia,* Vancouver, BC, Canada, 213p.

## TABLES

**Table 3.1: Summary of measurement priorities during different operation modes.**

| Measurements | Operation Modes | | |
|---|---|---|---|
| | **Driving** | **Load Test** | **Setup** |
| **Axial Load** | • Axial resistance to penetration<br>• Measure axial load to compare with PDA<br>• Skin friction can calculate from adjacent axial load measurements<br>• End bearing and skin friction component<br>• Residual stress | • Load capacity during load test<br>• Skin friction and end bearing component | • Not a primary measurement during pile setup |
| **Acceleration** | • Acceleration record for PDI type analysis. From acceleration to velocity to force. | • Not a primary measurement during load testing | • Not a primary measurement during pile setup |
| **Pore Pressure** | • Dynamic pore pressure generation<br>• Effective stress analysis | • Effective stress analysis | • Pore pressure dissipation over time<br>• Effective stress analysis |
| **Radial Stress** | • Radial stress during impact | • Radial stress during load testing | • Radial stress gain over time |
| **Inclination** | • Position of sensors with depth | • Position of sensors with depth | • Position of sensors with depth |
| **Temperature** | • Sensor correction | • Sensor correction | • Sensor correction |
| **Vertical Displacement** | • Number of blows / foot<br>• Drivability | • Displacement with load | • Not useful |
| **Chamber Pressure** | • Drivability<br>• Hammer efficiency | • Not a primary measurement during load testing | • Not a primary measurement during pile setup |

**Table 3.2: Sensors used in a RTP instrumented pipe and tip sections.**

| Sensor Type | Manufacturer / Model # | Measurement / Location |
|---|---|---|
| **Strain Gage** | Micro Measurements CEA-06-250UT-10C | • Axial resistance measurement<br>• Radial stress measurement<br>• Axial load transferred in thin wall cylinder |
| **Accelerometer** | Silicon Design 1221L-1000 | • Measures acceleration<br>• Attached to pore pressure module |
| **Pore Pressure Transducer** | Honeywell ABH500PSC1B | • Pore pressure measurement<br>• Secured with pore pressure module |
| **Temperature Sensor** | National Semiconductor LM20 | • Temperature<br>• Close to both set of strain gauges (Axial and Radial Measurements) |

**Table 3.3: Summary of sensors used above ground during pile installation, setup, and load testing.**

| Sensor | Manufacturer / Model | Measurement / Location |
|---|---|---|
| **String Potentiometer (250")** | Celesco / PT5A-250-N34-UP-500-M6M | • Displacement during pile driving and load test |
| **String Potentiometer (10")** | Celesco / PT1A-10-UP-500-MC4 | • Displacement during load test |
| **Pore Pressure Transducer** | Honeywell ABH500PSC1B | • Bounce chamber pressure |

**Table 3.4: Specification of sensors used in downhole with Geodaq.**

| Sensor | Signal Conditioner Model | Gain | Applied Excitation Voltage (V) | Signal Type |
|---|---|---|---|---|
| **Strain Gage** | Micro Measurements CEA-06-250UT-10C | 100 | 4.096 | Differential |
| **Accelerometer** | Silicon Design 1221L-1000 | 0.73 | 5 | Single ended |
| **Pore Pressure Transducer** | Honeywell ABH500PSC1B | 20 | 5 | Differential |
| **Temperature Sensor** | National Semiconductor LM20 | 0.73 | 5 | Single Ended |

**Table 3.5: Sampling rate, sample points, and sampling frequency used for different operating modes with the Geodaq system.**

| Operation Mode | Sampling Rate | Number of Sample Points | Desired time delay between samples (sec) |
|---|---|---|---|
| **Driving** | 8333 | 20000 | 1 |
| **Load Testing** | 8333 | 1000 | 1 |
| **Pile Setup and sensor calibration** | 8333 | 1000 | Varies starting from 1sec (increases with time) |

**Table 3.6: Components of NI DAQ system.**

| Component | Model | Function |
|---|---|---|
| **NI USB data acquisition unit** | NI-USB 6218 | Data acquisition, Digitize signals |
| **Phoenix Signal Conditioner** | Phoenix MCR-Strain Gage (LN) | Excitation, Gain and Filter |
| **ADAM Signal Conditioner** | ADAM 3016 | Excite the sensor, gain the signal |
| **DC Power Supply** | EGS Sola Heavy-Duty | 24 V DC power supply from AC supply, Excite the signal conditioners |

**Table 3.7: Gain and filters used for above ground sensors with NI-DAQ.**

| Sensor | Signal Conditioner Model | Gain | Applied Excitation Voltage (V) | Signal Type |
|---|---|---|---|---|
| **String potentiometer (250")** | Phoenix MCR-Strain Gage (LN) | 1 | 10 | Single Ended |
| **String potentiometer (9")** | Phoenix MCR-Strain Gage (LN) | 1 | 10 | Single Ended |
| **Pore Pressure Transducer** | ADAM 3016 | 100 | 5 | Differential |

**Table 3.8: Energy comparison between Becker hammer and laboratory simulated drop test.**

| | |
|---|---|
| Maximum Impact Energy Simulated in Laboratory (kJ) | 2.83 |
| Full throttle hammer energy from Becker Hammer (kJ) | 10.85 |

**Table3.9: Axial load calibration result details before and after the field testing at Oakland, CA.**

| Test Section | Calibration Factor (kips/count***) | | $R^2$ Value | |
|---|---|---|---|---|
| | Before Field Test | After Field Test | Before Field Test | After Field Test |
| **Tip section (S0)** | 0.0481 | Damaged* | 0.999981 | N/P |
| **S1** | 0.0300 | Damaged* | 0.999985 | N/P |
| **S2** | 0.0311 | 0.0312 | 0.999929 | 0.999974 |
| **S3** | 0.0310 | 0.0305* | 0.999965 | 0.952547 |
| **S4** | 0.0309 | No Correlation** | 0.999971 | N/P |
| **Above ground section (S5)** | 0.0303 | 0.0300 | 0.999994 | 0.999995 |

* Damaged on Installation 2 during final hard driving

** Inconsistent dynamic response from beginning of Installation 1

***Count is the least measurement of Geodaq. Here 16 bit system can generate ($2^{16} - 1$) counts in a signal.

N/P – Not possible

**Table 3.10: Radial stress calibration result details before and after the field testing at Oakland, CA.**

| Test Section | Calibration Factor (kips/count***) | | $R^2$ Value | |
|---|---|---|---|---|
| | Before Field Test | After Field Test | Before Field Test | After Field Test |
| **S1** | 0.1301 | Damaged* | 0.999355 | N/A |
| **S2** | 0.1299 | Damaged* | 0.999817 | N/A |
| **S3** | 0.1349 | Damaged** | 0.999412 | N/A |
| **S4** | 0.1303 | Damaged** | 0.999879 | N/A |

* Damaged on day 2 final hard driving

** No physical damage but gauge wiring was damaged

***Count is the least measurement of Geodaq. Here 16 bit system can generate ($2^{16} - 1$) counts in a signal.

N/A – Not available

**Table 3.11: Axial load calibration detail on the thin walled cylinder measuring radial stress before and after the field testing at Oakland, CA.**

| Test Section | Calibration Factor (kips/count) | | $R^2$ Value | |
|---|---|---|---|---|
| | Before Field Test | After Field Test | Before Field Test | After Field Test |
| **S1** | 0.0092 | Damaged* | 0.999621 | N/A |
| **S2** | 0.0090 | Damaged* | 0.999920 | N/A |
| **S3** | 0.0093 | Damaged** | 0.999527 | N/A |
| **S4** | 0.0091 | Damaged** | 0.999885 | N/A |

* Damaged on day 2 final hard driving

** No physical damage but gauge wirings got damaged

**Table 3.12: Pore pressure transducer calibration detail on RTP sections before and after the field testing at Oakland, CA.**

| Test Section | Calibration Factor (kips/count) | | $R^2$ Value | |
|---|---|---|---|---|
| | Before Field Test | After Field Test | Before Field Test | After Field Test |
| **S1** | 0.0153 | 0.0152 | 0.999916 | 0.999387 |
| **S2** | 0.0151 | 0.0152 | 0.999915 | 0.999855 |
| **S3** | 0.0149 | 0.0149 | 0.999882 | 0.999842 |
| **S4** | 0.0151 | 0.0151 | 0.999942 | 0.999946 |

**FIGURES**

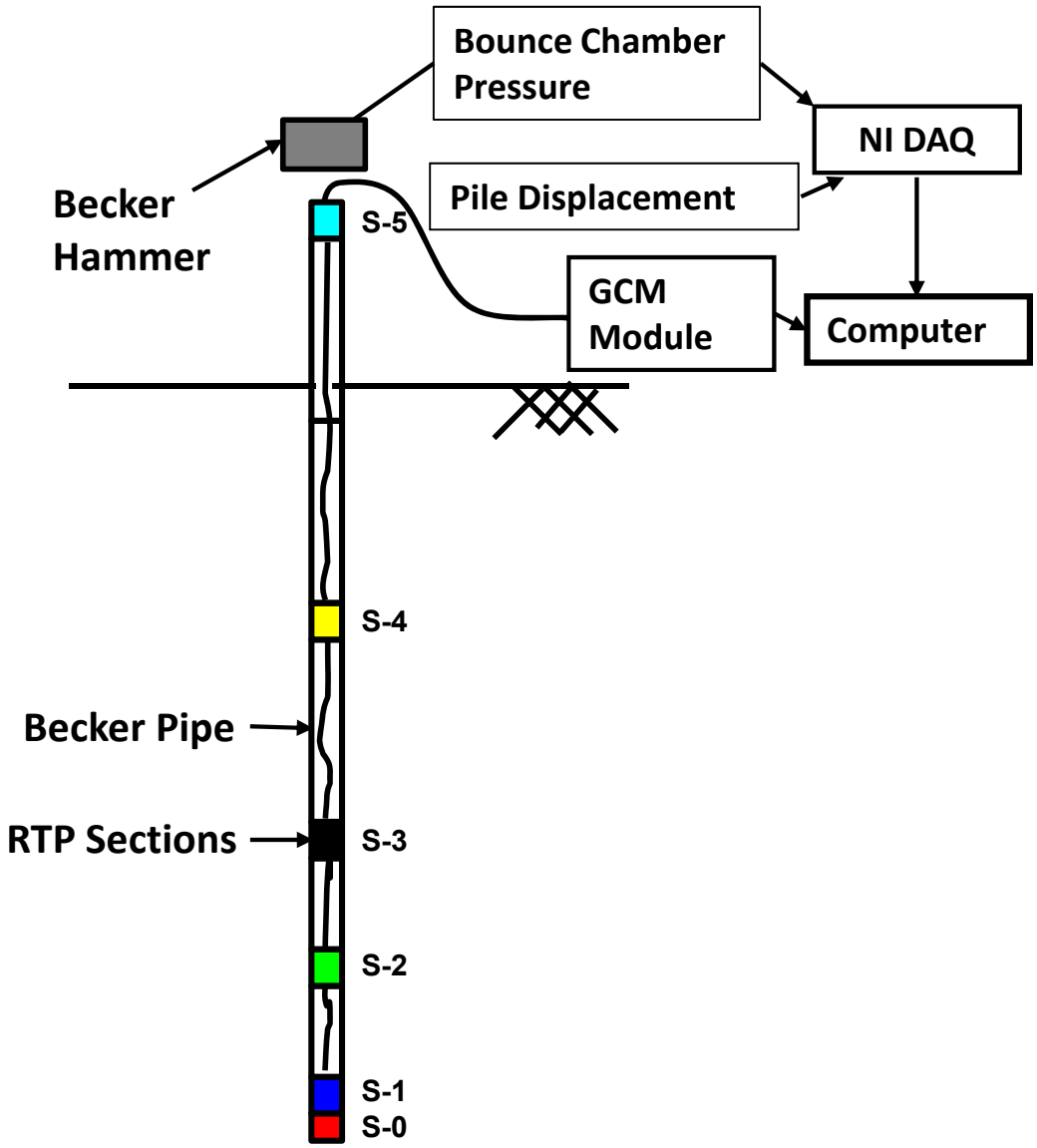


**Figure 3.1: Schematic diagram of RTP section assembly with above ground measurements and Becker hammer during driving (not to scale).**

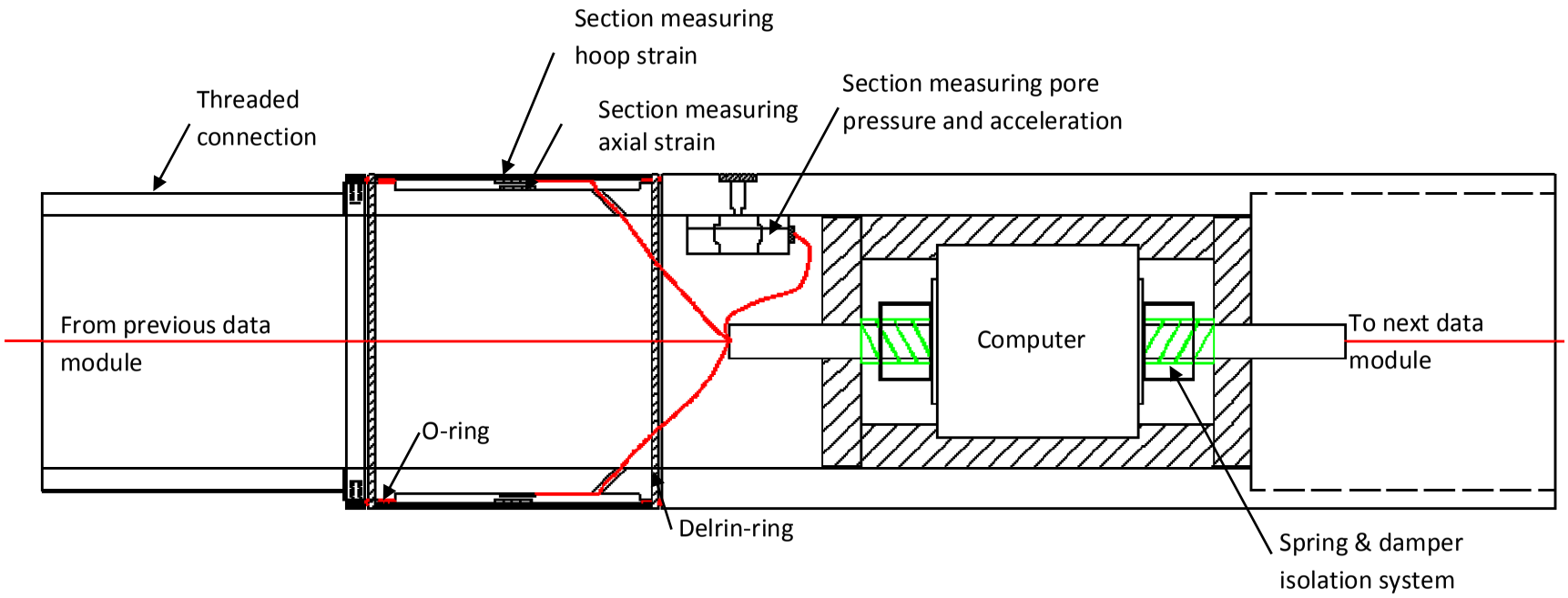


**Figure 3.2: Overall design cross section of the 61 cm (2 ft) instrumented RTP section.**

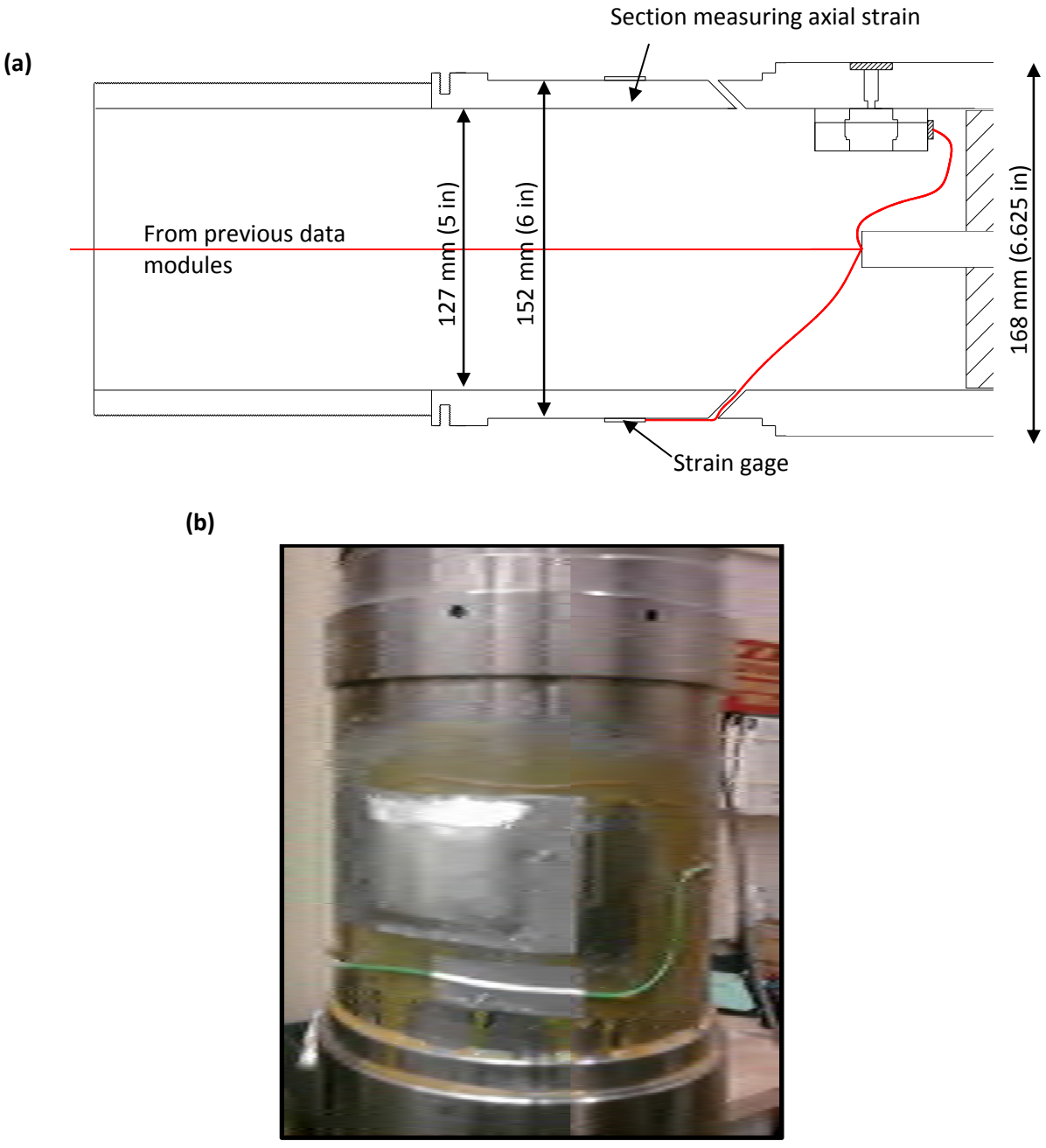


**Figure 3.3: Axial load measurement (a) section measuring axial strain and (b) picture of section measuring axial strain.**

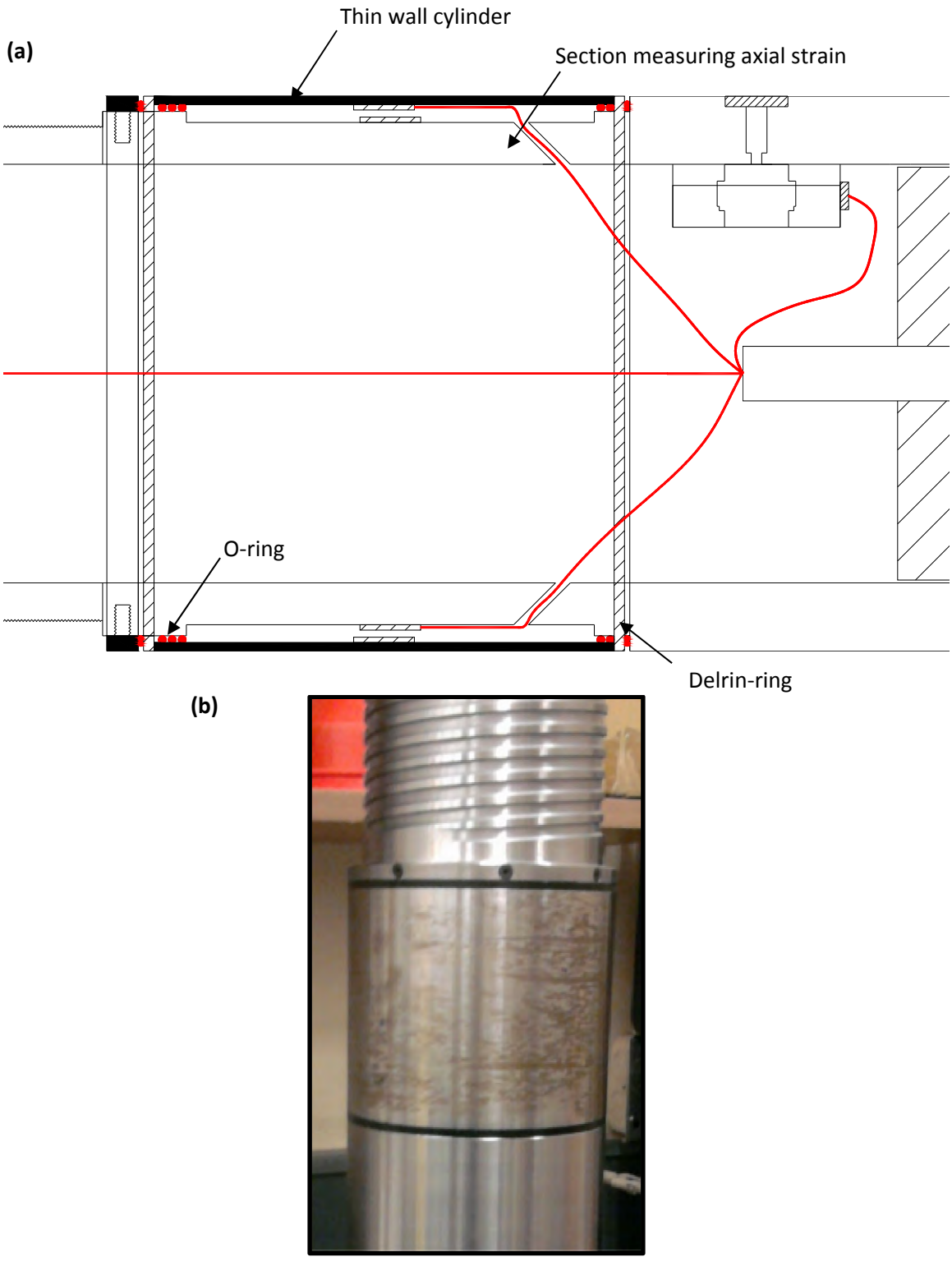


**Figure 3.4: Thin wall cylinder to measure radial stress in RTP sections. (a) Detail of thin wall cylinder in a RTP unit and (b) picture of assembly of thin wall cylinder in a RTP unit.**

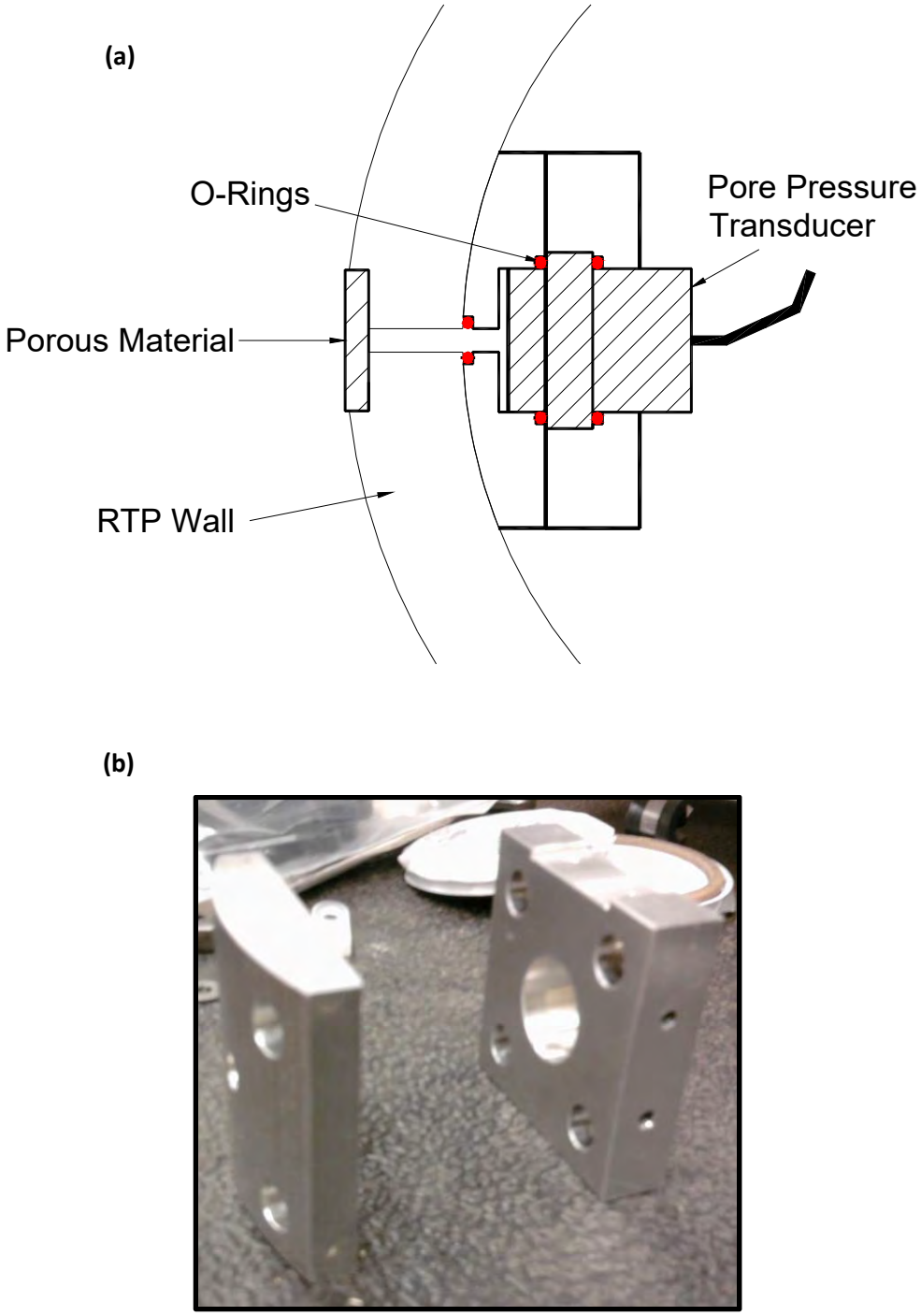


**Figure 3.5: Acceleration and pore pressure mounting system. (a) Acceleration and pore pressure module assembly against inner RTP wall and (b) picture of bulkhead components.**

(a)

(b)

(c)

(d)

**Figure 3.6: Pictures of porous filter saturation process before driving. (a) Porous hole of RTP unit is in upright position with a washer sealing, (b) silicon oil is filled in the cavity between pore pressure surface and RTP outer wall using a needle, (c) surface mount vacuum applied to remove air pockets, and (d) saturated porous stone in place.**

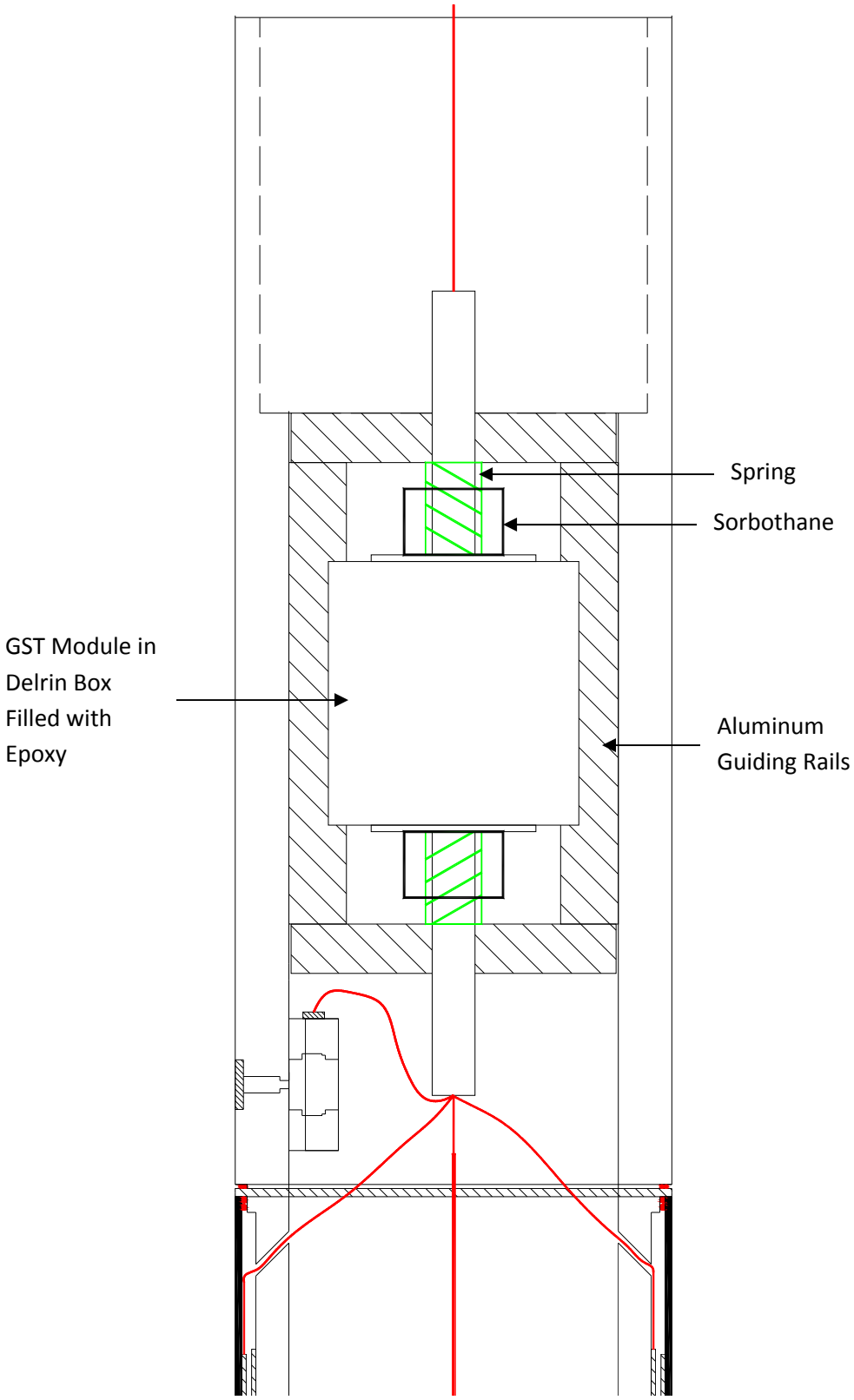


**Figure 3.7: Schematic of GST module and vibration isolation system assembly in RTP unit.**

(a)


(b)

**Figure 3.8: (a) Picture of GST units filled with epoxy and curing in the laboratory and (b) picture of GST module assembled inside the pipe section.**

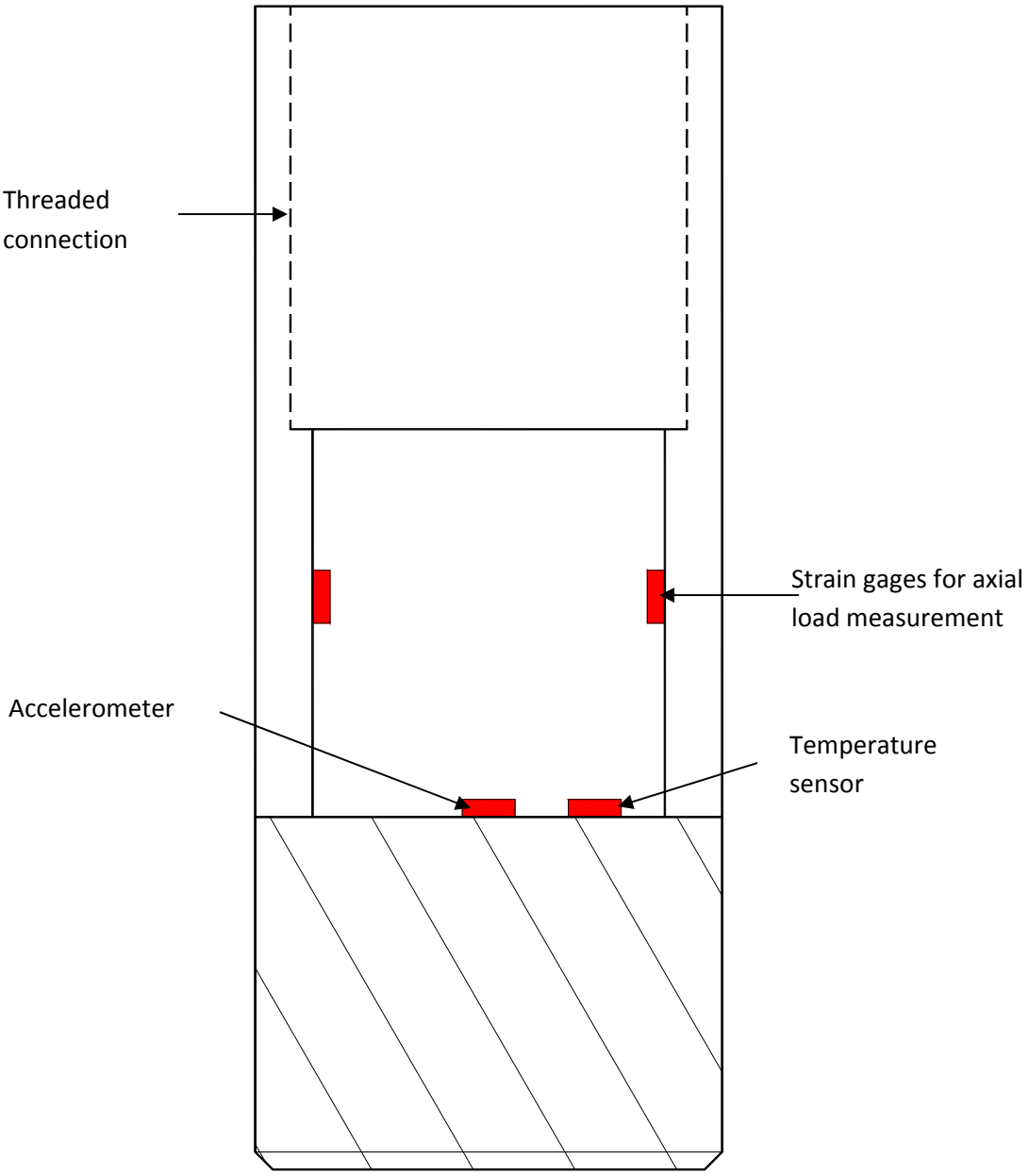


**Figure 3.9: Schematic of RTP driving shoe with mounted sensors.**

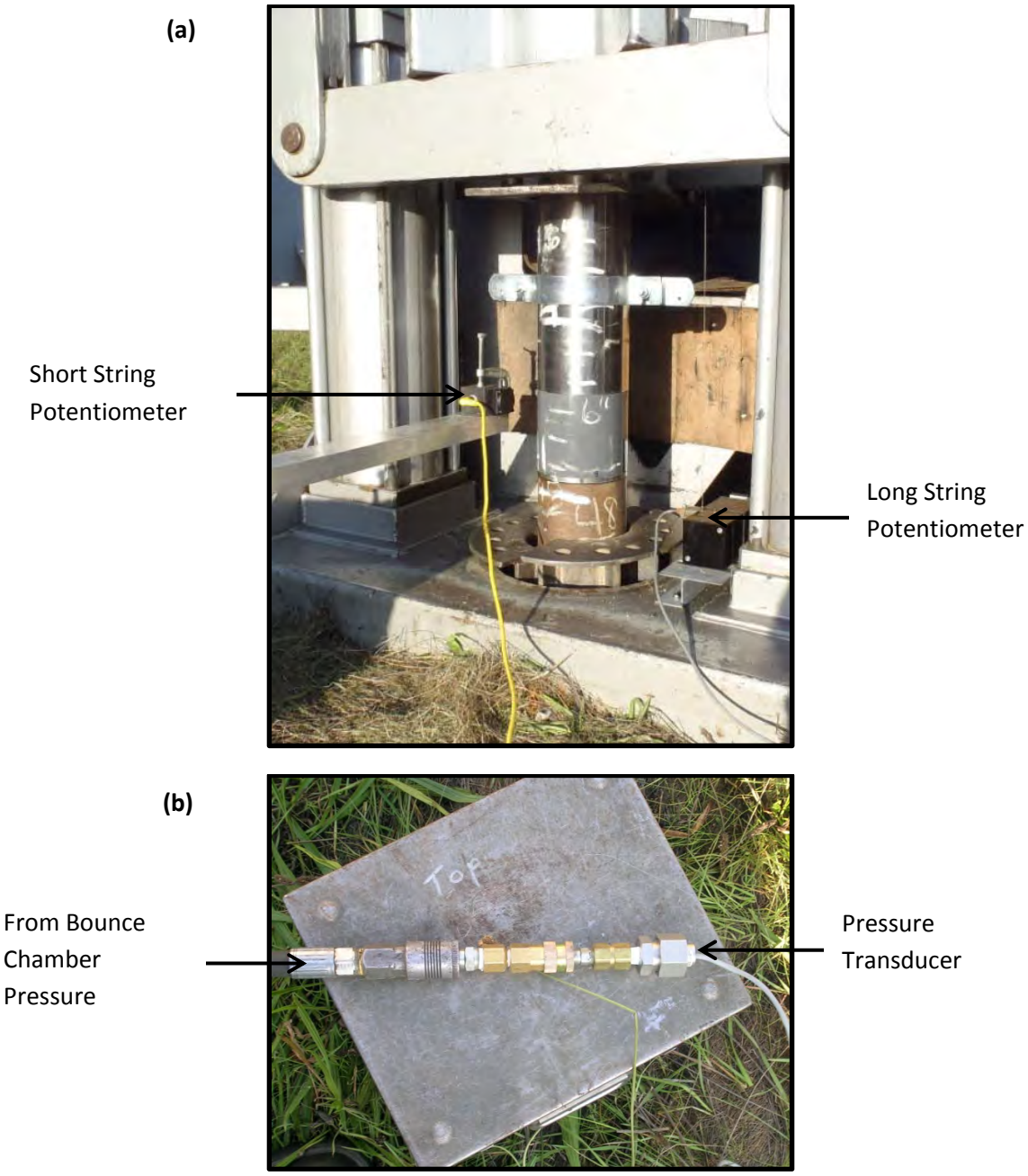


**Figure 3.10: Pictures of above ground sensors in field applications. (a) String potentiometer mounting for pullout load testing and (b) connection between pressure transducer and bounce chamber.**

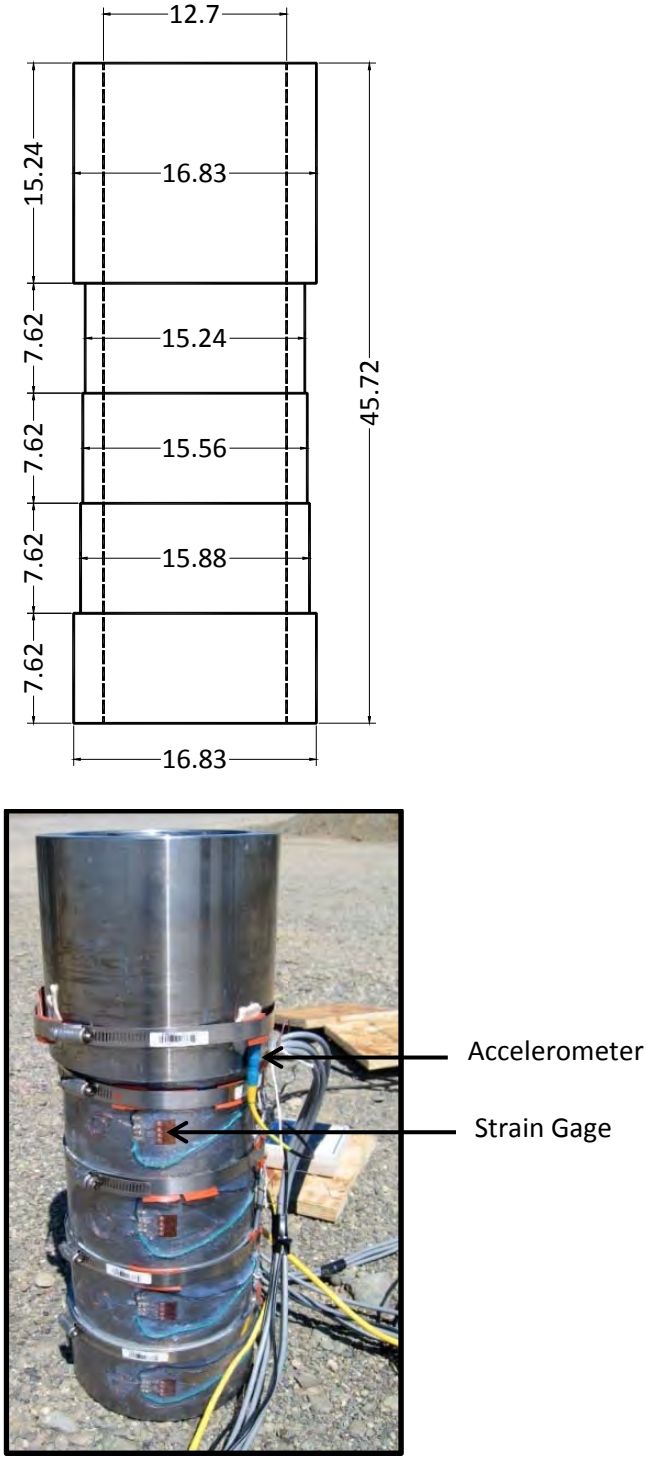


**Figure 3.11: Test section tested for geometrical design and Becker hammer performance. (a) Schematic with measurements in cm and (b) picture with instrumentation.**

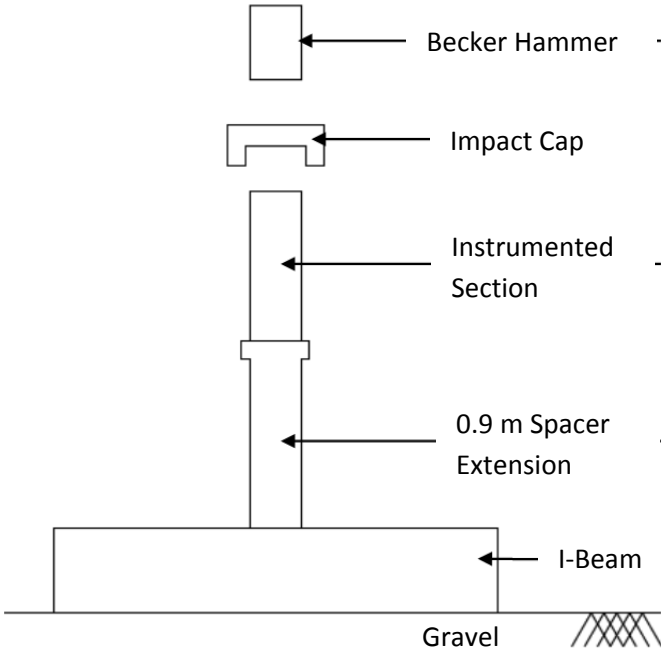


**Figure 3.12: Schematic diagram of test setup of instrumented section tested for geometrical design and Becker hammer performance.**

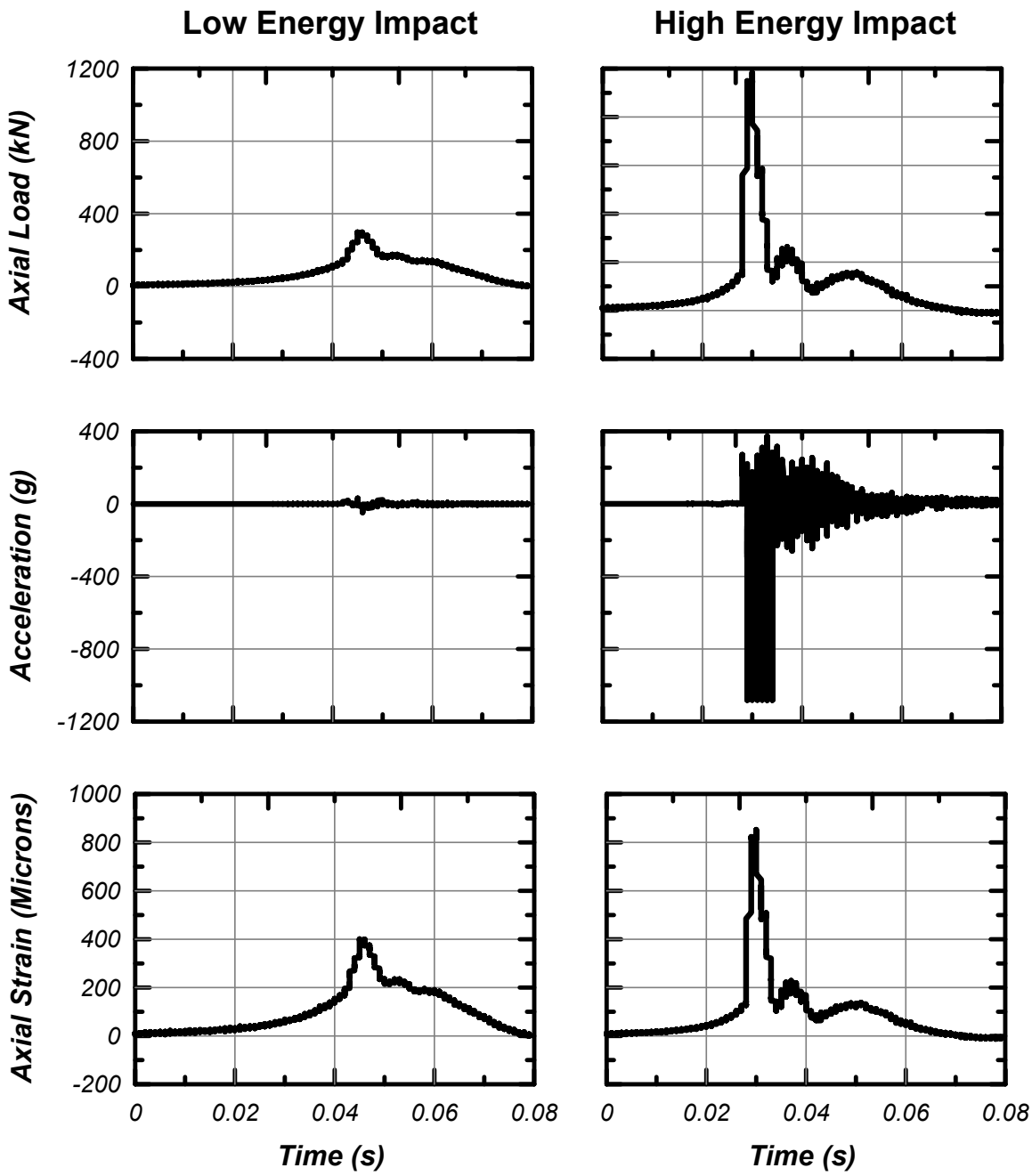


**Figure 3.13: Axial force, acceleration, and strain measurements during high and low energy impacts of Becker hammer from the field testing.**

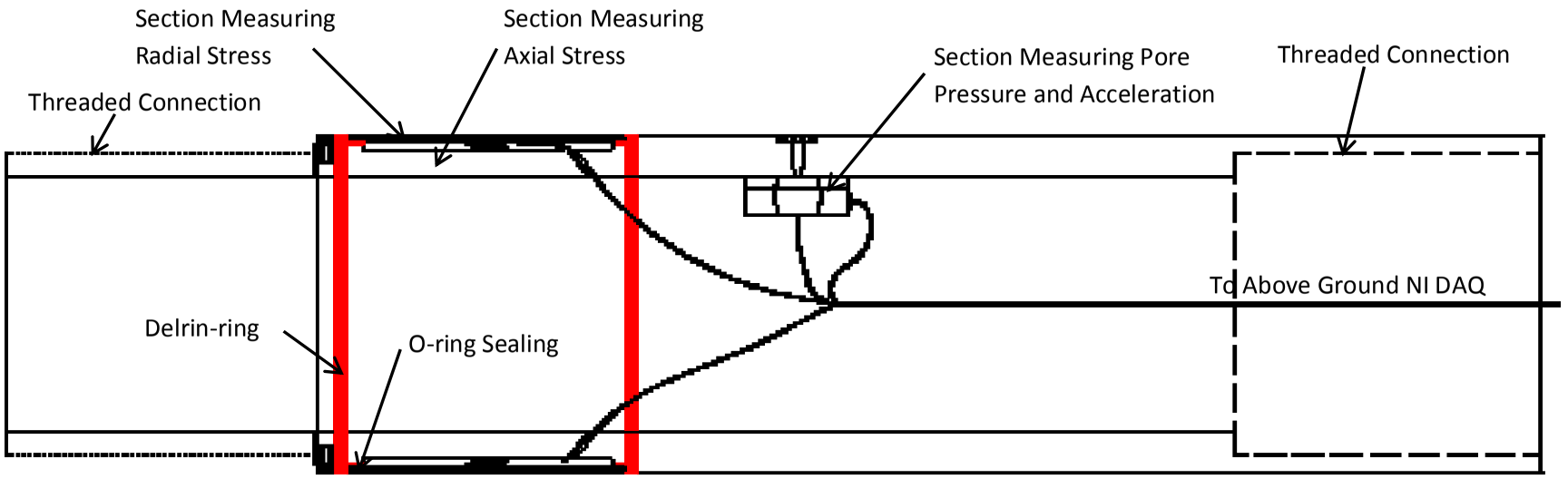


**Figure 3.14: Schematic of RTP section tested for design and sensor performance.**

(a)

(b)

(c)

(d)

**Figure 3.15: Pictures from field performance testing. (a) Hard wired RTP section connected to driving shoe, (b) driving shoe and RTP section assembly connected to regular Becker pipe section, (c) RTP string being driven into ground, and (d) pullout load testing in progress.**

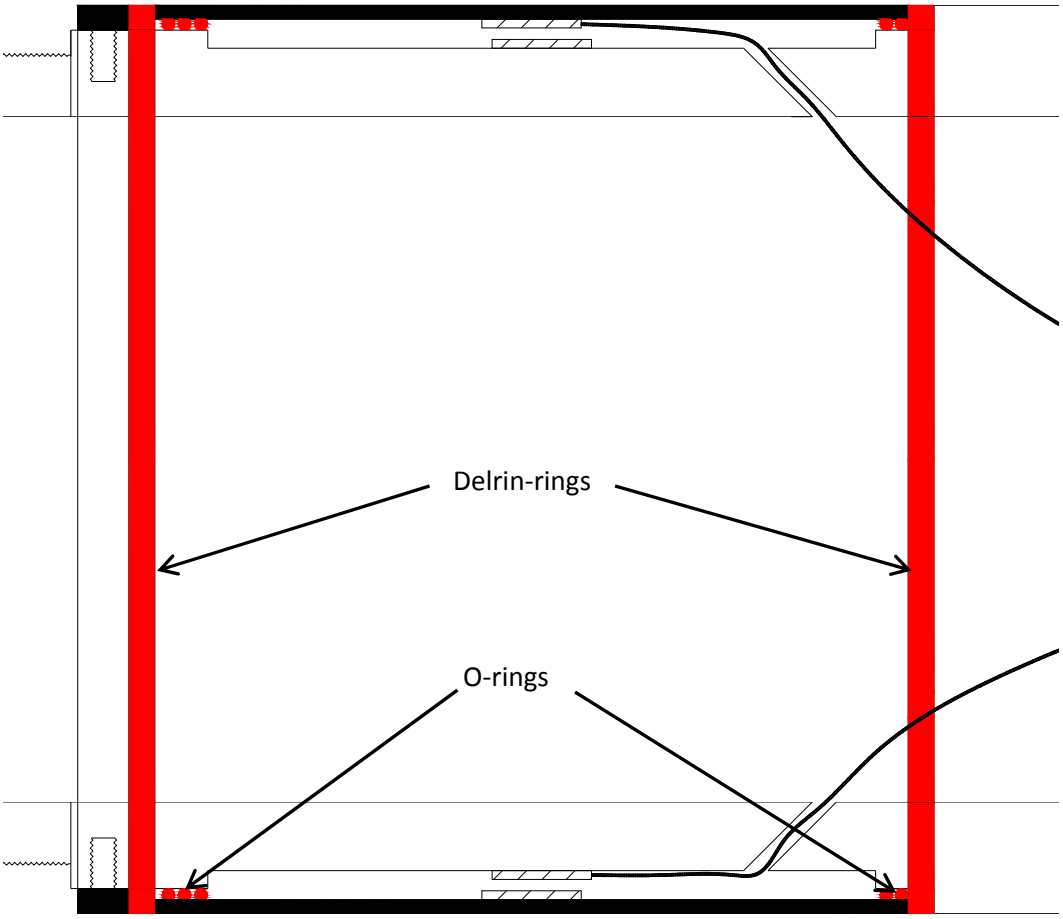


**Figure 3.16: Arrangement of O-rings and Delrin-rings as tested in the field for performance. Design was changed for the production unit after the test results.**

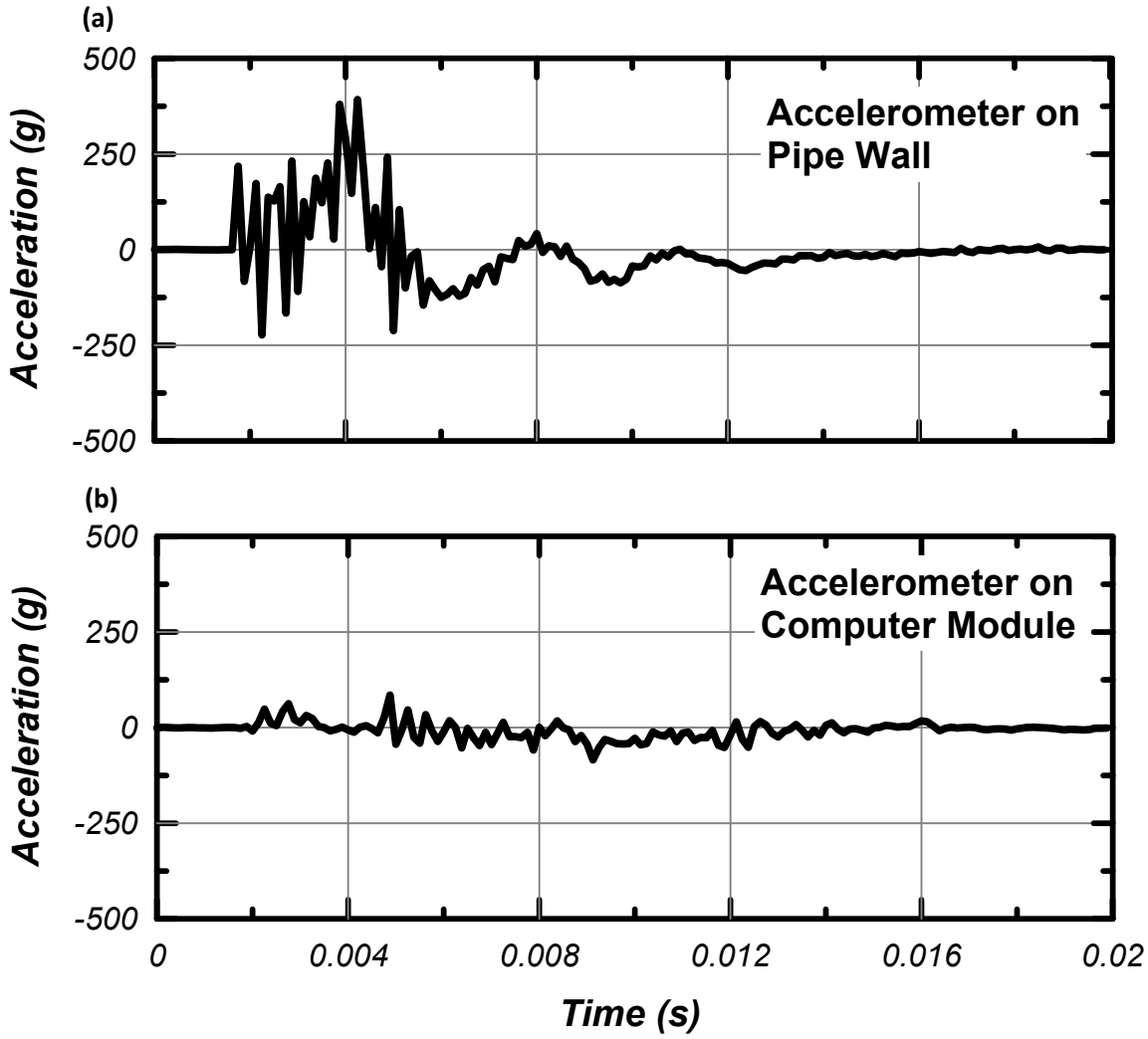


**Figure 3.17: Comparison between wall and vibration Isolation unit accelerations during drop test in UC Davis laboratory. (a) Acceleration measured on Becker pipe wall and (b) acceleration measured on vibration isolated computer unit.**

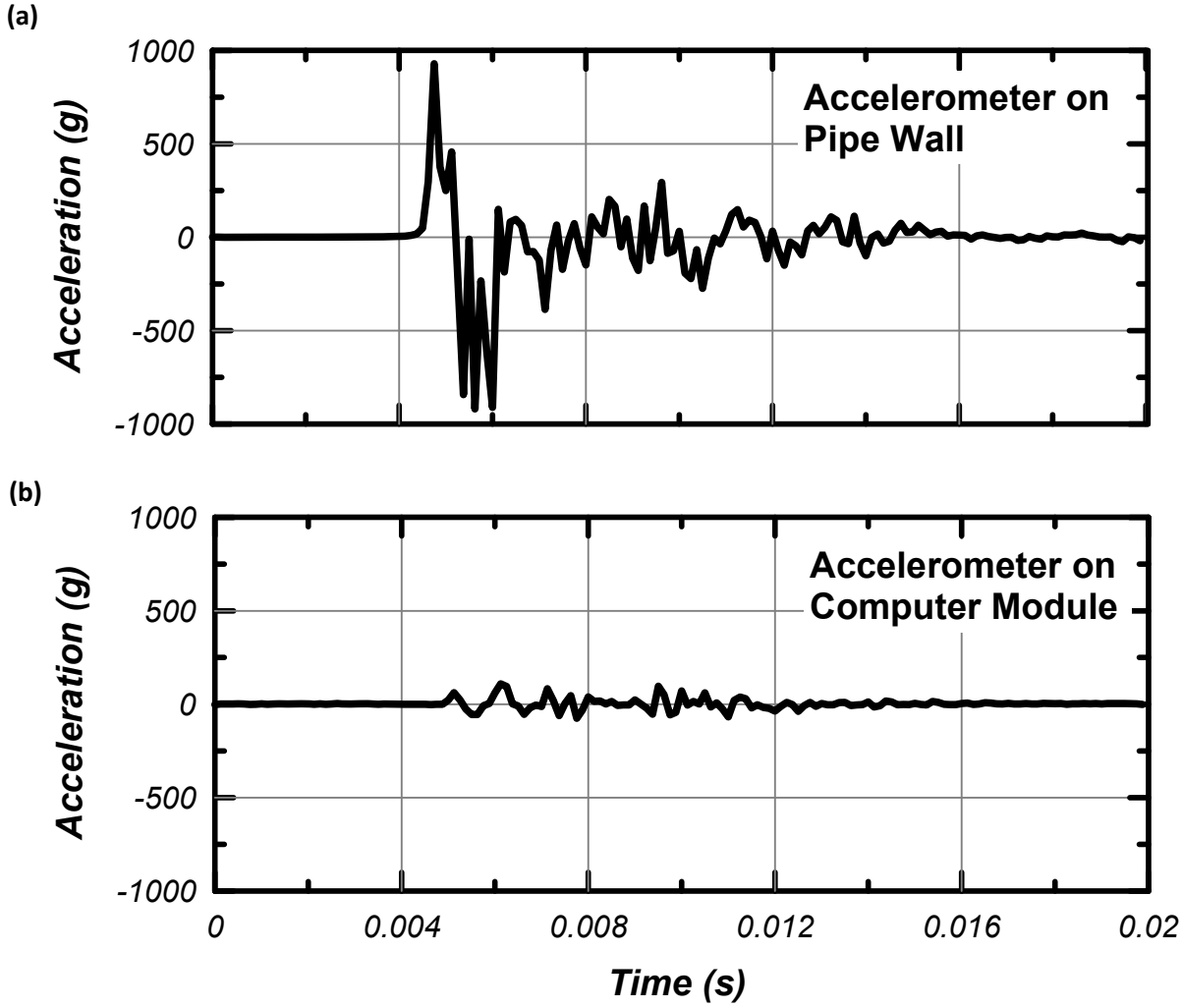


**Figure 3.18: Comparison between wall and vibration isolation unit accelerations during vibration isolation unit performance evaluation at Fontana, CA. (a) Acceleration measured on Becker pipe wall and (b) acceleration measured on vibration isolated computer unit.**

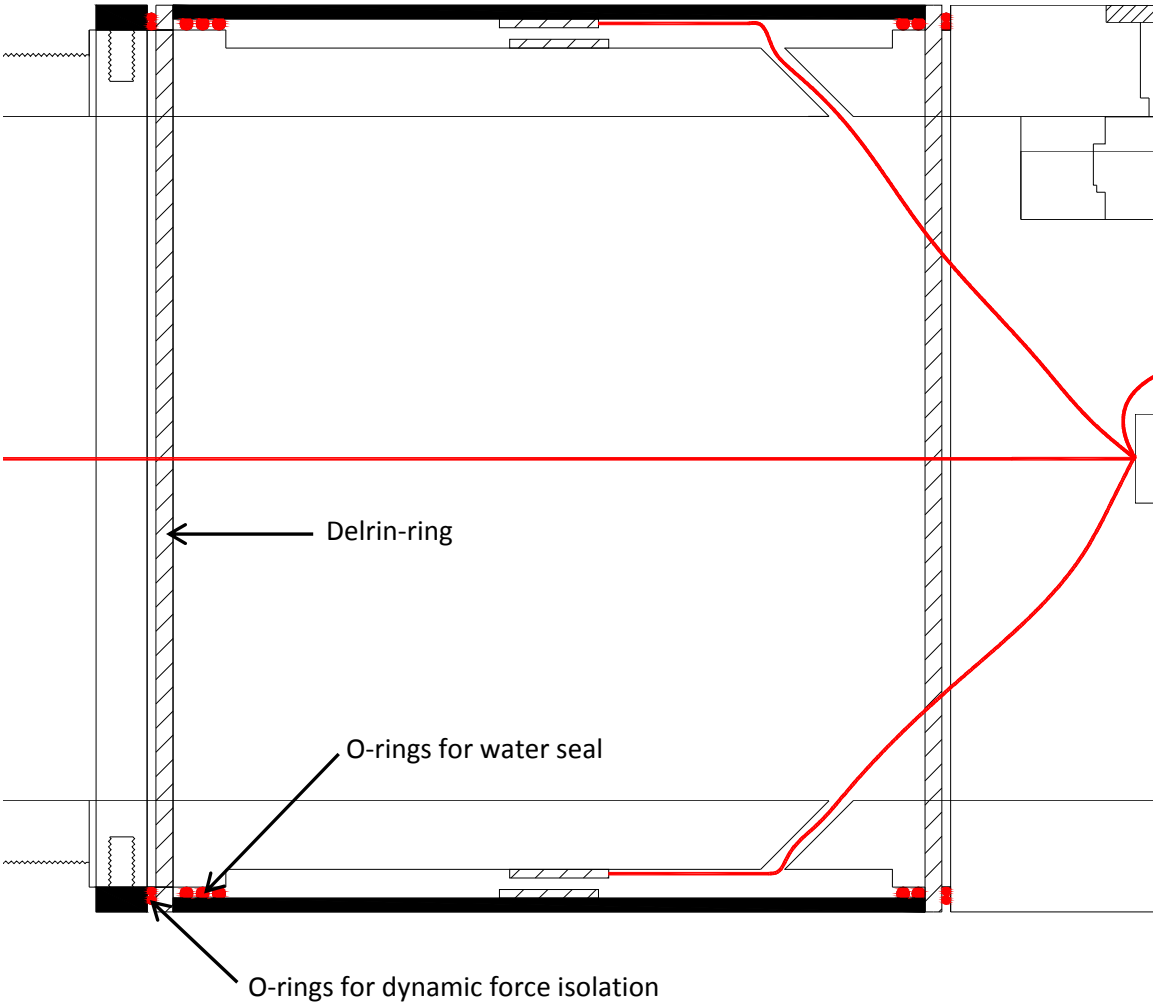


**Figure 3.19: Section measuring radial stress modified for dynamic force isolation by introducing soft O-rings as a cushion adjacent to thinner Delrin rings.**

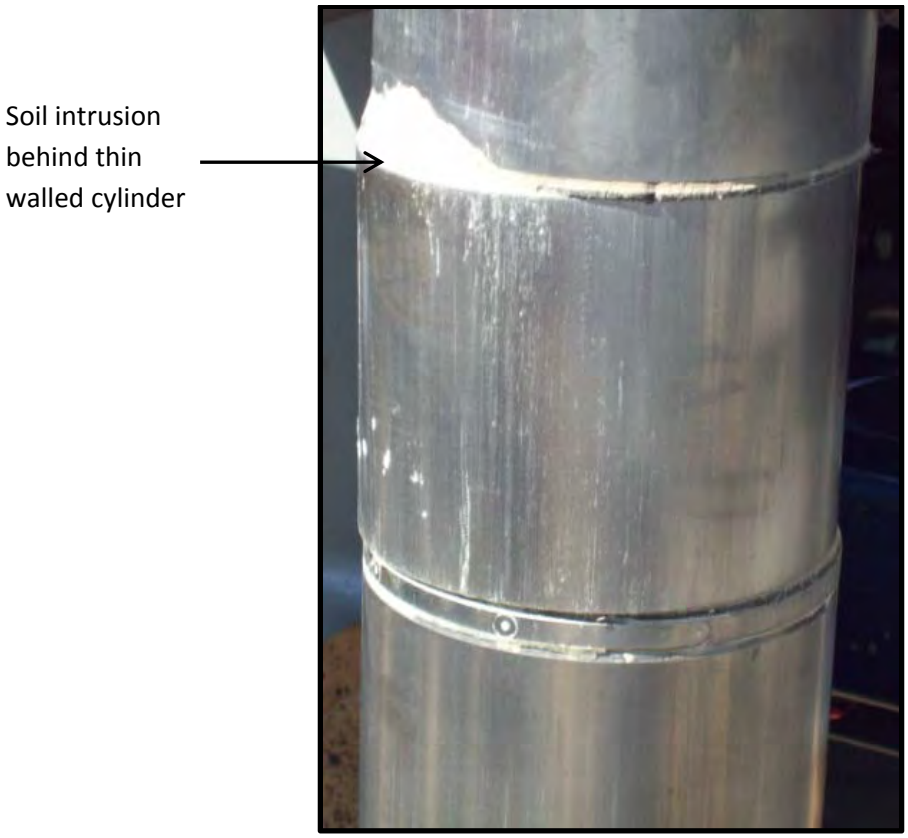


**Figure 3.20: Picture of damaged thin walled cylinder of instrumented section after hard driving condition encountered at Fontana, CA test site.**

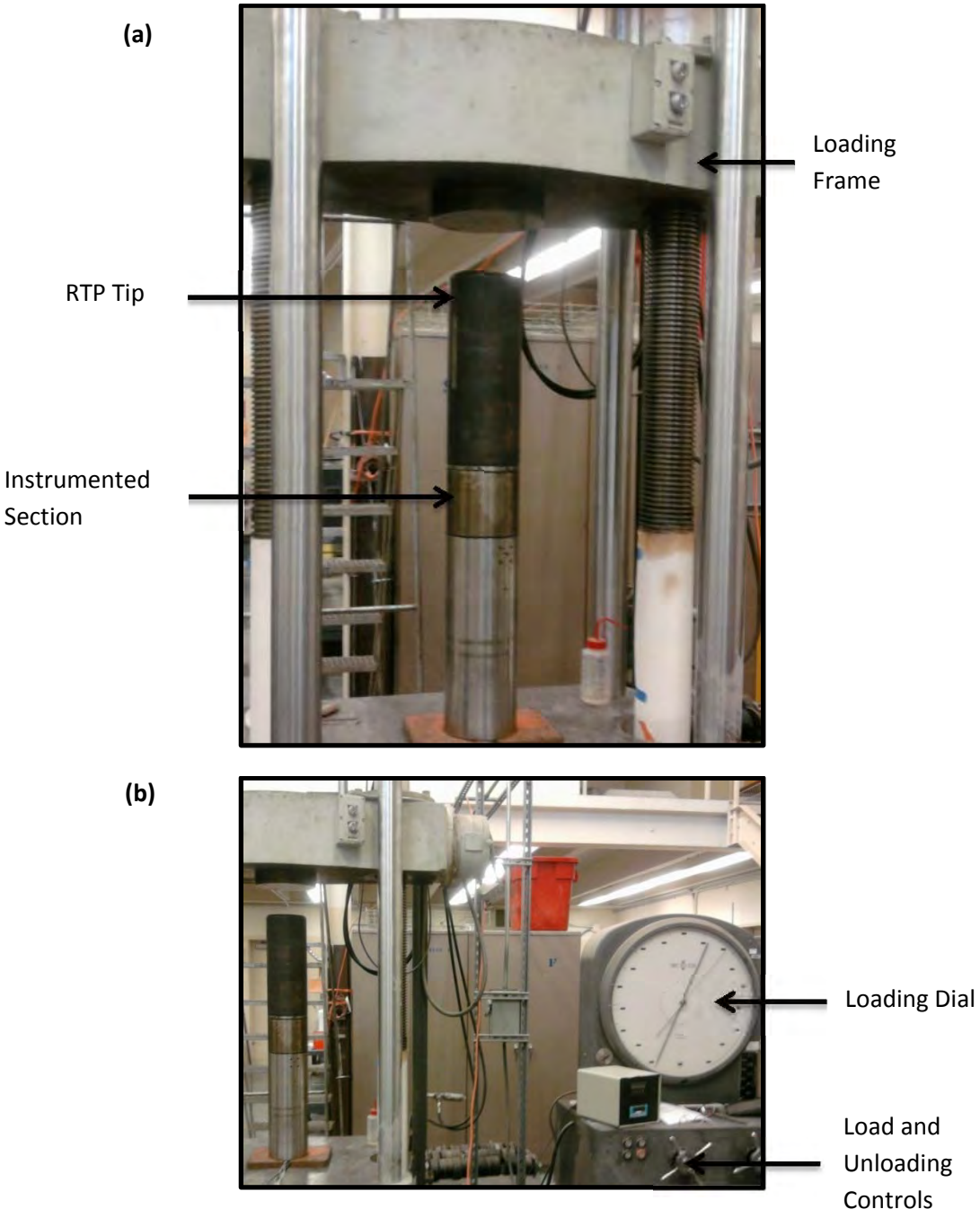


**Figure 3.21: RTP calibration in laboratory at University of California, Davis. (a) Tip section and an instrumented section of the RTP unit mounted for calibration on large structural loading frame and (b) controls of Tinius Olson load frame.**

(a)

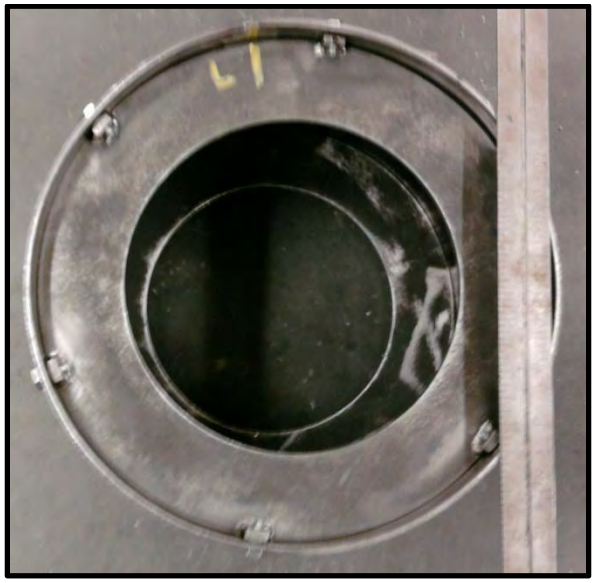

(b)

**Figure 3.22: Radial stress calibration chamber that contains a bladder that expands between inner wall of the calibration chamber and RTP's thin wall cylinder for radial stress measurement. (a) Top view and (b) side view.**

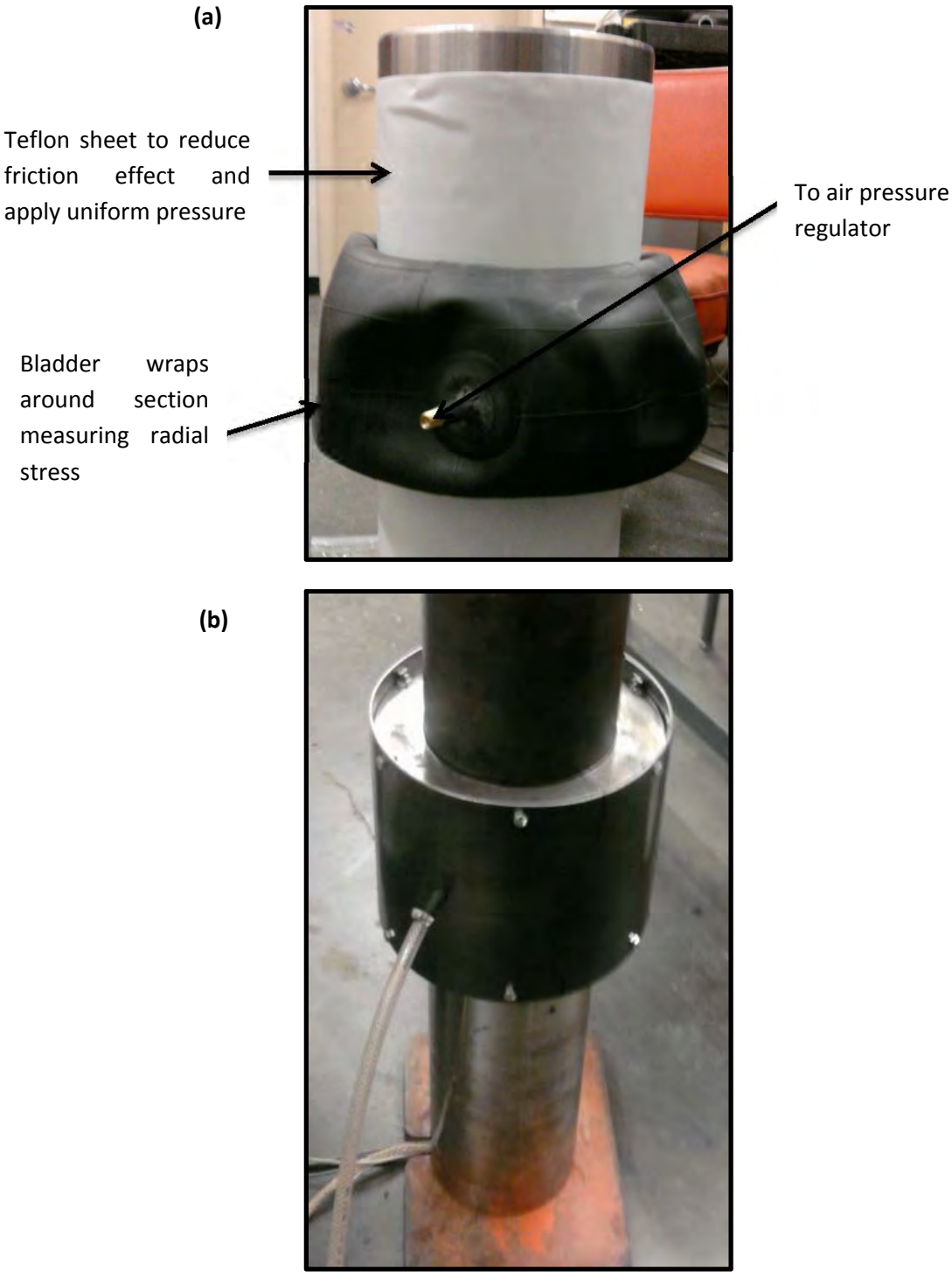


**Figure 3.23: (a) Bladder and calibration chamber assembly on thin wall cylinder to calibrate radial stress measurement. Teflon sheet and baby powder used to reduce friction and apply uniform pressure. (b) Inner tube inflated to desired pressures through air pressure regulator.**

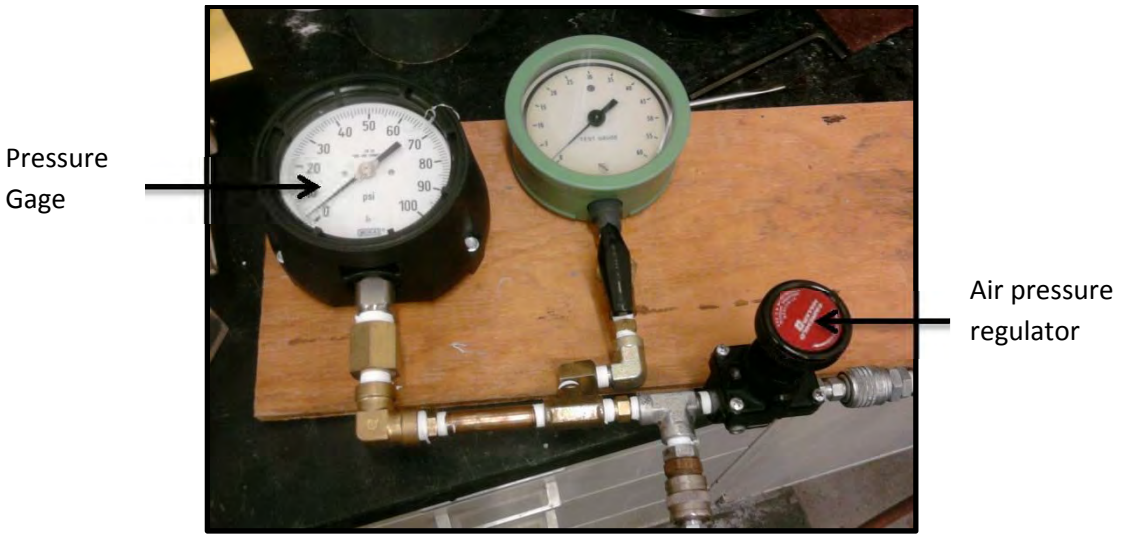


**Figure 3.24: Air pressure regulator and measurement gauges used in the calibration process.**

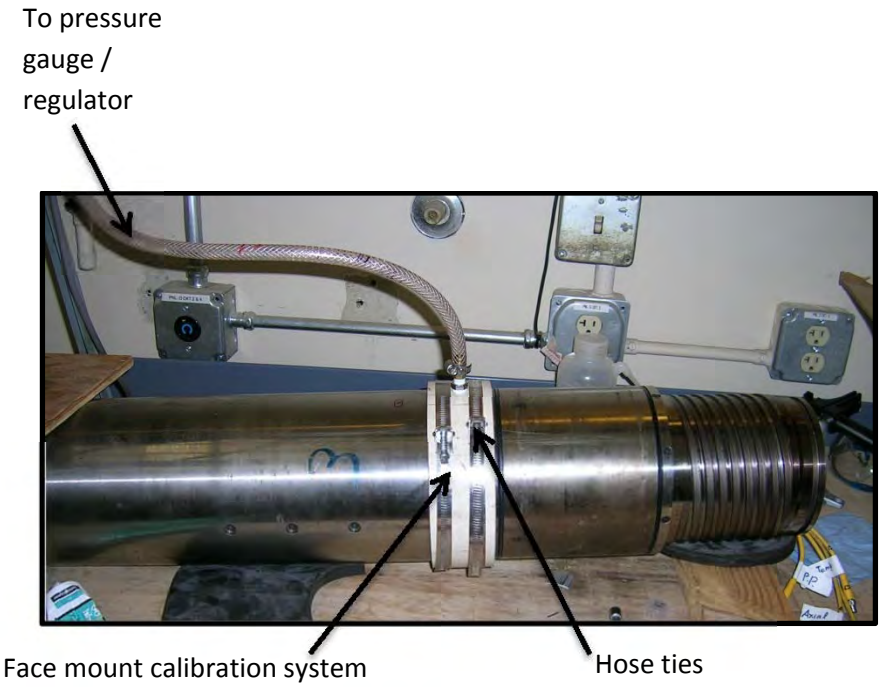


**Figure 3.25: Pore pressure calibration process. Face mount calibration unit secured against RTP section using hose clamps.**

# Chapter 4: Summary of Field Test Site and RTP Testing Program

A field testing program was performed to assess RTP performance during dynamic pile installation, setup, and tensile load testing following RTP development (which itself included three field testing events to finalize design of system components as described in Chapter 3). This chapter describes the field test site selected, including geologic history and insitu testing data obtained previously, and the overall testing program that included three RTP installations to 12.5 m or more over a period of three days.

## 4.1 Field Test Site

The field test site selected is located near the I-880 freeway in Oakland, CA. Specifically, it is located in the Southern Pacific Railroad Desert Yard southwest of the Grand Avenue Viaduct between the former Oakland Army Base and old Amtrak Station. The test site is directly adjacent to the northbound I-880 abutment. The location of the test site on a current map is presented in Figure 4.1.

The site location was selected in consultation with Caltrans. The test site property is owned and managed by Caltrans, and is directly adjacent to 'Site 2' that was developed during the I-880 Replacement Project (Service Contract No. 59V149) in the 1990s. The Caltrans Project Site 2 location and the adjacent site where the RTP was tested are indicted in Figure 4.2.

### 4.1.1 Regional Geology

The test site is located on the middle eastern side of San Francisco Bay. The general geological depositional sequence that occurred around the borders of the bay apply to the test site, and are summarized as follows. Bedrock exists at an elevation of about – 150 m (-500 ft). The geologic deposition processes during the Quaternary period (last 3M years) generated the stratigraphy in the upper 25 m of soil (the depth of interest for this study). The typical stratigraphic sequence as described by Holzer (personnel communication) and others (Rogers and Figuers 1991, Bonaparte and Mitchell 1979) for the east side of the bay is represented schematically in Figure 4.3. During the Pleistocene epoch fine grained sediments from coastal mountain rivers and creeks entered the bay. The coarse grained soil settled near the shore forming an alluvial fan while the finer grained soil remained suspended in the bay water prior to settling out and forming what is conventionally considered Old Bay Mud (OBM). The ice age at the end of the Pleistocene epoch (about 15k years ago) lowered the sea level by about -100 m to where the Farallon Islands (west of San Francisco) were part of dry land, resulting in the entire bay being above sea level. During this time period lowering of the water table resulted in desiccation and over-consolidation of OBM. Windblown sand dunes formed and migrated throughout the bay, forming what is today named Merritt Sand. Rivers and creeks continued to transport finer grained soils into, and through the bay, creating local channels of finer grained soils within the Merritt Sand deposit. The end of the ice age (about 10k years ago as the Holocene epoch began) resulted in sea level rise of about 100 m (up to today) and re-inundation of the bay with ocean water. The ocean water elevation has risen about 10 m over the last 6 thousand years (Atwater et al. 1977**)** with about 0.14 m rise in the last 100 years

(Cayen et al. 2006). This re-established the marine depositional processes, resulting in formation of Young Bay Mud. An alluvial fan was also formed at the base of the coastal mountains. Finally, man-made deposits of hydraulic fill and compacted fill have been created widely along the eastern side of San Francisco Bay for both industrial and residential development. A schematic showing the surface geological units are presented in Figure 4.4, with the test site indicated (Helley and Graymer 1997).

### 4.1.2 Test Site Stratigraphy

The test site stratigraphy was evaluated considering one boring with standard penetration tests (SPT) and two cone penetration test (CPT) soundings (without $u_2$ measurements) obtained during the Caltrans studies (Beddard et al. 1995). The location of the CPT soundings and the boring with SPT tests are indicated in Figure 4.5. As evident, the maximum spacing between these three locations was about 24 m in the north-south direction and about 3 m in the east-west direction (the primary direction of expected spatial variability). The SPT N value and the soil stratigraphy indicated by the engineer boring log is presented in Figure 4.6. The CPT soundings and stratigraphy inferred from soil behavior type using Robertson (1990) is presented in Figure 4.7. The interpretations differ somewhat, particularly near the upper surface and regarding the presence of the underlying clayey silt layer (Figure 4.8). Bore logging difference is mainly due to selection of sampling interval depths.

The representative soil stratigraphy model that was adopted and is consistent with both SPT N values and CPT data is presented in Figure 4.9. Overall, the stratigraphy profile to a depth of 15 m has six primary units. At the surface a compacted sandy fill layer exists to about 1 m depth, followed by a fine sand layer down to 3 m. From about 3 m to 7.7 m depth is a deposit of Young Bay Mud. The upper portion of the layer, which is near the ground water table, may be slightly overconsolidated. From 7.75 m to about 10 m depth is a dense sand layer, likely part of the Merritt Sand unit. A clayey silt layer exists from about 10 to 12 m depth. Interestingly, this layer was not reported in the engineer's boring log but was clearly detected (and is substantially different than the over and underlying sand layers) by both CPT soundings and during RTP testing. Below the clayey silt layer a dense sand layer continues beyond the depth of exploration. Though uncertain, the clayey silt layer may have been a temporary depositional ingression within the larger Merritt sand deposit. The ground water during RTP testing was at about 1.2 m depth.

### 4.1.3 Representative Engineering Properties of Soil Layers

Engineering properties of the YMB, two dense sand layers, and clayey silt layer are of primary interest for evaluation of the RTP. Unfortunately rigorous laboratory strength and consolidation testing was not reported as part of the Caltrans Site 2 study. The properties of YMB is well documented (e.g. Bonaparte and Mitchell 1979), and typically has a unit weight of about 15 kN/m$^3$, an overconsolidation ratio less than 3 at shallower depths and less than 1.5 at deeper depths (below 6 m depth), a normalized strength ratio of 0.3 based on triaxial

compression data, and a vertical consolidation coefficient of about 0.0003 $cm^2$/sec. A CPT $N_{kt}$ value of 12 for estimating undrained strength has been shown to provide reasonable agreement with laboratory strength data measured by unconfined compression test. The properties of the dense Merritt Sand layer were estimated from CPT data. The effective peak friction was estimated to be 45 degrees (based on Mayne et al. 2007) and the sand is relatively free draining with a permeability of 0.05 cm/sec or more. The properties of the underlying clayey silt layer are difficult to estimate based on CPT data since no $u_2$ pore pressure measurements were obtained; it is not clear whether drained, undrained, or partially drained conditions existed during cone penetration. However, following the $I_c$ based index proposed by Robertson (2009) and others (described in Lunne et al. 1996) the soil is likely more clay-like and therefore an estimate of undrained strength is more reasonable than an estimate of a drained friction angle. For a typical $N_{kt}$ range of 11 to 16 the corresponding undrained strength for the clayey silt layer would be between 123 and 178 kPa.

### 4.1.4 Caltrans Pile Load Test Program

The Caltrans I-880 Replacement Project at Site 2 included of installing and then load testing, under compression and/or tension, a series of test piles. Table 4.1 summarizes the previous pile load test results from Site 2. An example load test result is presented in Figure 4.11. Static pile load tests were performed on piles installed from 10.7 m (35 ft) to 13.1 m (43 ft), resulting in the pile tip being embedded in the relatively soft clayey silt layer from 10 to 12 m depth and lower dense sand layer beyond 12 m depth. The compression and tensile static

capacities were determined based on the Caltrans' 1.27 cm (0.5 in) pile displacement failure criteria and load tests were performed at least 20 days after installation (Beddard et al. 1995).

## 4.2 RTP Testing Program

The RTP testing program was designed to assess performance during dynamic pile installation, during pile setup as excess pore pressures dissipate, and during tensile static load testing. A total of three RTP installations to a depth of 12.5 m or more were performed, with one installation performed each day. Dynamic measurements during RTP installation were performed continually while setup and tension load tests were performed at the specific depths summarized in Table 4.2. The location of these three RTP installations was in close proximity to the soil boring and CPT soundings (Figure 4.6).

Dynamic RTP installation using the Becker hammer was measured throughout each RTP installation using the two parallel data acquisition systems described in chapter 3. The above ground data acquisition system (NI DAQ) provided continuous measurements at a 200 Hz measurement frequency of RTP head position (and therefore RTP tip depth) and hammer bounce chamber pressure during RTP installation. The below ground data acquisition system (Geodaq) obtained, ~2 second data packages recorded at 8333 Hz in all downhole instrumented RTP sections assembled. The data packages obtained by the downhole Geodaq GST modules then required about 60 seconds to transfer all the data uphole. Triggering of the Geodaq system was manual and occurred as frequently as possible during RTP installation.

In installation 3, at full depth of 12.6 m, pile setup (equilibration of excess pore pressures) was performed over a time period of 4 hours. It was monitored using the downhole Geodaq system. Measurements were obtained in all instrumented sections. As in consolidation-type measurements, time between consecutive samples increased as time progressed. RTP setup measurements were not obtained as part of the Installation 1 and 2 testing.

RTP tension (pull-out) load tests were performed using the Becker spider hydraulic extraction system. Tests were performed at the installation depths of about 9.3 m and 12.8 m in installation 1, 9.6 m and 13.3 m during Installation 2 and at 12.6 m in Installation 3 (Table 4.2). The load tests during Installation 1 and 2 were performed immediately after driving to the respective depth, resulting in the soil surrounding the RTP containing excess pore pressures and reduced effective stresses. The load test from Installation 3 at 12.6 m depth performed after excess pore pressure dissipation. Excess pore pressure dissipation resulted in the surrounding soil being re-consolidated and increased effective stresses. The Becker spider hydraulic extraction system was controlled manually by a hydraulic needle value, resulting in an average displacement rate that ranged from about 0.36 to 1.76 cm/min. This displacement rate was the slowest possible with the current Becker rig system. This rate needed to be lower further. This displacement rate exceeds that specified in the ASTM D3869 (2007) standard for static tension pile load testing using the Constant Rate of Uplift Method, which is 0.05 to 0.10 cm/min. However, it is slightly slower than that currently used in Becker pull-out tests performed for determining Becker pipe shaft resistance in gravel deposit explorations, which is about 2.5 to 7.5 cm/min. During the tension load tests the RTP head (above ground) displacement and the

long and short string potentiometers were monitored at a frequency of about 200 Hz with the NI-DAQ system using the setup pictured in Figure 3.10a. The instrumented sections and tip were sampled concurrently using the Geodaq system at a sampling frequency of about 8333 Hz. Unfortunately, the Geodaq system was unreliable during the pile load tests. While the system worked reliably during driving modes (maximum number of samples collected at high sampling rate, discrete packages of data approximately every minute) and during calibration / dissipation modes (small number of samples collected at high sampling rate, discrete packages sent at most every few seconds), the intermediate sampling configuration (lower sampling rate with more continuous transmission) required for pile load testing as applied in the field resulted in a conflict in the data transmission protocol and a loss of load data in most cases. It is noted that the source of these conflicts has been fixed for future operations.

**REFERENCES**


ASTM D3689-07., (2007). "Standard test methods for deep foundations under static axial tensile load." *ASTM international*, PA, 11p.

Atwater, B.F., Hedel, C.W., and Helley, E.J., (1977). "Late Quaternary depositional history, Holocene sea level changes, and vertical crustal movement, southern San Francisco Bay, California." *Geological Survey Professional Paper: 1014*, 15p.

Beddard, D.L., Speer, D., Swanson, K., (1995). "Site 2 summary report for Caltrans indicator pile test program on the I-880 replacement project." *Consultant Contract Management Branch Office of Structure External Liaison and Support and Geotechnical Support Branch Office of Structural Foundations, Service Contract No. 59V149,* Caltrans, CA.

Bonaparte, R. and Mitchell, J.K., (1979). "The properties of San Francisco bay mud at Hamilton air force base, California." *Department of Civil Engineering, University of California, Berkeley*. California, 186p.

Cayan, D., P. Bromirski, K. Hayhoe, M. Tyree, M. Dettinger, and R. Flick. (2006)., "Projecting future sea level." *CEC report CEC-500-2005-202-SF*, March

Helley, E.J. and Graymer, R.W., (1997). "Quaternary geology of Contra Costa County, and surrounding parts of Alameda, Marin, Sonoma, Solano, Sacramento, and San Joaquin Counties, CA: a digital database." *U.S. Geological Survey Open-File report: 97-98,* 12p

Holzer, T.L., (2010). Personal communication. *U.S. Geological Survey*.

Lunne, T., Robertson, P.K. and Powell, J.J.M., (1997). "Cone penetration testing in geotechnical practice." *Blackie Acadamic, EF Spon/Routledge Publishers*, New York.

Mayne, P.W. et al., (2007). "Cone penetration testing state-of-practice." *Synthesis on Cone Penetration Test, Synthesis Study, NCHRP Project 20-05,* Transportation Research Board, Washington, DC., 137p

Robertson, P.K., (2009). "Interpretation of cone penetration tests – a unified approach." *Canadian Geotechnical Journal,* 46: 1337-1355.

Rogers, J.D. and Figuers, S.H., (1991). "Engineering geologic characterization of the Greater Oakland – Alameda area, Alameda and San Francisco counties, California." *Final Report*

*to National Science Foundation, Grant BCS – 9003785*, *Rogers/Pacific, Inc*., Pleasant Hill, CA. 68p.

## TABLES

**Table 4.1: Static pile load test summary from prior Caltrans investigation at Site 2 (project test site).**

| Pile No. | Hammer Type | Installation Date | Test Date | Pile Tip Elevation (m) | Static Compression Capacity (kN) | Static Tensile Capacity (kN) |
|---|---|---|---|---|---|---|
| 2-H | VM2-25000 | 01/03/1994 | 02/02/1994 | -12.2 | 1601 | N/A |
| 2-H | VM2-25000 | 01/03/1994 | 02/03/1994 | -12.2 | N/A | 1000 |
| 2-L | D46-32 | 01/04/1994 | 02/01/1994 | -13.1 | 4448+ | N/A |
| 2-L | D46-32 | 01/04/1994 | 02/02/1994 | -13.1 | N/A | 3025 |
| 2-P | D62-22 | 12/30/1993 | 01/27/1994 | -12.3 | 3069 | N/A |
| 2-P | D62-22 | 12/30/1993 | 01/28/1994 | -12.3 | N/A | 1735 |
| 2-T | D46-32 | 01/04/1994 | 01/21/1994 | -10.7 | 3292 | N/A |
| 2-T | D46-32 | 01/04/1994 | 01/24/1994 | -10.7 | N/A | 1957 |
| 2-W | D62-22 | 12/30/1993 | 01/19/1994 | -12.3 | 4448+ | N/A |
| 2-W | D62-22 | 12/30/1993 | 01/20/1994 | -12.3 | N/A | 2669 |

N/A – Not Available

Notes:

1. Static Capacities shown are based on the Caltrans 1.27 cm pile failure criteria.
2. Piles 2-L, 2-T, and 2-W were installed closed ended.
3. All Piles were predrilled to a depth of 2.13 m (7 ft) with a 60.96 cm (24 in.) diameter auger.
4. All predrilled holes caved to the ground surface prior to pile placement.

**Table 4.2: Setup and tension load tests performed during RTP deployment at Oakland, CA test site.**

| Installation Number | RTP Tip Depth (m) | Soil Layer at RTP Tip | Setup Test | | Tension Load Test |
|---|---|---|---|---|---|
| | | | Performed (Yes/No) | Duration (hrs) | Performed (Yes/No) |
| 1 | 9.3 | Upper Dense Sand | No | N/A | Yes |
| 1 | 12.8 | Lower Dense Sand | No | N/A | Yes |
| 2 | 9.6 | Upper Dense Sand | No | N/A | Yes |
| 2 | 13.3 | Lower Dense Sand | No | N/A | Yes |
| 3 | 12.6 | Lower Dense Sand | Yes | 4 | Yes |

N/A – Not Available

**FIGURES**

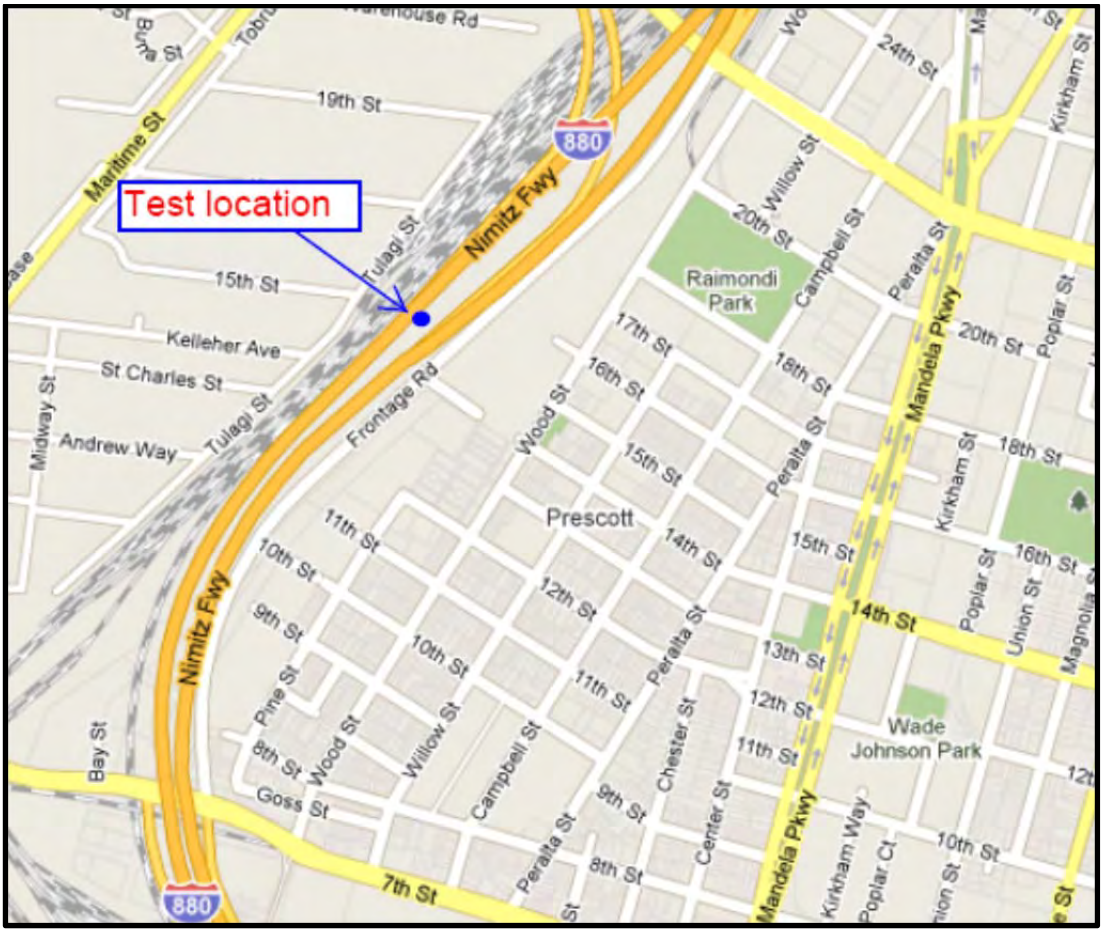


**Figure 4.1: Overall project plan for service on state highway in Alameda County in Oakland, CA.**

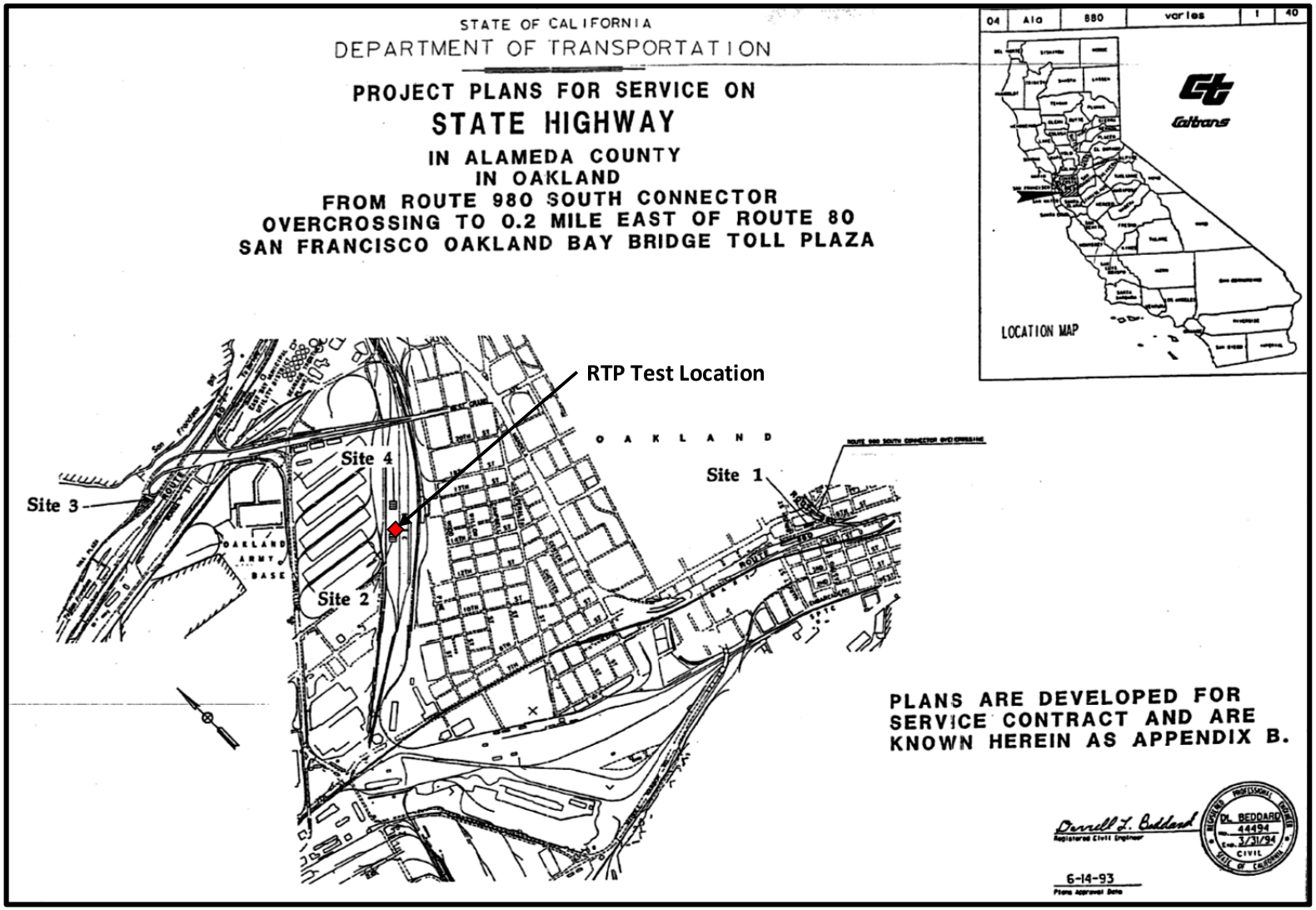


**Figure 4.2: Site 2 location and adjacent RTP test location indicated on original Caltrans (1995) report map.**

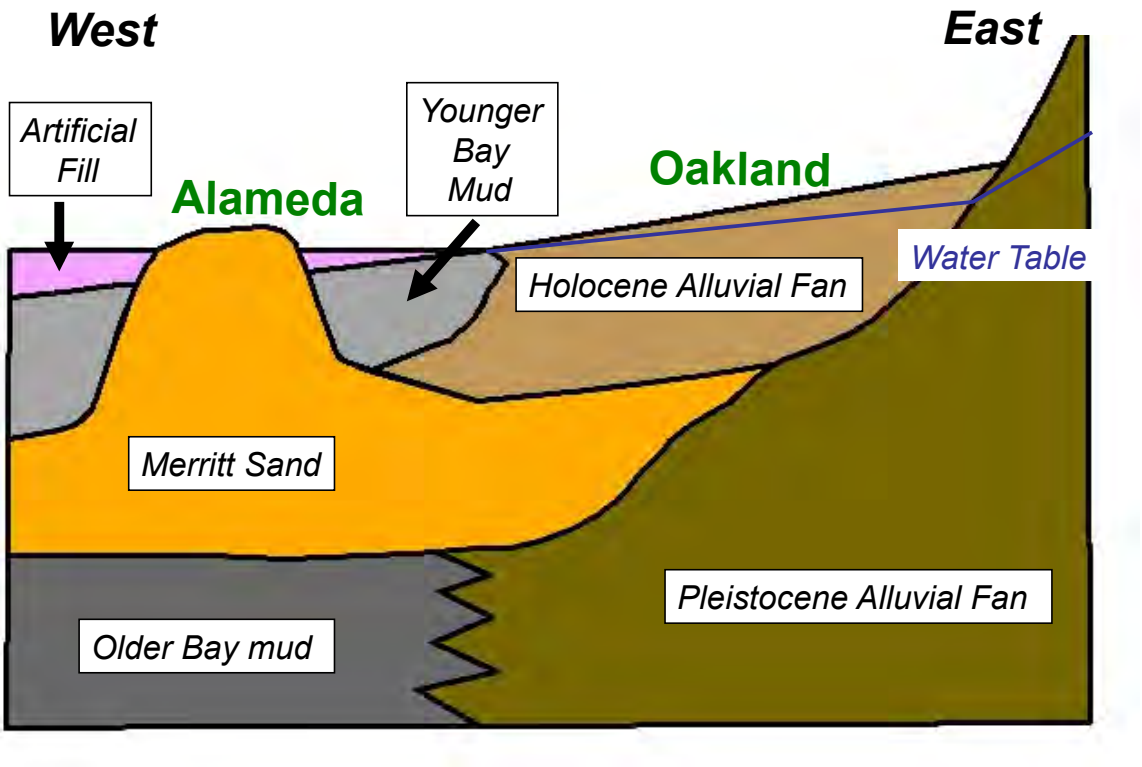


**Figure 4.3: Schematic cross-section of the geologic layering in the eastern side of the San Francisco Bay (Tom Holzer, personal communication 2010).**

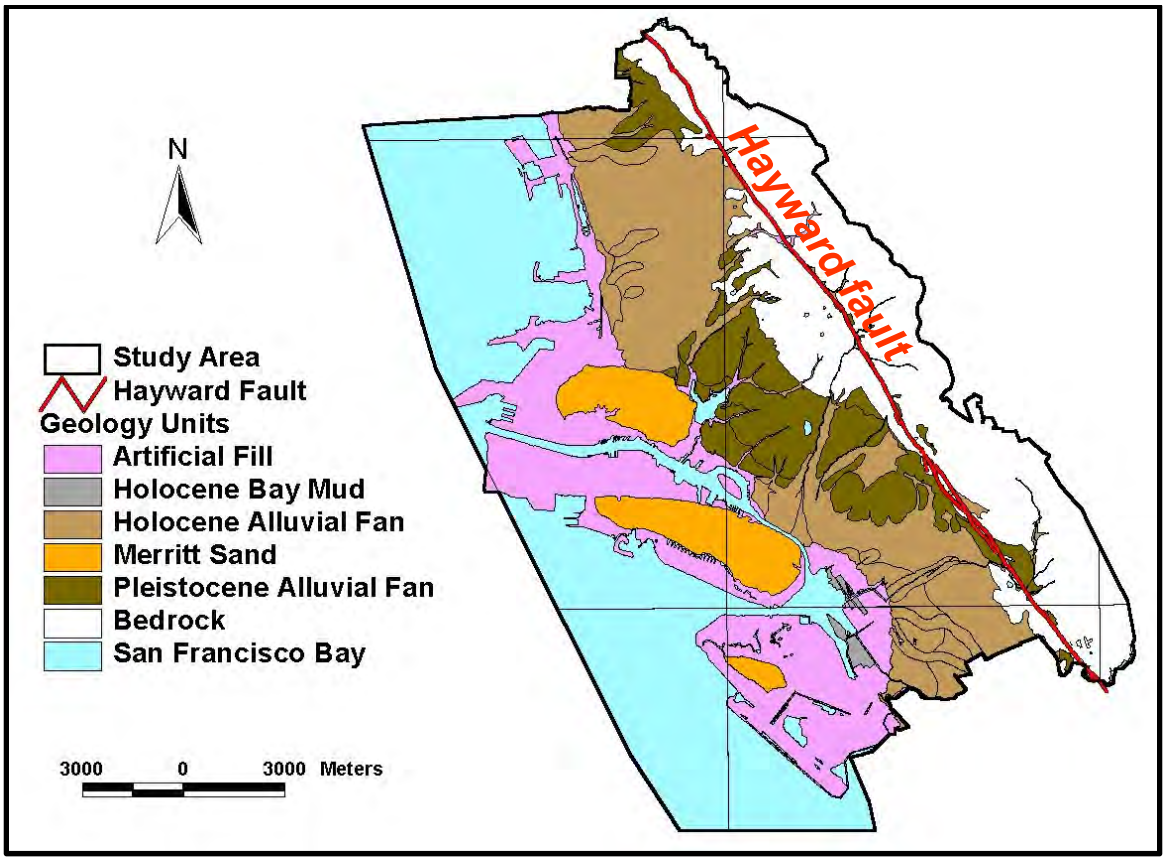


**Figure 4.4: Schematic surficial geologic units along the eastern side of the San Francisco Bay with location of test site indicated (Helley and Graymer 1997).**

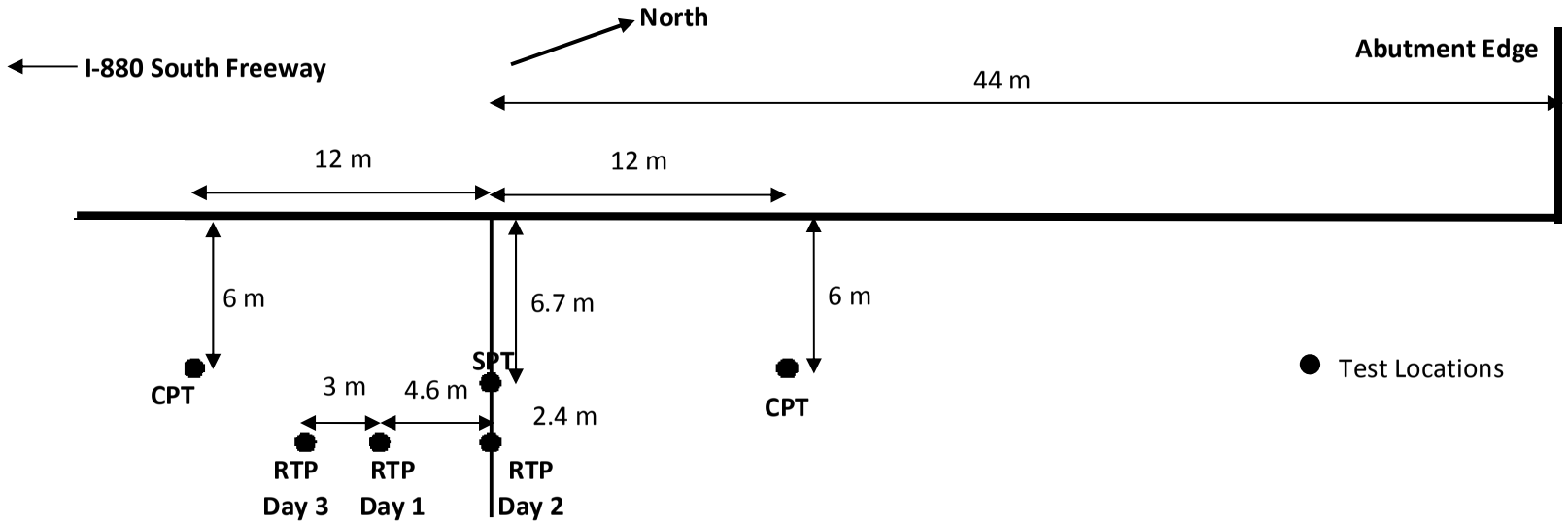


**Figure 4.5: RTP test locations near I-880 abutment along with CPT sounding and SPT drilling locations.**

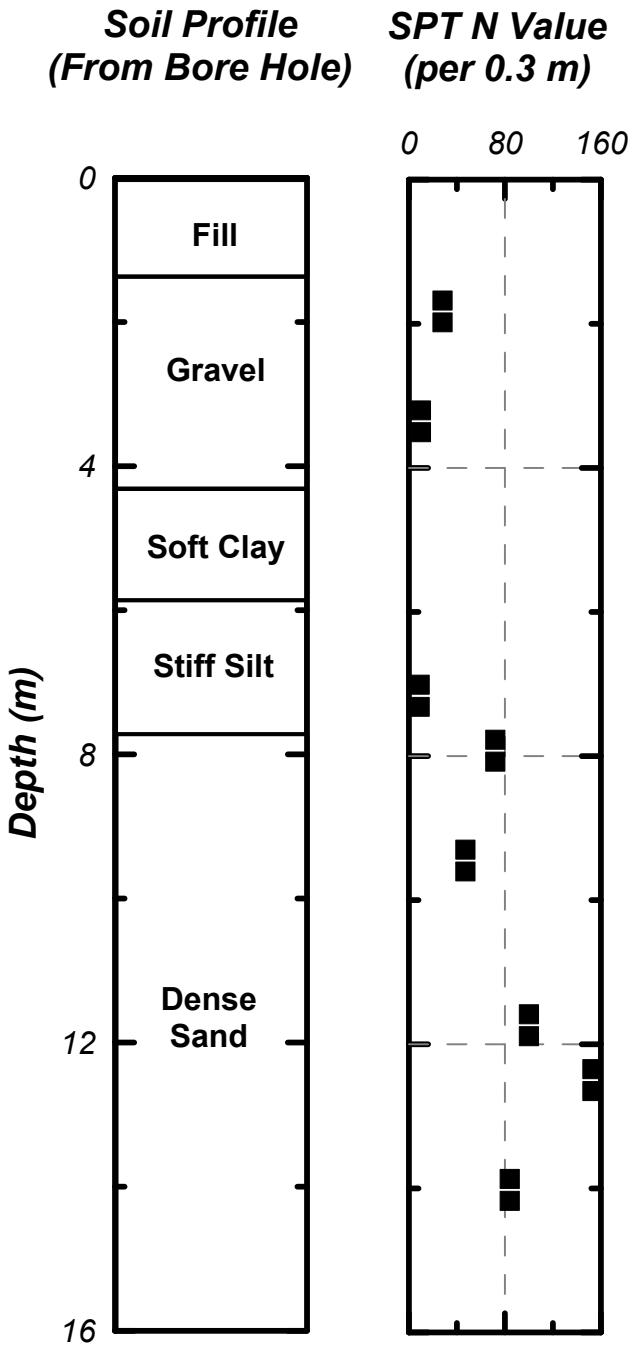


**Figure 4.6: Soil bore log and SPT N values obtained by Caltrans (Beddard et al. 1995).**

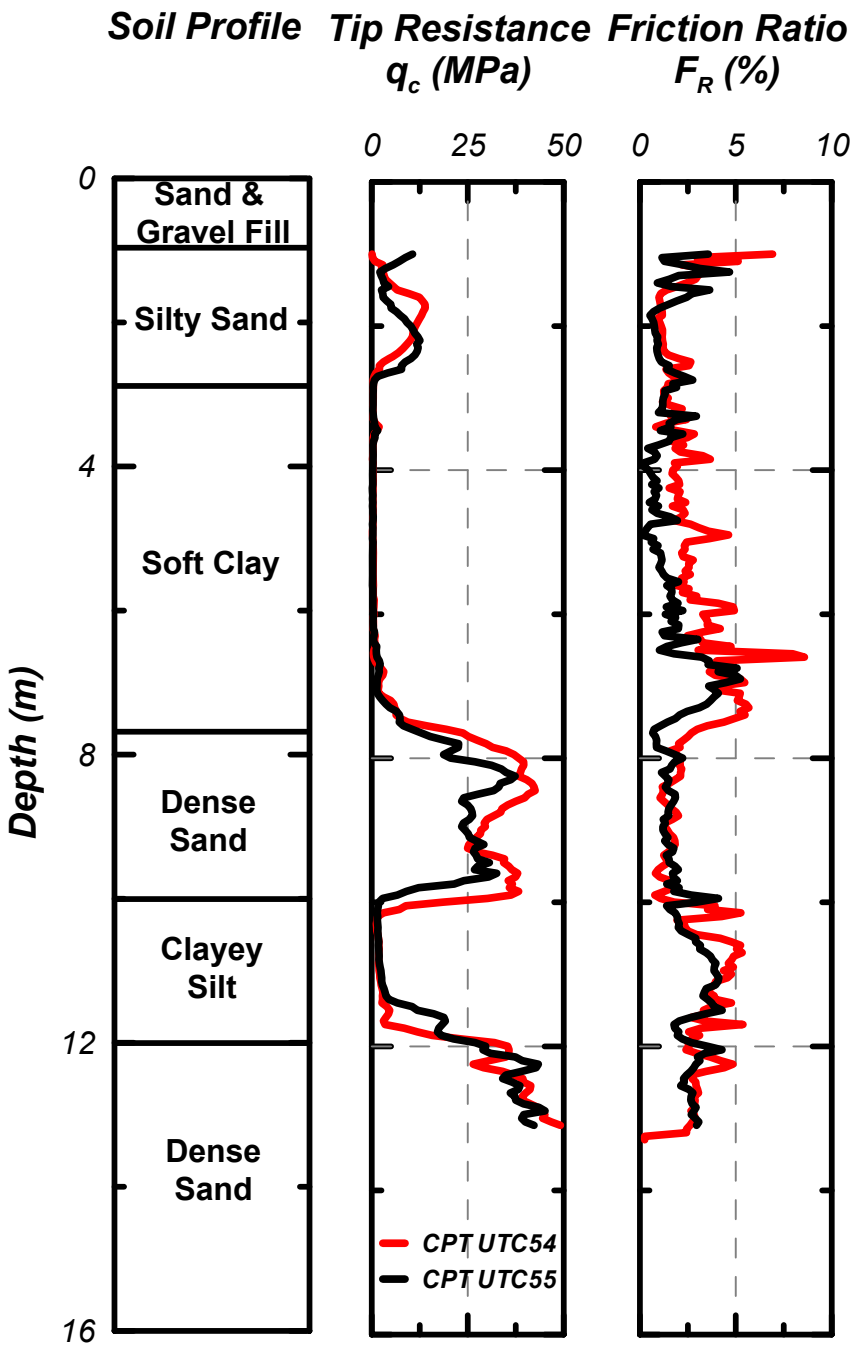


**Figure 4.7: CPT soundings and soil behavior type profile interpreted using Robertson (1990).**

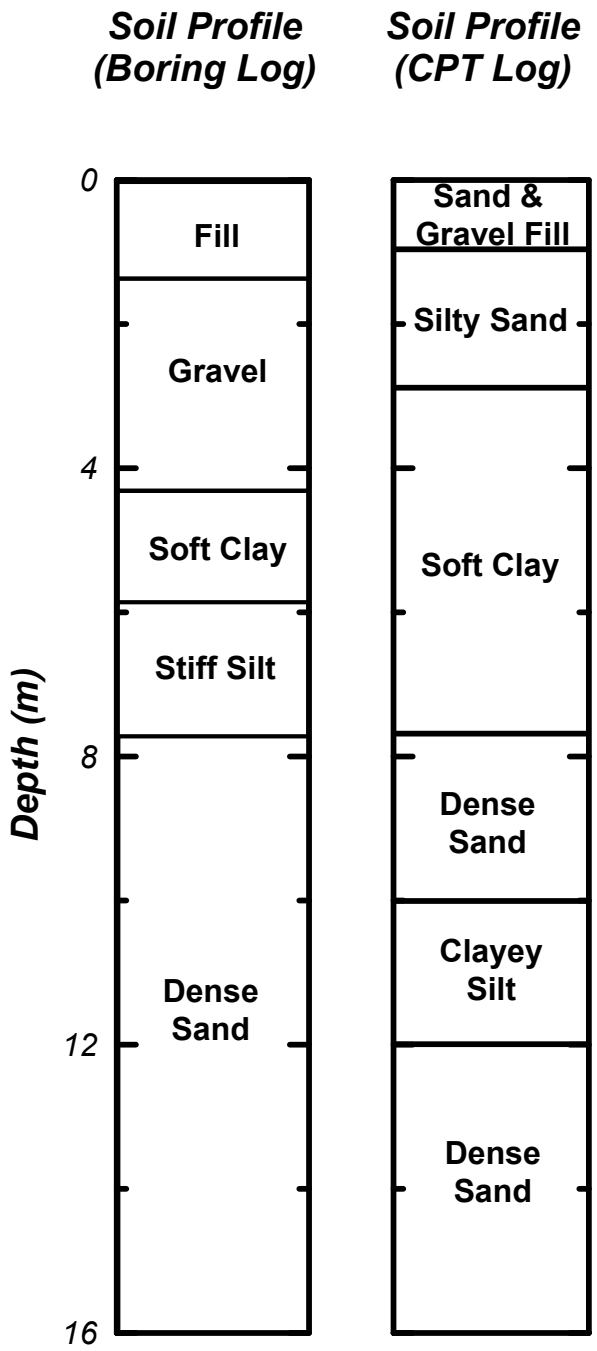


**Figure 4.8: Comparison of soil strata obtained from borehole data and constructed from CPT sounding data.**

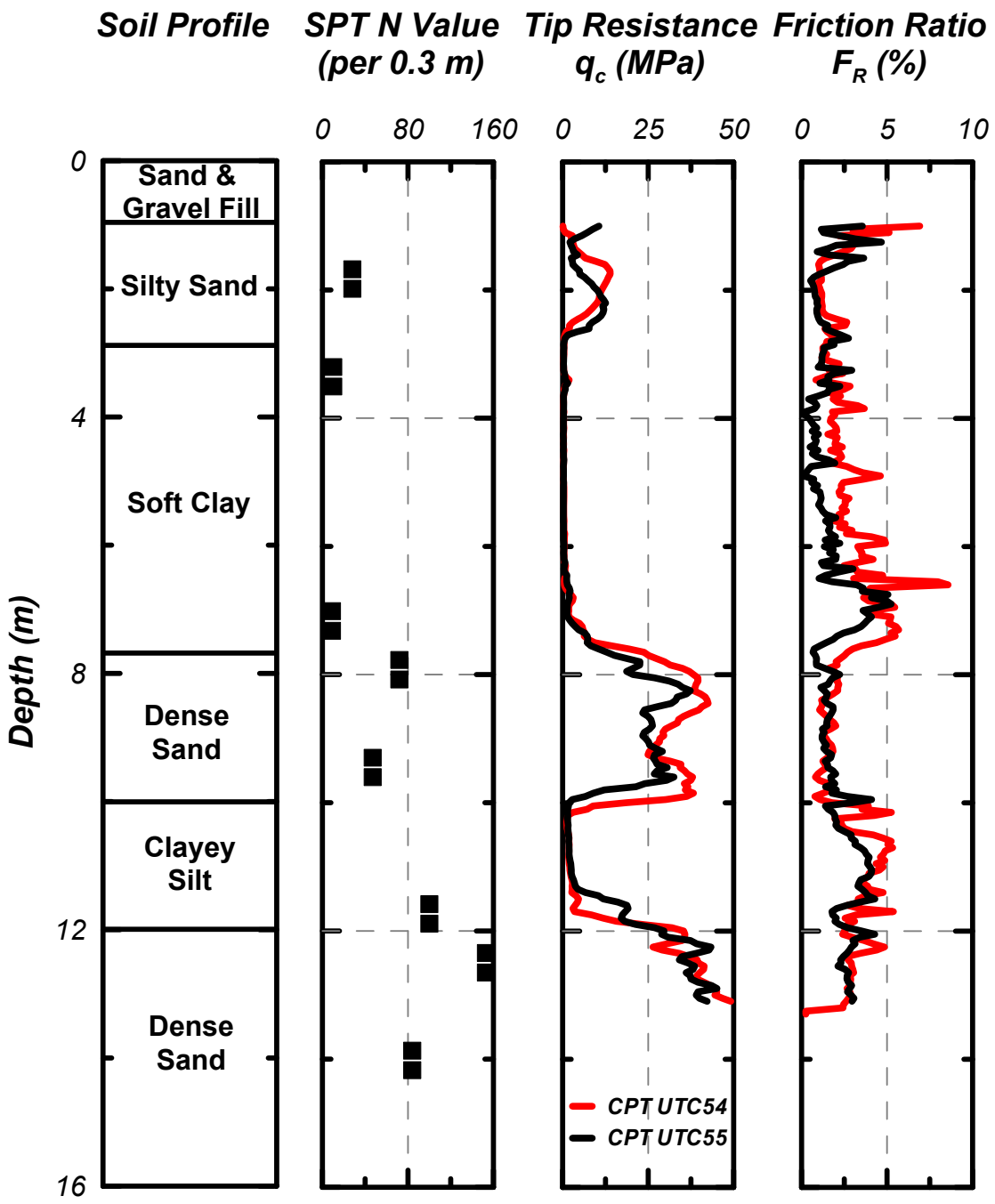


**Figure 4.9: Representative soil stratigraphy model alongside SPT N values and CPT soundings data.**

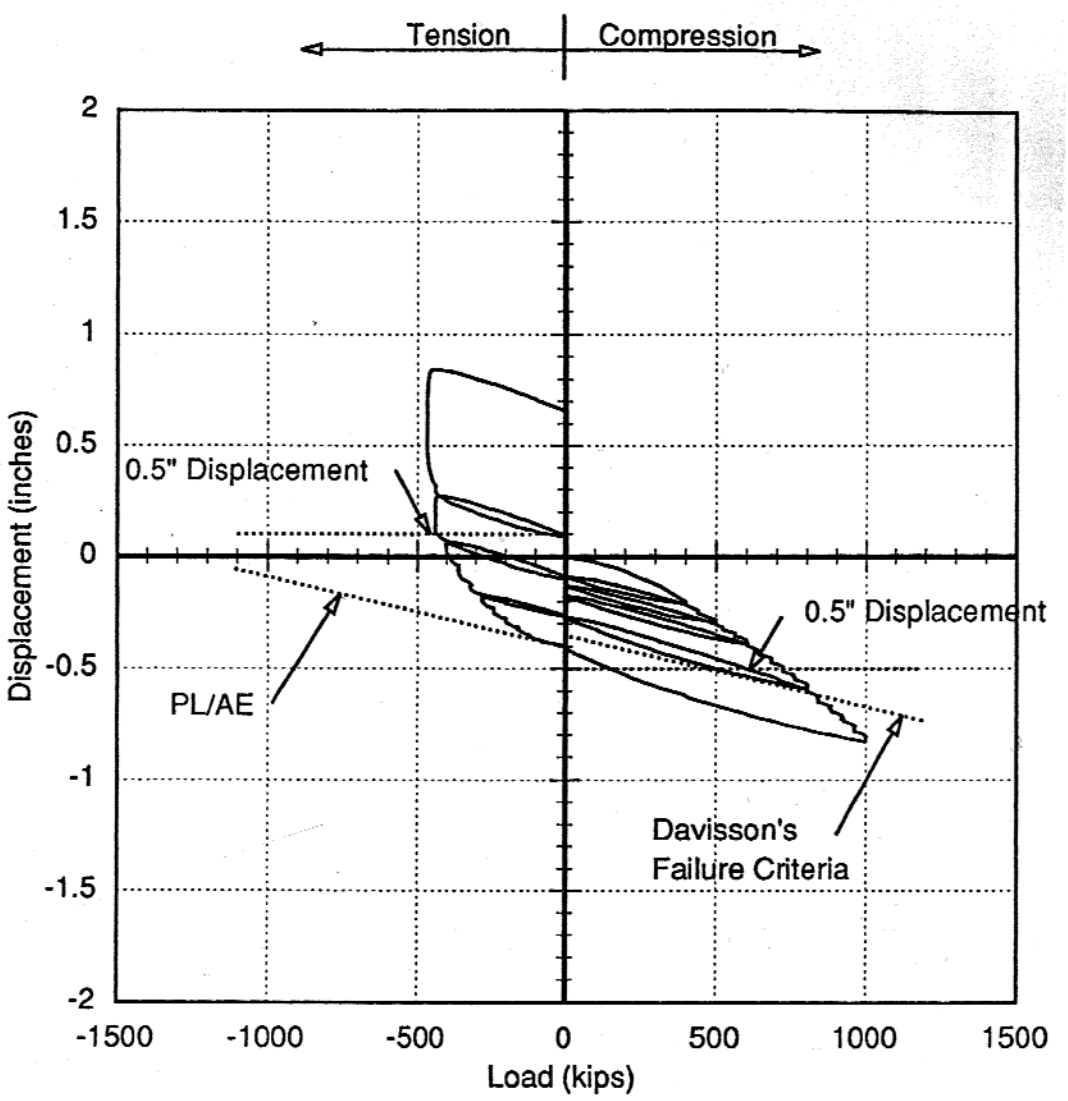


**Figure 4.10: Representative pile load test result from pile number 2-T performed as part of I-880 Replacement Project at Site 2.**

# Chapter 5: Reusable Test Pile (RTP) Performance during Driven Installation

This chapter focuses on the performance of the RTP system during driven installation in the field. Content presented includes driving records to illustrate the drivability of RTP system with the Becker hammer system, bounce chamber pressure records to show the variations in energy induced by Becker hammer with driving difficulty, and driving dynamics including wave propagation along the RTP system for various driving conditions and PDA type analysis. The driving analysis is presented for four driving depths that collectively represent a broad range of driving conditions from easy driving to driving refusal. Driving conditions are analyzed for RTP tip depths of 3.96 m (13 ft) when the tip is just entering the soft clay layer (3 m depth), at 9.3 m (30.5 ft) depth where the tip section is near the bottom of the upper dense sand layer, at 10.7 m (35 ft) depth where the tip section is in the middle of the softer clayey silt layer, and at the final penetration depth (~ 12.8 m, 42 ft) in the lower dense sand layer where the Becker driving system encountered penetration refusal.

## 5.1 Driving Records

The penetration resistance during driving with the Becker Penetration Test (BPT) can be monitored using a 'blow count per foot' metric in a manner similar to the SPT N-value. The measured blow count per foot for the RTP system, $N_{RTP}$, provides an indication of soil resistance for a given hammer energy and can be used to identify changes in soil resistance. However, soil

along the entire length of the RTP provides driving resistance due to the uniform cross-sectional area (i.e. there is no oversize driving bit like the BPT standardized test or the SPT test). This differs from the SPT where penetration resistance is only due to the soil in contact with the split spoon sampler.

The RTP driving record was obtained by monitoring the displacement of the top of the RTP continuously during the driving process using the long string potentiometer and NI-DAQ system described in Chapter 3. A summary of the measured $N_{RTP}$ profiles is presented in Figure 5.1. As evident, a high level of repeatability was achieved, with differences primarily occurring during penetration in the deeper dense sand layers.

A comparison between the $N_{RTP}$ profiles and nearby CPT soundings and SPT N-value profiles is presented in Figure 5.2. Caltrans obtained these insitu test measurements during prior studies (Beddard et al. 1995) at the same location. The proximity of the insitu tests with the RTP installation locations was, in general, less than 12.3 m (detailed arrangement presented in Figure 4.6).

The overall trends between the $N_{RTP}$ profile and the SPT data are similar. It is noted that the SPT advanced by 'weight of rod' through the soft clay layer and a SPT N-value was not obtained in the middle of the lower clayey silt layer. On Installation 2 and 3, the RTP also experienced free-fall under self weight during penetration through the soft clay layer, typically between depths of 3.0 m and 7.75 m depth. However, Installation 1 experienced low level soil resistance that resulted in higher displacement for each hammer blow in this soil region. In Figure 5.1 the corresponding $N_{RTP}$ value for Installation 2 and Installation 3 are reported as 0

and the $N_{RTP}$ value for Installation 1 is reported as less than 3. Although $N_{RTP}$ value for Installation 1 was very low, the bounce chamber pressure created during the impact registered values between 70 – 90 kPa. Installation 2 and 3 shows 0 kPa bounce chamber pressure as the RTP experienced free fall penetration.

The trends between the $N_{RTP}$ profile and the CPT sounding also generally agree, with the important exception during penetration through the lower clayey silt layer between depths of 10 m and 12 m. The cone tip measurement, $q_c$, within this layer is less than ~2 MPa, indicating minimal tip resistance. However, the $N_{RTP}$ value within this same layer remains relatively high at about 50 blows per 0.3 m. This is due to the $N_{RTP}$ being influenced by the total soil resistance along the entire length of the RTP pile. As a result, the $N_{RTP}$ is relatively high due the significant shaft friction that is generated in the overlying dense sand layer. This shows that the $N_{RTP}$ value alone may not be a reliable indicator of softer stratigraphic layers underlying harder stratigraphic layers.

## 5.2 Bounce Chamber Pressure during Driving

The efficiency of the Becker hammer varies during RTP driving and is generally dependent on the difficulty of driving conditions. Harder and Seed (1986) utilized the maximum bounce chamber pressure generated after a hammer blow as an indicator of hammer energy. The bounce chamber exists above the hammer mass (Figure 2.20). Following a hammer impact and simultaneous diesel combustion, the hammer mass accelerates upwards

while the pile accelerates downward. The air in the bounce chamber compresses during relative upward movement of the hammer, eventually reaching a maximum value when the hammer mass reverses direction and begins to move downwards. The upward acceleration of the hammer mass is dependent on driving conditions. The mass of RTP is higher than that of the hammer. During hard driving, RTP acceleration is low therefore the hammer acceleration is high. The higher hammer mass acceleration results in a higher bounce pressure, and overall higher hammer energy. During soft driving the opposite is true; upward mass acceleration is reduced, the bounce pressure is reduced, and hammer energy is lower. The bounce pressure in the RTP system was continuously monitored using a pressure transducer connected directly to the bounce chamber and the NI-DAQ data acquisition system (described in Chapter 3).

The measured relationship between the $N_{RTP}$ value and the bounce pressure is presented in Figure 5.3a for data from all three RTP installations (Installations 1 through 3). As evident, the range of both the $N_{RTP}$ values and maximum bounce pressures recorded is wide ranging. The $N_{RTP}$ values range from 2 to 220 while the bounce pressure ranges from 31.7 to 197.3 kPa (4.6 to 28.6 psi). The zero $N_{RTP}$ values and corresponding 0 kPa bounce pressures during the free fall through soft clay is not presented here as semi-logarithmic space is used. Penetration through the clay layer reported with lower $N_{RTP}$ values and corresponding lower bounce chamber pressures. On the other hand, penetration through the lower dense sand layer has very high values of bounce chamber pressure corresponding to higher $N_{RTP}$ values. Figure 5.3b presents the $N_{RTP}$ values separated by the soil type that the RTP tip is penetrating. Overall, there is a correlation in semi-logarithmic space between bounce chamber pressure and $N_{RTP}$.

The hammer energy correction method proposed by Harder and Seed (1986) is presented in Figures 5.3a and b for reference. The lower bounding line corresponds to the idealized relationship between bounce chamber pressure and Becker Penetration Test N-value known as hammer calibration combustion rating curve (property of hammer). The series of contour lines intersecting this reference line provide guidance for data correction obtained at lower hammer efficiencies. A data point falling on one of the contours should be corrected to the reference line following the contours.

The $N_{RTP}$ data presented herein was not corrected to this hammer efficiency reference condition because the force acting on the RTP pile from the hammer impact is measured directly (and presented below). Nonetheless, it is interesting that the data obtained by the RTP exceeds the correction range proposed by the method. Comparatively easier (low $N_{RTP}$ values) and harder (high $N_{RTP}$ values) driving conditions were experienced. Also, hammer efficiencies greater than rated were also observed (indicated by data lying below calibration combustion rating curve).

## 5.3 Blow Counts and Bounce Chamber Pressure under Different Driving Conditions

The RTP driving conditions and the corresponding bounce chamber pressure was evaluated considering penetration at four different depths. These depths represent easy driving conditions at about 4 m (13 ft) as the RTP is entering the soft clay layer, hard driving conditions at about 9m (30 ft) as the RTP is driven through the upper dense sand layer,

moderate driving conditions with high shaft friction and low tip resistance at about 11 m (35 ft) as the RTP is driven through the lower clayey silt layer, and hard driving conditions prior to refusal at about 13 m (42 ft) as the RTP is driven into the lower dense sand layer. The following provides a systematic discussion on the RTP driving performance for these four representative conditions.

### 5.3.1 Soft Driving Condition as RTP Enters Clay Layer at about 4 m

RTP penetration through the soft clay layer represents the easiest driving conditions that are realistically possible. In fact, immediately following the hammer blows while the RTP penetrated the upper half of the clay layer presented in this section, the RTP pile free-fell under self weight to the bottom of the clay layer (starting at a depth of about 4 m). Reduced driving conditions in the soft clay layer were evident from a depth of about 4 m and down to the base of the clay layer at about 7 m. It is noted that the soil profile generated from CPT sounding indicated the soft clay layer to begin at a depth of about 2.75 m. The difference between the top of the clay layer as detected by the CPT and the depth where easy RTP driving conditions began is attributed to some over-consolidation of the upper portion of the clay layer and spatial variability between the location of the CPT sounding and the RTP installation. In fact, the depth of easy driving was observed to increase between Installations 1 and 3, again reflecting local variability in layer boundary elevations.

The blow count and corresponding bounce chamber pressure recording with time for penetration over the final 0.3 m (1 ft) interval recorded prior to RTP free fall conditions is presented in Figures 5.4 through 5.6 for Installations 1 through 3. As evident, very few hammer blows, between 3 and 5, were required to advance the RTP by 0.3 m (1 ft). These soft driving conditions resulted in large displacements for each hammer impact. Installation 2 and 3 averaged about 0.1 m (0.3 ft) penetration per hammer blow while Installation 1 averaged about 0.04 m (0.14 ft) penetration per impact. The comparatively lower penetration per blow in Installation 1 is attributed to the weight of the RTP at this depth during driving being about 115 kg less than that for Installations 2 and 3 (517 kg for Installation 2 and 3 compared to 402 kg for Installation 1). Installation 1 had the different RTP assembly than installation 2 and 3.

The large displacements and rapid penetration of the RTP through the clay layer, which has very low permeability, results in driving conditions that can be considered undrained. The average undrained shear strength of the sensitive clay for this soft driving condition is about 12 kPa (250 psf, based on the CPT $q_c$ measurement and an $N_{kt}$ value of 13). The stress at the tip of the RTP pile given its diameter and weight, and assuming negligible shaft resistance, would result in 177 kPa for Installation 1 and 228 kPa for Installation 2 and 3. Assuming an end bearing factor of 11 (per Fleming et al. 2009), and the estimated undrained strength, the unit based capacity is estimated to be 132 kPa. It is noted that the rapid penetration conditions differ from conventional static end bearing analysis. Firstly, the rate of loading is higher, which could result in an increase in undrained strength and some inertial resistance. At the same time the rapid loading may degrade and remold the soil more quickly, resulting in strength reduction. Nonetheless, this value is below the applied stress on Installation 2 and 3 indicating

that bearing capacity failure is likely and comparable to the stress at tip on Installation 1, still indicating that bearing capacity failure is likely provided the negligible shaft friction component. Shaft friction is neglected in this argument based on dynamic degradation and remolding of material will reduce its strength.

The bounce chamber pressure time history also provides an indication of the soft driving conditions encountered during penetration of the clay layer. Immediately after impact the hammer piston travels upward due to the reaction diesel combustion in the lower chamber. As stated previously, under hard driving conditions compression in the upper chamber is higher (i.e. bounce chamber pressure is higher) and under soft driving conditions the pressure is reduced. Figures 5.4 to 5.6 present bounce chamber pressure measurements as tip penetration approaches the soft clay for all three installations.

For all recordings the bounce chamber pressure reaches zero value during hammer impact since the bounce chamber is vented and then increases to a maximum value when the hammer mass reaches its maximum height. During Installations 2 and 3 the maximum bounce pressure obtained begins at a pressure of about 40 kPa (6 psi) and then decreases down below 28 kPa (4 psi) after three hammer impacts as the RTP free fall condition is approached. For the slightly harder driving conditions encountered during Installation 1 the bounce chamber pressure value was relatively constant and remained at about 85 kPa (12.5 psi).

RTP depth during driving plots presented in Figures 5.4 to 5.6 also indicate that the RTP continues to slowly advance into the clay layer between each hammer impact; RTP pile movement is continuous during the entire 0.3 m of penetration. This slow advancement

between hammer blows is evident as a mild slope of RTP depth versus time. Installations 2 and 3 the RTP driven depth showed about 0.1 m (0.3 ft) penetration between the first and second hammer blows. On the other hand, the plot for Installation 1 shows a very mild slope between hammer blows, indicating that the RTP reached a stable condition between hammer blows.

### 5.3.2 Hard Driving Condition as RTP Penetrates Upper Dense Sand Layer at about 9 m depth

RTP driving conditions through the upper dense sand layer represent hard driving conditions that can be sustained and lead to successful penetration with the Becker hammer system. The upper dense sand layer begins at a depth of 7.5 m (24.6 ft) and extends down to a depth of 9.9 m (32.5 ft). The RTP penetration blow counts per 0.3 m advancement and corresponding bounce chamber pressure with time for penetration from 9.14 m (30 ft) to 9.45 m (31 ft) are presented in Figures 5.7 to 5.12. Each figure includes an additional figure showing a magnified time scale of the driving record to better examine performance for an individual, representative blow. It is noted that the wire of the string potentiometer itself vibrates during driving, resulting in the steady noise band of about 3 mm and the initial decrease in displacement to a stable value following each hammer blow.

Hard driving conditions result in a small displacement per hammer blow, and therefore a higher blow count per 0.3 m (1 ft) of penetration. During Installation 1 (Figure 5.7) penetration required 90 blows per 0.3 m, resulting in an average displacement per blow of 0.003 m (0.01 ft). Installation 2 and 3 records shows 55 and 70 blows per 0.3 m penetration,

respectively, and resulted in 0.005 m (0.018 ft) and 0.004 m (0.014 ft) penetration for each blow.

The number of blows per foot applied by Becker hammer system is dependent on the energy efficiency of the hammer impacts. In this layer the energy efficiency was higher than during penetration of the soft layer, and yet many more hammer blows were required. The recording presented for Installation 1 in this layer includes the hammer performance immediately following starting of the hammer. The Becker hammer does not immediately operate at its full capacity on the first blow. Instead, the bounce pressure is initially low and then gradually increasing with subsequent blows (Figure 5.7). As the hammer reaches a steady state condition the energy (and bounce pressure) becomes consistent and the RTP is advanced at a steady rate. This trend is also evident during Installation 3 when driving was stopped to add an additional pipe section to the RTP. As evident in Figure 5.11 with two sets of plots, driving first occurred from 9.14 m to 9.33 m followed by additional driving after a pipe section had been added from 9.33 m penetration depth. This variation in Becker hammer energy, even during penetration of a uniform profile, highlights the necessary of correcting Becker hammer blow counts for the hammer energy level.

The RTP displacement time history recorded by the string potentiometer successfully captures the number of blows per foot. However, the displacement per hammer blow is very small. During driving the Becker rig experiences vibrations that result in the string potentiometer wire continuous vibrating. The magnitude of these vibrations relative to the displacement per pile blow is sufficiently high that it is evident in the magnified plots.

Nonetheless, it was evident that the RTP does not continue to move between hammer impacts as was observed earlier during penetration through the soft clay.

The harder driving conditions directly result in the hammer efficiency increasing as indicated by the measured increase in bounce chamber pressure. The bounce chamber pressure averaged 165 kPa (24 psi), 200 kPa (29 psi), and 186 kPa (27 psi) during 0.3 m of penetration during Installations 1, 2, and 3, respectively.

### 5.3.3 Moderate Driving Condition as RTP Penetrates Clayey Silt Layer at about 11 m depth

Continued penetration of the RTP at the site resulted in the tip penetrating the softer clayey silt layer after penetrating the overlying dense sand layer. This condition is somewhat unique, and not one that was directly considered when developing the Becker Penetration Test methods (Harder and Seed 1986, Sy 1993). The condition of a softer layer underlying a denser layer occur frequently when earthen construction works placed dense compacted fill on natural soft deposits (e.g. dams, abutments, levees over soft alluvial soils). RTP penetration with this variation of soil layering results in the shaft friction in the upper sand layer, not the tip resistance in the clayey silt layer, providing the primary resistance.

The softer clayey silt layer underlying the dense sand begins at a depth of about 9.9 m (32.5 ft) and extends down to a depth of 12 m (39 ft). The RTP penetration blow counts and corresponding bounce chamber pressure with time for penetration from 10.4 m (34 ft) to 10.7

m (35 ft) are presented in Figures 5.13 to 5.18. As above, an accompanying figure showing the magnified time scale is presented.

The $N_{RTP}$ value, resultant displacement per impact, and corresponding maximum bounce chamber pressure all reflect the slightly easier driving condition relative to the above sand layer. Installation 1 records show an $N_{RTP}$ value of 36 (0.009 m (0.028 ft) penetration per impact) and a corresponding bounce chamber pressure of about 165 kPa (24 psi). Installation 2 records contain similar trends ($N_{RTP}$ = 42, 0.007 m (0.024 ft) penetration per impact, average bounce chamber pressure = 138 KPa (20 psi)). Installation 3 exhibited slightly easier driving ($N_{RPT}$ = 29, 0.01 m (0.034 ft) penetration per impact, average bounce chamber pressure = 172 kPa (25 psi)).

### 5.3.4 Hard Driving Condition to Refusal as RTP Penetrates Lower Dense Sand Layer at about 13 m.

The RTP was continually advanced until driving refusal conditions were encountered at a depth of about 12.8 m in the underlying dense sand layer. RTP advancement was generally ceased, except in Installation 2, when the $N_{RTP}$ value approached 150 or more (estimated by extrapolating number of blows measured for a smaller increment of displacement). This section describes the hard driving conditions encountered prior to refusal. The lower dense sand layer starts from a depth of 12 m (39.5 ft) and continues below the depth of investigation. Driving was terminated at depths of 12.8 m (42 ft), 13 m (43 ft), and 12.6 m (41.5 ft) for

Installations 1, 2, and 3, respectively. It is noted that the greater depth of penetration for Installation 2 occurred as the objective was, in part, to assess RTP system robustness during driving refusal conditions. The $N_{RTP}$ value for this Installation was closer to 300. Under these latter driving conditions the thin walled cylinder hoop strain measurement deformed and soil penetrated in the gap behind the cylinder where the strain gages were installed (similar to what was described in Section 3.4.1.2). This resulted in damages to many hoop strain (radial stress) measurements and some of the axial force measurements. However, the structural integrity of the pipe section overall as well as of the remaining sensors was maintained.

The very difficult driving conditions encountered are evident in the $N_{RTP}$ values, displacement per hammer impact, and average bounce chamber pressure recordings. The $N_{RTP}$ values and corresponding bounce chamber pressure with time are presented for 0.3 m of penetration prior to refusal conditions in Figures 5.19 to 5.24. Installation 1 had an $N_{RTP}$ value of 111, a corresponding average penetration of 0.003 m (0.009 ft) per hammer impact, and an average maximum bounce chamber pressure of 186 kPa (27 psi). The harder driving conditions for Installation 2 are evident in respective values of 195 blows / 0.3 m, 0.0015 m (0.005 ft) penetration per blow, and 200 kPa (29 psi) average maximum bounce chamber pressure. Values for Installation 3 were similar to Installation 1 ($N_{RTP}$ = 75, 0.004 m (0.013 ft) penetration per blow, and 165 kPa (24 psi) average maximum bounce chamber pressure.

## 5.4 RTP Installation Driving Dynamics

Measurements of axial force and acceleration within each instrumented module as well as in the tip section were monitored during RTP installation using the Geodaq system (described in Chapter 3), enabling dynamic wave propagation analysis and pile driving analysis (PDA). Herein measurements and analysis are presented for the four driving conditions (and associated installation depths) described previously. Figure 5.25 presents a schematic outlining the position of the tip and each instrumented section when measurements were recorded for the four different conditions during Installation 1.

The as-recorded strain data required post-processing before it could be used for analysis. The analog low-pass antialiasing filter circuit was set too low during fabrication of the data acquisition units, which affected the magnitude and phase of the recorded signal at frequencies of interest in the analysis (about 400 Hz). A correction algorithm using a simple inverse transfer function was developed after field testing. The algorithm was determined to recover more than 95% of the higher frequency signals of interest (between about 300 Hz and 1 kHz). This correction algorithm was applied in frequency domain after removing residual driving stresses from the time history if any existed (residual driving stresses are recorded as a constant offset in force). The residual force offset value was then reapplied to the record after correction of the high frequency data.

### 5.4.1 Wave Propagation

Dynamic wave propagation through each instrumented section and the tip in the RTP pile for the different depths and installation events is presented. Acceleration and axial load measurements at each instrumentation location show the impact wave propagation downward to the pile tip and the reflected wave as it returns to the pile top. Figures 5.26 to 5.29 present the results for each section with annotations indicating the section depth below the ground surface and the vertical spacing to the next instrumented section below. Figures also include the conventional 0L/c (impact wave) and 2L/c (reflective wave) reference lines, where L is the length from the measurement location to the pile tip and c is the wave velocity (equal to 5142 m/s for the RTP steel pipe), indicating the times when the impact wave first passes an instrumentation location and when the reflected wave then passes the instrument location. Wave velocity was back calculated based on the time required for the wave to travel to the pile tip and return to the top instrumented section. This velocity was consistently used in all subsequent calculations. Impact wave time at top section was picked by visual interpretation and then following impact wave and reflection wave times at different sections were calculated using the distances between instrumentations and wave velocity. If an instrumented section was not connected to the RTP pile the respective plot is labeled with “NA” (not applicable). If a sensor was not functioning properly and no data was obtained the respective plot is labeled with “NP” (not possible).

#### 5.4.1.1 Wave Propagation for Soft Driving Conditions as RTP Enters Soft Clay Layer

The last set of axial load and acceleration recordings prior to the RTP pile penetrating the soft clay layer is presented in Figure 5.26 for Installation 1. The pile length was 4.76 m (15.625 ft), which corresponds to a 2L/c time for the top RTP section of 0.002 seconds.

During the soft driving condition, with low $N_{RTP}$ values and bounce chamber pressures, the recorded dynamic accelerations and axial loads are relatively low. The maximum acceleration recorded at the RTP pile top as the impact wave travels downward is about 250 g. However acceleration reached closer to 500 g as the pile and hammer travels together due to the easier penetration condition and pile hammer strike again during travelling. The maximum dynamic axial force in the top RTP section is also relatively low, and is less than 445 kN (100 kips). There is also a difference immediately prior to hammer impact. The accelerometer recording is stable and remains close to 0 g as expected. However, the recorded axial force time history gradually increases, ramping upwards, prior to the actual hammer impact. This ramping is associated with the force applied to the RTP pile while the pressure inside the diesel compression chamber of the hammer increases as the impact mass moves downwards. This ramping is recorded, with decreasing magnitude, in all RTP measurement locations.

The propagation of the impact wave downward through the RTP is clearly evident in both the acceleration and axial force records. The maximum acceleration remains approximately constant while the axial force decreases with depth down to a value of about 222 kN (50 kips). The reduction in axial force is due to the dynamic shaft resistance along the RTP. The axial load measurement within the RTP tip shows the end bearing as well as the shaft

friction that occurs along the bottom 21.6 cm (8.5 in) of the RTP pile wall. On the other hand, the top instrumented section indicates the total load applied to the pile. Thus, the dynamic axial force difference between any two sections is the average dynamic shaft resistance between them. In this case the shaft resistance provides about 50% of the driving resistance.

#### 5.4.1.2 Wave Propagation for Hard Driving Conditions as RTP Penetrates Upper Sand Layer

The hard driving conditions during RTP penetration of the upper dense sand layer expectedly result in an increase in overall maximum dynamic acceleration and axial force. Figure 5.27 presents the wave propagation recordings for these hard driving conditions for Installation 1.

The maximum acceleration measurement is in the range of 750 g throughout the RTP length. The maximum axial force measurement at the top is about 900 kN (200 kips) and at the tip it is about 700 kN (157 kips). However, the axial load measurements at other two intermediate sections were reading more than that on the top. This is unexpected. Axial residual stresses stored in the RTP sections due to driving (about 100 kN) and reflective waves from joint and impedance contrasts could contribute to this unexpected behavior. Overall the acceleration and force time histories are consistent with those typically observed for the hard driving conditions (Fang 1991).

#### 5.4.1.3 Wave Propagation for Moderate Driving Condition as RTP Penetrates Clayey Silt Layer

RTP installation into the soft clayey silt layer below the dense sand layer results highlights how the distribution of penetration resistance between tip and shaft resistance can vary significantly. Figure 5.28 presents the recording for Installation 1.

The moderate driving condition, with relatively high shaft friction and minimal tip resistance, produce moderately high accelerations and axial force measurement at the surface. The maximum acceleration, occurring during hammer impact, is about 500 g throughout the RTP length (at all measurement locations). This is about 50% of that encountered during penetration of the dense sand layer, indicating that the maximum acceleration is primarily dependent on the pile tip resistance. The axial force, also maximum during the initial hammer impact, is about 800 kN (180 kips) at the RTP top instrumented section above the ground and remains at this magnitude until the top of the upper dense sand layer (depth of 8.23 m and position of instrumented section S2), indicating minimal shaft resistance generated in the top fill and soft clay layers. The axial force then decreases significantly within the dense sand layer due to high shaft friction, arriving at the RTP tip (section S0) with a value of about 250 kN (56 kips).

#### 5.4.1.4 Wave Propagation for Hard Driving Condition to Refusal as RTP Penetrates Lower Dense Sand Layer

RTP driving in the lower dense sand layer to a refusal condition results in the highest acceleration and force measurements obtained. Also, since the total RTP length (including above ground stickup) was 15.13 m (49.625 ft) wave propagation is captured more clearly. It is noted that the eventual operational conditions for the RTP on Caltrans projects will be for about 10 to 40 m lengths. Therefore results for this RTP length may be most representative of what may be generated on future Caltrans projects. Figure 5.29 presents the dynamic recordings for Installation 1 at this depth.

The near-refusal hard driving conditions yield very high acceleration and axial force measurements. The maximum acceleration is almost 1000 g near tip and about 750 g at top. The accelerometer at the tip experiences the effect of reflection wave before it registered the peak acceleration from initial impact wave. The arrival time for impact and reflection wave is also presented in Figure 5.29. The maximum axial force at the RTP top is about 950 kN (215 kips). This value reduced to about 600 kN (135 kips) at the tip as expected due to the high shaft friction in upper dense sand layer. However, sections S3 and S2 show almost 1100 kN (247 kips) axial force and indicate very low shaft resistance in upper dense sand layer. Shaft resistance (function of radial effective stress) reduces as a function of normalized distance from the pile tip (Lehane et al. 1993). Here the pile tip advanced almost 3.5 m beyond the bottom of upper dense sand layer, resulting in a reduction in shaft resistance. Section S3 shows almost

same axial force measurement as the top above ground section, indicating that negligible shaft resistance is provided by fill material and clay layers.

#### 5.4.1.5 Wave Propagation Compilation for Entire Driving Record

Compilation of the dynamic driving data obtained throughout RTP installation enables overall trends with depth to be investigated. Figure 5.30 presents, versus depth, the (a) maximum force measured at the RTP head and tip, (b) the dynamic shaft resistance (determined as the different between the maximum force at the head and tip), and (c) the ratio of the tip force to the total force applied at the RTP head. The dynamic force profiles capture the driving conditions with depth and the different driving conditions discussed previously. The dynamic shaft resistance does not increase significantly until the RTP penetrates the upper dense sand layer. Below this depth the shaft friction increases rapidly. The shaft resistance then decreases again as the RTP penetrates through the clayey silt layer. The proportion of the overall driving force that is generated by the RTP tip resistance remains relatively high, above 50% until the RTP penetrates the clayey silt layer. In this layer the RTP tip force decreases significantly and nearly all the penetration resistance is due to shaft resistance.

A comparison of the RTP driving force to the CPT $q_c$ measurement is presented in Figure 5.31. The RTP dynamic resistance is presented in units of stress by dividing the measured axial force by the projected area of the RTP tip (0.022 $m^2$), and is denoted with the term $q_{dyn\_RTP}$. The RTP dynamic penetration resistance, $q_{dyn\_RTP}$, is computed and presented for both the maximum

force recorded at the RTP head and tip. Overall, the $q_{dyn\_RTP}$ values, regardless of whether the recorded head or tip force is used, track the CPT $q_c$ profile. During penetration of the two dense sand layers the RTP tip $q_{dyn\_RTP}$ values are slightly below the $q_c$ values while the RTP head $q_{dyn\_RTP}$ values are slightly above. However, significant differences exist during penetration of the soft clayey silt layer. In this layer the RTP tip resistance is a small percentage of the overall driving resistance. As a result the $q_{dyn\_RTP}$ values based on the RTP head significantly over estimate this layer. In fact, it could be argued that they do not even detect the softer layer. However, the $q_{dyn\_RTP}$ values based on the RTP tip do much better at detecting the softer layer.

### 5.4.2 Stress Wave Analysis during Pile Driving

Analysis of pile driving using simultaneous measurements of axial force (from strain gage measurements) and acceleration (from accelerometers) provide further insight into pile driving conditions. The acceleration time history was integrated to obtain a velocity time history, and then integrated a second time to obtain a displacement time history at the measurement location. The velocity time history was used with the impedance concept to obtain an estimate of an equivalent force time history (Timoshenko et al. 1970). Comparison of the directly-measured axial force history with the velocity impedance-based force estimate provides unique insight into quality of collected data, pile resistance, and capacity (Goble et al. 1980). In addition, the energy input for a given hammer blow can be estimated using the force and velocity time histories. Force and velocity are only proportional for unidirectional wave propagation in an unbounded medium and thus only exists in the absence of wave reflection.

For this reason, proportionality is only expected for the short period of time immediately following the hammer impact at the pile head. Herein results of these analyses are presented for the four driving conditions discussed previously and are then compiled and compared over the entire installation depth.

Data processing and analysis was required for presentation of the data in the following plots. It is known that the RTP acceleration and velocity before and after the hammer impact event must be 0 g and 0 m/sec, respectively. Therefore two corrections were applied to the acceleration time history record. First, the mild constant slope in the acceleration record that existed and was almost equal before and after the hammer impact event was removed by re-zeroing the data about a linear trend line that was fitted to the slope prior to hammer impact. The mild slope (typically 0.3 g / second to 10 g / second, note the noise level in acceleration caption is about ± 0.5 g) was attributed to sensor warming immediately after powering up (which occurred prior to every measurement obtained). Second, an offset between the pre and post hammer impact acceleration was observed. This offset was general less than ± 3 g and was attributed to the accelerometer performance during the hammer impact event. A ($1\text{-}cos\theta$) function was used correct the post impact mean acceleration value to 0 g. The ($1\text{-}cos\theta$) function was applied within a time window defined to start at the beginning of the hammer impact (when acceleration first increased rapidly) and end when the impact signal had attenuated to small values. The end value typically occurred at a time corresponding to about 15-20 L/c after hammer impact and when the velocity and recorded strain-based force measurement were close to zero. The same method of correction was applied to the

integrated velocity time history in order to ensure 0 m/sec velocity prior to and after impact without any drift.

The impedance based force calculation used the following equation:

$$F = v \times \frac{EA}{c}$$

where v is the velocity, E is the elastic modulus of the steel (E = 206,843 MPa for the RTP pile), A is the cross-sectional area of the pile (A = 0.0096 $m^2$ for the instrumented sections), and c is the wave speed through steel (c = 15,316 m/s obtained from $c = \sqrt{\frac{E}{\rho}}$ where steel density $\rho$ = 7,833 kg/$m^3$) (Timoshenko 1970, Measurements Groups, Inc. 1988). It is noted that this equation is based on a simplified solution for an unbounded rod in air. The pipe connection joints between sections and the varying sidewall thickness violate this assumption as these generate some amount of upward reflected waves during downward wave propagation. However, this error was estimated to be less than 15% and therefore use of this equation is considered reasonable for initial evaluations (it is also the standard equation used by industry). In addition, a rigorous solution for wave propagation near the driving head, accounting for the changes in section area along the upper instrumented sections showed the potential error due to using this impedance would be quite small (Ghafghazi, personal communication). Finally, the energy time history was computed from the strain gage based force and displacement time histories.

A representative set of plots obtained with the data processing method is presented in Figure 5.32, which is a single measurement record from the RTP head during hard driving

through the upper dense sand layer. Plots of corrected acceleration, integrated velocity, and integrated displacement are first presented, followed by the direct strain gage force measurement recording. For comparison, the impedance velocity based force estimate is also presented in the latter plot. Finally, the energy time history plot is presented. The energy is presented as a percentage of the theoretical maximum possible energy, which is equal to 10.85 kJ based on the Becker hammer specifications.

#### 5.4.2.1 Stress Wave Analysis for Soft Driving Conditions as RTP Enters Soft Clay Layer

Analysis of the easy driving condition through the soft clay layer is presented in Figure 5.33. Results are presented for both measurements at the RTP head (Figure 5.33a) and tip (Figure 5.33b). Composite plots of direct strain gage force measurements and for impedance velocity based force (v*z force) estimates are presented together. The computed displacement and energy time histories are also presented together. During driving through the soft clay layer the RTP is rather short (5.3 m in length), resulting in a head and tip measurement separation distance of 4.6 m (15 ft). As a result the time delay between the downward impact wave and the upward reflective wave even at the top section is very short (about 0.0019 sec). In fact, the 2L/c time period is less than the duration of the impact wave. This is captured in the higher frequency oscillations within the hammer impact duration (i.e. frequency of wave reflection is higher than frequency of hammer impact). Figure 5.33 also presents the wave travel time for 0L/c, 1L/c, and 2L/c.

The direct strain gage measurement from the head section from Figure 5.33 shows about 550 kN of axial force and tip section shows about 250 kN of axial force. Top section reading indicates the total load transfer to the pile while the tip section reading indicates the amount of load transfer to the tip. Here more than 50% of total dynamic resistance comes from shaft resistance between the head and tip section. Although the instrumented section at the bottom is referred to as the tip section, the instrumentation measuring axial load is located 0.2 m behind the tip in Installation 1 and 0.6 m behind the tip in Installations 2 and 3. Shaft resistance generated from this short-section also contributed to the axial force, and to a noticeable degree when the tip was embedded in the dense sand layers.

Impedance based force values are calculated based on an acceleration record from each section. Figure 5.33 shows that the impedance based force for the head section and tip section is higher than the strain gage measured force. This behavior can be expected in the tip section since wave reflects back much quicker as it has to travel through very short section. Generally it is expected to see good agreement at the head section until the reflective wave begins to return (at about 1L/c). However, Figure 5.33a presents impedance based force showing higher axial force than the measured axial force at the time of 0L/c. This behavior is unexpected and detailed reanalysis of the force and accelerometer measurements and of the calculation schemes implemented did not identify any errors. While further work is needed, it is hypothesized that this difference may be due to the impedance contrasts at changes in cross-section area (e.g. reduced wall thickness for axial load strain gages). Nonetheless, the longer period of impedance based force and low magnitude of axial force shows the relatively easy driving condition.

Displacement calculation from the acceleration measurement shows that the head displaced by 3.5 cm and the tip displaced by 3 cm. Head and tip displacements are almost equal and show the uniform displacement of the RTP during the single impact analyzed. This agrees well with the physical measurement (presented in section 5.3.1) in the field that showed the RTP head displaced by 4.3 cm per impact at this depth. The larger displacement during the impact also reflects the easy driving condition.

Energy calculation at the top (based on measured force and acceleration measurements) shows that about 52% of theoretical maximum hammer energy is transferred to the head section. The tip section received about 38% of the maximum theoretical hammer energy. Energy transfer from head to tip is reduced by the work done in shaft resistance.

#### 5.4.2.2 Stress Wave Analysis for Hard Driving Conditions as RTP Enters Upper Sand Layer

Pile driving analysis for the harder driving conditions encountered as the RTP penetrates the upper dense sand layer are presented in Figure 5.34. During this driving recording the RTP length was 12.6 m (41.3 ft), resulting in the head and tip measurements being separated by 12.1 m (39.6 ft). The RTP tip was at a depth of 9.3 m (30.5 ft).

Strain measured force at the head and tip shows lower magnitude compared to the force calculated based on measured acceleration records. Although the calculated and measured peak forces do not agree, they follow the same trend up to the time period of 2L/c. The strain based axial force difference between the head and tip section shows the dynamic

shaft resistance. The head section shows about 900 kN of peak force and the tip section shows about 600 kN of peak force. Impedance based force at head section is about 40% higher than the strain measured force. The magnitude of the force measurement and wave pattern of impedance based force reflects the hard driving condition.

The displacement plot in Figure 5.34 shows that head section displaced less than 0.25 cm during the single impact while the tip section also displaced about 0.25 cm. However, the RTP head displaced more initially (about 1.25 cm) due to elastic pile compression. The above ground measurement obtained using the string potentiometer (discussed in section 5.3.2) shows the corresponding RTP head displacement of 0.33 cm, which agree well.

The energy time history shows that 30% of the theoretical maximum hammer energy is transferred to the head section. The tip section received about 15% of the total rated hammer energy, resulting in 55% of applied hammer energy consumed by the shaft resistance.

#### 5.4.2.3 Stress Wave Analysis for Moderate Driving Condition as RTP Enters Clayey Silt Layer

Pile driving analysis for when the RTP penetrated the softer clayey silt layer that underlies the upper dense sand layer is presented in Figure 5.35. The pile length and measurement spacing is the same as for penetration through the upper dense sand layer (section 5.4.2.2).

The measurements differ significantly between the head and tip due to the RTP tip force being much smaller than the shaft resistance. The RTP head measures about 800 kN axial force

and the tip measures less than 300 kN of axial force. Here more than 60% of the total force is generated from shaft resistance.

Impedance based force at the pile head shows good agreement with the measured strain based force beyond the 1L/c time period, although the impedance based force shows about 10% more magnitude at peak. The low tip force but high acceleration makes it unlikely to expect agreement between then impedance based force measured force at the tip. The impedance based force is 400% more than the measured strain based force at the tip section.

The displacement time history of Figure 5.35 shows that the RTP head displaced by 1.0 cm and the tip displaced by about 0.8 cm. The field measurement (section 5.3.3) shows the corresponding displacement of the RTP head to be 0.9 cm, which agrees with the calculated value.

Energy time history plots in Figure 5.35 shows that RTP head section received about 42% of theoretical total hammer energy. The RTP tip section received about 7% of the energy, resulting in more than 80% of the imparted energy being absorbed in shaft resistance.

#### 5.4.2.4 Stress Wave Analysis for Hard Driving Condition to Refusal as RTP Enters Lower Dense Sand Layer

Driving analysis during hard driving conditions as the RTP approaches refusal in the lower dense sand layer is presented in Figure 5.36. The head and tip measurements were separated by 14.9m (49 ft).

Here the tip force became much higher than the previous clayey silt layer. The RTP tip force measurement is about 600 kN while the RTP head measured about 900 kN total axial force. Here the tip force contributes more than 67% of the total dynamic axial force.

The impedance based axial force is estimated to be about 1300 kN at the head. However, the strain measured axial force was recorded to be 900 kN. Again the peaks are not agreed but the overall trend on RTP head measurements agrees reasonably.

The displacement history on Figure 5.36 shows the total displacement in RTP head due to impact is about 0.4 cm and in the tip is about 0 cm (i.e. no significant permanent displacement from the hammer impact). The RTP head section value of 0.4 cm agrees reasonably with the field string potentiometer average displacement of 0.3 cm. The difference between the head (0.4 cm) and tip (0 cm) displacement may be due to elastic shortening of the RTP length and the generation of residual stresses or due to variations in how the integration scheme is applied. Overall, it is not likely that 0.4 cm of elastic shortening that remained (and was not recovered) after a single hammer blow occurred since the pile was already near refusal conditions, but elastic shortening of this magnitude is possible with multiple blows.

The Becker hammer supplied about 37% of the maximum theoretical energy per impact at this depth. Of this a negligible amount reached the RTP tip, with more than 90% of the energy consumed through shaft resistance.

#### 5.4.2.5 Stress Wave Analysis Compilation for Entire Driving Record

Compilation of data from the entire driving record for the permanent hammer displacement per blow and the estimated energy efficiency (calculated based on ratio between energy at pile head and theoretical hammer energy) are presented in Figure 5.37 along with $N_{RTP}$ profiles and corresponding average displacement per hammer impact values. The relationship between the average RTP displacement based on the $N_{RTP}$ value and that estimated from representative hammer blows is plotted directly in Figure 5.38.

The displacement calculated for a particular blow using the acceleration record follows closely the trend of average displacement calculated from the number of blows per 0.3 m penetration (Figures 5.37 and 5.38). The average displacement from the direct displacement measurements is reported per 0.3 m depth increment without accounting for variations in stratigraphy. On the other hand displacement based on acceleration is the calculated displacement for a particular single pile impact corresponding to a specific pile depth. Therefore it is reasonable to expect these to differ as the RTP section approaches stratigraphic transitions. Figure 5.37 and 5.38 indicate this behavior in a few locations (e.g. at depth of 7.9 m as the RTP begins to enter the upper dense sand layer). Nonetheless, overall the two methods agree very well.

The energy efficiency is also shown to vary with soil layers. Energy efficiency is computed using the strain based force and the velocity over the impact time period that was obtained from the acceleration record. The hammer produced high energy as RTP tip

approached and penetrated the dense layer. In general Becker hammer operates at efficiencies between 20% and 40% of its theoretical maximum value.

## 5.5 Conclusions

This chapter presented RTP performance during driven installation. During driving bounce chamber pressure and displacement were measured separately and number of blow count per 0.3 m depth was obtained. Analysis was performed to understand the behavior of bounce chamber pressure monitoring and driving records with varying soil layers. Acceleration and axial force measurement of different sections at different depths during installation were analyzed to understand the effect of different driving conditions on wave propagation and the dynamic load distribution behavior during driving. Stress wave analysis was performed to assess wave quality and dynamic pile loading. Dynamic axial force at the head and tip were compare to evaluate the load distribution, and impedance based force analysis was performed to compare with the measured strain based force. Although peak force values differed somewhat, in general both showed good agreement up to a normalized time of 1L/c. The pile head displacement calculated using the acceleration record was shown to agree well with the average displacement measured directly in the field using the sting potentiometer.

**REFERENCES**


Beddard, D.L., Speer, D., Swanson, K., (1995). "Site 2 summary report for Caltrans indicator pile test program on the I-880 replacement project." *Consultant Contract Management Branch Office of Structure External Liaison and Support and Geotechnical Support Branch Office of Structural Foundations, Service Contract No. 59V149,* Caltrans, CA.

Feng, H.Y., (1991). "Foundation engineering handbook." *2nd edition, Van Nostrand Reinhold,* New York, 923p.

Fleming, W.G.K., Weltman, A.J., Randolph, M.F., and Elson, W.K., (2009). "Piling engineering." *3rd edition, Taylor and Francis*, New York, 398p.

Ghafghazi, M., (2012). Personal communication, University of California, Davis.

Goble, G.G., Rausche, F., and Likins, G.E., (1980). "The analysis of pile driving – a state of the art." *Proceedings of the 1st International Conference on the Application of Stress-Wave Theory on Piles,* Stockholm, Sweden, 131-161.

Harder, Jr., L.F. and Seed, H.B., (1986). "Determination of penetration resistance for coarse-grained soils using the Becker hammer drill." *Report UCB/EERC-86/06, Earthquake Engineering Research Center, University of California, Berkeley,* CA. 144p.

Lehane, B.M., Jardine, R.J., Bond, A.J., Frank, R., (1993). "Mechanisms of shaft friction in sand from instrumented pile tests." *Journal of Geotechnical Engineering, ASCE*, 119(1): 19-35.

Measurements Group, Inc., (1988). "Strain gage based transducers – Their design and construction." *Measurements Group, Inc.*, Raleigh, NC. 79p.

Sy, A. (1993). "Energy measurements and correlations of the Standard penetration test (SPT) and the Becker penetration test (BPT)." *Ph.D. thesis, Department of Civil Engineering, University of British Columbia,* Vancouver, BC, Canada. 219p.

Timoshenko, S.P. and Goodier, J.N., (1970). "Theory of elasticity." *3rd edition, McGraw-Hill Inc.* New York. 567p.

**FIGURES**

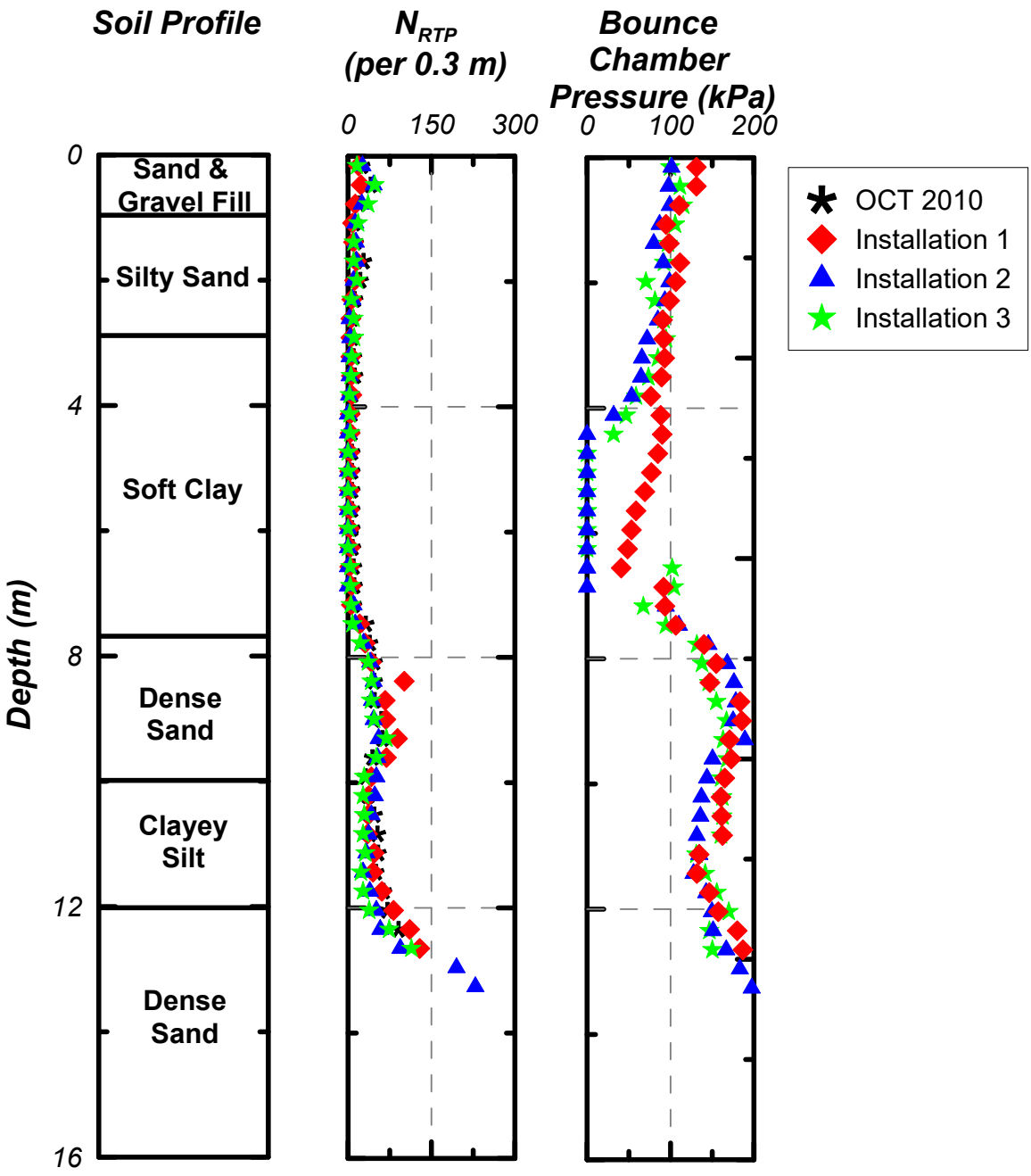


**Figure 5.1: RTP N value and bounce chamber pressure profiles from Oakland, CA test site.**

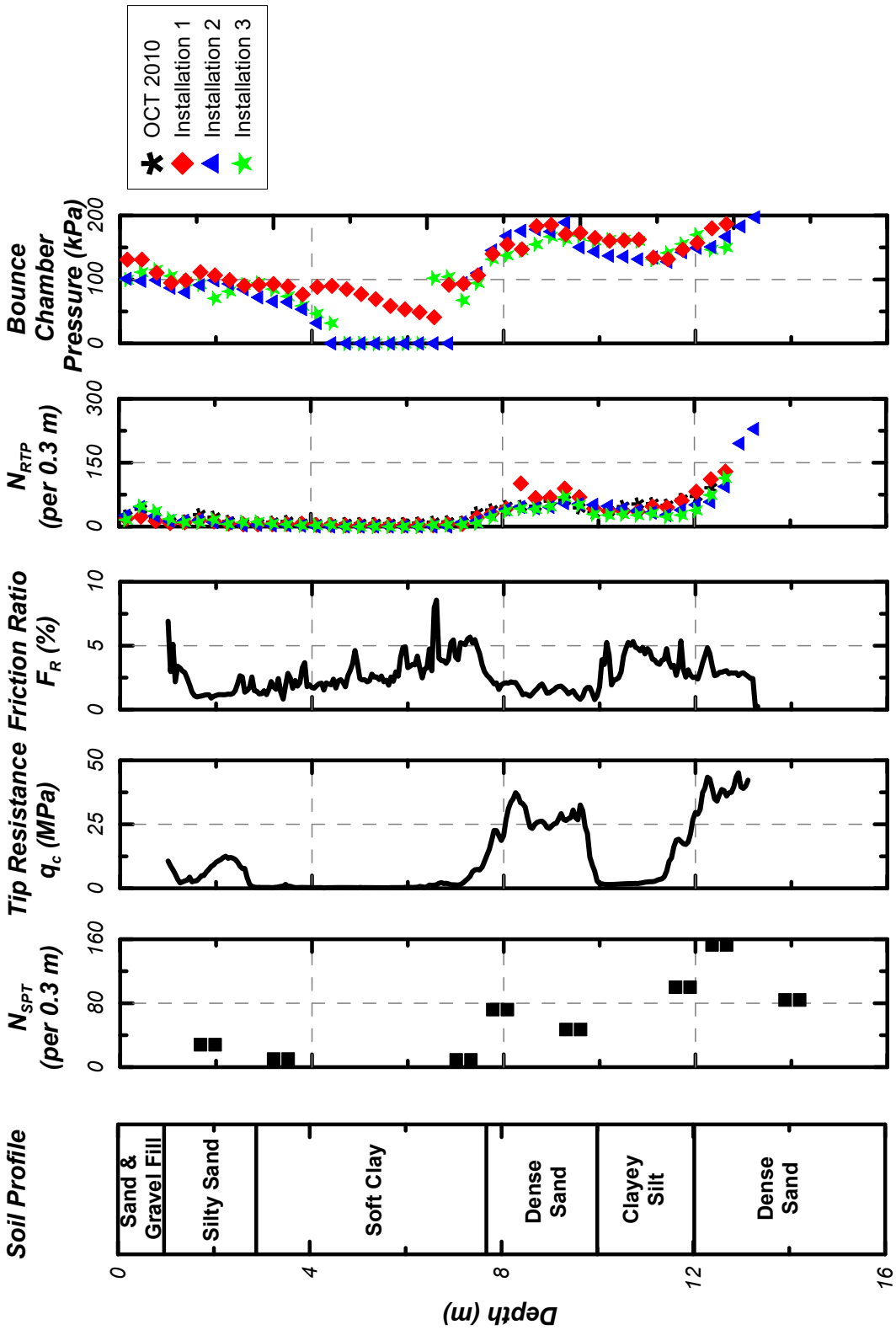


Figure 5.2: RTP N value and bounce chamber pressure profiles compared with other in situ test results.

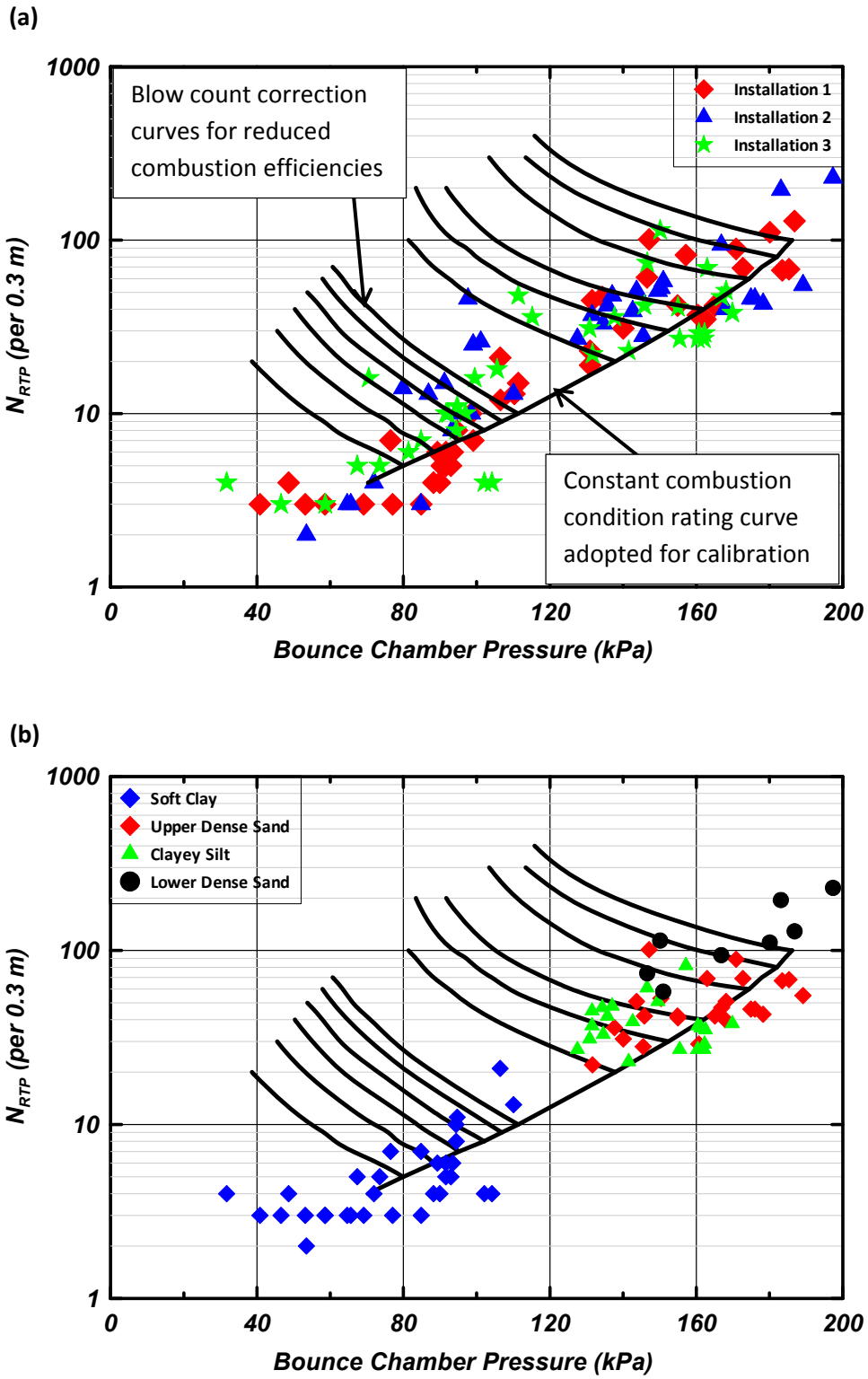


**Figure 5.3: Variation of $N_{RTP}$ values with measured bounce chamber pressure. Curves proposed by Harder and Seed (1986) presented for reference. (a) $N_{RTP}$ values separated by installation and (b) $N_{RTP}$ values separated by soil type that the RTP tip penetrating.**

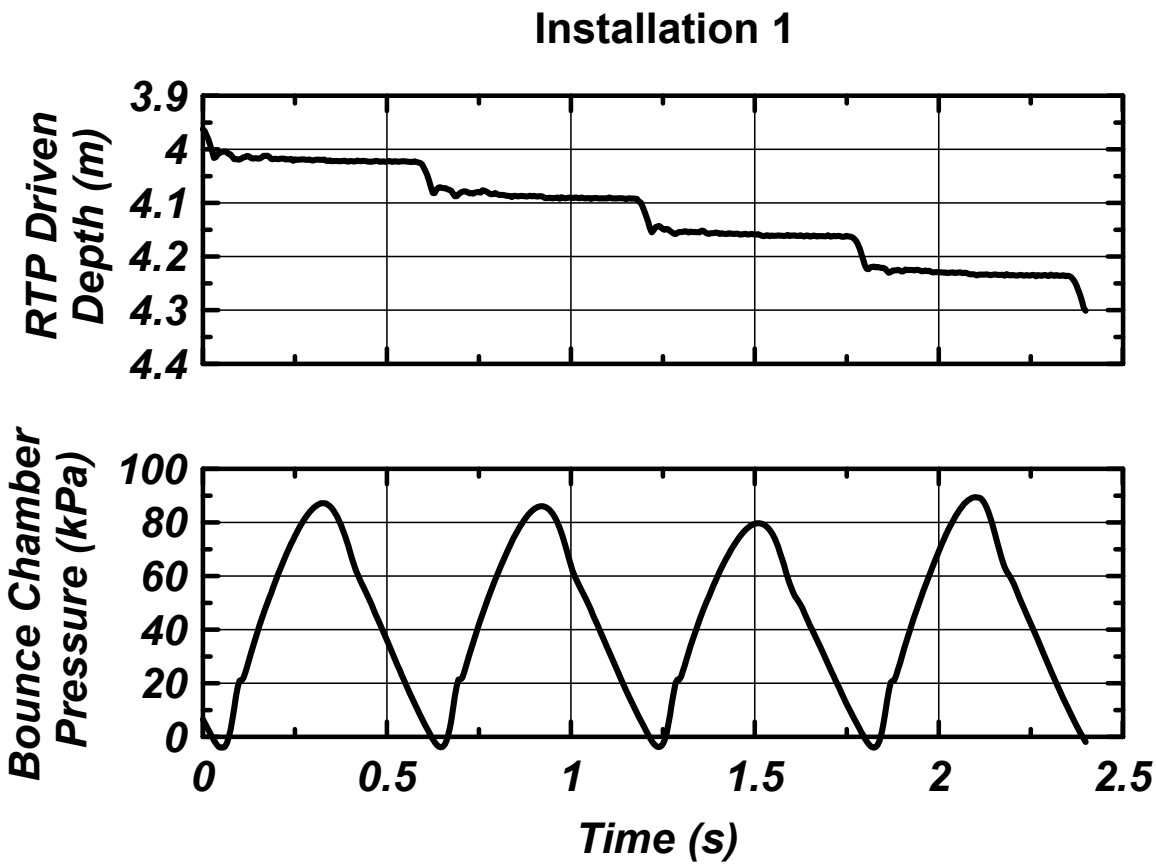


**Figure 5.4: RTP driven depth and bounce chamber pressure measured just before entering into soft clay layer. Record obtained from installation 1 driving from 3.96 m (13 feet) to 4.27 m (14 feet) depth.**

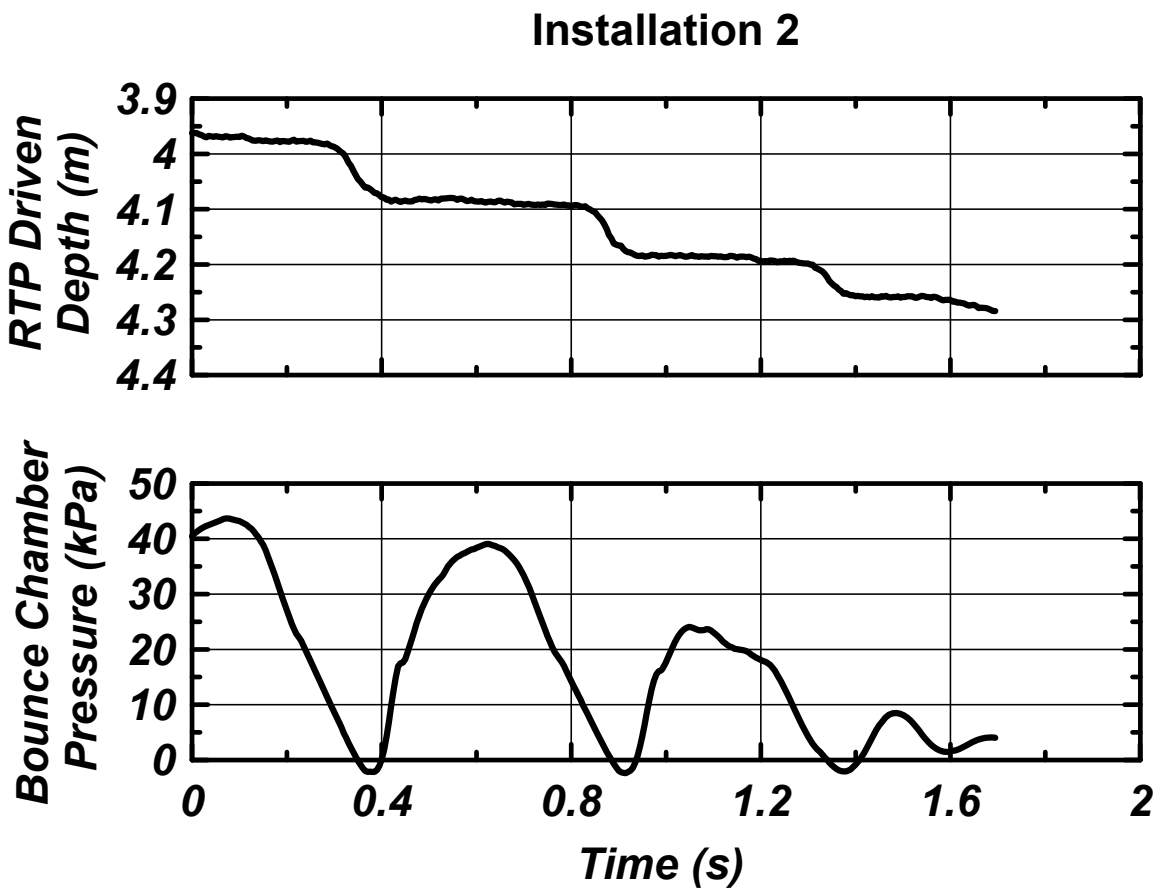


**Figure 5.5: RTP driven depth and bounce chamber pressure measured just before entering into soft clay layer. Record obtained from installation 2 driving from 3.96 m (13 feet) to 4.27 m (14 feet) depth.**

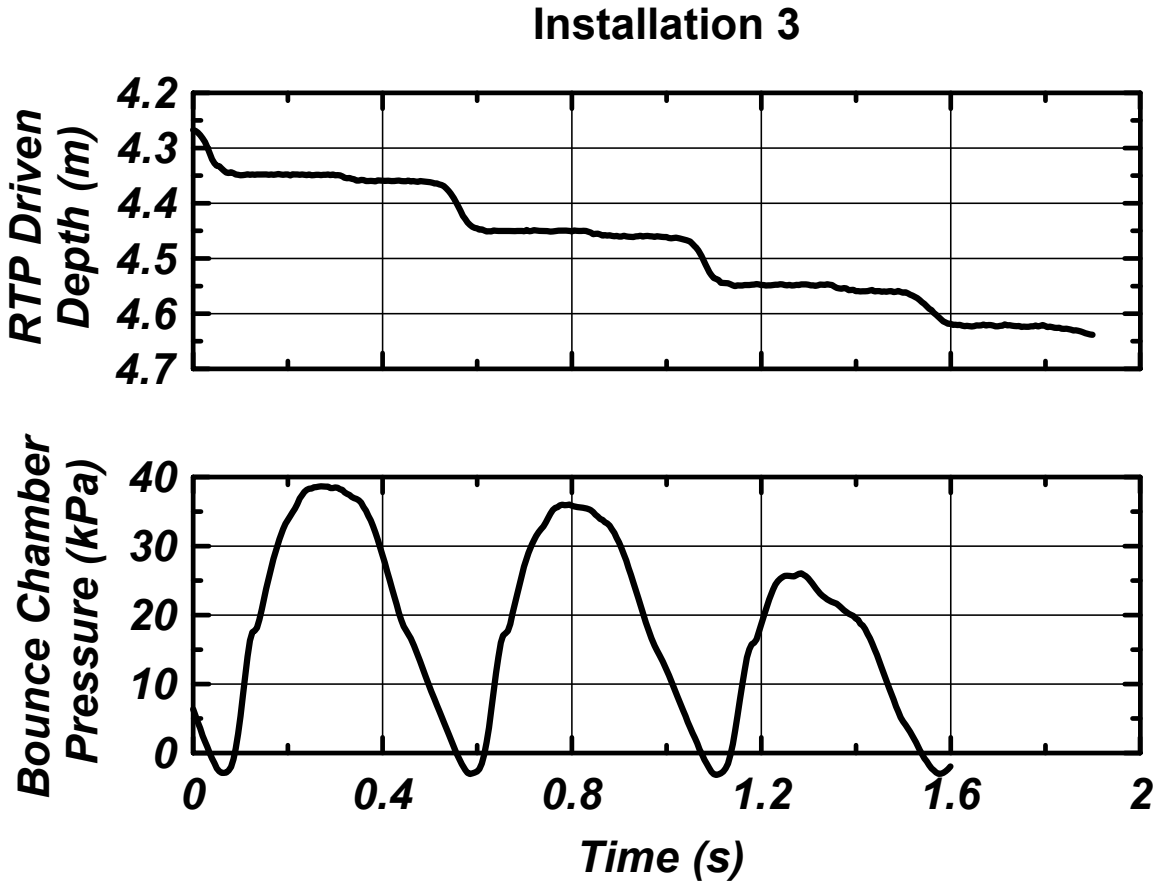


**Figure 5.6: RTP driven depth and bounce chamber pressure measured just before entering into soft clay layer. Record obtained from installation 3 driving from 4.27 m (14 feet) to 4.57 m (15 feet) depth.**

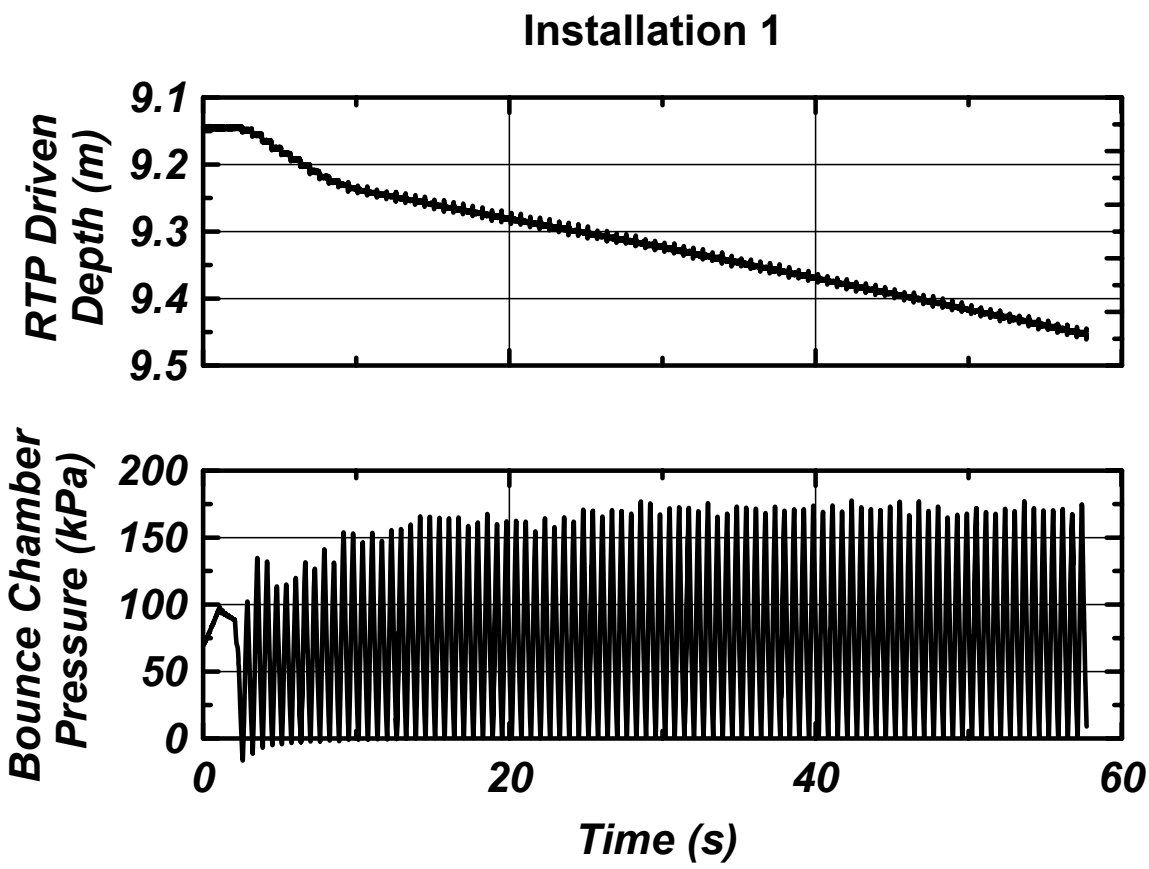


**Figure 5.7: RTP driven depth and bounce chamber pressure measured in the middle of upper dense sand layer. Record obtained from installation 1 driving from 9.14 m (30 feet) to 9.45 m (31 feet) depth.**

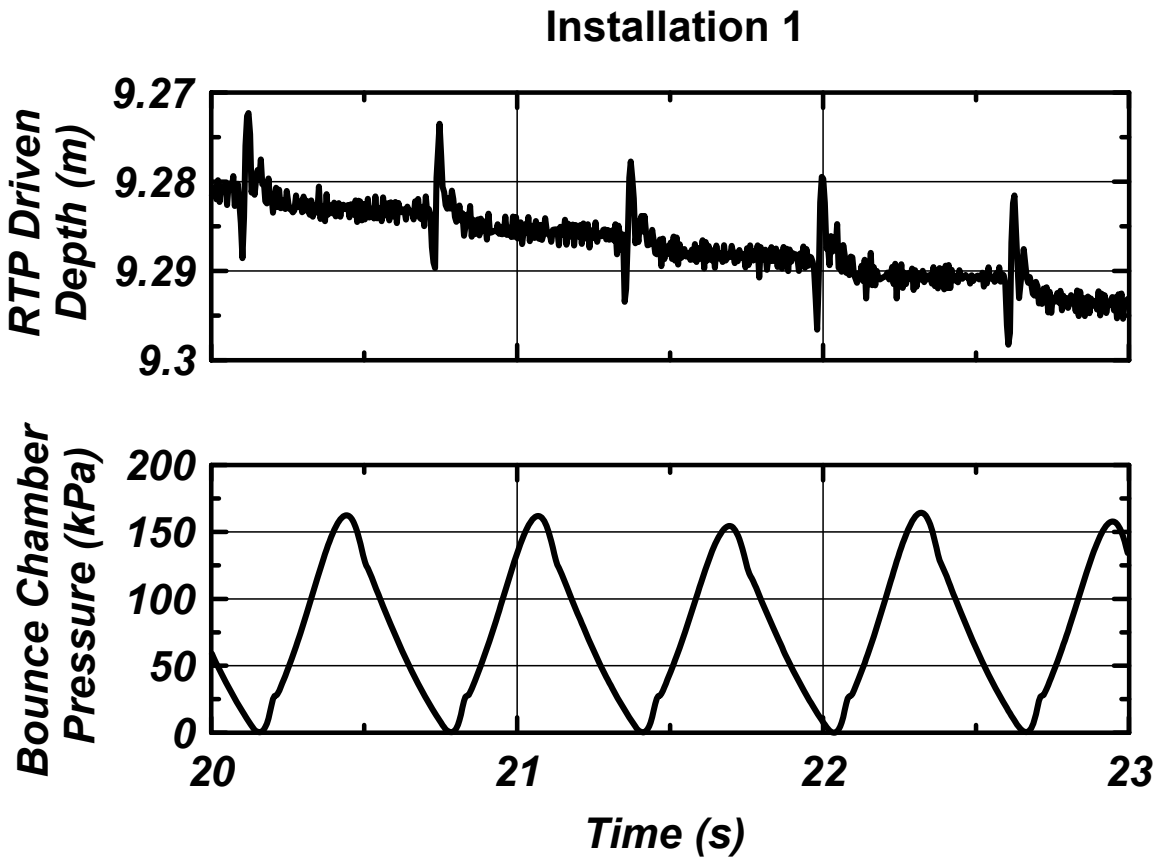


**Figure 5.8: RTP driven depth and bounce chamber pressure measured in the middle of upper dense sand layer. Record obtained from installation 1 driving from 9.14 m (30 feet) to 9.45 m (31 feet) depth. Time scales are magnified to show the performance for individual blow.**

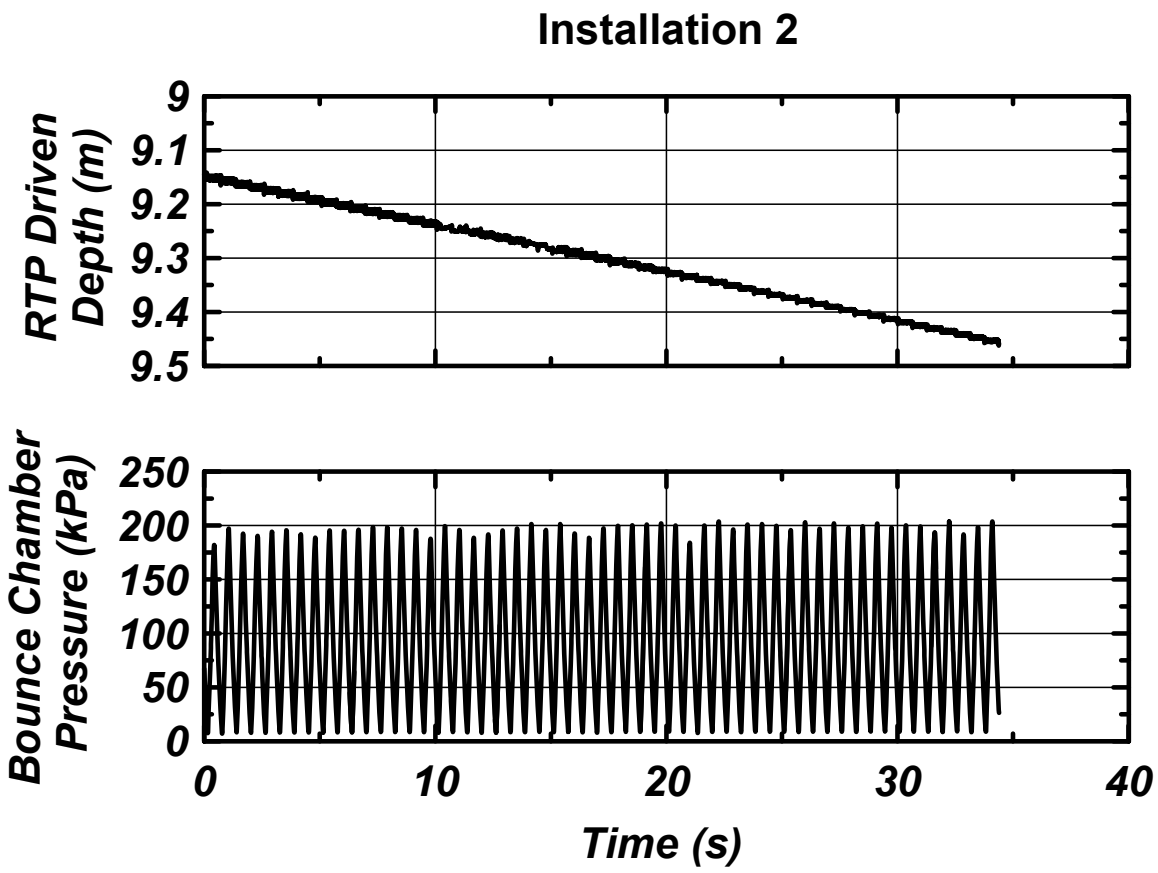


**Figure 5.9: RTP driven depth and bounce chamber pressure measured in the middle of upper dense sand layer. Record obtained from installation 2 driving from 9.14 m (30 feet) to 9.45 m (31 feet) depth.**

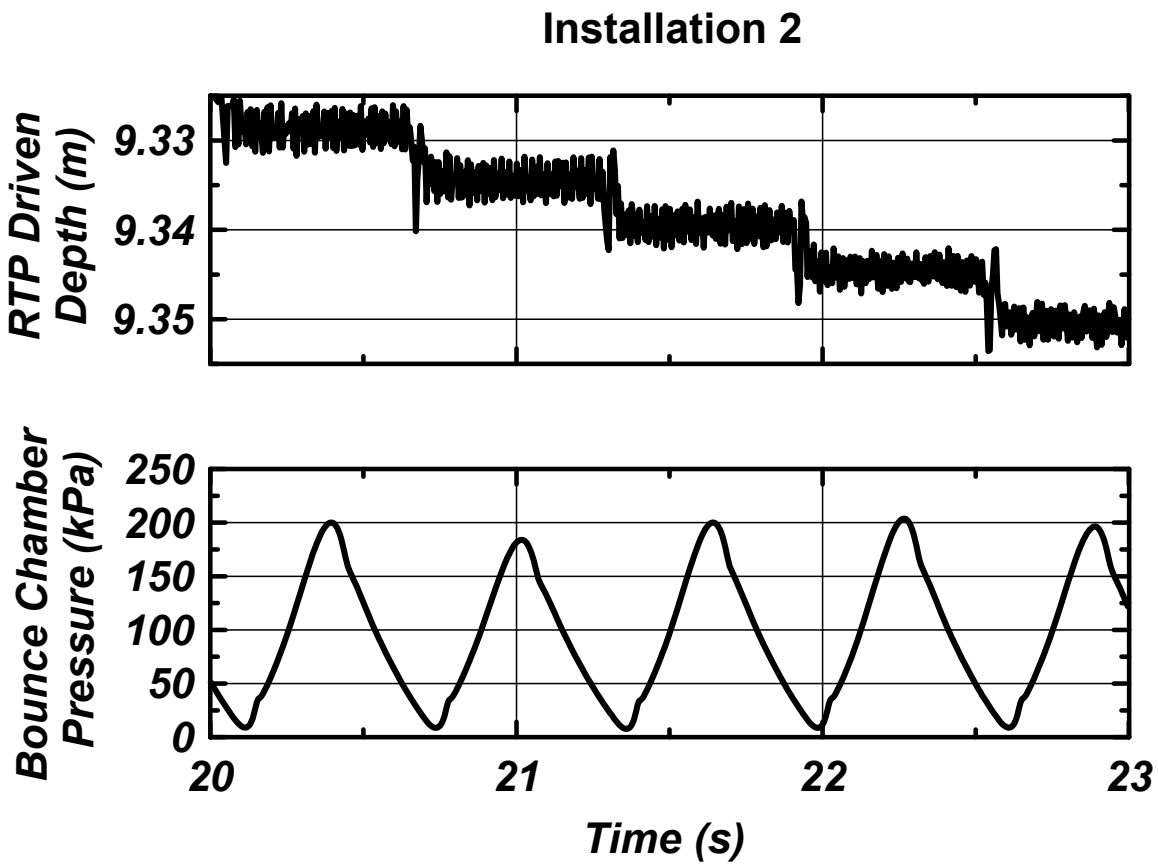


**Figure 5.10: RTP driven depth and bounce chamber pressure measured in the middle of upper dense sand layer. Record obtained from installation 2 driving from 9.14 m (30 feet) to 9.45 m (31 feet) depth. Time scales are magnified to show the performance for individual blow.**

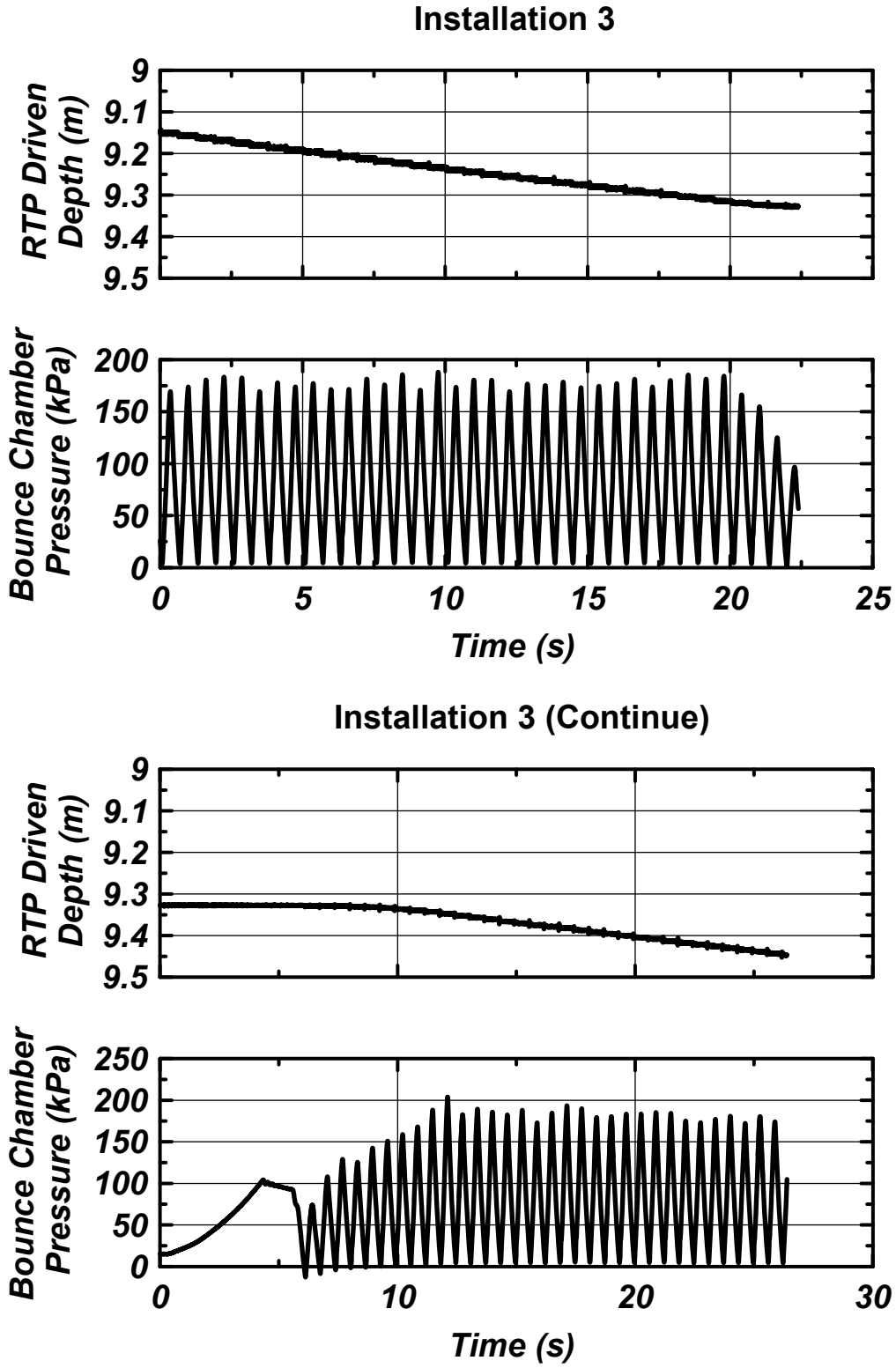


**Figure 5.11: RTP driven depth and bounce chamber pressure measured in the middle of upper dense sand layer. Record obtained from installation 3 driving from 9.14 m (30 feet) to 9.45 m (31 feet) depth.**

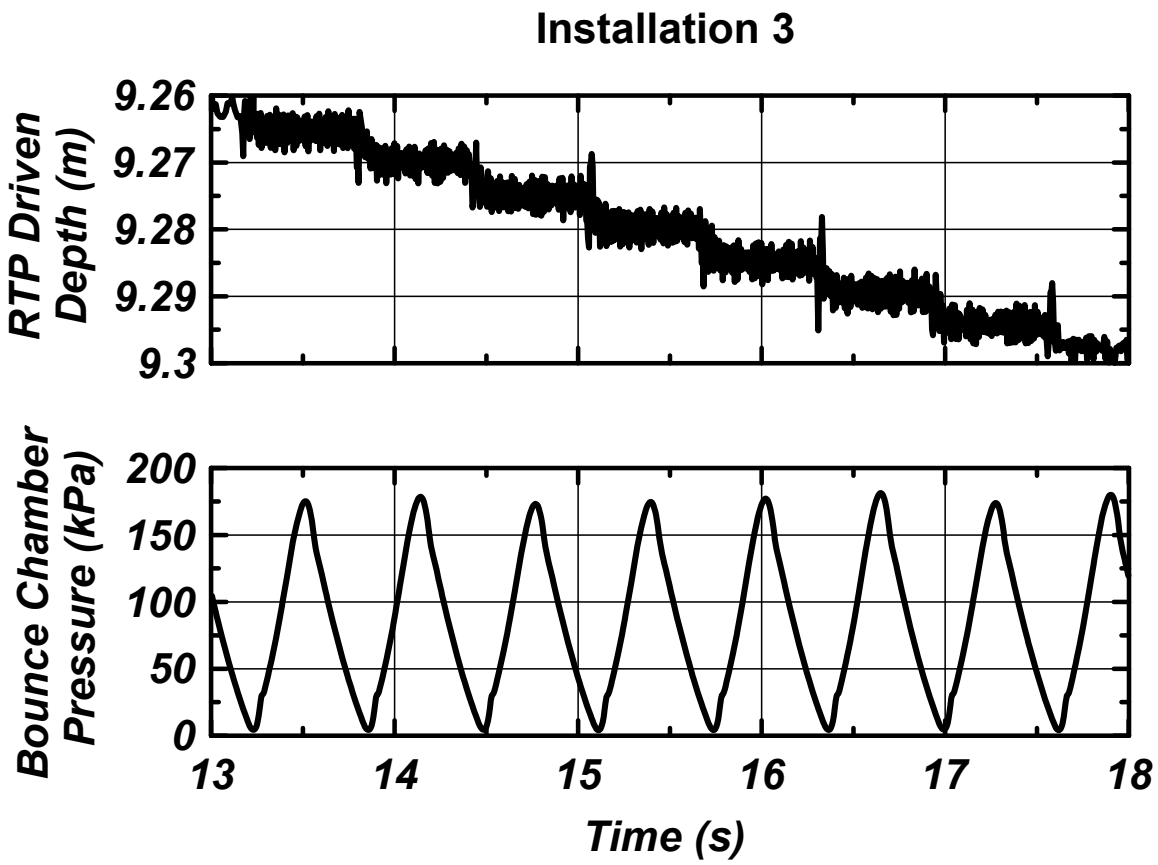


**Figure 5.12: RTP driven depth and bounce chamber pressure measured in the middle of upper dense sand layer. Record obtained from installation 3 driving from 9.14 m (30 feet) to 9.45 m (31 feet) depth. Time scales are magnified to show the performance for individual blow.**

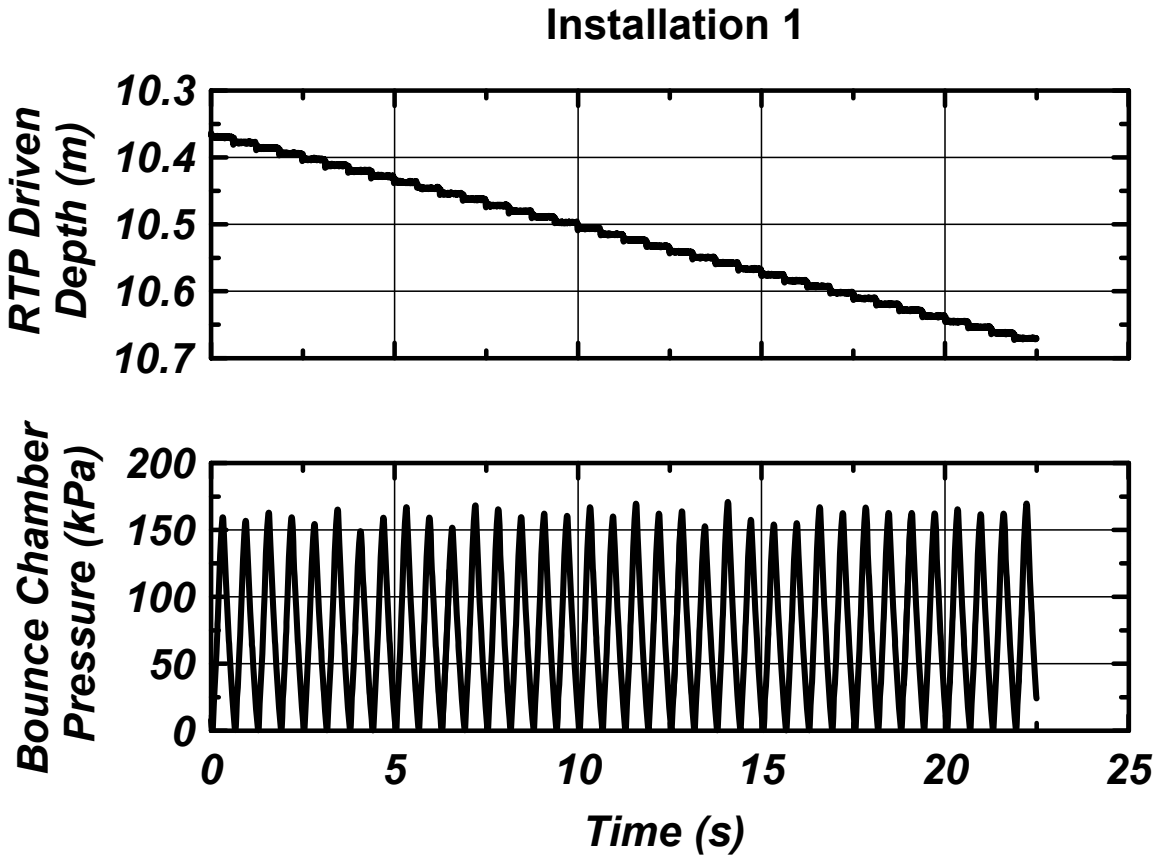


**Figure 5.13: RTP driven depth and bounce chamber pressure measured in the middle of clayey silt layer. Record obtained from installation 1 driving from 10.36 m (34 feet) to 10.67 m (35 feet) depth.**

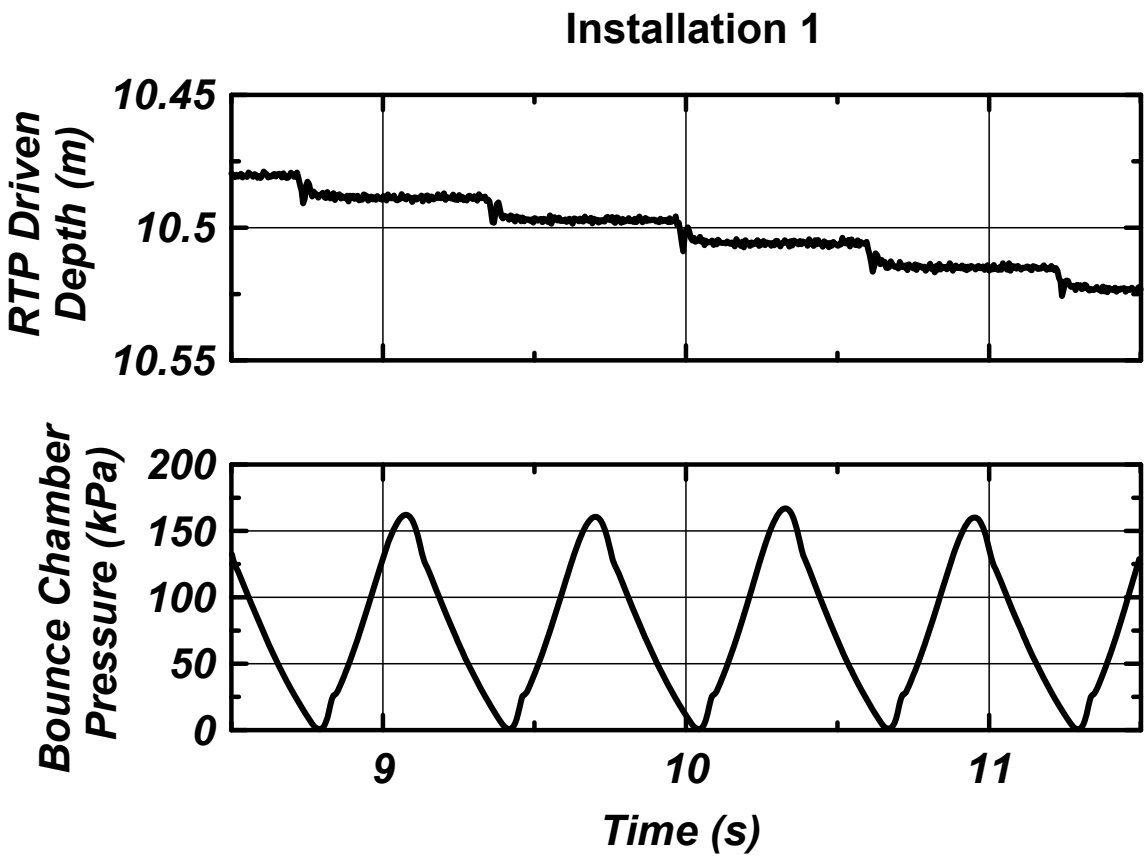


**Figure 5.14: RTP driven depth and bounce chamber pressure measured in the middle of upper dense sand layer. Record obtained from installation 1 driving from 10.36 m (34 feet) to 10.67 m (35 feet) depth. Time scales are magnified to show the performance for individual blow.**

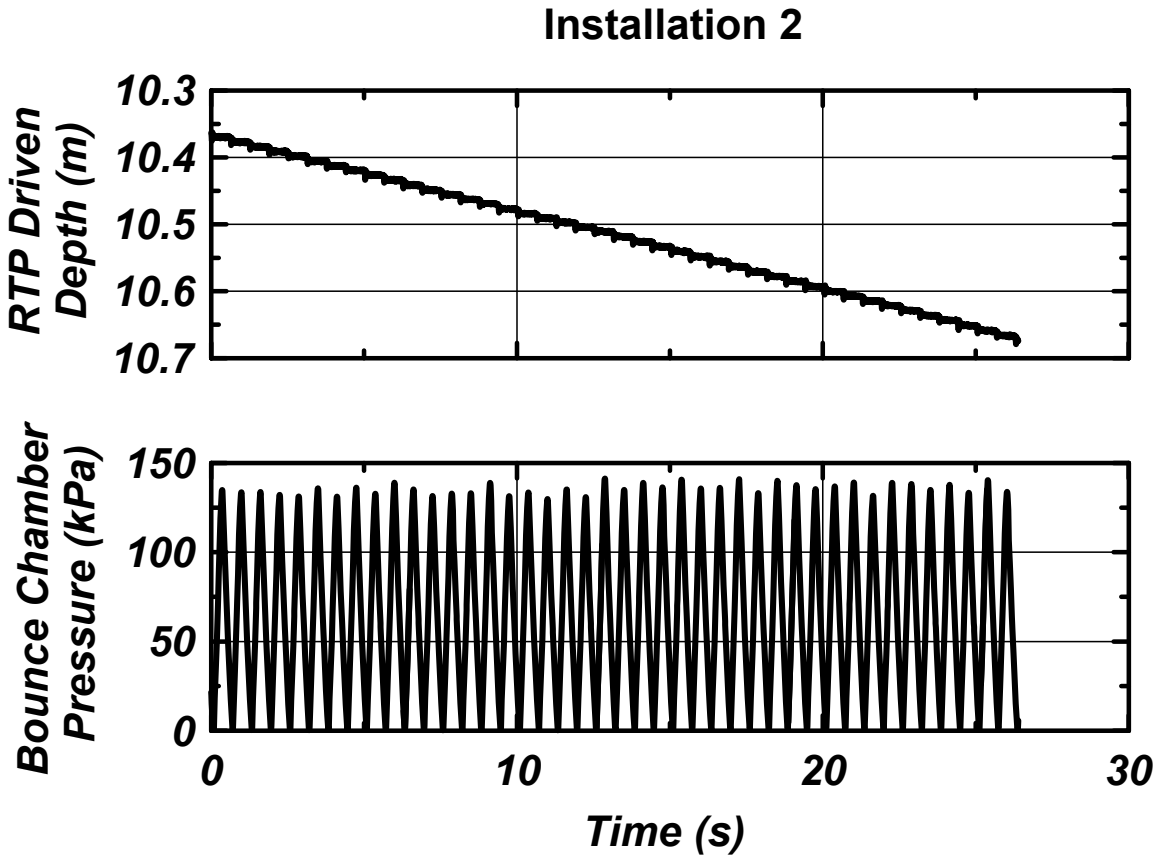


**Figure 5.15: RTP driven depth and bounce chamber pressure measured in the middle of clayey silt layer. Record obtained from installation 2 driving from 10.36 m (34 feet) to 10.67 m (35 feet) depth.**

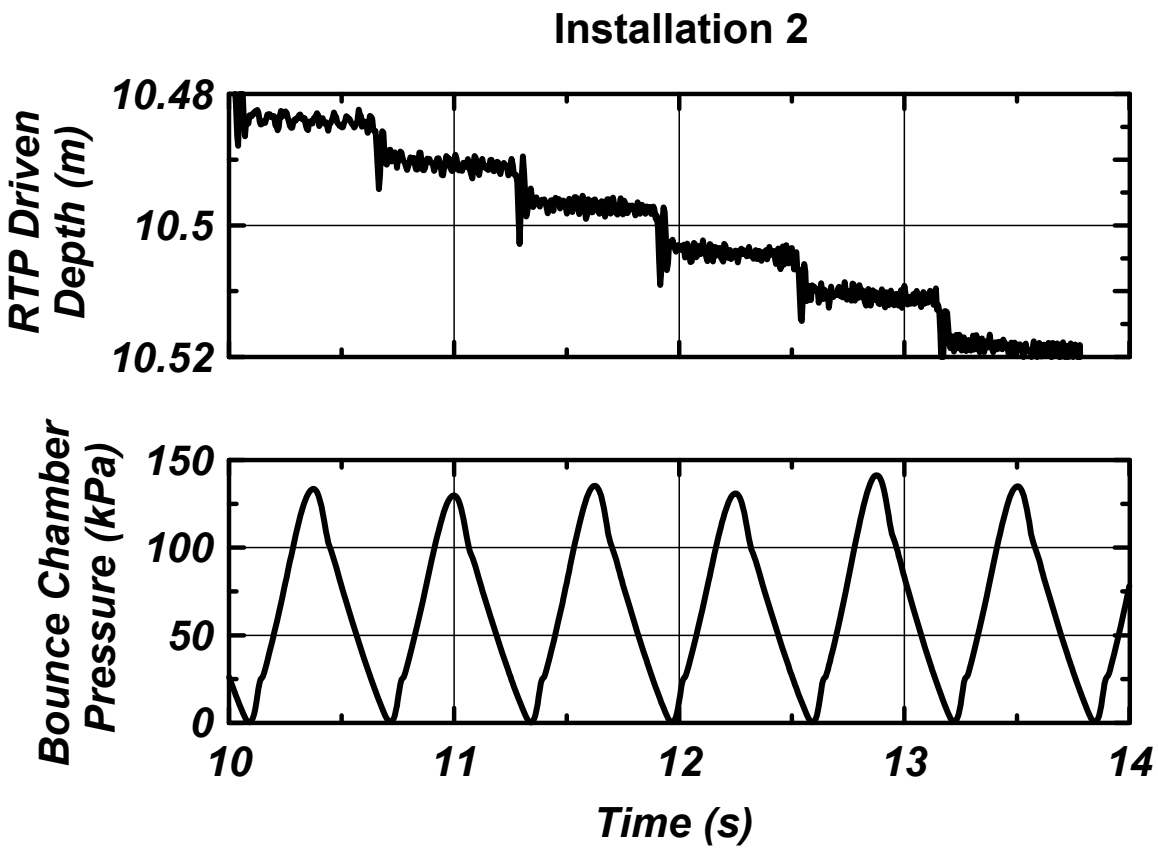


**Figure 5.16: RTP driven depth and bounce chamber pressure measured in the middle of upper dense sand layer. Record obtained from installation 2 driving from 10.36 m (34 feet) to 10.67 m (35 feet) depth. Time scales are magnified to show the performance for individual blow.**

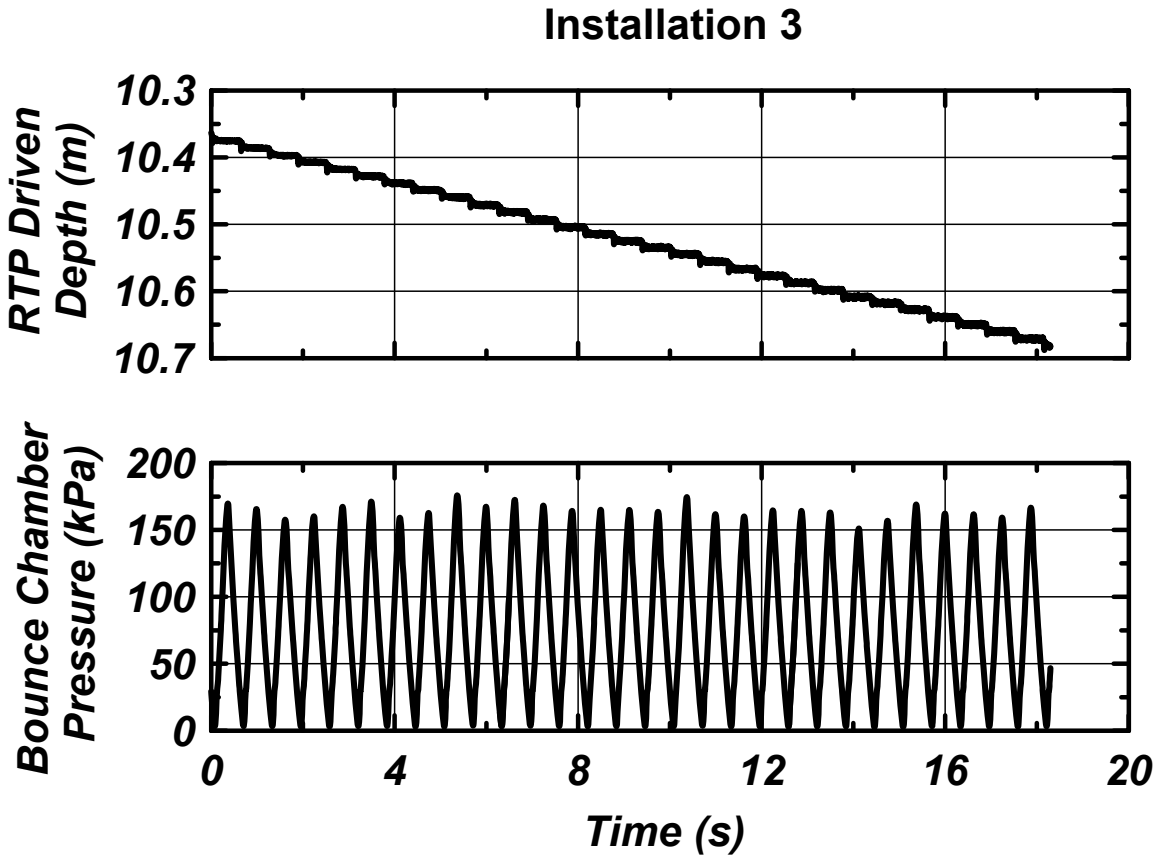


**Figure 5.17: RTP driven depth and bounce chamber pressure measured in the middle of clayey silt layer. Record obtained from installation 3 driving from 10.36 m (34 feet) to 10.67 m (35 feet) depth.**

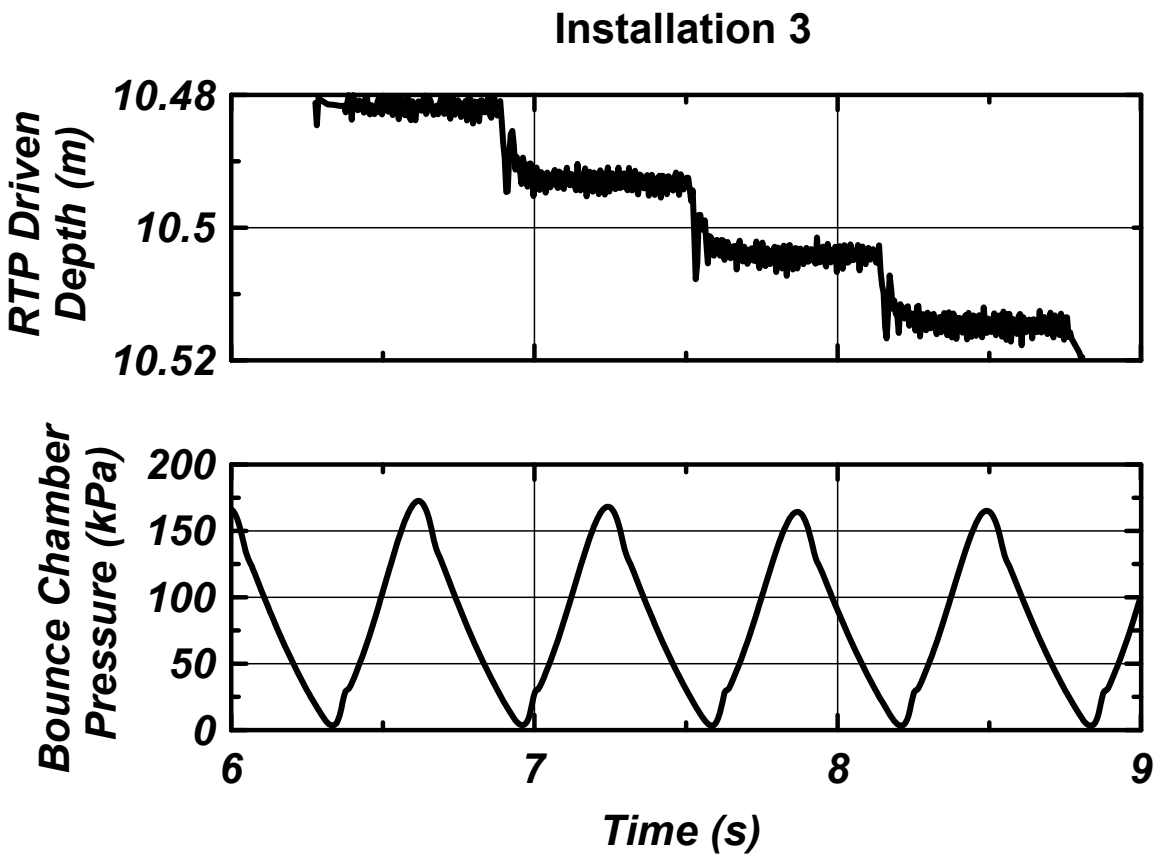


**Figure 5.18: RTP driven depth and bounce chamber pressure measured in the middle of upper dense sand layer. Record obtained from installation 3 driving from 10.36 m (34 feet) to 10.67 m (35 feet) depth. Time scales are magnified to show the performance for individual blow.**

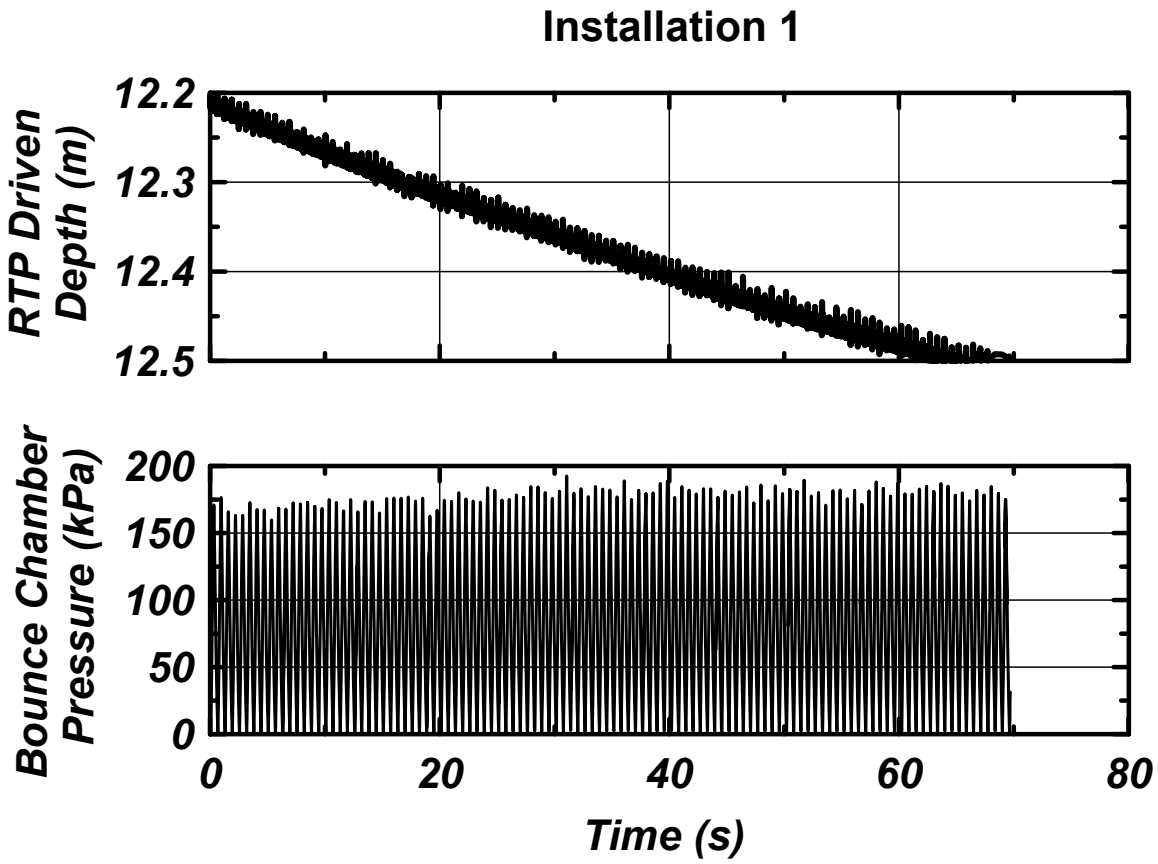


**Figure 5.19: RTP driven depth and bounce chamber pressure measured in the lower dense sand layer before refusal. Record obtained from installation 1 driving from 12.19 m (40 feet) to 12.50 m (41 feet) depth.**

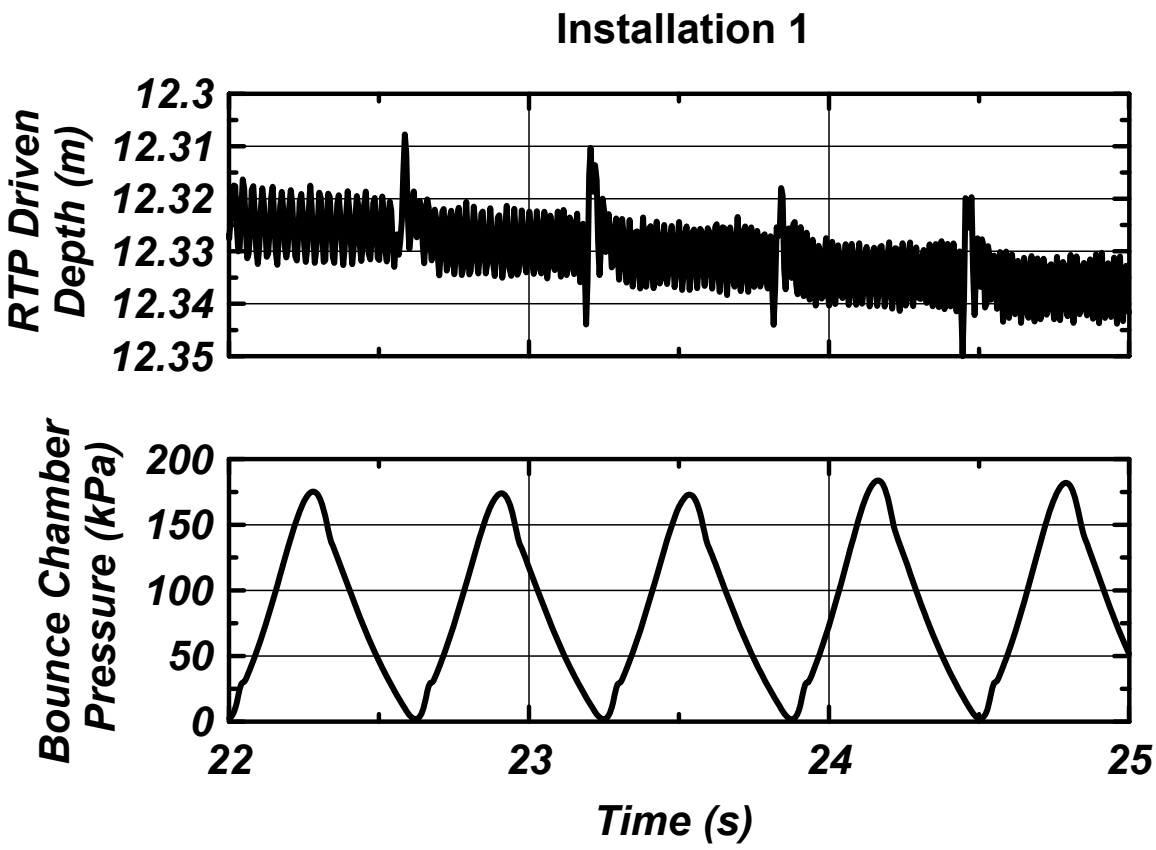


**Figure 5.20: RTP driven depth and bounce chamber pressure measured in the lower dense sand layer before refusal. Record obtained from installation 1 driving from 12.19 m (40 feet) to 12.50 m (41 feet) depth. Time scales are magnified to show the performance for individual blow.**

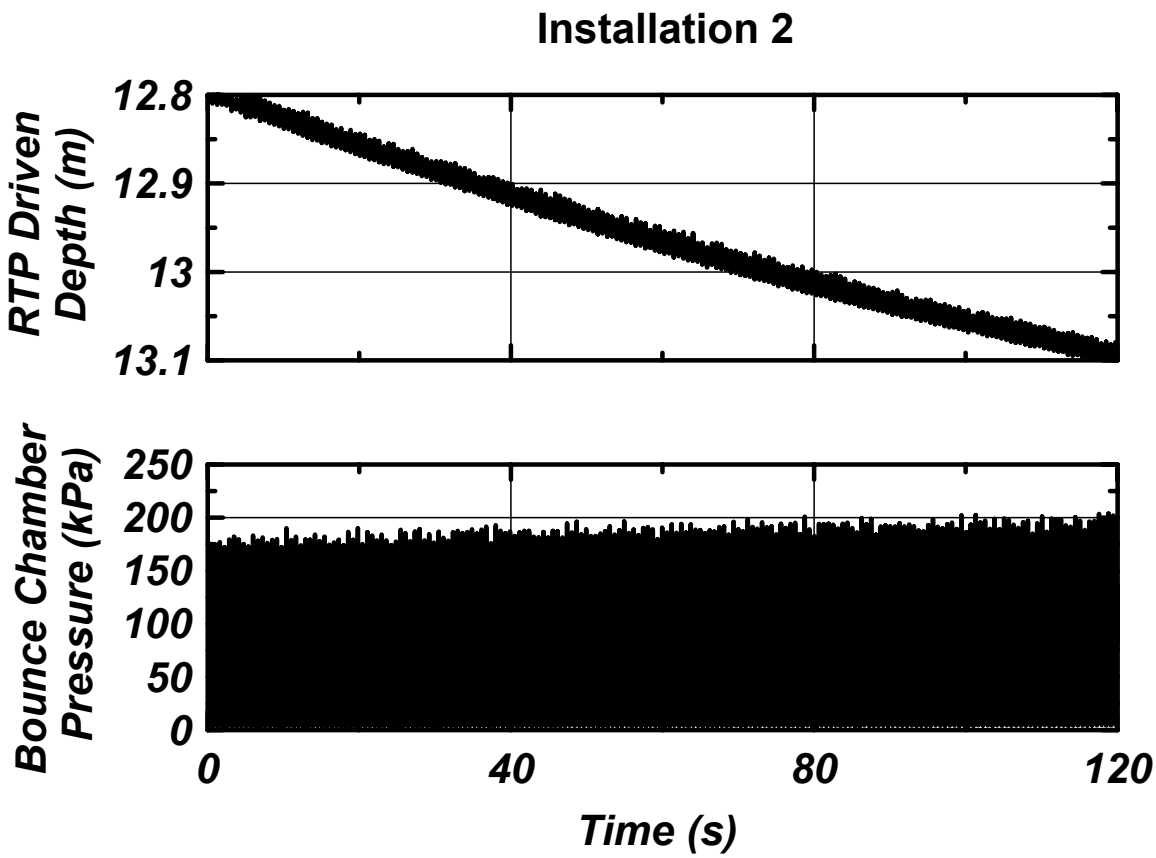


**Figure 5.21: RTP driven depth and bounce chamber pressure measured in the lower dense sand layer before refusal. Record obtained from installation 2 driving from 12.80 m (42 feet) to 13.11 m (43 feet) depth.**

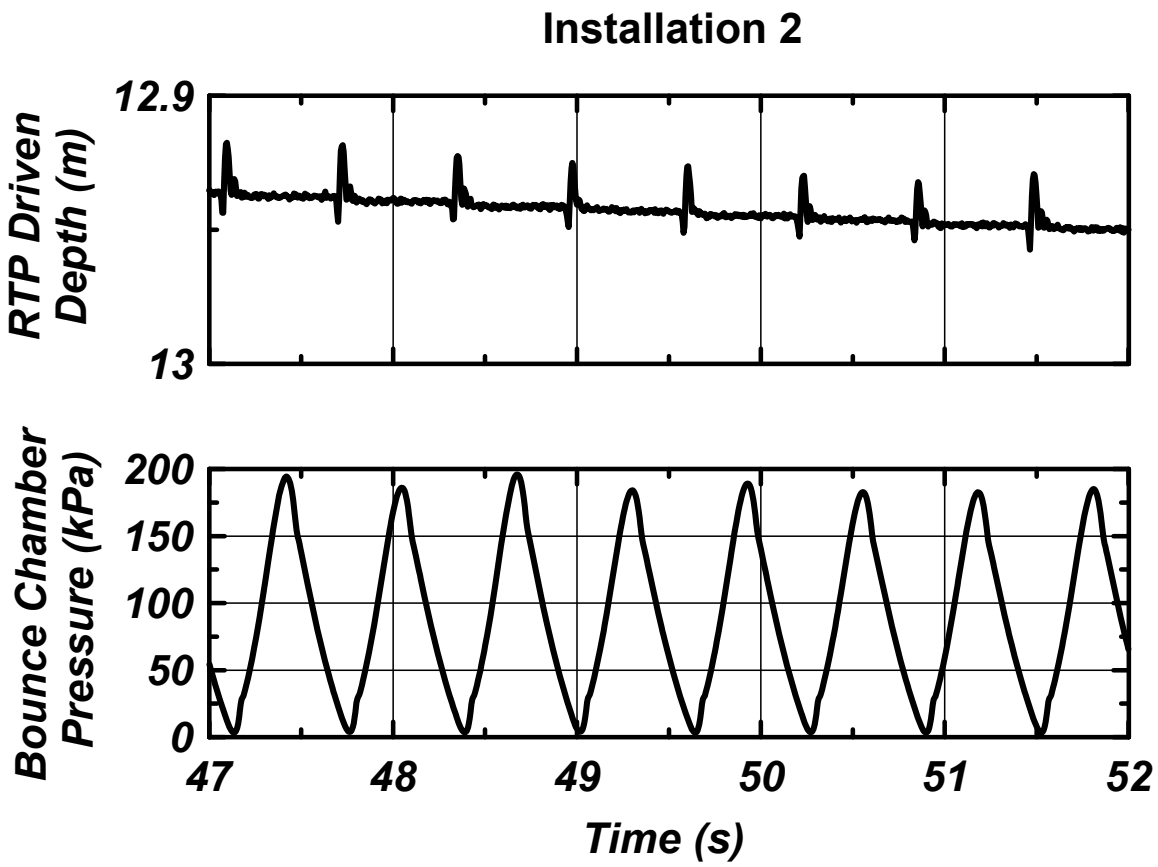


**Figure 5.22: RTP driven depth and bounce chamber pressure measured in the lower dense sand layer before refusal. Record obtained from installation 2 driving from 12.80 m (42 feet) to 13.11 m (43 feet) depth. Time scales are magnified to show the performance for individual blow.**

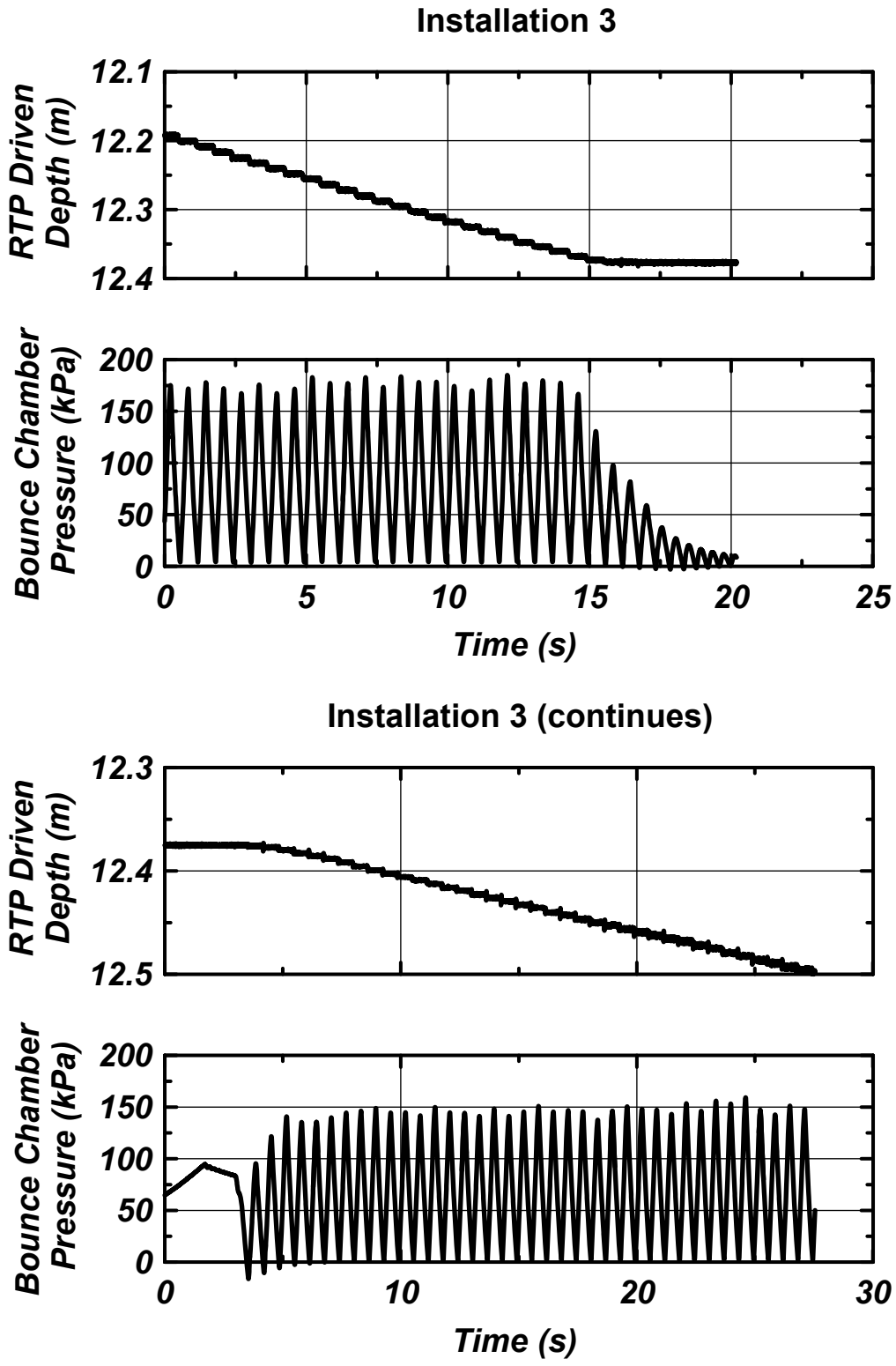


**Figure 5.23: RTP driven depth and bounce chamber pressure measured in the lower dense sand layer before refusal. Record obtained from installation 3 driving from 12.19 m (40 feet) to 12.5 m (41 feet) depth.**

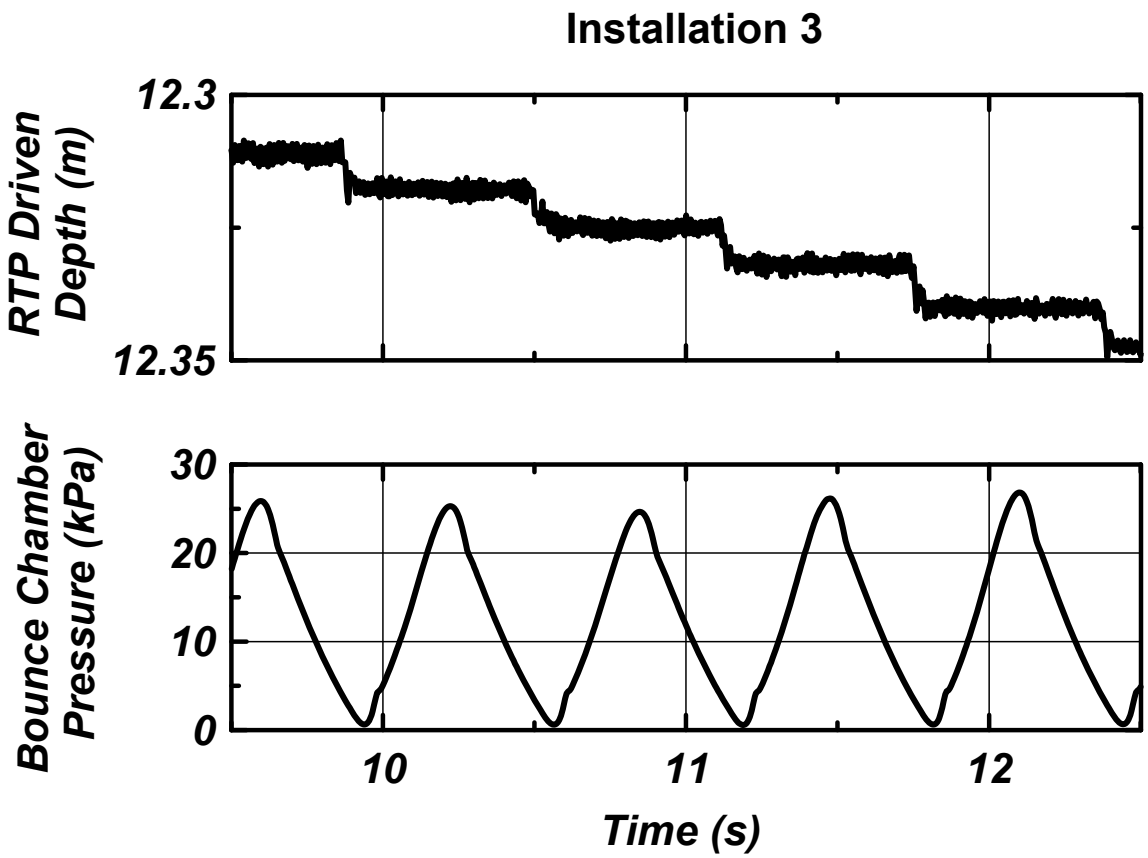


**Figure 5.24: RTP driven depth and bounce chamber pressure measured in the lower dense sand layer before refusal. Record obtained from installation 3 driving from 12.19 m (40 feet) to 12.5 m (41 feet) depth. Time scales are magnified to show the performance for individual blow.**

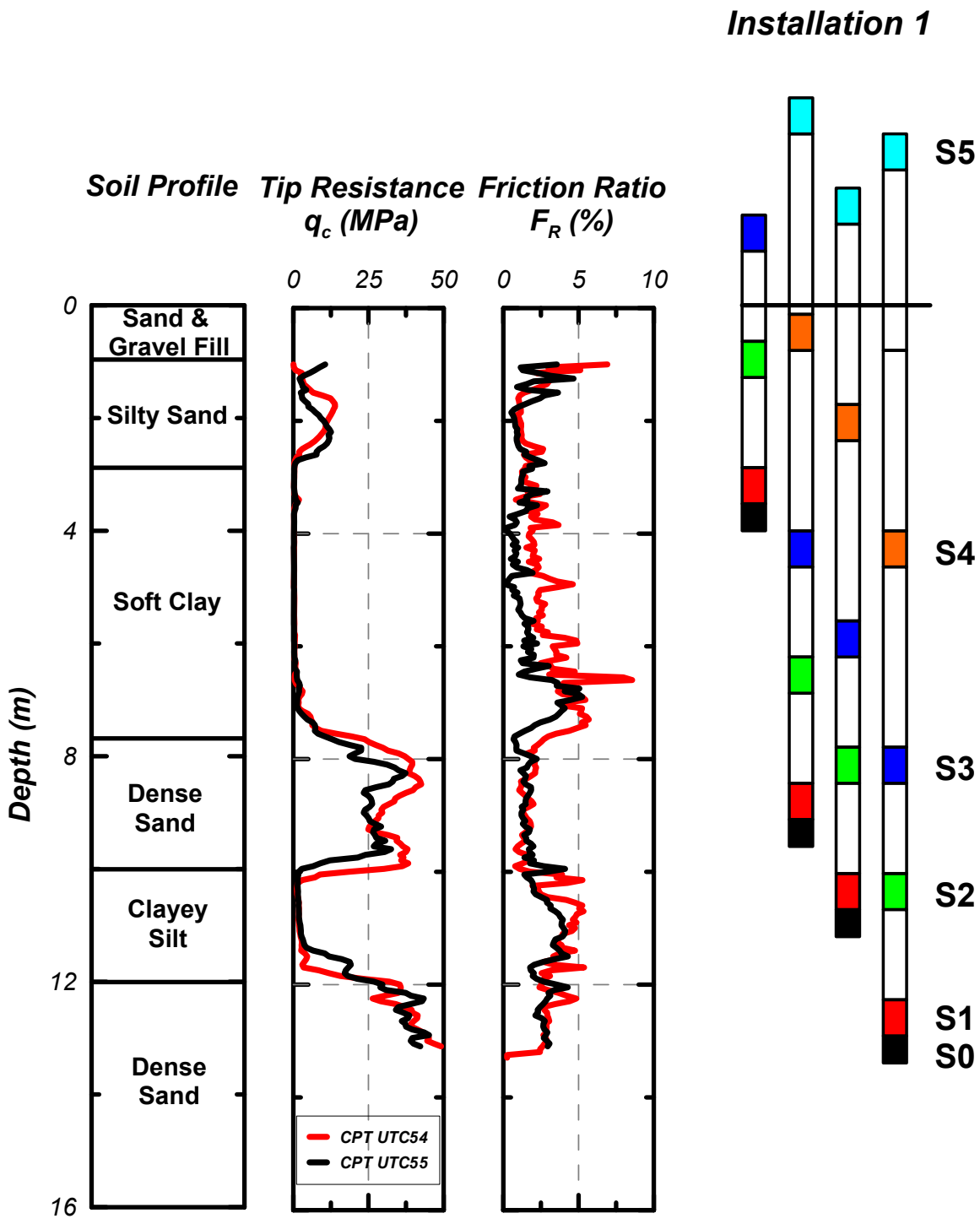


**Figure 5.25: Typical RTP string configuration and locations at different depths on used for the data analysis. Installation 1 is shown here as an example.**

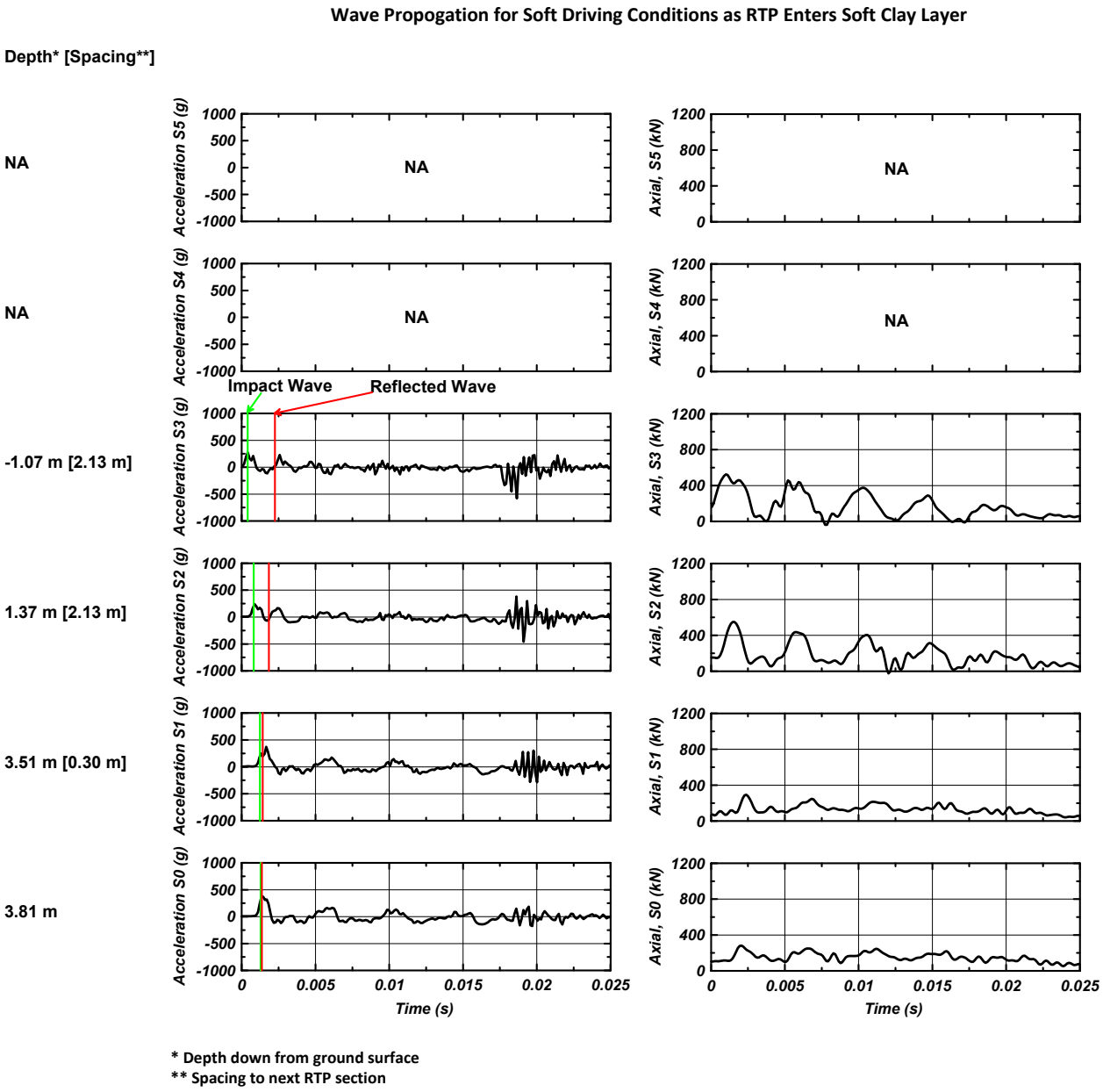


**Figure 5.26: Single impact wave propagation acceleration and axial force time histories of RTP pile penetrating soft clay layer at 3.81 m (12.5 ft) depth during installation 1.**

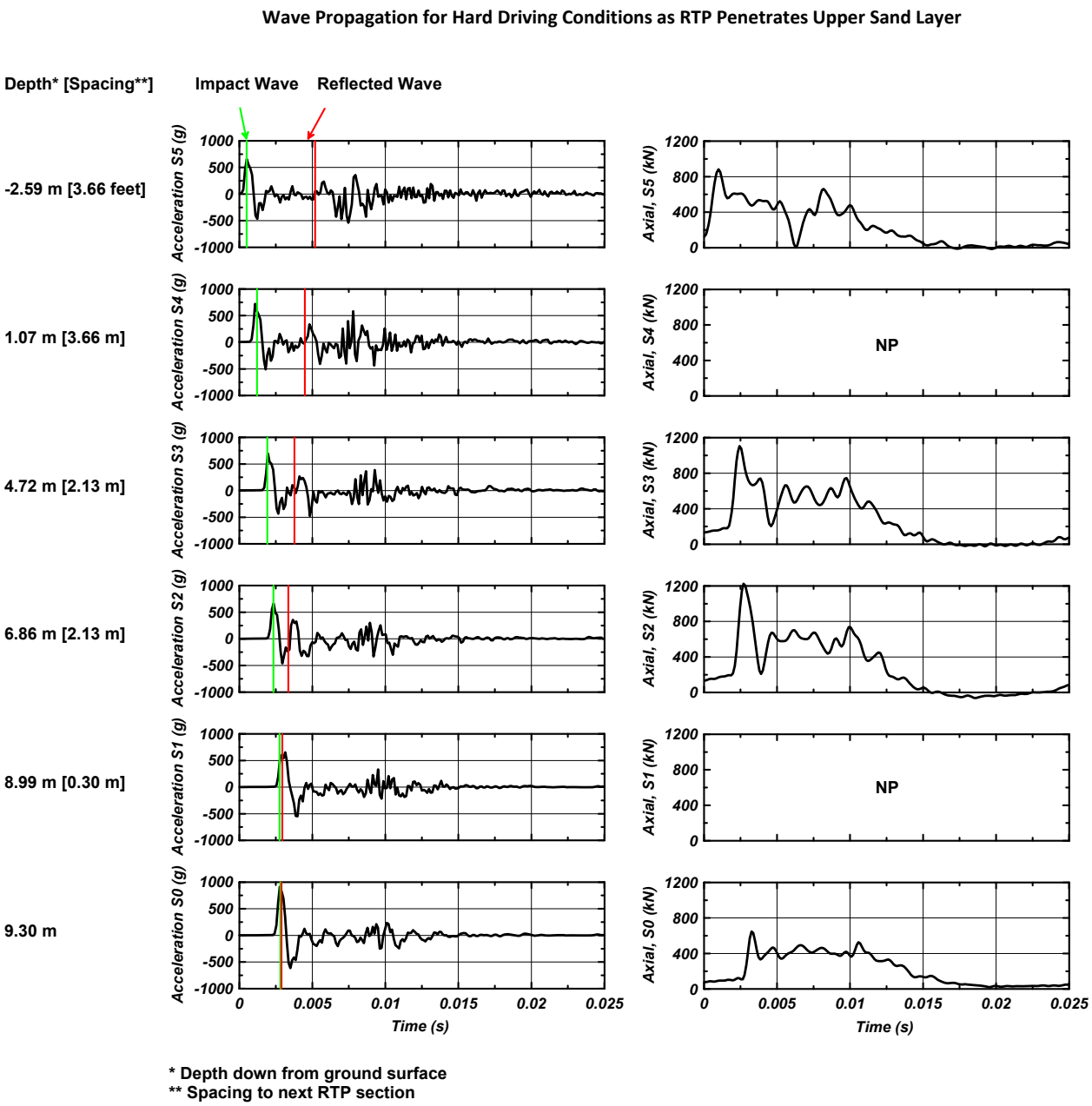


**Figure 5.27: Single impact wave propagation acceleration and axial force time histories of RTP pile penetrating upper dense sand layer at 9.30 m (30.5 ft) depth during installation 1.**

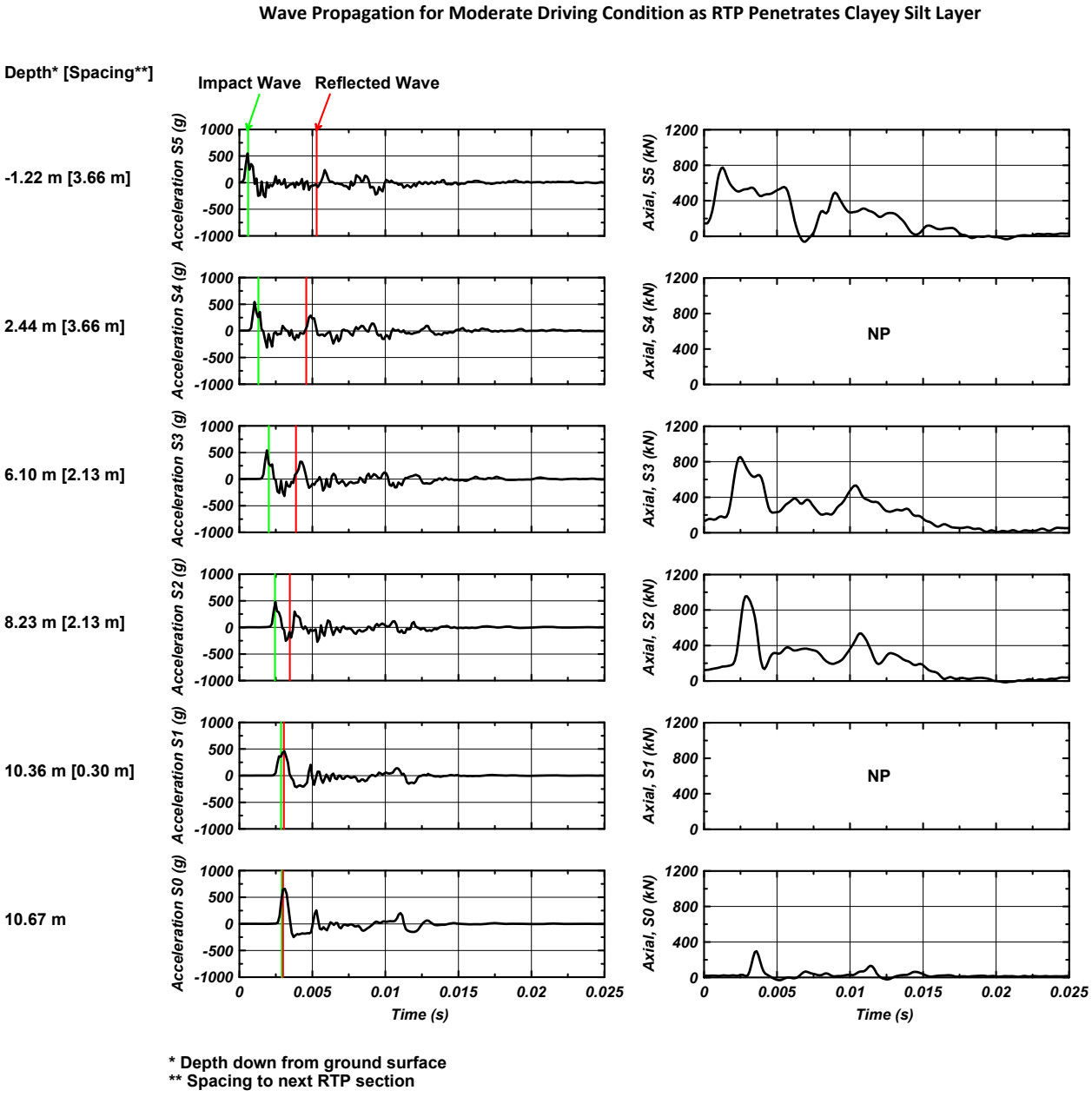


**Figure 5.28: Single impact wave propagation acceleration and axial force time histories of RTP pile penetrating clayey silt layer at 10.67 m (35 ft) depth during installation 1.**

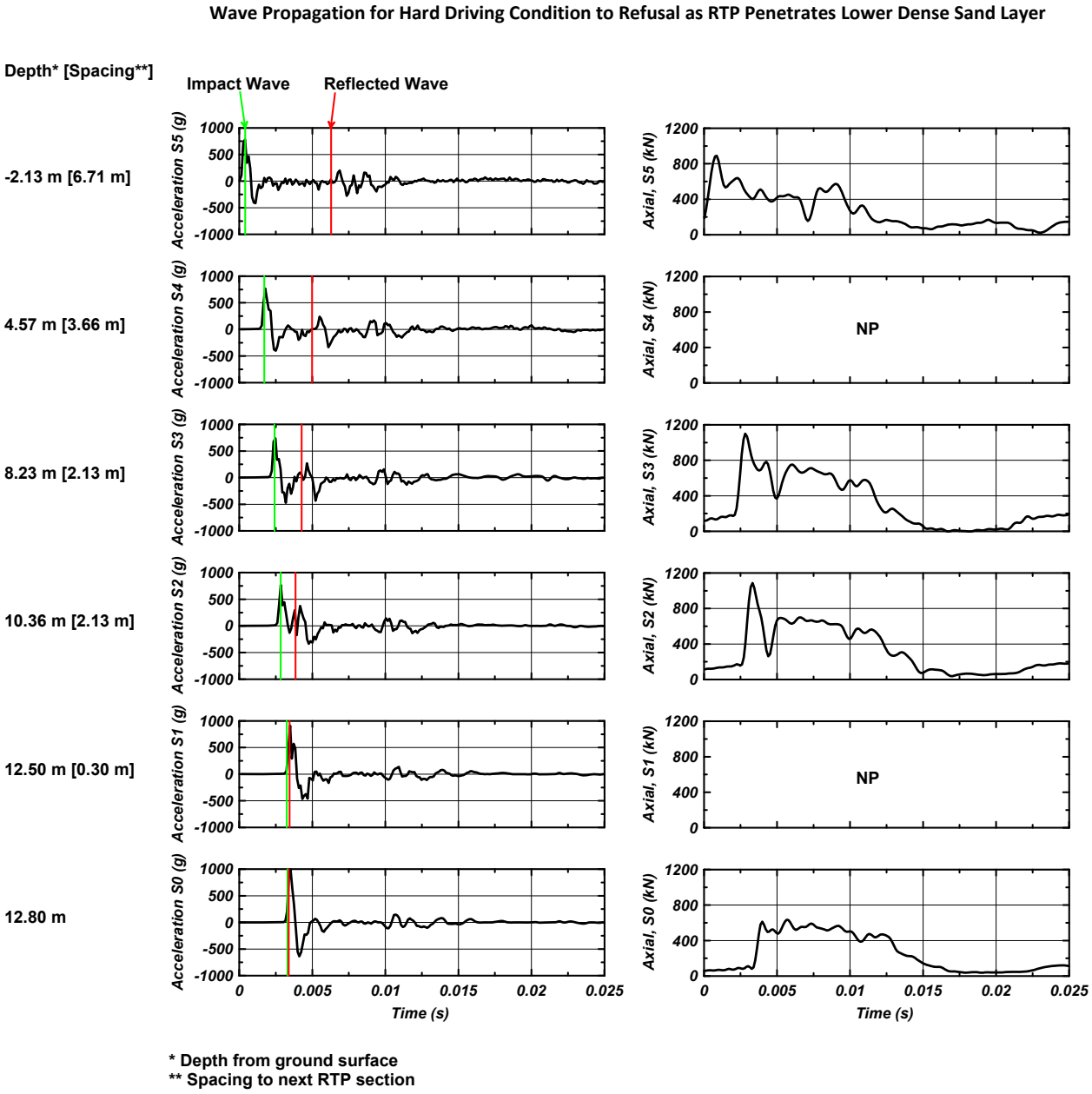


**Figure 5.29: Single impact wave propagation acceleration and axial force time histories of RTP pile penetrating lower dense sand layer at 12.80 m (42 ft) depth during installation 1.**

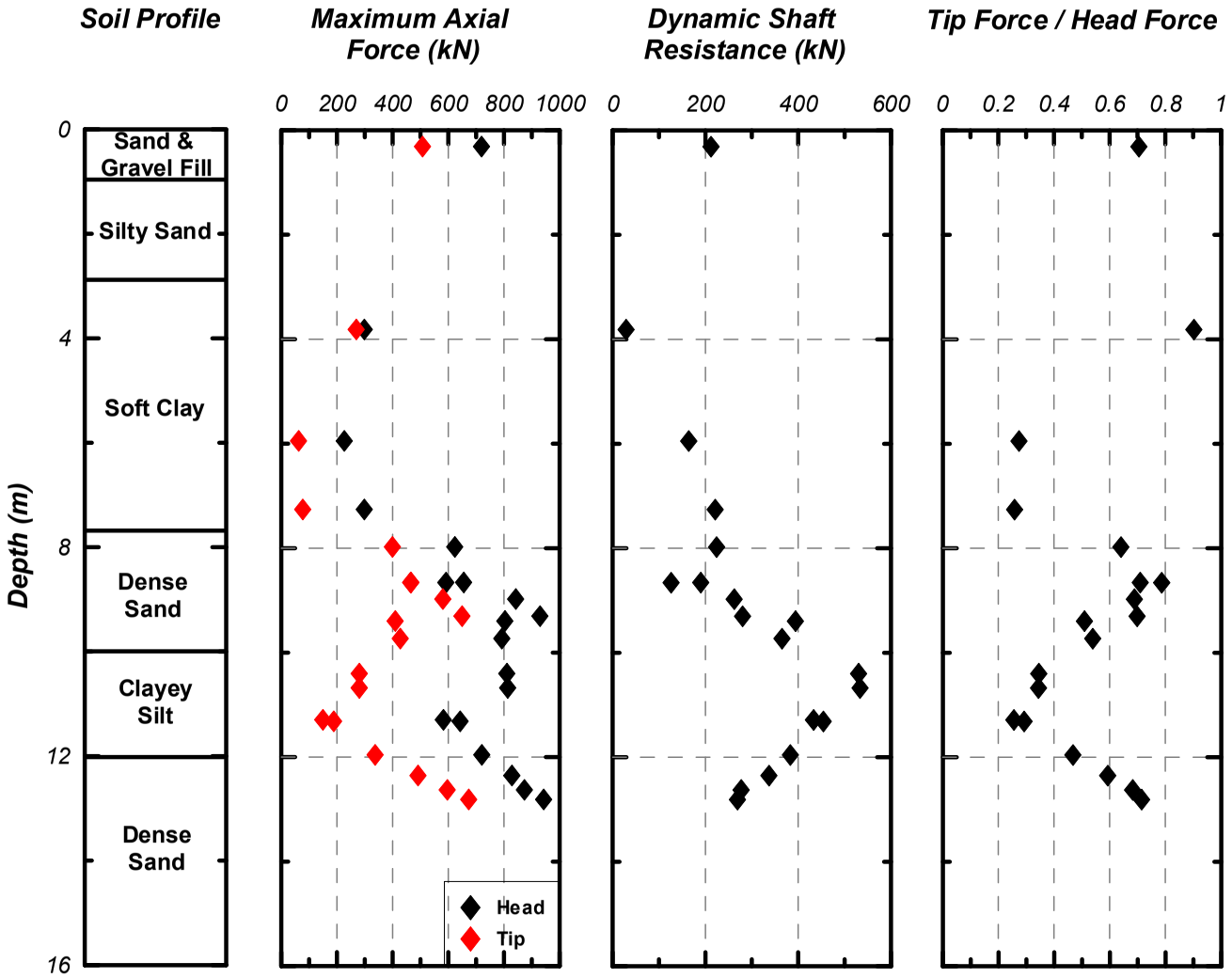


**Figure 5.30: Variation of maximum axial force measured at RTP head and tip, dynamic shaft resistance, and ratio of the tip axial force to total axial force applied at the top with penetration depth.**

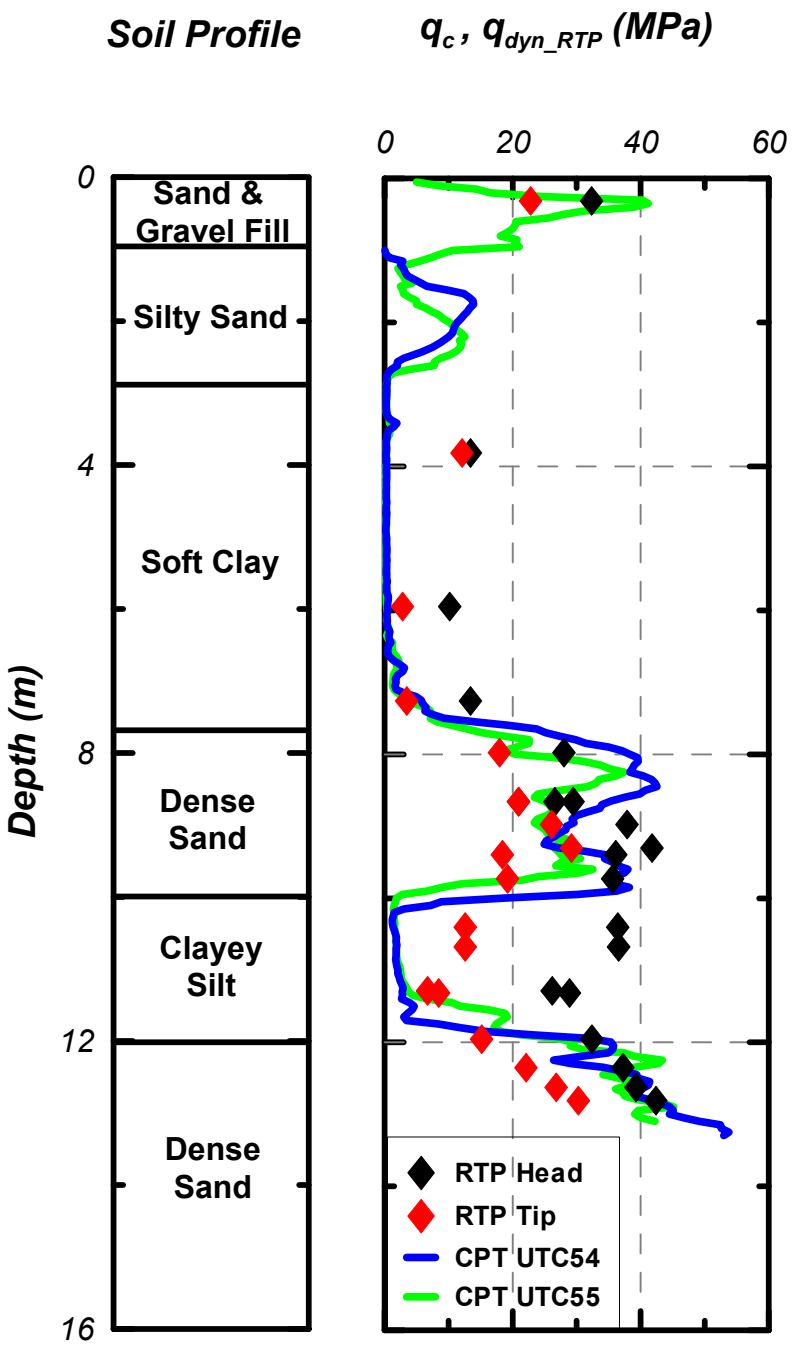


**Figure 5.31: Comparison of RTP head and tip dynamic penetration resistances with cone penetration resistance at same test site.**

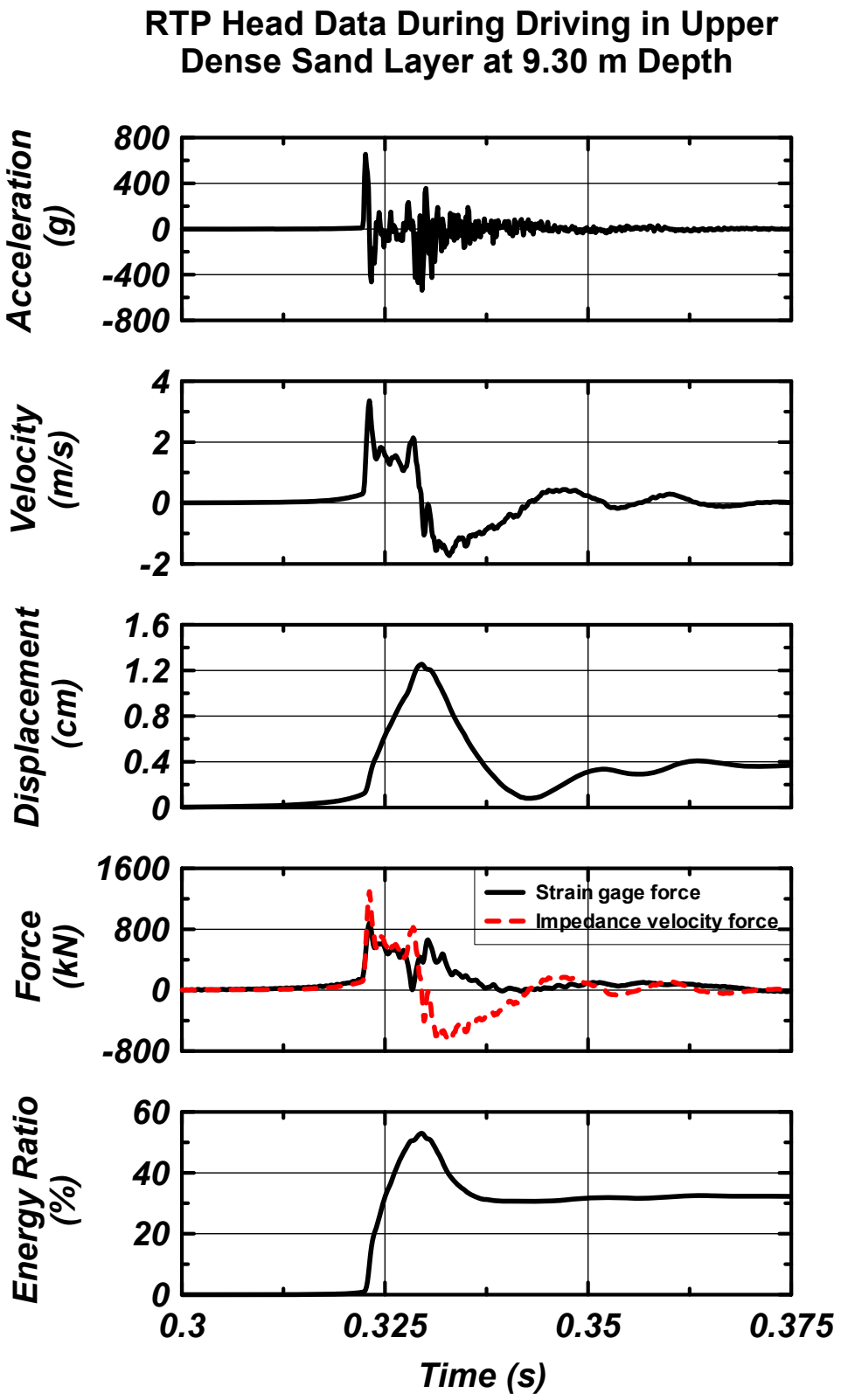


**Figure 5.32: RTP force correction and PDA analysis. Example set of plot from RTP head data during driving in upper dense sand layer at 9.30 m depth.**

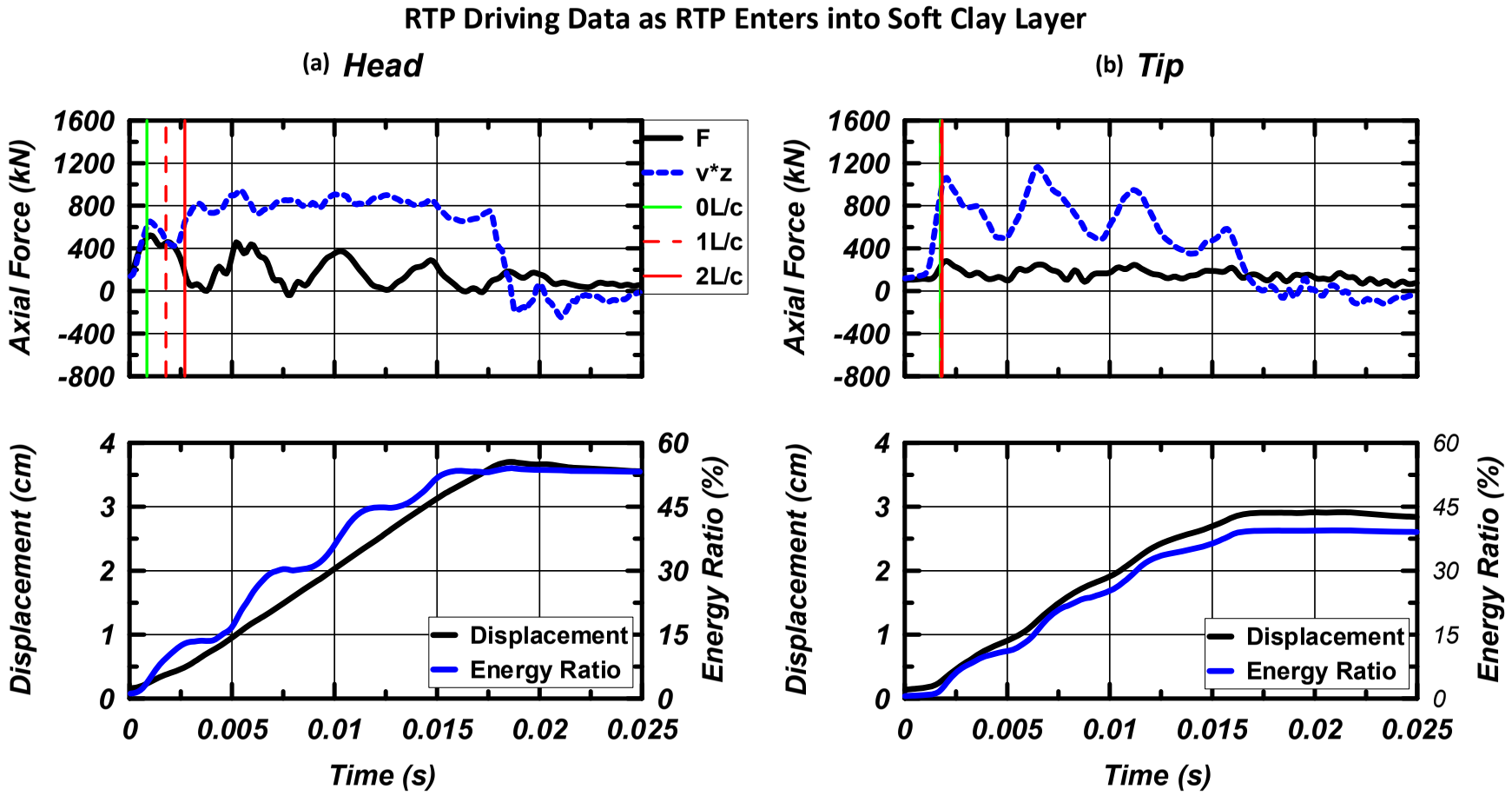


Figure 5.33: Analysis of RTP driving data for easy driving condition through soft clay layer (a) data from top section and (b) data from tip section.

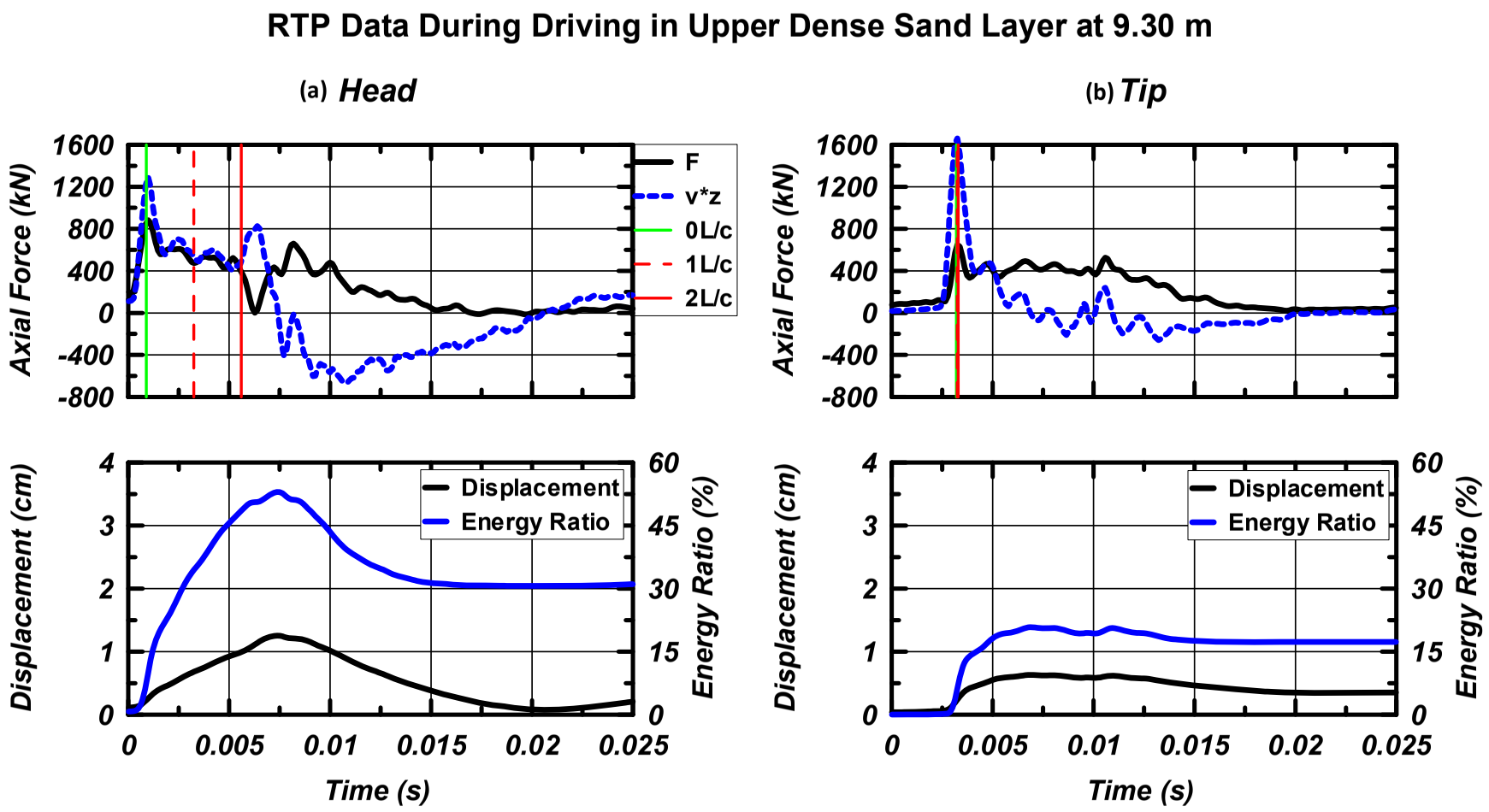


Figure 5.34: Analysis of RTP driving data for hard driving condition through upper dense sand layer (a) data from top section and (b) data from tip section.

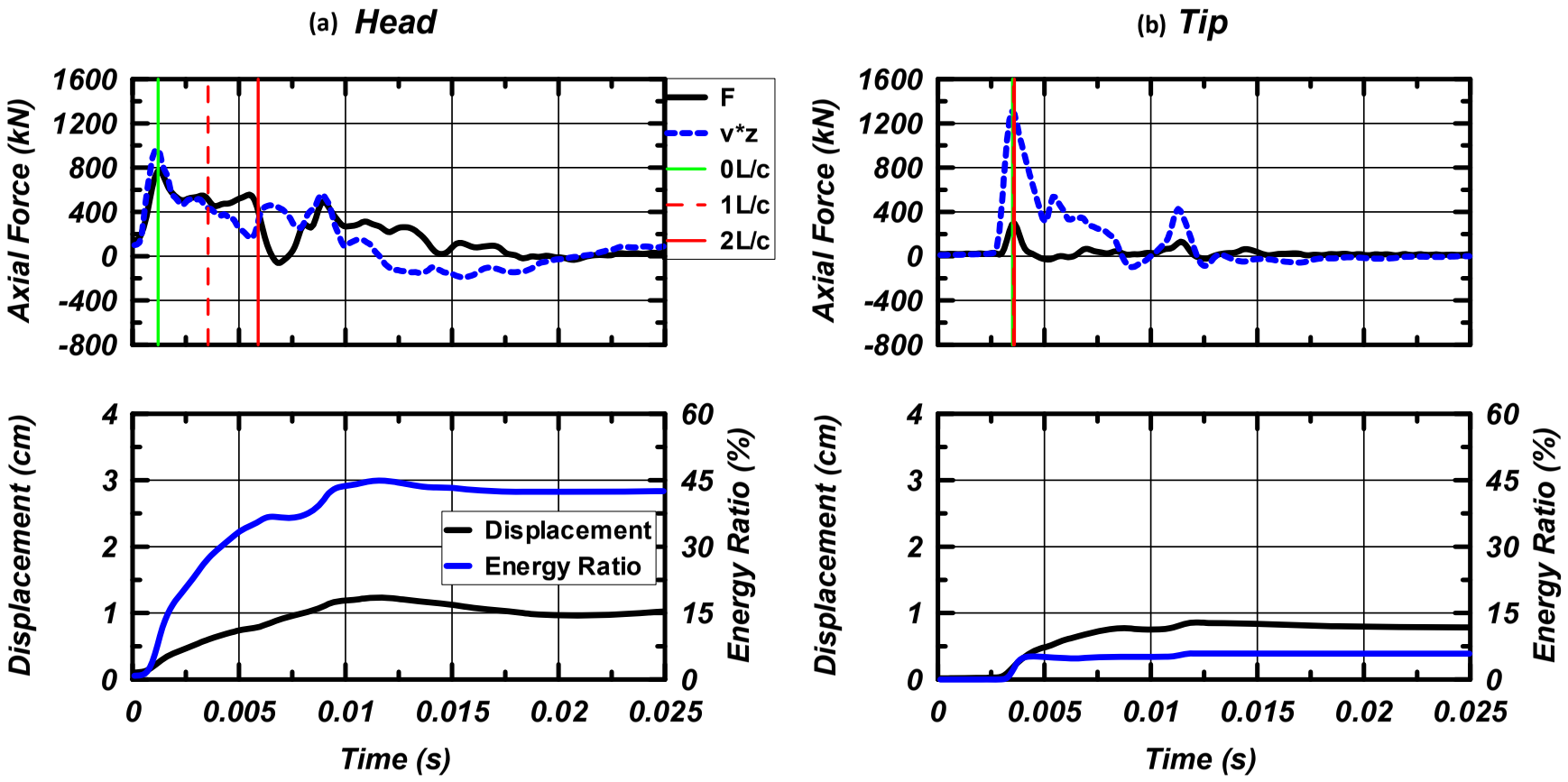


Figure 5.35: Analysis of RTP driving data for moderate driving condition through clayey silt layer (a) data from top section and (b) data from tip section.

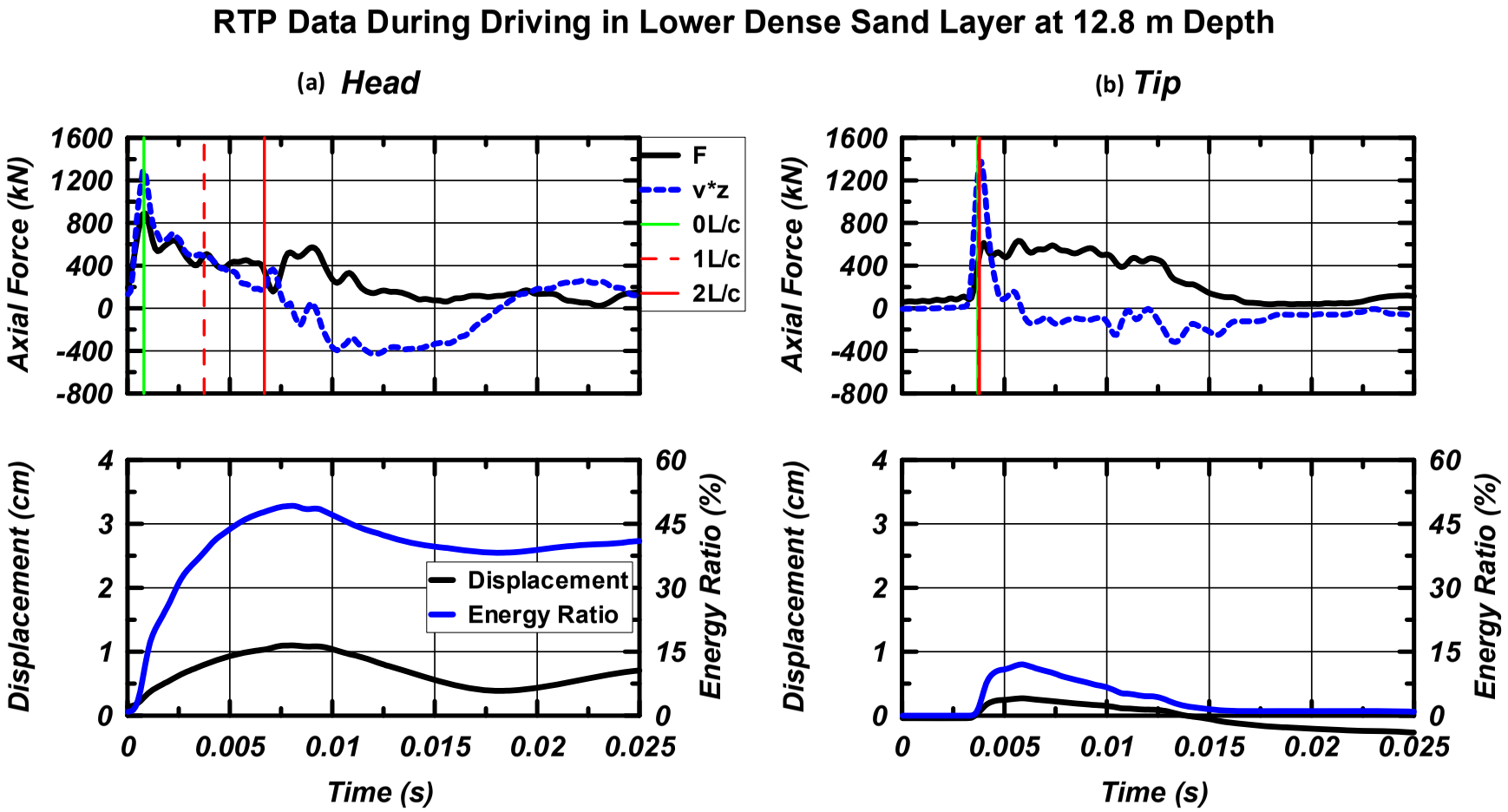


Figure 5.36: Analysis of RTP driving data for hard driving condition in lower dense sand (a) data from top section and (b) data from tip section.

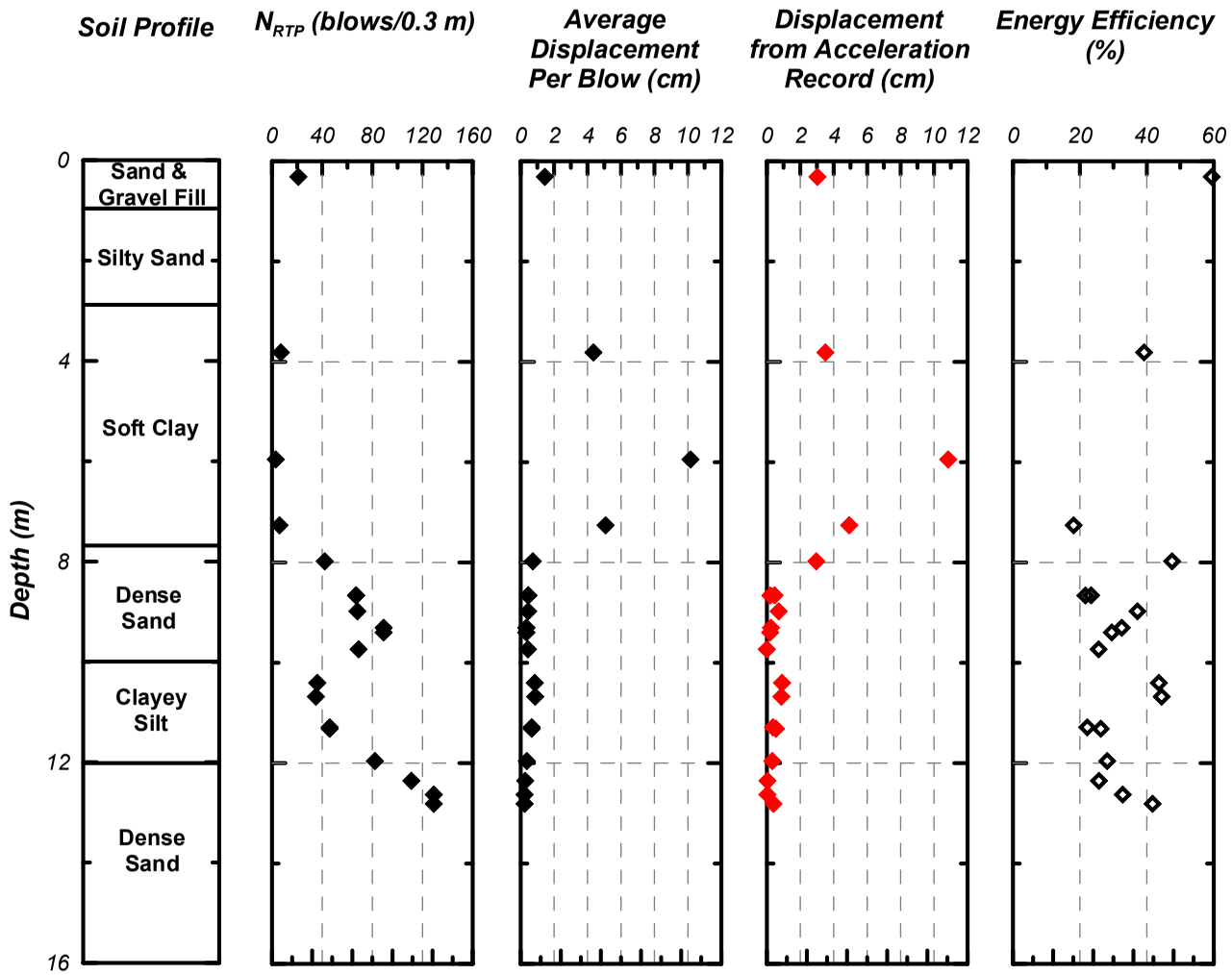


**Figure 5.37: Compiled driving data from installation 1 for displacement calculated from acceleration record and corresponding energy efficiency at the RTP head presented along with $N_{RTP}$ and corresponding displacement caused by $N_{RTP}$.**

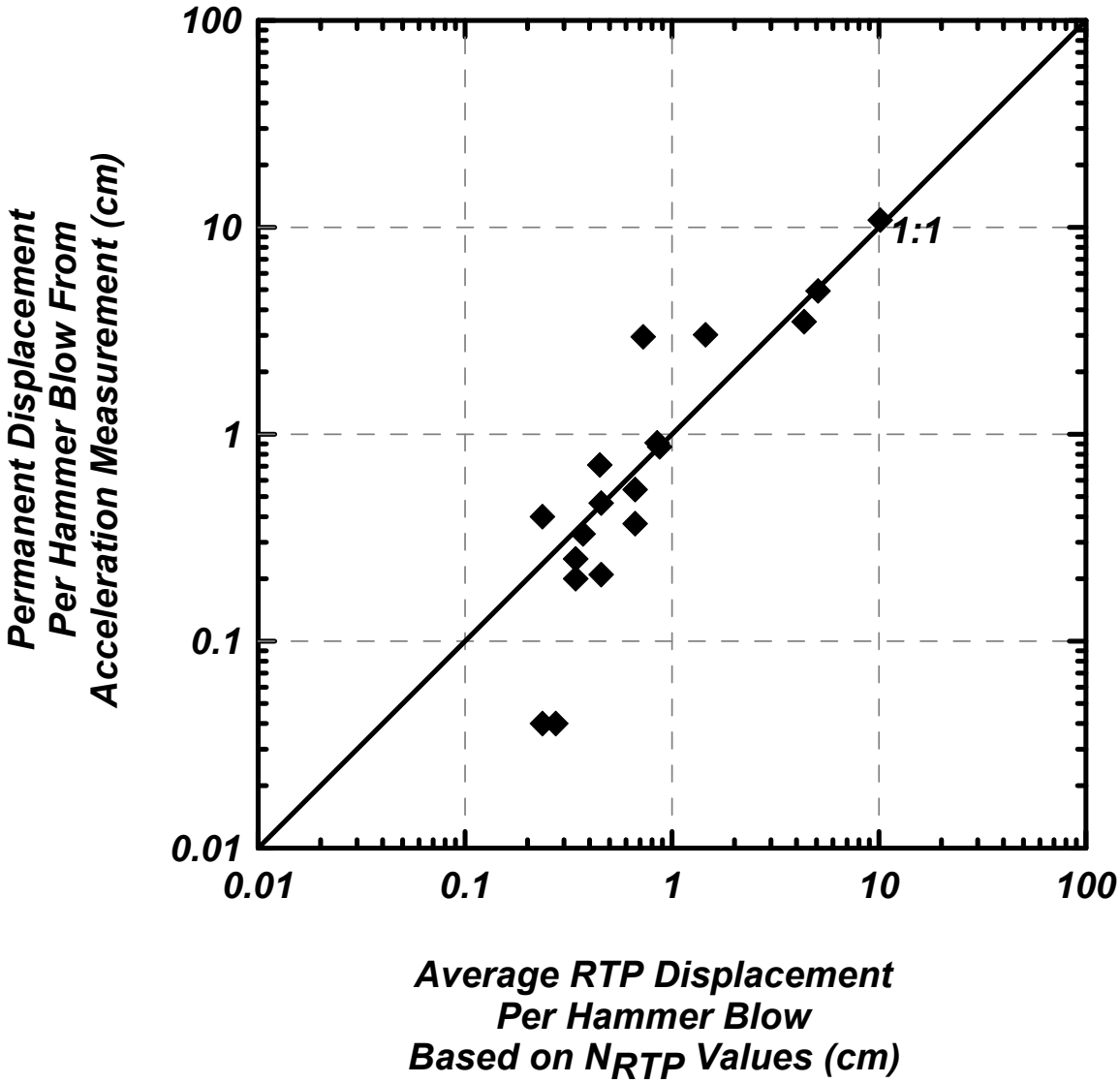


**Figure 5.38: Comparison of displacement calculated from acceleration measurement with the average displacement calculated from number of blows measured in the field.**

# Chapter 6: RTP performance during Loading

This chapter examines the residual stress that develops in the RTP during driving, the dissipation of excess pore pressure during RTP setup following driving, and the performance of the RTP under tensile loading performed immediately after installation and also following four hours of pile setup. Results during RTP driving and two tensile load tests from Installation 1, and results during RTP setup and subsequent load test from Installation 3 are presented and examined in this section. Tensile load test locations of RTP during Installation 1 and 3 are presented in Figure 6.1. It is noted that certain sensors were damaged during Installation 1 hard driving as the RTP penetrated the lower sand layer; this resulted in damaged sensors and a reduced quality data set for subsequent analysis.

## 6.2 Residual Stresses Developed in RTP Sections during Driving

During driving, residual axial stresses (reported and discussed as forces herein) can develop within the RTP due to elastic pile shortening during hammer impact and sufficient shaft friction developing along the upper portion of the pile that prevents complete elastic rebound. The processes of residual stress formation in piles has been studied and documented by several researchers, with a summary presented by Altaee et al. (1992a, b).

The magnitude of residual forces developed in the RTP when installed at the Oakland test site were concentrated at depth in the sand layers since the surficial layers and soft clay layer do not provide significant shaft friction (a specific estimate is provided in a subsequent

section). The residual force measured in the instrumented sections S0 (located at pile tip and at a normalized distance h/D = 1.3 where h is the distance behind the tip and D is the RTP outer diameter), S2 (instrumented section @ h/D = 15.6), and S3 (instrumented section @ h/D = 28.3) is presented in Figure 6.2. It is noted that section S4 responded inconsistently during driving and S5 was never driven below the ground surface; therefore data from neither section is included herein. The figure also indicates the site stratigraphy and the location of the instrumented sections when the RTP had been installed to the final penetration depth of 12.8 m. For context, a force of about 20 kN is applied when the Becker hammer system is lowered and rests statically on the top of the RTP before dynamic driving is initiated. The data presented are consistent with expectations, though additional data from future deployments is desirable for more detailed examination.

The magnitude of the residual axial forces within the RTP expectedly increases with depth, particularly once the dense sand layers are encountered, and remain generally constant with continued pile penetration. The residual force through the upper soft clay, which ends at about 7.7 m depth, is relatively small and equal to about 20 kN or less. Initial penetration into the upper dense sand layer does not increase the residual force either as insufficient shaft resistance exists above this location. However, in the lower portion of the upper dense sand layer the residual stress increases significantly to between 80 and 100 kN, the highest values recorded. As the RTP section enters the clayey silt layer the residual force in the tip section (S0) reduces again as the tip section is able to elastically expand (downward) to reduce the stress in the tip section. Penetration in to the lower dense sand layer results in an immediate increase in residual force since the overlying upper sand layer provides the reaction shaft

friction required to create the residual force. The residual force during penetration through the lower dense sand section varies, but generally remains high.

The distribution of residual axial force within the RTP pile during driving can be examined to a limited extent with the data from the three instrumented sections obtained. Figure 6.2 contains symbols indicating the sensor locations when the RTP tip had penetrated to depths of 10.2, 11.7, and 12.6 m (i.e. data points with the same symbol were obtained at the same point in time during RTP installation). At the full RTP penetration depth of 12.6 m (square symbols) the residual force is highest at section S2, which is positioned near the bottom of the upper dense sand layer. The residual force decreases rapidly at shallower depths as the soils become softer. At shallower penetration depths the upper two sections (S2 and S3) are located in the soft clay layer, which limits the ability to estimate residual force distribution in the lower layers where it is primarily expected to occur. Future testing is needed with additional instrumented sections and with thicker stratigraphic layers so that at least one axial force measurement can be made within each layer to properly assess the residual force distribution.

The measurements of residual radial stress during penetration follow expectations as it generally increases with depth and as the more dense and stiff sand layers are encountered. Residual radial stress measurements from sections S2 (h/D = 15.6), S3 (h/D = 28.3), and S4 (h/D = 50.0) are presented in Figure 6.3. The residual stress measurements near the RTP tip (S0 and S1) are not reported as the sensors were damaged during driving into the lower dense sand layer. Therefore the following limited conclusions can be drawn. The residual stress is about three times larger in the upper sand layer (1000 kPa) compared to in the soft clay layer (300 kPa

near bottom of layer). The measured radial stress is approximately equal at the shallower depths in the clay layer with no particular trends as the h/D ratio increases from 16 to 50 evident. However, as documented by Lehane et al. (1993) and others, the degradation of radial stress and unit shaft friction as a function of h/D primarily occurs within a distance of 15 h/D; at further distances (> h/D values) further degradation is very gradual.

## 6.3 Short Term Setup of RTP Following Installation

During pile setup, excess pore pressure, which was generated during pile driving, will gradually dissipate at a rate dependent on the soil's rate of consolidation and geometric factors. In soft, near normally consolidated (contractive) clays, excess pore pressure dissipation results in consolidation to a denser state and an increase in effective stress. In sands dissipation occurs rapidly, often within hours after pile installation. Fleming et al. (2009), citing numerical work by Randolph et al. (1979) and Randolph and Wroth (1979) and experimental work by McClelland (1969), and Seed and Reese (1955), have shown pile capacity to increase by a factor of two or more in clays with a low over consolidated ratio (OCR) while the effect is less and variable in high OCR clays. Effect on axial capacity in sands is less significant, but can increase by up to 100% over time due to pore pressure dissipation and other thixotropic processes (Chow et al. 1998, Fleming et al. 2009).

RTP Installation 3 consisted of penetration to 12.6 m depth immediately followed by a 4.0 hour time period to allow for (partial) pile setup. During this time period the top of the RTP

was not subjected to loading and monitoring of pore pressure occurred as described in Chapter 4.2. Measurements of pore pressure versus time from two depths, one at 6.3 m depth (section S4) located in the soft clay layer and one at 11.8 m depth (section S2) located in the lower dense sand layer, are presented in Figure 6.4. The hydrostatic value estimated for each respective depth is also indicated in Figure 6.4. Pore pressure measurements from section S3 is not reported due to desaturation of the porous stone while the sensor was above ground and/or in the upper fill material.

Pore pressure dissipation in time follows expected trends in both the clay and sand, with about 50% excess pore pressure dissipation occurring in the clay after 4.0 hrs (14,730 seconds) and about 100% dissipation occurring in the sand after 0.41 hrs (about 1500 seconds). The excess pore pressure in the clay immediately following driving of about 78.3 kPa remains constant until about 1500 seconds, after which the data follows the conventional trend of dissipation for normally consolidated soils (Fleming et al. 2009). Dissipation of the excess pore pressure in the lower dense sand layer begins immediately after driving, beginning with an excess pore pressure of 91.1 kPa, and decreases to the hydrostatic value of 109.5 kPa rapidly. After reaching the hydrostatic pressure the pore pressure varies slightly, which may be due to dissipation of adjacent layers.

The coefficient of consolidation in the clay and sand layer was estimated to be 0.019 $cm^2$/sec (0.003 $in^2$/sec) and 1.29 $cm^2$/sec (0.2 $in^2$/sec), respectively. These estimations are based on modeling solid pile penetration in an elastic-perfectly plastic soil as described in

Fleming et al. (2009) (and based on Randolph 2003) which examines radial consolidation as a function of pile diameter using a normalized time factor ($T_{eq}$) in the following form

$$T_{eq} = \frac{c_h \times t}{d_{eq}^2}$$

where $d_{eq}$ is the equivalent diameter of a pile and $c_h$ is the horizontal coefficient of consolidation. For the RTP $d_{eq}$ is equal to the outer diameter since it is closed ended. Figure 6.5 presents the associated relationship between normalized excess pore pressure ratio and the equivalent normalized time factor. The solution presented is for a rigidity index, $I_r = {}^{G}/_{S_u}$ (where $G$ is the shear modulus and $S_u$ is the undrained strength) of 100, which is a typical value for soft normally consolidated clays. A $c_h$ value of 0.019 $cm^2$/sec for the soft clay is obtained assuming 50% consolidation at a time of 15,000 seconds and that an $I_r$ value of 100 is reasonable. Estimation of $c_h$ for the sand is complicated due to the difficult in specifying an appropriate $I_r$ value. However, it is likely that the actual value of $I_r$ is larger than 100. Therefore, a rough approximation (possibly reasonable to one order of magnitude) is that the $c_h$ of sand is equal to 1.29 $cm^2$/sec.

## 6.4 Pile Load Test - Pullout Testing

Pile load tests were performed immediately after driving and also following a setup period of 4.0 hours. Results from each, and a comparison between them are presented below.

### 6.4.1 Pile Load Test Results without Setup

Tension load tests performed during Installation 1 immediately after driving to depths of 9.3 and 12.8 m show that the RTP is capable of measuring total pile capacity and the distribution of load along the pile length. The RTP performed well during driving through the clay, upper sand, and clayey silt layers, resulting in a relatively clear dataset for examination of the tension load test performed following penetration to 9.3 m. During subsequent penetration to the termination depth of 12.8 m very difficult driving conditions were encountered (as discussed in Chapter 5.3.4 with >150 blows / 0.3 m penetration), such that certain sensors (particularly the radial stress cells, which also damaged some of the axial load cells due to the proximity of the strain gage locations) were damaged. Therefore only the axial load distribution is examined for the latter test.

Measurements of axial load, pore pressure, and radial stress during the RTP tension load test after penetration to 9.3 m (30.5 ft) are presented in Figure 6.6a. The maximum capacity is reached within about 5 mm of RTP displacement. Instrumented sections at shallower depths, S2 and S3 in the soft clay at 6.7 and 4.5 m depth, respectively, and S4 in the upper fill at a depth of 0.88 m, have comparable load distribution curves that stabilize at about 325 kN tensile load. The similarity in the curves and initial values of approximately 0 kN prior to loading are due to the soft clay and surficial soil layers having negligible shaft friction. In contrast, the two measurements at the tip (S0 at 8.8 m depth and S1 at 9.1 m depth) are located near the bottom of the upper dense sand layer at a depth where the unit shaft resistance is significant. The residual forces in S0 and S1 prior to the tension test are due to the prior loading history. The

difference in magnitude between the S0 and S1 measurement at large displacements is due to the 0.28 m separation distance between sensors over which shaft resistance acts. Similarly, the S0 is non-zero due to the axial load sensor (strain gages) being positioned approximately 0.21 m from the RTP tip. From this load test data the unit shaft resistance between axial force measurement locations can be estimated as summarized in Table 6.1. Of particular interest is the estimated shaft resistance between instrumented locations S0 and S1, and between S2 and S3 as these intervals are positioned entirely within a single soil layer. The unit shaft resistance is estimated to be 1.2 kPa in the clay layer and 331 kPa in the upper dense sand layer. The low shaft friction value for the clay is reasonable given observation of free fall of the RTP under self weight during installation and the associated shearing and remolding of the clay.

During the tension load test the pore pressure and radial stress measurements evolve in a manner generally consistent with the axial load data (Figure 6.6 b and c). At the end of driving as the pile load test is initiated excess pore pressure exists in both the clay (S2 and S3) and upper sand (S1) while no significant excess pore pressure is generated near the surface (S4). During the pile load test, the excess pore pressure in the clay layer does not change appreciably; this is attributed to the intensive shearing process during pile installation being the primary source of pore pressure generation and the rate of consolidation (as discussed above) being sufficiently low such that the time duration of the load test (~5 min) was very small relative to the time required for consolidation (4.0 hr). The initial radial stress measurements increased with depth for measurements S2, S3, and S4 (S1 is not reported because it was damaged during driving to this depth). The radial stress in the soft clay did not change significantly during the tension load test due to the time duration of loading being less than

that for consolidation. The radial stress measurement S4 in the fill material near the ground surface increases with loading. The increase observed is likely either due to dilation of the granular fill around the RTP or because of initial non-verticality of the RTP resulting in horizontal loading of the thin walled cylinder as the tension load is applied (i.e. vertical pullout resulted in a small amount of lateral RTP movement and concentrated horizontal loading of the thin walled cylinder).

The results of the second tension load test performed immediately after driving to a depth of 12.8 m during Installation 1 was consistent with the load test at shallower depths (Figure 6.7). Penetration of an additional 3.3 m increased the capacity to about 450 kN, a 125 kN increase. The increase in total capacity is attributed to full penetration into the upper dense sand layer and about 1.5 m penetration into the lower dense sand layer. Again, the soft clay layer generates negligible shaft resistance.

A comparison of the load test results from performed at RTP tip depths of 9.3 and 12.8 m is shown in Figure 6.8. The required displacement to reach total capacity is about 4 mm for the shallower depth and about 8 mm for the deeper depth (though 80% of capacity is obtained after 6 mm of displacement). The difference in capacity again is attributed to the additional penetration down into the lower dense sand layer

### 6.4.2 Pile Load Test Results Following Setup

The tension load test performed on Installation 3 following driving to a depth of 12.6 m and a setup time of 4.0 hours (Figure 6.9) resulted in an increase in capacity of about 100 kN relative to the comparable load test without setup (Installation 1 to depth of 12.8 m discussed above). The displacement required to reach full pullout capacity again occurred before about 10 mm of displacement (though issues with displacement rate and data acquisition compromised the integrity of the data up to maximum load). The increase in capacity is attributed primarily to the increase in shaft resistance in the lower clayey silt layer and the upper soft clay due to consolidation during setup (dissipation of excess pore pressured induced by driving). This is evident in Figure 6.10, which presents the load displacement curves from Installation 1 (immediate loading) and 3 (loading after setup) following driving to 12.8 m depth at comparable measurement depths at the top of the clayey silt layer (S2 for Installation 1 and S3 for Installation 3) and near the surface (S4 for Installation 1 and S5 for Installation 3). The overall increase in capacity is evident based on the near surface measurements. The measurement at about 10 m depth has a load difference opposite than expected; the capacity following immediate loading from Installation 1 is greater than that following setup from installation 3. The source of this difference is unclear, but may be linked to the magnitude of residual stress existing before the pullout test (the residual stress offset is about equal to the observed stress difference). Unfortunately no pore pressure measurements were obtained within the silty clay layer so it was not possible to determine the magnitude of excess pore pressure generated or the rate at which the excess pore pressure dissipated. However, based

on the CPT data and boring log record it is likely that full dissipation occurred within the 4.0 hours of setup time.

### 6.4.3 Pile Load Test Results Compared to CPT Based Pile Design Method

The tensile load capacity of the RTP after installation to depths of 9.3 and 12.6 m estimated using the Canadian Foundation Engineering Manual (CFEM) CPT based method (Canadian Geotechnical Society 2006) compares reasonably with the RTP measurements performed in the field and presented above. In this section the distribution of shaft friction as well as the total pull out capacity of the RTP using the CFEM method is presented.

The CFEM method was selected as the comparison design methodology because (1) it is an established, time proven procedure, (2) it is flexible in that it can be applied to all soil types and layered stratigraphies, and (3) it provides some consideration to pile and installation type. The CFEM method was developed based on a diverse pile load test database that enabled specification of empirical factors applied to the cone tip resistance to estimate shaft capacity based on both pile (and installation) method and soil type as determined from the CPT and boring logs. The unit shaft resistance, $q_s$, is determined as the lesser of a direct estimate based on the cone $q_c$ measurement and an empirical limiting shaft resistance, $q_{s\_lim}$, based on the load test data base. The cone based estimate is defined as

$$q_s = \frac{q_c}{\propto}$$

where $\alpha$ is the shaft resistance factor. The $\alpha$ and $q_{s\_lim}$ factors for the four soil types encountered at the project site given RTP driven installation (defined as Category IIB in the method) are tabulated in Table 6.2.

The profile of unit shaft resistance using the CFEM method, include entire profiles for the $q_c$ based estimate and for the $q_{s\_lim}$ values is presented in Figure 6.11. The lesser of the two values at each depth comprise the recommended profile for design (red line labeled as CFEM in Figure 6.11). The comparison of average unit shaft resistance calculated using RTP and CPT based is shown in Table 6.3. The unit shaft resistances estimated based on the CFEM method is higher (about 800%) in the clay layer compared to the RTP measurements (Figure 6.11 and Table 6.3). This difference is expected as the RTP measurements for Installation 1 were obtained immediately after RTP installation while the CFEM method was developed to estimate the long term shaft resistance after pile setup.

The cumulative shaft distribution for a tension load test for the RTP installed to depths of 9.3 and 12.8 m is presented in Figure 6.12. As evident, the cumulative resistance profiles indicate that about 68% of the capacity for the RTP installed to a depth of 9.3 m is due to the 2.1 m penetration into the upper sand layer. For the RTP installed to a depth of 12.6 m about 69% of capacity is due to the two dense sand layers.

A comparison of the three tension load tests with the CFEM estimated cumulative shaft distributions indicate a reasonable agreement, but with the CFEM method consistently underestimating capacity by about 50% or less. Even the cumulative shaft distribution based on only the CFEM $q_c$ estimate without applying a limiting shaft resistance underestimates the

measured capacity. Comparison of the Installation 1, 9.3 m depth, without setup test indicates that the primary source of difference between the methods is in the unit shaft friction in the upper dense sand layer. Similarly, the unit shaft resistance also appears to be underestimated for the lower dense sand layer for tests performed after installation to 12.8 m.

## 6.5 Summary

This chapter has presented and examined the results of residual axial loads and radial stresses during and at the end of driving, pile setup in terms of excess pore pressure dissipation over 4 hours following pile installation, three tension pile load tests, and a comparison of the load test results with that predicted with the CFEM design method. The RTP data obtained was of reasonable quality, but damage and failure of the radial stress measurement (by deformation of the thin walled cylinder and soil ingress behind it that damaged the radial stress and axial load Wheatstone bridge strain gages and wiring) resulted in an incomplete data set.

Overall the measurements obtained with the RTP were consistent with expectation. Namely, the residual driving forces developed within the dense sand layers due to higher shaft resistance, the dissipation of excess pore pressures in the soft clay layer occurred in a manner and rate consistent with the soil properties and pile geometry, the dissipation in the lower sand layer occurred more rapidly due to higher permeability, the RTP tension capacity increased with an increase in driving distance and pile setup, the sand layers were the primary contributors to the tension capacity, and the CFEM method was shown to under predict the RTP field test data.

**REFERENCES**


Altaee, A., Fellenius, B.H., and Evgin, E., (1992a) "Axial load transfer for piles in sand. I. Tests on an instrumented precast pile", *Canadian Geotechnical Journal, Vol. 29*, pp. 11-20.

Altaee, A., Evgin, E., and Fellenius, B.H., (1992b) "Axial load transfer for piles in sand. II. Numerical Analysis", *Canadian Geotechnical Journal, Vol. 29*, pp. 21-30.

Canadian Geotechnical Society (2006) *Canadian Foundation Engineering Manual*, 4th Edition, 488 p.

Fleming, K., Weltman, A., Randolph, M., and Elson, K., (2009) "Piling Engineering", *3rd Edition,* Taylor & Francis, New York, N.Y., 398 p.

McClelland, B., Focht, J.A., and Emrich, W.J., (1969) "Problems in design and installation of offshore piles", *ASCE J. Soil Mech. and Found. Div.*, Vol. 6, pp. 1491–1513.

Randolph, M.F., (2003) "43rd Rankine Lecture: Science and empiricism in pile foundation design", *Géotechnique*, Vol. 53, No. 10, pp. 847–875.

Randolph, M.F., Carter, J.P., and Wroth, C.P., (1979) "Driven piles in clay – the effects of installation and subsequent consolidation", *Géotechnique*, Vol. 29, No. 4, pp. 361–393.

Randolph, M.F. and Wroth, C.P. (1979) "An analytical solution for the consolidation around a driven pile", *Int. J. Num. and Anal. Methods in Geomechanics*, Vol. 3, pp. 217–229.

Seed, H.B. and Reese, L.C. (1955) "The action of soft clay along friction piles", *Proc. ASCE*, Publication 81, Paper 842.

**TABLES**

**Table 6.1: Comparison of unit shaft friction values obtained from CPT and RTP measurements at the penetration depth of 9.3 m.**

| Depth (m) | Soil Layer | Average Unit Shaft Friction (kPa) |
|---|---|---|
| 4.5 – 6.7 | Soft Clay | 1.2 |
| 6.7 – 8.8 | 50% Soft Clay<br>50% Upper Dense Sand | 165 |
| 8.8 – 9.1 | Upper Dense Sand | 331 |

**Table 6.2: CFEM method factors for $\alpha$ and $q_{s\_max\_lim}$ for the soil layers at the project site. Calculations of average shaft friction are based on these factors.**

| Soil Type | $\alpha$ factor | $q_{s\_max\_lim}$ (kPa) |
|---|---|---|
| Silty Sand | 200 | 80 |
| Soft Clay | 30 | 15 |
| Dense Sand | 200 | 120 |
| Clayey Silt | 120 | 35 |

**Table 6.3: Comparison of unit shaft friction values obtained from CPT and RTP measurements at the penetration depth of 9.3 m.**

| Depth (m) | Soil Layer | Average Unit Shaft Friction (kPa) | | | |
|---|---|---|---|---|---|
| | | RTP based | CPT based | | |
| | | | $q_s=q_c/\alpha$ | $q_{s\_max\_lim}$ | CFEM |
| 4.5 – 6.7 | Soft Clay | 1.2 | 15 | 15 | 10 |
| 6.7 – 8.8 | 50% Soft Clay<br>50% Upper Dense Sand | 165 | 124 | 76 | 70 |
| 8.8 – 9.1 | Upper Dense Sand | 331 | 124 | 120 | 120 |

**FIGURES**

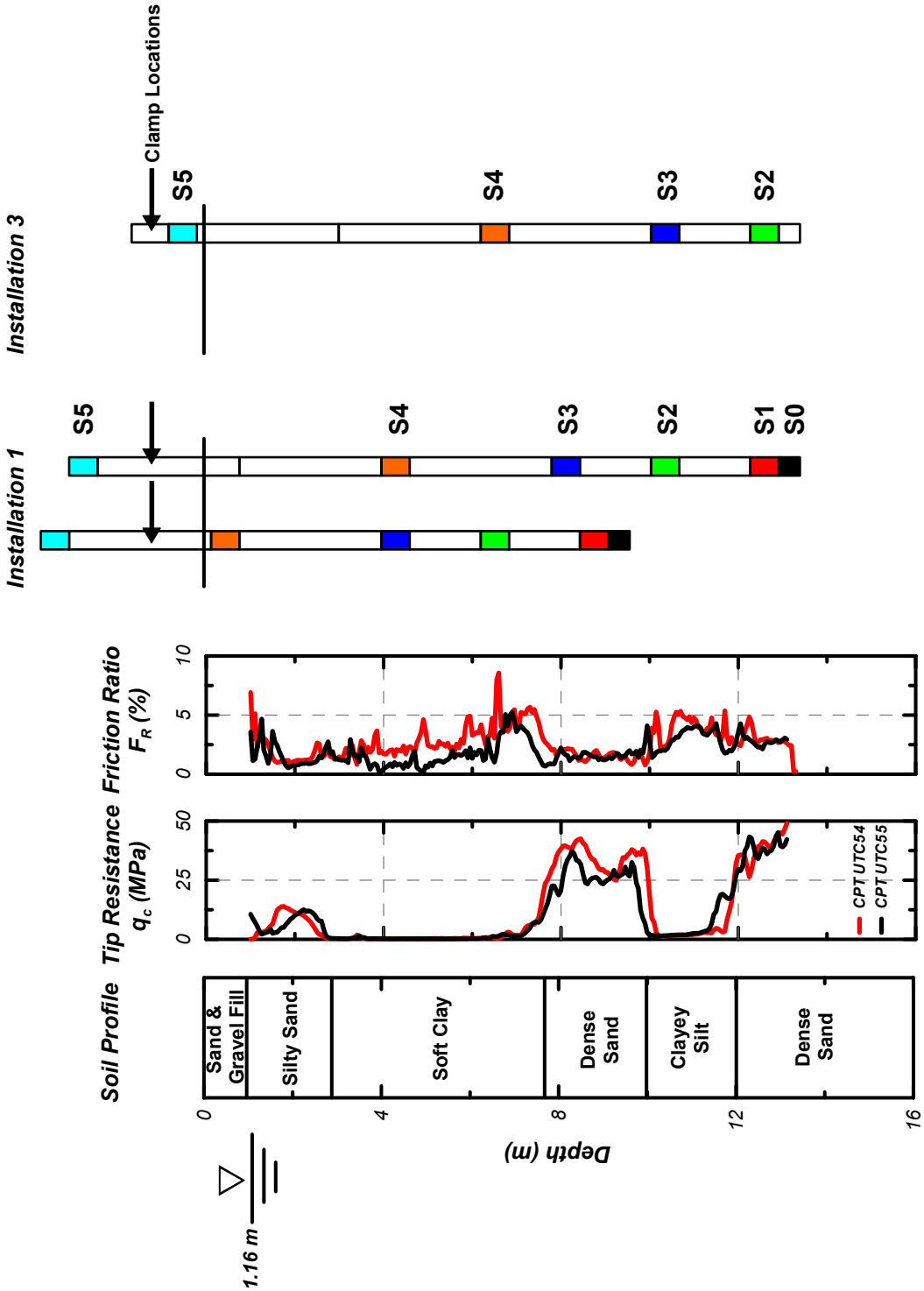


**Figure 6.1: Schematic of RTP locations during tension load testing in installations 1 and 3.**

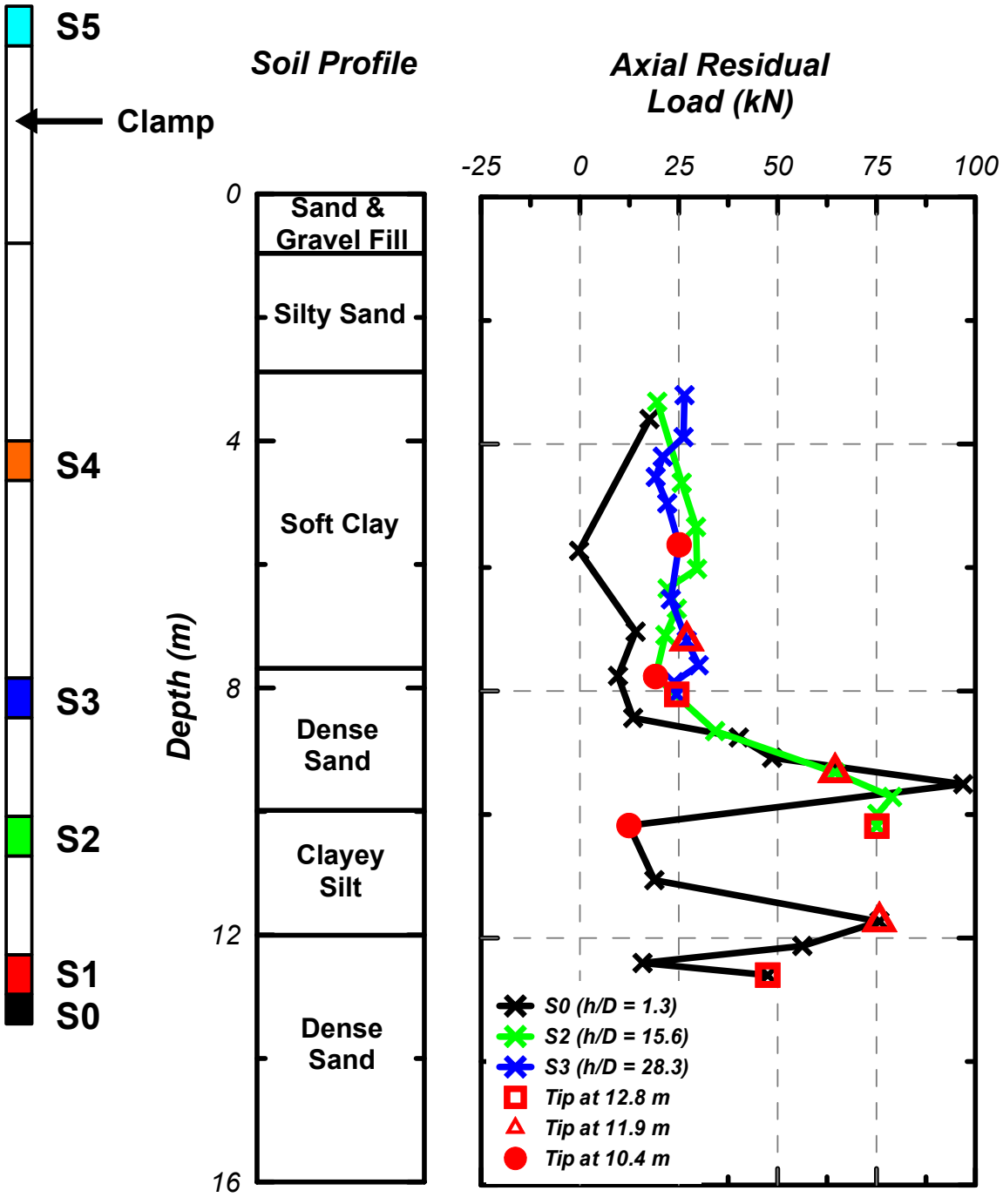


**Figure 6.2: Residual axial force on tip and two other instrumented sections with penetration depth of each section presented with site stratigraphy. Measurements obtained at every location where symbol is presented. The set of measurements when tip was at 12.8 m is indicated with open box symbol, set of measurements when tip was at 11.9 m is indicated by open triangle symbol, and set of measurements when tip was at 10.4 m is indicated by closed circle symbol.**

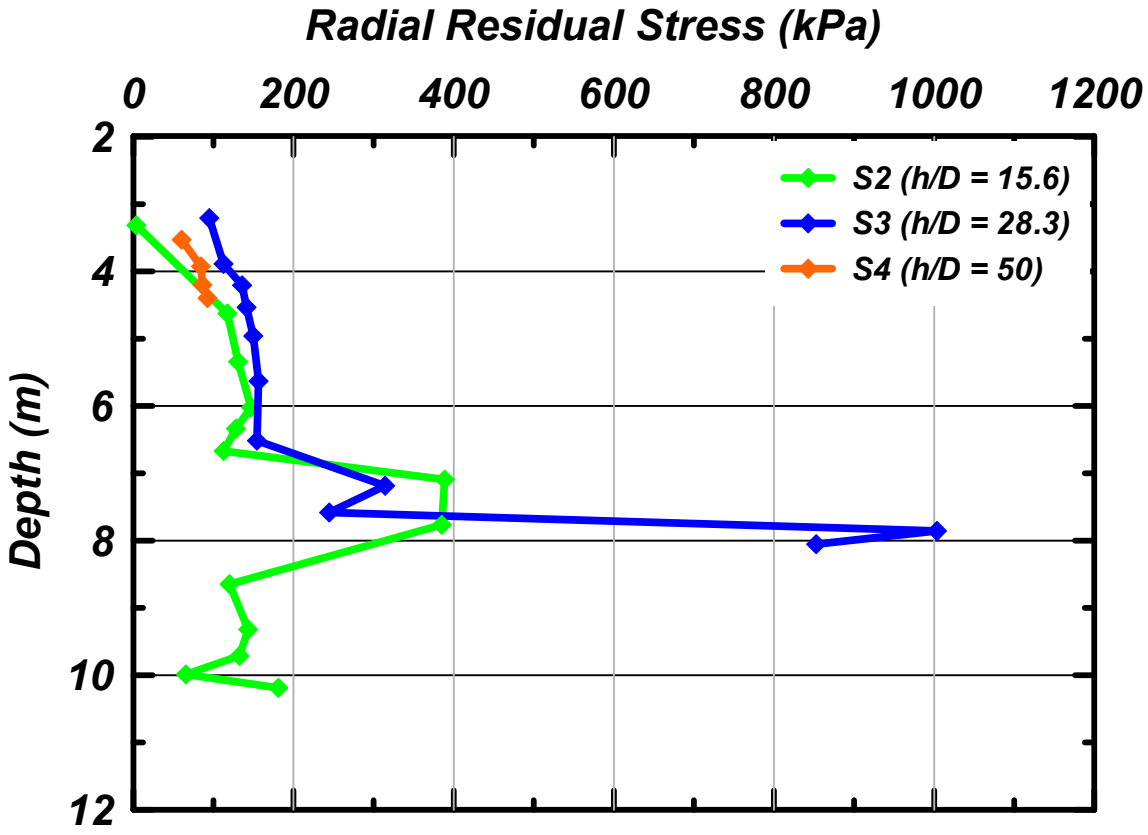


**Figure 6.3: Residual radial stress measurements from instrumented sections versus penetration depth. Data presented was obtained stable values following dynamic driving.**

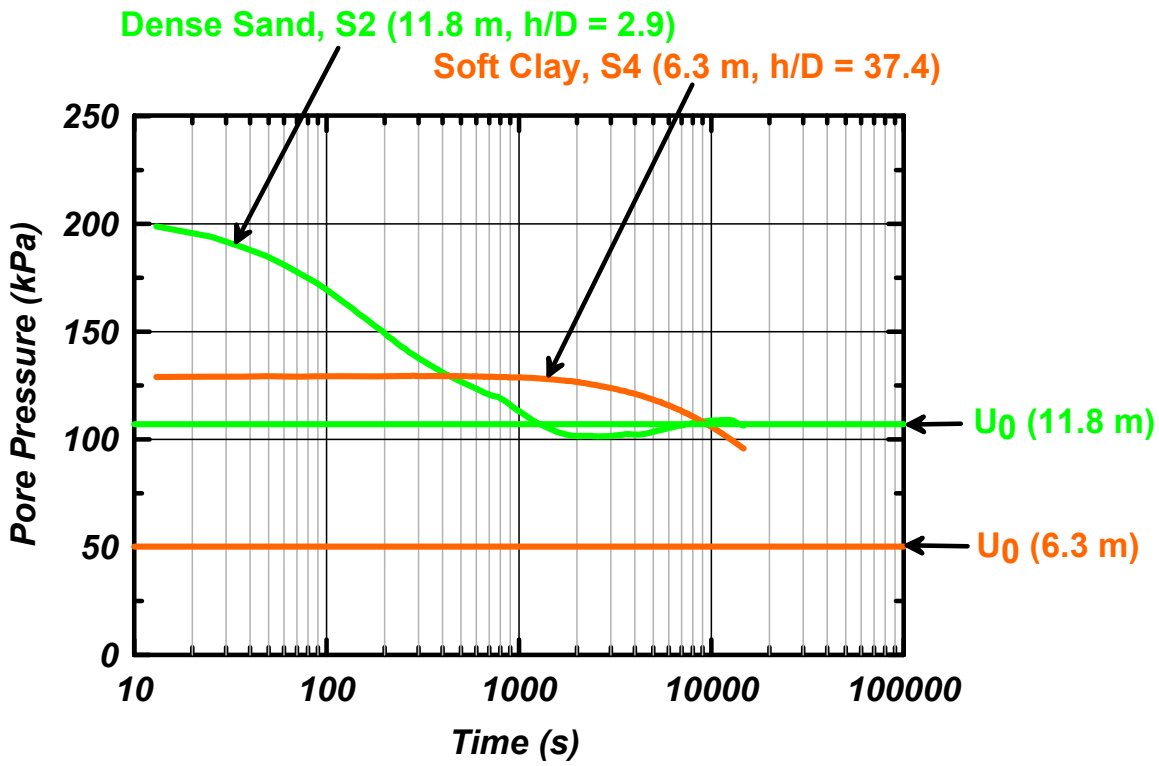


**Figure 6.4: Pore pressure dissipation in lower dense sand and soft clay layer during RTP setup period**

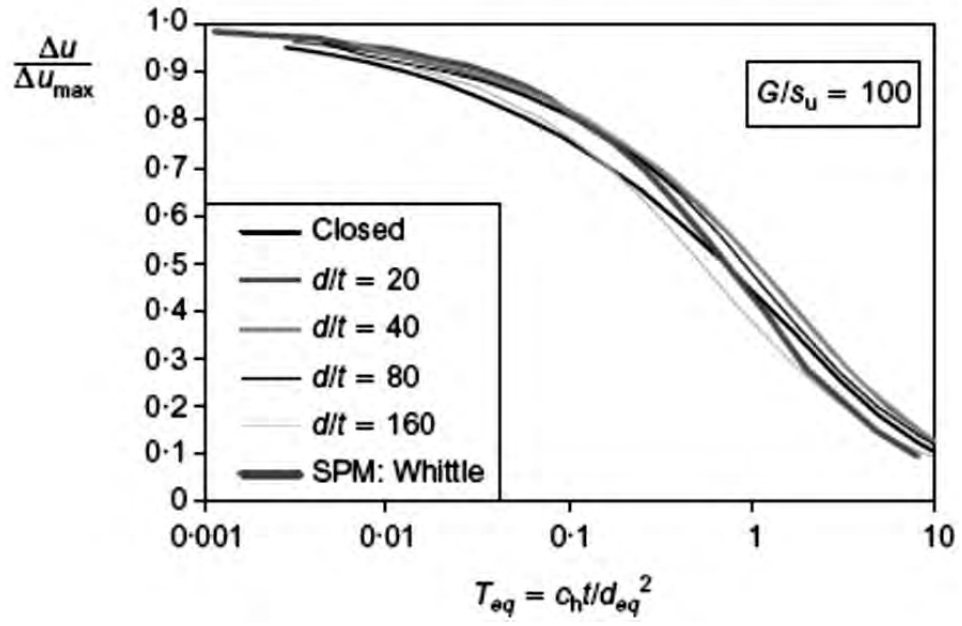


**Figure 6.5: Dissipation of excess pore pressure ratio of normally consolidated soils at pile shaft (Fleming et al. 2009)**

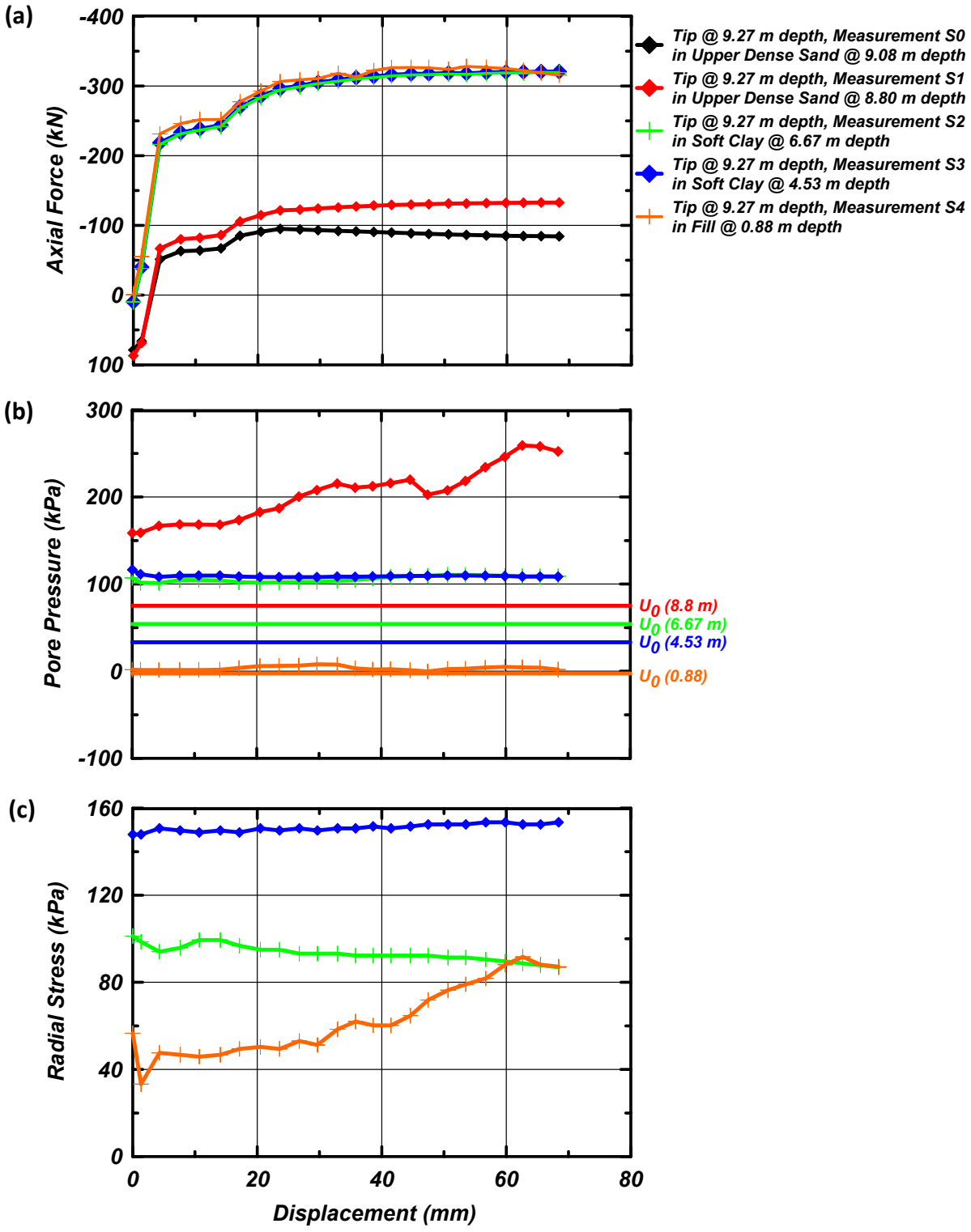


**Figure 6.6: Measurement during tension load test with displacement, (a) axial load, (b) pore pressure, and (c) radial stress. Test performed at RTP tip penetration depth of 9.3 m.**

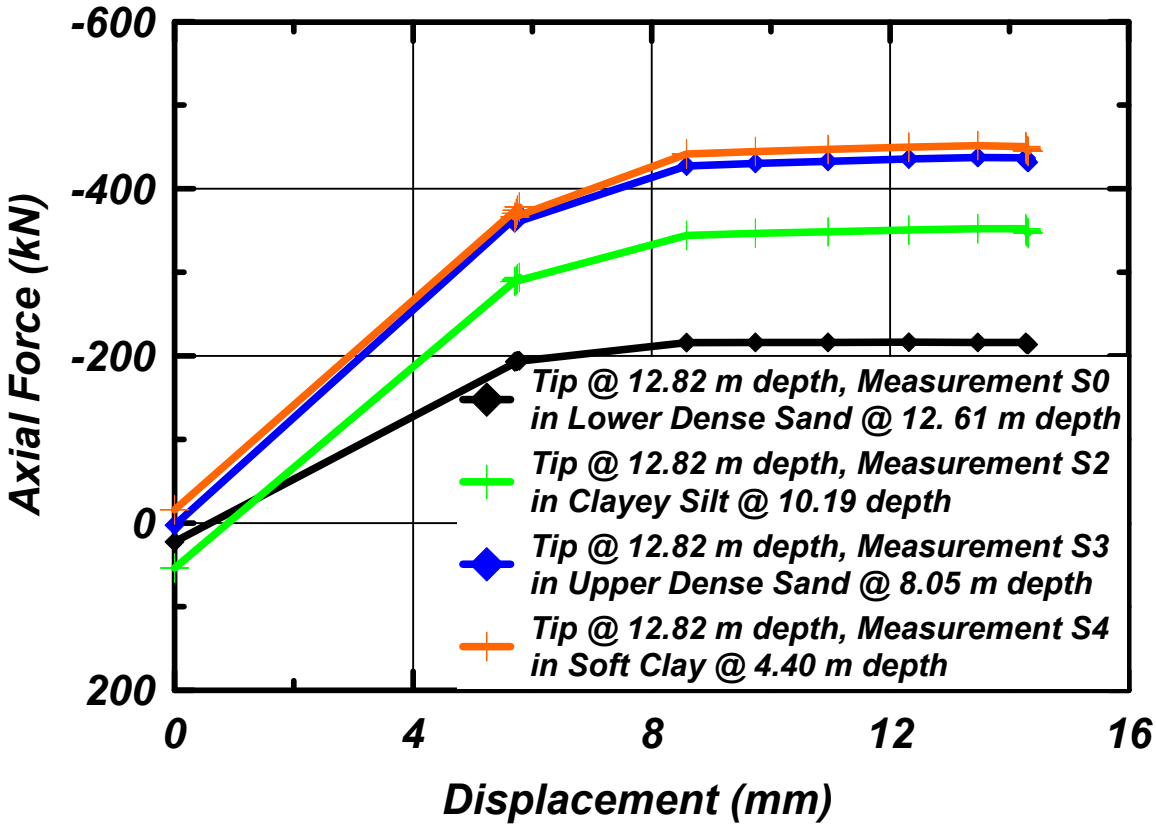


**Figure 6.7: Tension pile load test result with RTP tip driven to 12.8 m depth. Test performed immediately after driving.**

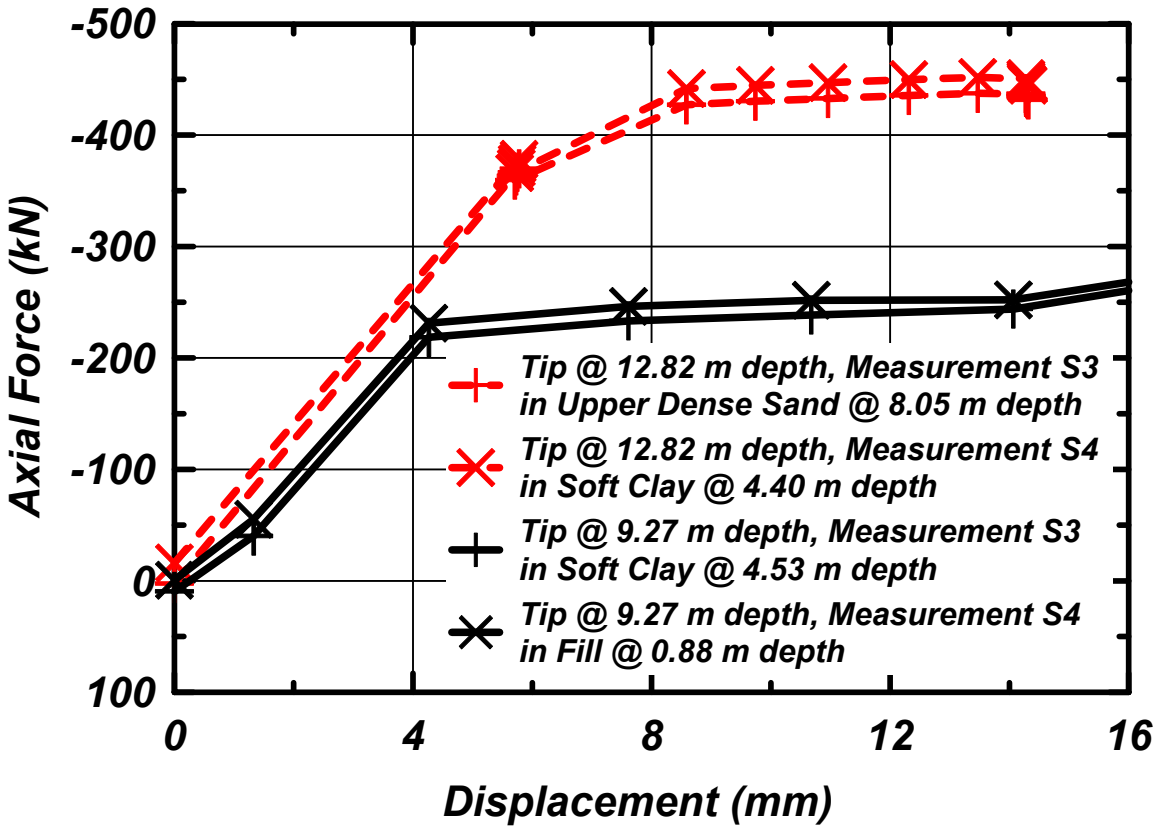


**Figure 6.8: Comparison of tension pile load test results at shallower depth (9.3 m) and deeper depth (12.8 m).**

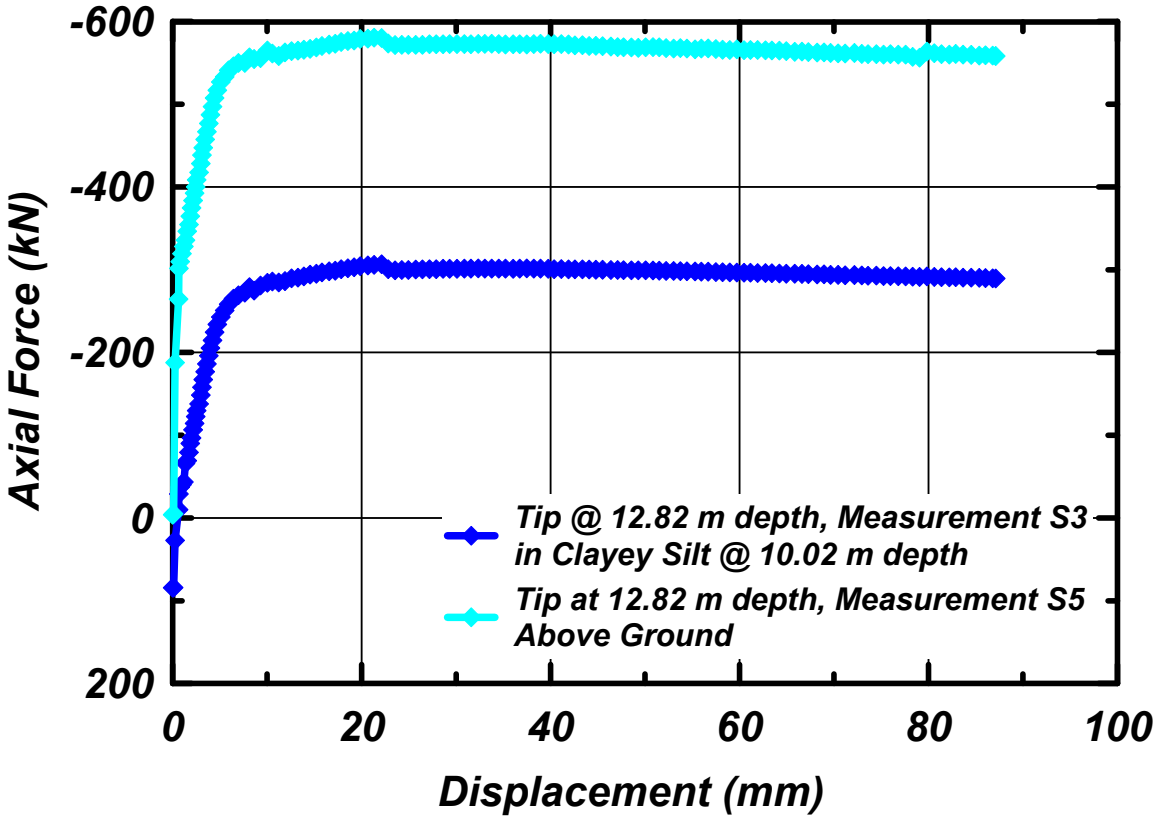


**Figure 6.9: Tension pile load test result with RTP tip driven to 12.8 m depth. Test performed after setup period of 4 hours.**

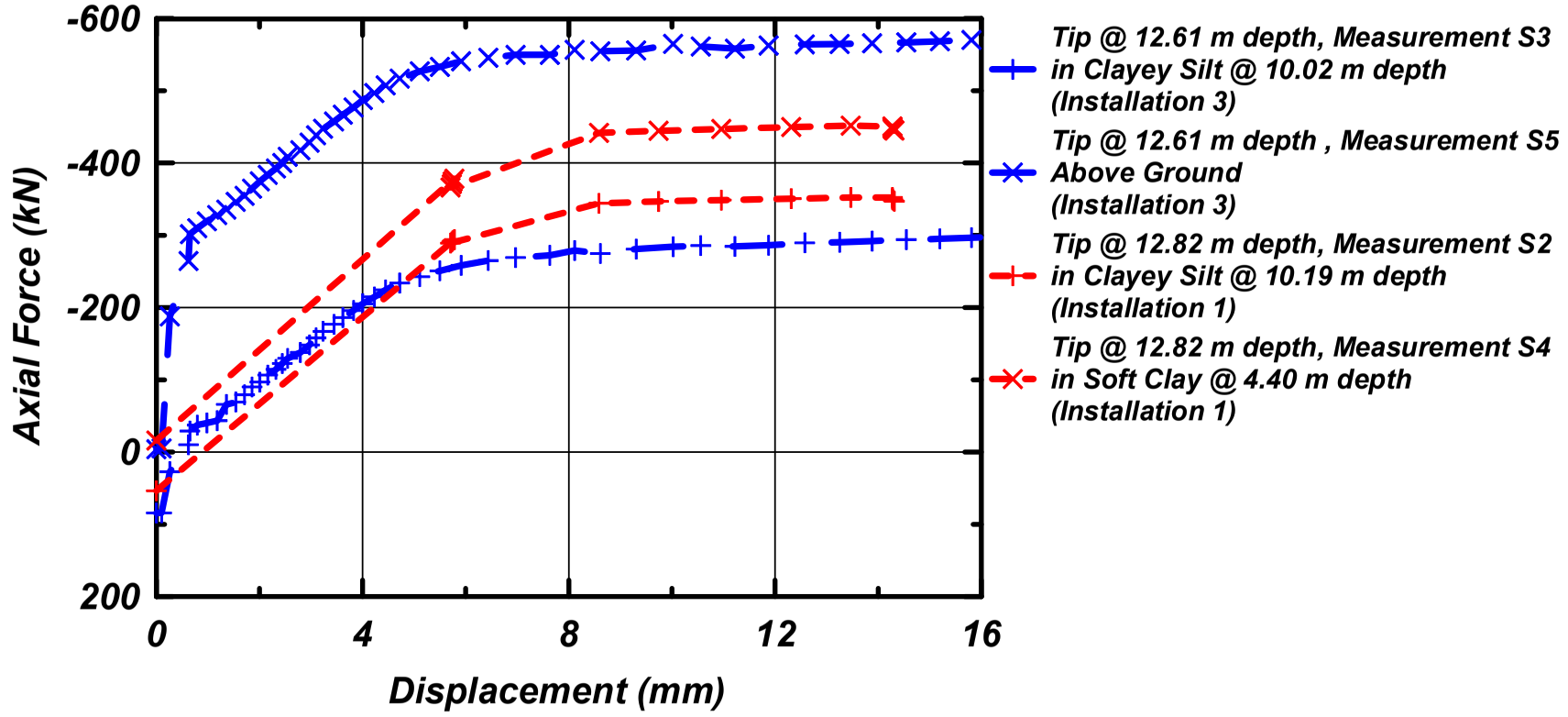


**Figure 6.10: Comparison of tension load tests performed immediately after RTP installation (Installation 1) and after pile setup period of 4 hours (Installation 3). In both cases pile tip is driven to the lower dense sand layer.**

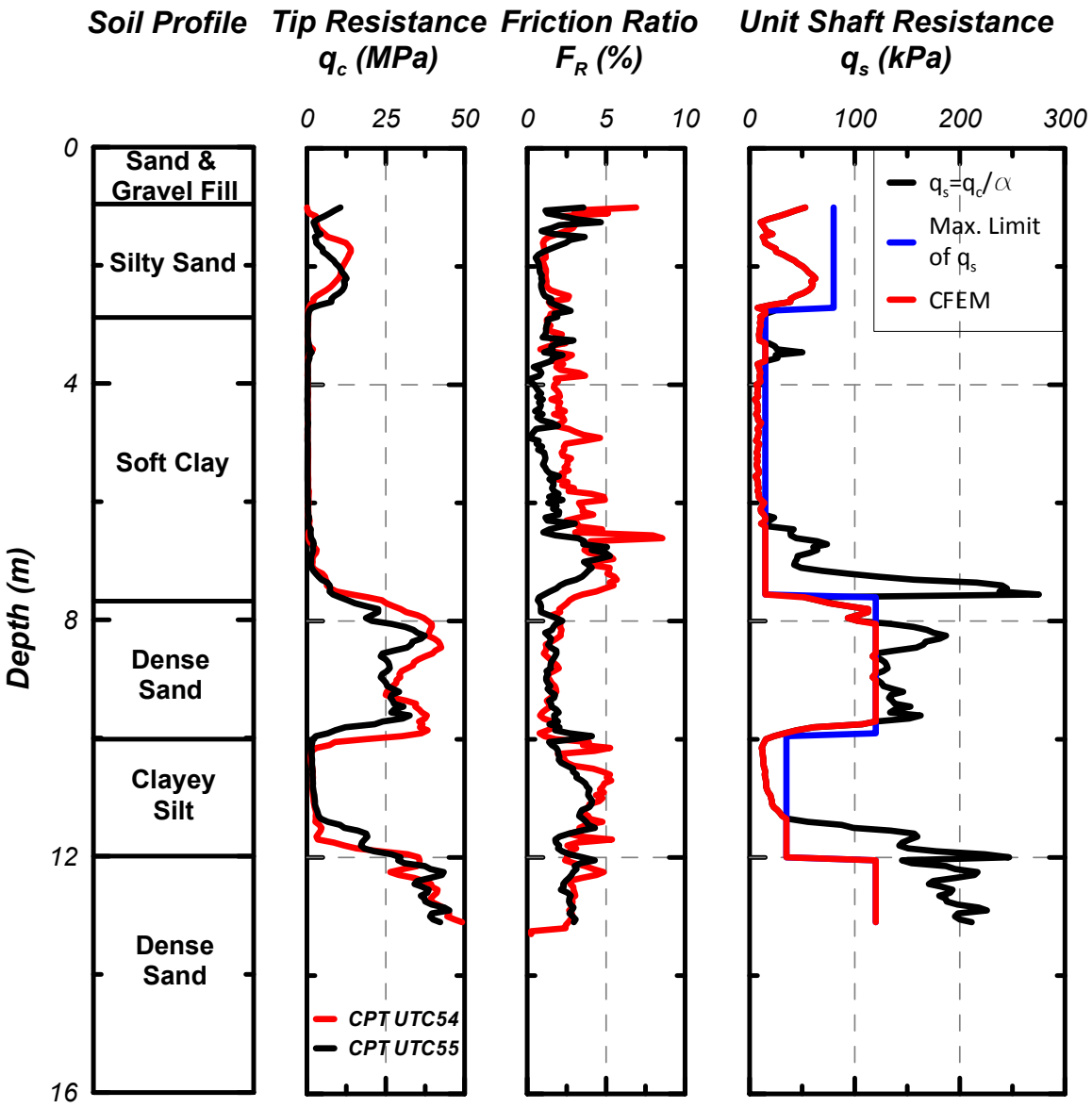


**Figure 6.11: Calculated unit shaft resistance profile based on the CFEM maximum allowable value of $q_s$ (blue line), the $q_s$ as a fraction of $q_c$ (black line), and the recommended CFEM value (red line, which is lesser of blue line and black line). CPT records and soil profile presented for completion.**

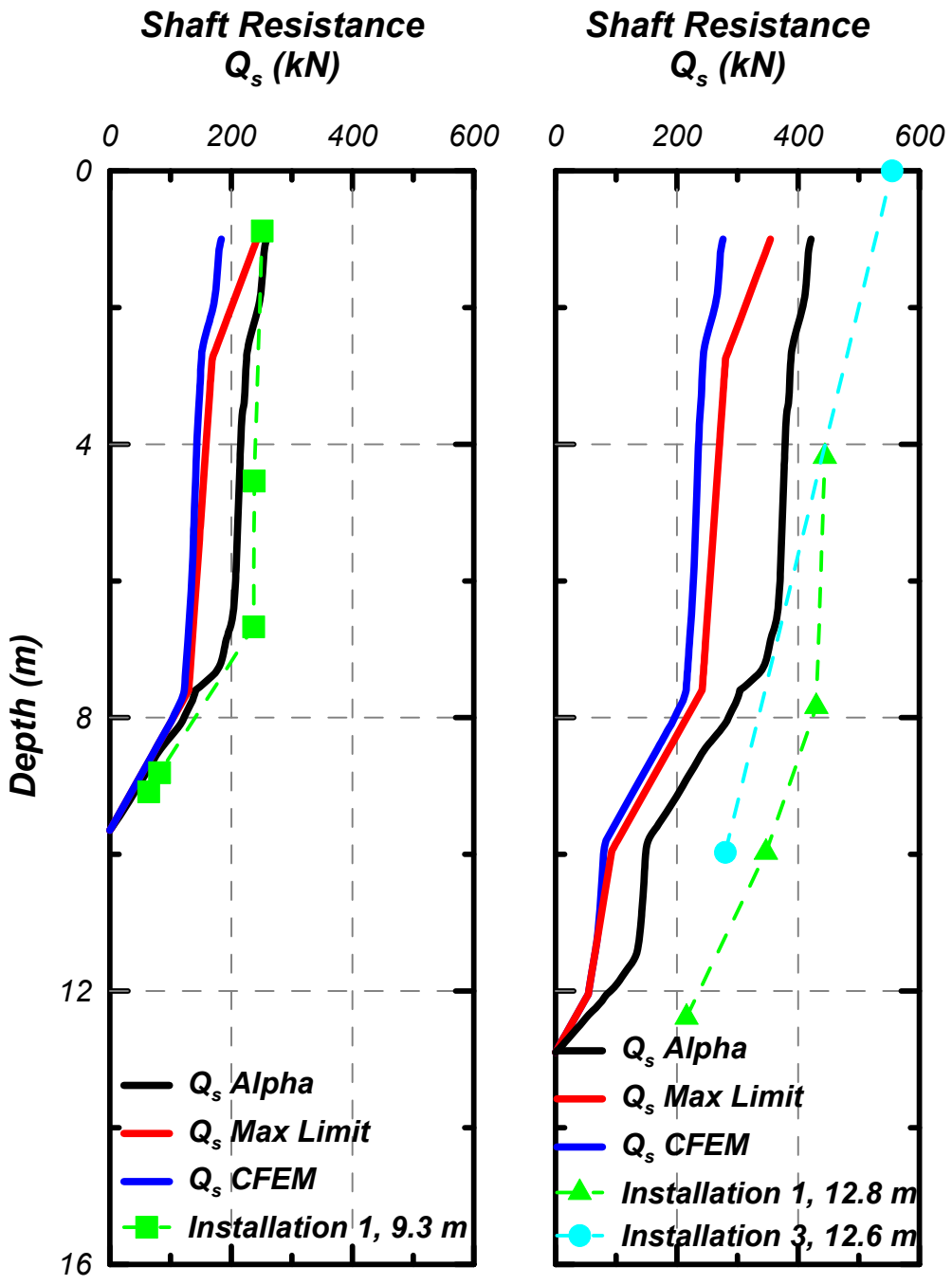


**Figure 6.12: Comparison of cumulative shaft distribution calculated for RTP based on CPT records and shaft resistance measured in field using RTP instrumented sections. Instrumentation locations for installation 1 and installation 2 are about 0.2 m and 0.6 m behind the toe.**

# Chapter 7: Conclusions and Recommendations for Future Work

The objective of this dissertation was to develop a reusable test pile (RTP) as an in situ device deployed during the site investigation phase of a project and which produces measurements during dynamic installation, pile setup, and load testing that would be used to improve the design of the full scale piling foundation system eventually installed at the project site. Overall this objective has been accomplished; a new RTP device with capabilities never achieved previously has been produced. The Conclusions section highlights the design process, the RTP design fabricated, tested, and calibrated, the test program executed at the Oakland, CA test site, and RTP measurements capture during dynamic driving, pile setup, and pile tension load tests. This work also revealed which aspects of the RTP system worked well and which require additional improvements. The second section, Recommendations for Future Work, addresses opportunities for improvement.

## 7.1 Conclusions

Chapter 3 presented details of the design, fabrication, calibration, and prototyping of the RTP system. The performance requirements of the RTP included practical constraints to enable routine use and some constraints to ensure insitu measurements to improve the design of driven piles. The most significant constraints were installation by an industry standard pile driving hammer and deployment using industry standard equipment. Both of these constraints had not been accomplished in previous projects on instrumented piles. The RTP system consists

of short instrumented sections which can be connected in series with Becker pipe sections. The modular design also allows the RTP configuration to be adapted to project-specific conditions and minimizes the amount of equipment that is RTP specific. Each section is instrumented to measure axial force, radial stress, acceleration, and pore pressure. The closed-end driving shoe is instrumented to measure axial resistance and acceleration. Details of the system developed for each measurement were presented. Each RTP section contains a data acquisition module that filters, gains, and performs analog to digital conversion of sensor signals before transmitting the signal above ground. A second data acquisition system provides continuous measurements of pile head displacement and Becker hammer performance (via bounce chamber pressure measurements). During development a series of intermediate testing programs were required to test and evaluate prototype designs before the final RTP system was fabricated. Particular challenges in the design were the down hole computer isolation system, radial stress measurement system with the thin walled cylinders, and saturation of the pore pressure sensor. In addition, fixtures and equipment to perform sensor calibration before and after field testing were developed and presented.

Chapter 4 presented details of the Oakland, CA test site and of the field testing program that was performed. The Oakland, CA test site is owned by Caltrans and is located adjacent to where prior pile load tests were performed as part of the I-880 expansion project in the 1990s. The site was well suited for the first RTP deployment as the stratigraphy at the site included a strong crust, a soft clay layer where easy driving conditions occurred, and deeper dense sand layers where driving resistance reached refusal conditions. The field testing program consisted of three primary installation events, one occurring on each day. In all installation events

measurements during pile driving and tension load testing were obtained. During Installation 1 and 2 pile load tests were performed at two different penetration depths, both immediately after pile installation. Installation 3 included RTP installation directly to 12.6 m, followed by a 4 hour setup time prior to a tension load test.

Chapter 5 examined RTP performance during dynamic pile installation. Above ground measurements of pile driving resistance, captured by blows per 0.3 m and displacement per pile blow, and Becker hammer efficiency, captured by hammer bounce chamber pressure, were used to examine RTP system performance during penetration through the soft clay layer, the upper dense sand layer, the silty clay layer, and the lower dense sand layer until refusal conditions occurred. Immediately prior to RTP free-fall in the soft clay the displacement per blow was very large (about 7 cm) and the hammer efficiency was very low. This contrasted refusal driving conditions where the displacement per blow was about 0.03 cm. The acceleration and force time histories recorded during select blows as the RTP penetrated the four soil layers were also analyzed for all instrumented sections. The propagation of the impact wave from the hammer down through the RTP sections and the following reflection wave back up through the RTP was clearly captured. These results are promising as a complete set of dynamic data along the RTP length would likely improve estimation of load distribution using CAPWAP type programs. In addition, the acceleration and force measurements recorded above ground were analyzed in a pile driving analysis manner. The impedance based force estimated from the velocity time history (integrated from the acceleration record) was compared to the direct strain based time history. There was good overall agreement in the shape of the

recorded signal between 0 and 1 L/c, but the amplitude of the impedance based force was higher than the strain based estimate.

Chapter 6 examined the development of residual stresses during driving, pore pressure dissipation during a pile setup time of 4.0 hours, and three tension load tests (two from Installation 1 and one from Installation 3). It was shown that significant residual stresses did not develop until the RTP penetrated the upper and lower dense sand layers. When residual stresses did develop the shaft resistance in upper and lower dense sand layer was significant enough to prevent complete elastic rebound following a hammer impact. During the 4.0 hour time period for pile setup the excess pore pressure (generated during driving) in the soft clay approached 50% consolidation while the excess pore pressure in the upper dense sand layer dissipated fully within 0.4 hours. Estimates of $c_h$ from the dissipation data were consistent with that expected. Tension load tests performed immediately after installation to depths of 9.3 and 12.6 m captured the load distribution with depth and the overall tensile load capacity. Expectedly the load increased with penetration depth, primarily after further penetration into the dense sand layers. The RTP capacity was also shown to increase by 25% follow the 4.0 hour pile setup period. The increase in capacity was attributed to full reconsolidation around the RTP in the lower silty clay layer and in the sand layers and partial reconsolidation in the soft clay layer.

## 7.2 Recommendations for Future Work

The first generation design of the RTP has revealed components that performed well and components that require design improvements. Clear successes include the integrated design with the Becker drilling system, the pore pressure measurement system, the axial force Wheatstone bridge design, the accelerometer measurements, the vibration isolation of the downhole data acquisition system, and the above ground measurements of RTP head position and hammer bounce chamber pressure. The most significant issue in the first generation design is the radial stress measurement system. The results are consistent with what many previous researchers have found; it is tremendously difficult, if not impossible, to achieve the robustness required to survive dynamic driving and the resolution required to accurately measure the static radial stress. It is likely not realistic to include a radial stress measurement in future RTP generations. Second, the first generation downhole data acquisition system, although it survived and performed well for data collection during driving, setup and pullout test, it is recommended to increase the capability of the downhole data acquisition for higher sampling rates and more memories, and increased data communication bandwidth to collect more data. Second, the vibration isolation system, though successful in protecting the down hole computer system, was difficult to assemble and to perform maintenance on in the field. Similarly, the permanent wiring of sensors and cabling to the pipe section made maintenance difficult. Redesign to improve efficiency in assembly and performing maintenance on RTP instrumented sections is recommended. Third, the pore pressure measurement performed well when saturation was maintained, but desaturation did occur for certain sensors. Improvements in the saturation process are recommended. Fourth, additional work is needed

to understand the difference in the PDA analysis between the impedance and strain based force measurements. The possible source(s) of the difference was investigated (changes in pile cross section area, changes in material properties, joint connections, use of only one accelerometer, data acquisition system) but no definitive source was identified. Fifth, an integrated data acquisition system for both the down hole and above ground measurements is recommended as the lack of synchronization in the first generation design was problematic in post-processing. Sixth, a LabView based GUI control module to control data acquisition as well as to evaluate data recorded in real time is recommended.

In addition to RTP equipment improvements in the second generation design there are other additional recommendations for future work. First, it is recommended that Great West Drilling improve the hydraulic control system to ensure that the displacement rate during tension load tests is constant and at a speed acceptable by ASTM standards. Second, it is recommended that the RTP be deployed at several additional Caltrans project sites in California where full scale driven displacement piles have been installed and load tested so that a direct side by side comparison between installation performance and pile load tests can be made. Third, it is recommended that the data obtained from several sites be integrated and used to develop a new design framework based directly on RTP measurements. Fourth, CAPWAP type analysis should be performed on RTP measurements to determine if RTP measurements along the pile depth can improve prediction of full scale capacity.